NRL Memorandum Report 4373

Detailed Modelling of Combustion Systems

ELAINE S. ORAN AND JAY P. BORIS

Laboratory for Computational Physics

November 12, 1980

NAVAL RESEARCH LABORATORY
Washington, D.C.

(14) NRL-MR-4371

SECURITY CLASSIFICATION OF THIS PAGE (When Data Entered)

REPORT DOCUMENTATION PAGE	READ INSTRUCTIONS BEFORE COMPLETING FORM
1. REPORT NUMBER: NRL Memorandum Report 4371 / 2. GOVT ACCESSION NO.: AD-A092 284	3. RECIPIENT'S CATALOG NUMBER
4. TITLE (and Subtitle): (C) DETAILED MODELLING OF COMBUSTION SYSTEMS	5. TYPE OF REPORT & PERIOD COVERED: (9) Interim report on a continuing NRL problem.
	6. PERFORMING ORG. REPORT NUMBER
7. AUTHOR(s): (10) Elaine S. Oran and Jay P. Boris	8. CONTRACT OR GRANT NUMBER(s): (16) RR02402
9. PERFORMING ORGANIZATION NAME AND ADDRESS: Naval Research Laboratory, Washington, D.C. 20375	10. PROGRAM ELEMENT, PROJECT, TASK AREA & WORK UNIT NUMBERS: (17) 61153N; RR0240241; NRL Problem No. 62-0572-0-0
11. CONTROLLING OFFICE NAME AND ADDRESS: (12) 226 (11) 12	12. REPORT DATE: November 1980
	13. NUMBER OF PAGES: 225
14. MONITORING AGENCY NAME & ADDRESS (if different from Controlling Office)	15. SECURITY CLASS. (of this report): UNCLASSIFIED
	15a. DECLASSIFICATION/DOWNGRADING SCHEDULE

16. DISTRIBUTION STATEMENT (of this Report)

Approved for public release; distribution unlimited.

17. DISTRIBUTION STATEMENT (of the abstract entered in Block 20, if different from Report)

18. SUPPLEMENTARY NOTES

19. KEY WORDS (Continue on reverse side if necessary and identify by block number)

Modelling
Flames
Detonations
Computational Physics
Combustion

20. ABSTRACT (Continue on reverse side if necessary and identify by block number)

The purpose of this paper is to acquaint the reader with some of the basic principles of detailed modelling as applied to combustion systems. Detailed modelling is also known as numerical simulation. It can be used to describe the chemical and physical evolution of a complex reactive flow system by solving numerically the governing time-dependent conservation equations for mass, momentum and energy. → next page

(Continued)

DD FORM 1 JAN 73 1473 EDITION OF 1 NOV 65 IS OBSOLETE
S/N 0102-014-6601

20. ABSTRACT (Continued)

cont.→ Solving these equations requires input data such as the species present, the chemical reactions that can occur, transport coefficients for viscosity, thermal conductivity, molecular diffusion, and thermal diffusion, the equation of state for the various materials present, and a set of boundary, source and initial conditions. Given this information, the equations contain in principle all the information we might want from the largest macroscopic space scales down to the point where the fluid approximation itself breaks down. Flame, detonation, turbulence phenomena, and all multi-dimensional effects are included in the solutions of these equations.

The real question is then: how in practice do we extract the information we want? There are severe restrictions imposed on our modelling capability by the finite computer memory, storage, and processing speeds available with even the best of today's computer hardware. Thus the solutions we arrive at are restricted and depend on both the time and space regimes we can afford to study and the numerical methods we have available to resolve them.

An important goal of detailed modelling is to develop a computational model with a well-understood range of validity. This model can then be used in a predictive role to evaluate the feasibility and validity of new concepts. It can also be used to interpret experimental measurements, to extend our knowledge to new parameter regimes, and perhaps as an engineering design tool. Throughout these various applications, the model may serve as an excellent way to test our understanding of the interactions of the individual physical processes which control the behavior of a reactive flow system.

Modelling combustion systems has its own particular problems because of the strong interaction between the energy release from chemical reactions and the dynamics of fluid motion. Release of chemical energy generates gradients in temperature, pressure, and density. These gradients in turn influence the transport of mass, momentum, and energy in the system. On a large scale, the gradients may generate vorticity or affect the diffusion of mass and energy. On a microscopic scale, they are the origin of the turbulence which drastically affects macroscopic mixing and burning velocities. Properly describing the strong interplay between chemistry and fluid dynamics is the real challenge of modelling combustion.

We have purposely concluded this paper on a rather challenging note by discussing turbulence, a major stumbling block in combustion. A thorough review of all of the current approaches to both reactive and non-reactive turbulence would require at least several volumes. Instead, we have tried to describe some of the physical processes which lead to and control turbulence in reactive, incompressible flows. Our point of view is that of modeller looking for an adequate representation and we outline what features we would like the representation and associated evolution algorithms to have.

CONTENTS

DETAILED MODELLING OF COMBUSTION SYSTEMS

I. INTRODUCTION

The purpose of this paper is to acquaint the reader with some of the basic principles of detailed modelling as applied to combustion systems. Detailed modelling is also known as numerical simulation. It can be used to describe the chemical and physical evolution of a complex reactive flow system by solving numerically the governing time-dependent conservation equations for mass, momentum and energy.

Solving these equations requires input data such as the species present, the chemical reactions that can occur, transport coefficients for viscosity, thermal conductivity, molecular diffusion, and thermal diffusion, the equation of state for the various materials present, and a set of boundary, source and initial conditions. Given this information, the equations contain in principle all the information we might want from the largest macroscopic space scales down to the point where the fluid approximation itself breaks down. Flame, detonation, turbulence phenomena, and all multi-dimensional effects are included in the solutions of these equations.

The real question is then: how in practice do we extract the information we want? There are severe restrictions imposed on our modelling capability by the finite computer memory, storage, and processing speeds available with even the best of today's computer hardware. Thus the solutions we arrive at are restricted and depend on both the time and space regimes we can afford to study and the numerical methods we have available to resolve them.

An important goal of detailed modelling is to develop a computational model with a well-understood range of validity. This model can then be used in a predictive role to evaluate the

Manuscript submitted August 19, 1980.

feasibility and validity of new concepts. It can also be used to interpret experimental measurements, to extend our knowledge to new parameter regimes, and perhaps as an engineering design tool. Throughout these various applications, the model may serve as an excellent way to test our understanding of the interactions of the individual physical processes which control the behavior of a reactive flow system.

Modelling combustion systems has its own particular problems because of the strong interaction between the energy released from chemical reactions and the dynamics of fluid motion. Release of chemical energy generates gradients in temperature, pressure, and density. These gradients in turn influence the tranport of mass, momentum, and energy in the system. On a large scale, the gradients may generate vorticity or affect the diffusion of mass and energy. On a microscopic scale, they are the origin of the turbulence which drastically affects macroscopic mixing and burning velocities. Properly describing the strong interplay between chemistry and fluid dynamics is the real challenge of modelling combustion.

Table I.1 lists some of the major chemical and physical processes which might need to be considered for an accurate description of a complicated combustion system. Multi-phase processes such as surface catalysis and soot formation can be important even when we are primarily interested in gas phase combustion. For most interesting systems, the basic chemical reaction scheme, the individual chemical rates, the optical opacities, or the effects of surface reactions are not well known. Thus the first problem that must be solved is modelling the controlling fundamental processes separately.

The paper's discussion of the detailed modelling of combustion systems is confined to the gas phase: we have omitted heterogeneous effects and radiation transport. Section II is devoted to defining the problem we wish to solve, describing the types of time, space, physical and geometric complexity which models must handle, and then illustrating these with examples

Section III provides an introduction to some of the basic features of finite difference solutions of the individual terms in the conservation equations. The various types of terms are classified and simple solution algorithms are derived. This section provides the background necessary for understanding the specific numerical techniques discussed in Sections IV, V, and VI, which deal with solving the more complicated terms representing the chemical reactions, hydrodynamics, and diffusive transport processes occurring in combustion systems. Section VII deals with techniques for coupling the solutions of the equations representing these processes.

Sections VII and IX, which summarize some of the results of detailed modelling of gas phase combustion calculations, are far from comprehensive. The goal is to give the reader an idea of what kind of work has been done to date and how these models may be used. We emphasize that we have not dealt with phenomenological models, but rather with models that will guide our intuition and which, together with experiments and analytic theory, will give us the material upon which phenomenological models can be based.

We have purposely concluded this paper on a rather challenging note by discussing turbulence, a major stumbling block in combustion. A thorough review of all of the current approaches to both reactive and non-reactive turbulence would require at least several volumes. Instead, we have tried to describe some of the physical processes which lead to and control turbulence in reactive, incompressible flows. Our point of view is that of modeller looking for an adequate representation and we outline what features we would like the representation and associated evolution algorithms to have.

How to Read this Article

The sections of this paper can be grouped into five parts which may be read as units.

(1) This introduction and Section II present a statement of the fundamental equations we wish to solve and the problems inherent in obtaining their solution.

(2) Sections III, V, and VII deal with the origin of the numerical problems we must face. The first of these, Section III, should be at least skimmed before preceeding to Section V.

(3) Sections IV and VI discuss chemical and diffusive transport equations.

(4) Sections VII and IX are a representative review of the literature which shows how detailed models have been used.

(5) Finally, Section X describes the problems we must deal with if we wish to develop a model of turbulence to be incorporated in a detailed model of combustion. Section VII, which discusses the coupling of models for phenomena which vary on widely divergent time and space scales, is good background material for Section X.

A Glossary is provided which defines those variables used in more than one section of the paper.

Table I.1
Fundamental Processes in Combustion

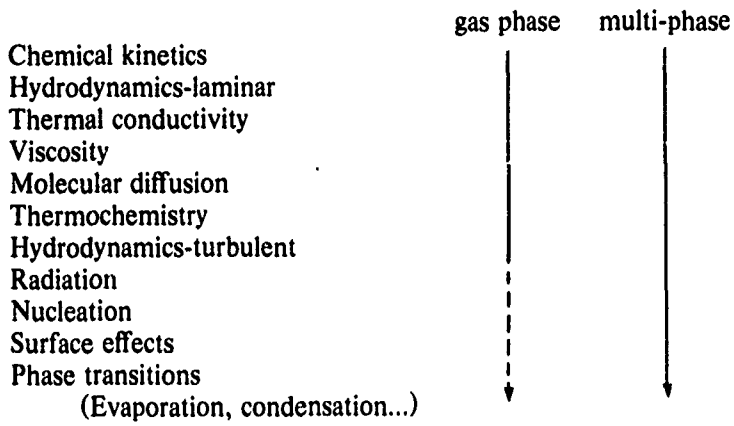

II. THE DETAILED MODELLING PROBLEM

II.A. Conservation Equations

The basic equations which a detailed reactive flow model proposes to solve are the time-dependent equations for conservation of mass, momentum and energy. These may be written as [1,2]

$$\frac{\partial \rho}{\partial t} = -\underline{\nabla} \cdot \rho \underline{v} \tag{II.1}$$

$$\frac{\partial n_j}{\partial t} = -\underline{\nabla} \cdot n_j \underline{V}_j - \underline{\nabla} \cdot n_j \underline{v} + Q_j - L_j n_j \tag{II.2}$$

$$\frac{\partial (\rho \underline{v})}{\partial t} = -\underline{\nabla} \cdot (\rho \underline{v}\underline{v}) - \underline{\nabla} P + \underline{\nabla}\, \eta (\underline{\nabla} \underline{v} + (\underline{\nabla} \underline{v})^T) - \frac{2}{3} \underline{\nabla} (\eta [\underline{\nabla} \cdot \underline{v}]) \tag{II.3}$$

$$\frac{\partial \mathscr{E}}{\partial t} = -\nabla \cdot E \underline{v} - \nabla \cdot P \underline{v} - \underline{\nabla} \cdot \underline{Q} \tag{II.4}$$

where the heat flux, Q, is defined as

$$Q = -\lambda \underline{\nabla} T + \sum_j n_j h_j \underline{V}_j + k_B T \sum_{j,k} \frac{n_j}{N M_j} \frac{D_j^T}{D_{jk}} (\underline{V}_j - \underline{V}_k) \tag{II.5}$$

The ρ, $\rho \underline{v}$, $\mathscr{E}$ and P are the total mass, momentum, energy density, and pressure, respectively and $\underline{v}$ is the fluid velocity. The $\{n_i\}$ and $\{\underline{V}_i\}$ are the number density and the diffusion velocities of the individual chemical species. The quantities η and λ represent the shear viscosity and the thermal conductivity of the gas mixture at specified $\{n_j\}$ and temperature, T. The coefficient of bulk viscosity is assumed to be negligible. The $\{Q_j\}$ and $\{L_j\}$ refer to chemical production and loss processes for species j. The last two terms in Eq. (II.5) represent the local change in energy due to molecular diffusion and chemical reactions which must be added to the fluid dynamic energy density. The quantities $\{h_j\}$ are the temperature dependent enthalpies for each species and the $\{D_{jk}\}$ and $\{D_j^T\}$ are the sets of binary and thermal diffusion coefficients, respectively. The superscript "T" in Eq. III.3 indicates the transpose operation and k_B is Boltzmann's constant.

Throughout this paper the ideal gas law is assumed so that

$$P = Nk_B T, \tag{II.6}$$

where N is the total number density,

$$N = \sum_j n_j. \tag{II.7}$$

Quantities are given in cgs °K units. Thus we may write the internal energy per unit volume as

$$\epsilon = \sum_j n_j h_j - P = H - P. \tag{II.8}$$

The internal energy is related to the pressure and total energy by

$$\epsilon = \frac{P}{\gamma - 1} = \mathscr{E} - \frac{1}{2}\rho v^2 - \sum_j h_{oj} n_j \equiv E - \frac{1}{2}\rho v^2 \tag{II.9}$$

where γ is the ratio of specific heats, $\{h_{oj}\}$ is the set of heats of formation at 0°K of the species j, and E is the total energy minus the total heat of formation.

Combining Eqs. (II.8) and (II.9), we obtain

$$\gamma = \frac{H}{H - P}, \tag{II.10}$$

which may be evaluated from $\{h_i\}$. When it is required, the equation-of-state, Eqs. (II.6) or (II.8), may be replaced by other forms.

The diffusion velocities $\{\underline{V}_j\}$ are found by inverting the following matrix equation:

$$S_j = \sum_k \frac{n_j n_k}{N^2 D_{jk}} (\underline{V}_k - \underline{V}_j) \equiv \sum_k W_{jk} (\underline{V}_k - \underline{V}_j), \tag{II.11}$$

where the source terms S_j are defined as [3]

$$S_j \equiv \underline{\nabla}(n_j/N) - (\rho_j/\rho - n_j/N) \frac{\nabla P}{P} - \sum_k \frac{n_j n_k}{N^2 D_{jk}} (D_k^T/\rho_k - D_j^T/\rho_j) \frac{\nabla T}{T}. \tag{II.12}$$

Equation (II.10) is also subject to the constraint

$$\sum_j \rho_j \underline{V}_j = 0. \tag{II.13}$$

Quantities such as the chemical rates which appear in the $\{Q_j\}$ and $\{L_j\}$, the η, λ, $\{D_{jk}\}$

and $\{D_j^T\}$, as well as any coefficients which might be added to represent turbulence, are input submodels. Their values are based on experiments, theoretical calculations, or simply educated guesses.

Equations (II.1-13) as written encompass both flame and detonation phenomena. The specific problem modelled is determined by the initial conditions, the boundary conditions, the set of chemical constituents and their thermophysical and chemical properties. These conditions often determine the choice of solution technique, which is a major theme in the remainder of this paper.

II.B. Problems in Modelling Reactive Flows

In the previous section several generic problems associated with the solution of Eqs. (II.1-12) were described. These problems, which must be overcome in order to accurately model transient combustion systems, are associated with the

- multiple time scales,
- multiple space scales,
- geometric complexity, and
- physical complexity

in the systems to be modeled.

The first class of problems arises as the result of trying to represent phenomena characterized by very different time scales. In ordinary flame and detonation problems these scales range over many orders of magnitude. When phenomena are modelled that have characteristic times of variation shorter than the timestep one can afford, the equations describing these phenomena are usually called "stiff." Models of sound waves are stiff with respect to the timestep one wishes to employ when modelling a flame. The equations describing many chemical reaction rates are stiff with respect to convection, diffusion, or even sound wave timestep

criteria. Two distinct modelling approaches, global implicit and time-split asymptotic, have been developed to help resolve these temporally stiff phenomena in a calculation. The two approaches are described in Section VII.

The second class of problems involves the huge disparity in space scales occurring in combustion problems. To model the steep gradients at a flame front, a grid spacing of 10^{-3} cm or smaller might be required. To model convection, grid spacings of 1 to 10 cm might be adequate. Complex phenomena such as turbulence, which occur on intermediate spatial scales, present a particular modelling problem. It would be a pipedream to expect a numerical calculation to faithfully reproduce physical phenomena with scale lengths shorter than a cell size. Therefore, to calculate realistic profiles of physical variables, a certain cell spacing is required to obtain a given accuracy. Choosing a method which maximizes accuracy with a minimum number of grid points is a major concern in detailed modelling.

The third set of obstacles arises because of the geometric complexity associated with real systems. Most of the detailed models developed to date have been one-dimensional. Thus they give a very limited picture of how the energy release affects the hydrodynamics. Even though many processes in a combustion systems can be modelled in one-dimension, there are others, such as boundary layer growth, or the formation of vortices and separating flows, which clearly require at least two-dimensional hydrodynamics. Real combustion systems are at least two-dimensional, with unusual boundary conditions and internal sources and sinks. However, even with sixth generation parallel processing computers available, what can be achieved with two-dimensional detailed models is still limited by computer time and storage requirements.

Currently, one-dimensional models can be best used to look in detail at the coupling of a very large number of species interactions in a geometry that is an approximation to reality. Processes such as radiation transport, turbulence, or the effects of material heterogeneity can be included either as empirically or theoretically derived submodels. Two- and three-dimensional models are best used to study either flow properties or other macroscopic structures. In these

latter models, the chemical reaction scheme is usually quite idealized or parameterized.

The final set of obstacles to detailed modelling concerns physical complexity. Combustion systems usually have many interacting species. These are represented by sets of many coupled equations which must be solved simultaneously. Complicated ordinary differential equations describing the chemical reactions or large matrices describing the molecular diffusion process are costly and increase calculation time orders of magnitude over idealized or empirical models. Table I.1, which lists the fundamental processes occurring in combustion, shows that even in what might appear to be a gas phase problem the reactive flow problem is subject to the effects of heterogeneity. Before a model of a whole combustion system can be assembled, each individual process must be separately understood and modelled. These submodels are either incorporated into the larger detailed model directly or, if the time and space scales are too disparate, must be incorporated phenomenologically. For example, diffusion and thermal conductivity between a wall and the reacting gas can be studied separately and then incorporated directly into a detailed combustion model. Turbulence, however, can be modelled on its own space scales only in idealized cases. These more fundamental models must be used to develop phenomenological models for use in the macroscopic detailed model. Resolution and computational cost prevent incorporating the detailed turbulence model directly.

Often there are cases where the submodels are poorly known or misunderstood, which might occur for chemical rates, thermochemical data, or transport coefficients. A typical example is shown in Fig. II.1, which shows the rate at 300°K for the reaction $HO + O_3 \rightarrow HO_2 + O_2$ as a function of the year of the measurement. We note with amusement and chagrin that if we were modelling a kinetics scheme which incorporated this reaction before 1970, the rate would be uncertain by five orders of magnitude! Similar tales of woe also exist for thermochemical data. One use of modelling is to test the importance of specific chemical rates, and examples of this type of application are given in Sections IV and IX.

II.C. Introduction to the Gedanken Flame Experiment

In order to illustrate how the cost of a computation grows when the requirements needed to model systems characterized by large temporal and spatial disparities are met, we have chosen to analyze a gedanken flame experiment. This analysis is concluded at the end of Section VII. There it is shown how the application of various numerical algorithms introduced in the coming sections may be used to reduce this calculation to a tractable computational problem.

Consider a closed tube one meter long which contains a combustible gas mixture. We wish to calculate how the physical properties such as temperature, species densities, and position of the flame front change after the mixture is ignited at one end. The burning gas can be described, we assume, by a chemical kinetics reaction rate scheme which involves some tens of species and hundreds of chemical rates. For now we will assume one-dimensional propagation along the tube. Boundary layer formation and turbulence will be ignored. We further assume that the flame front moves at an average velocity of 100 cm/sec.

Table II.1 summarizes the pertiment time and space scales in this problem. If we assume that the speed of sound is 10^5 cm/sec, a timestep of about 10^{-9} sec would be required to resolve the motion of sound waves bouncing across the chamber. Chemical time-steps, as mentioned above, are about 10^{-6} sec. This number may be reduced drastically if the reaction rates or density changes are very fast. It takes a sound wave about 10^{-3} seconds to cross the 1 meter system and it takes the flame front about one second to cross. We further assume that the flame zone is about 10^{-2} cm wide and that it takes grid spacings of 10^{-3} cm to resolve the steep gradients in density and temperature. In those portions of the tube on either side of the flame front, we assume that 1 cm spacings are adequate.

To estimate the computational expense of this calculation, we use 10^{-3} seconds of computer time as a reasonable estimate of the time it takes to integrate each grid point for one timestep (a single point-step). This estimate includes a solution of all of the chemical and

hydrodynamic equations and is based on a detailed model of a hydrogen-oxygen flame problem. Figure II.2 shows the information in Table II.1 cast into a graph of space versus time. Since the scales are logarithmic, a calculation of the number of point-steps and then of the needed computer time requires exponentiation. Thus it appears that 3000 years of computer time is required tc calculate the 10^{14} point-steps involved in representing the finest resolved space and time scales!

Of course this is unacceptable. Ideally such a simple calculation should be done in 100 seconds, as indicated by the smaller rectangle in Fig. II.2. We need numerical algorithms which have fine resolution in time and space only where it is required. Furthermore, these algorithms should be optimized to take advantage of what is known about the physics and chemistry of the problem. Sections III, IV, V, and VII present some of the background necessary to understand the principles of numerical simulation.

Table II.1

Important Scales in Gedanken Flame Experiment

Timescales		Spacescales	
Δt	sec	Δx	cm
Sound Speed (Courant Limit)	10^{-9}	Flame Resolution	10^{-3}
Chemistry Reactions	10^{-6}	Flame Zone	10^{-2}
Sound Transit Time	10^{-3}	Diffusion Scale	10^{-1}
Flame Transit Time	1	Convective Scales	10
		System Size	100

$V_f = 100$ cm/sec

III. SOME GENERAL NUMERICAL CONSIDERATIONS

This section discusses generally the major problems encountered in solving numerically the different types of terms occurring in Eqs. (II.1)-(II.13). Sections IV through VII present ways to solve equations containing these terms when they are applied specifically to combustion systems. Primarily finite difference techniques are considered. Other methods, such as finite elements, spectral methods or characteristic methods for solution of continuity equations (Section V) are mentioned briefly, but they have not yet been used to solve the full set of coupled reactive flow equations.

Since the set of reactive flow equations presented at the beginning of Section II is coupled and nonlinear, it is impossible to give a priori a comprehensive analysis of numerical accuracy and stability. For any particular problem, however, these equations may contain the four generic types of terms listed in Table III.1 below. By analyzing these simple, linear, constant coefficient cases, many of the numerical difficulties which also appear in the coupled nonlinear problem can be studied. The discussion also illustrates the strengths and weaknesses of the classical methods for solving the individual terms.

Choosing the best algorithms involves dealing with the nonlinear and non-uniform complexities of a real system. Making these choices under differing conditions is a major theme of this paper. Section VII discusses coupling the numerical representations of the individual physical phenomena into a complex overall model.

III.A. Source, Sink, Coupling, and Chemical Kinetics Terms

The simple equation

$$\frac{\partial A}{\partial t} = \gamma A + B \tag{III.1}$$

represents a number of local phenomena such as source terms, $B(\underline{x}, t)$, sink terms, $-\gamma(\underline{x}, t)\, A(\underline{x}, t)$, and coupling terms between equations. For example, if A is a two component

vector containing a thermal and a vibrational temperature, terms such as $(\gamma A + B)$ express temperature equilibration at the rate $-\gamma$. If A were a vector of chemical reactants, Eq. (III.1) would look like the typical chemical kinetic rate equations.

The discussion of Eq. (III.1) presented here first derives the analytic solution which results when γ and B are constant. This solution is then compared with those derived from explicit, implicit, and asymptotic finite difference techniques. We conclude that the most accurate and cost-effective technique is a combination of an explicit or centered method when the timestep it requires is affordable (normal equations) and an asymptotic method when the timestep required for stability is too small for practical applications (stiff equations).

When γ and B are constant, Eq. (III.1) has the theoretical solution

$$A(t) = \left[A(0) + \frac{B}{\gamma}\right] e^{\gamma t} - \frac{B}{\gamma}, \tag{III.2}$$

which is correct whether γ is positive or negative. Equation (III.1) can be written in a simple finite-difference form

$$\frac{A^\tau - A^{\tau-1}}{\delta t} = \gamma \left[f A^\tau + (1-f) A^{\tau-1}\right] + B \tag{III.3}$$

where $A^\tau \equiv A(\tau \delta t)$ and δt is the finite difference timestep. The implicitness parameter, f, ranges from 0 to 1 and determines whether the right hand side of Eq. (III.3) is evaluated fully at the new time ($f = 1$, full implicit scheme), or at the old time ($f = 0$, fully explicit scheme), or somewhere in between. Equation (III.3) can be solved formally for A^τ,

$$A^\tau = \left[A(0) + \frac{B}{\gamma}\right] E(\gamma \delta t) - \frac{B}{\gamma} \tag{III.4}$$

where $E(\gamma \delta t)$ is a finite-difference approximation to the exponential function which may be written as

$$E(\gamma \delta t) \equiv \frac{1 + (1-f)\gamma \delta t}{1 - f \gamma \delta t}. \tag{III.5}$$

The best approximation to the exponential occurs when $f = 1/2$. Then

$$E(\gamma\delta t) \equiv 1 + \gamma\delta t + \frac{(\gamma\delta t)^2}{2} + \frac{(\gamma\delta t)^3}{4} + \ldots \tag{III.6}$$

which is correct through second order and has a third order error term $\frac{(\gamma\delta t)^3}{12}$.

Figure III.1 displays these solutions for the case when $\gamma < 0$ and $B = 0$. The solutions go asymptotically to $B/\gamma = 0$ and start with $A(0) = A^0 = 1$. They represent a stable equilibration or relaxation which is characteristic of most coupling and chemical kinetic processes. The three panels show the results of numerical integrations which were performed using timesteps $-1/2\gamma$, $-1/\gamma$, and $-2/\gamma$. The characteristic relaxation time is $(-\gamma)^{-1}$. The four solutions in each panel shown for each choice of timestep are labelled by the letters e, c, i, t, where

t = analytical solution,

e = explicit solution ($f = 0$)

c = centered solution ($f = 1/2$), and

i = implicit solution ($f = 1$).

When $-\gamma\delta t$ is small, all of the numerical solutions are stable. The centered solution, $f = 1/2$, is nearly indistinguishable from the exact theoretical solution. The explicit solution is lower than the exact $A(t)$ solution by about as much as the implicit solution errs by being too high. But all of the methods replicate the general behavior of the exact solution and they are all stable. Unfortunately, ensuring $-\gamma\delta t \lesssim 1$ everywhere at each timestep can be expensive computationally when the equations are "stiff", which means here that $-\gamma \frac{A}{dA/dt} \gg 1$.

When $-\gamma\delta t = 1$, the centered solution still approximates the exact solution very well, although the implicit solution is noticeably less accurate than it was when the timestep was smaller. The explicit solution displays a rather singular behavior: it goes exactly to zero in one timestep and then stays there in that asymptotic state. All solutions are stable and still behave essentially physically.

As the timestep is increased further to $-\gamma\delta t = 2$ in the third panel, the explicit solution displays the odd behavior of oscillating at fixed amplitude about the asymptotic $A = 0$ state. This situation is the borderline of classical stability for the explicit solution, but, as noted in panel two, the solution was obviously incorrect even when δt was a factor of two smaller, $\delta t = -1/\gamma$. For δt larger than $-1/\gamma$, the explicitly computed value of A may go below zero and then change sign on each timestep. This occurs because $E\ (\gamma\delta t)$ becomes negative.

Most integrations of the coupled systems of equations cannot accept the mathematically stable but physically bizarre behavior shown in the third panel. Chemical kinetics calculations, for example, go explosively unstable when species number densities are negative. An important guideline in computational physics is that the numerical timestep should always be chosen at least a factor of two smaller than required by the term with the most stringent stability condition. Practical stability is about a factor of two more expensive than mathematical stability.

When $-\gamma\delta t = 2$, the centered solution is still behaving acceptably but has reached the limiting case before instability occurs in the form of negative values of A. Here we also see that the implicit solution is behaving physically and stably. This guaranteed stability is the lure of the implicit approach. Unfortunately the error in the implicit solution, relative to the rapidly decaying theoretical curve (unlabelled in panel 3), has grown over that in the previous two panels. This potentially large error in the relaxation rate of stiff equations is the hidden sting. Thus we note that the practical timestep stability condition for an explicit method is also the effective accuracy condition for the corresponding implicit method.

There are many situations where the damping nature of an implicit algorithm will make any large relative errors progressively less important, but there are also physically unstable situations where the errors are important. Thus there has been a concentrated effort to develop other methods specifically designed to treat $-\gamma\delta t >> 1$ integrations. These are asymptotic approaches in which convergence is guaranteed only for $(\gamma\delta t)$ large, whereas the methods above are based on a Taylor-series expansion which converges when $(\gamma\delta t)$ is small

To derive an asymptotic solution to Eq. (III.1), the right hand side is set equal to zero and then dA/dt is successively approximated using earlier asymptotic solutions. For example, to lowest order

$$\gamma(\tau)A^{\tau} = -B(\tau) + \frac{dA}{dt}(\tau) \tag{III.7}$$

yields $A^{\tau} \approx -B(\tau)/\gamma(\tau)$. The time derivative of A can be approximated using this lowest order solution. The time dependence of γ and B are now included because the asymptotic analysis must take into account the external and the non-linear coupling which represent multiple-timescale facets of the problem.

Since

$$\frac{dA}{dt}(\tau) \approx \left[\frac{B(\tau)}{\gamma(\tau)} - \frac{B(\tau-1)}{\gamma(\tau-1)}\right]/\delta t \tag{III.8}$$

then to next order,

$$A^{\tau} \approx \frac{-B(\tau)}{\gamma(\tau)} + \frac{\left[\dfrac{B(\tau)}{\gamma(\tau)} - \dfrac{B(\tau-1)}{\gamma(\tau-1)}\right]}{\gamma\,\delta t} + \ldots. \tag{III.9}$$

An expansion like this is adequate only when $(\gamma\delta t)$ is large. When $\gamma\delta t = -2$,

$$A^{\tau} \approx \frac{-3}{2}\frac{B(\tau)}{\gamma(\tau)} + \frac{1}{2}\frac{B(\tau-1)}{\gamma(\tau-1)}. \tag{III.10}$$

When $\gamma\delta t = -1$,

$$A^{\tau} \approx -2\frac{B(\tau)}{\gamma(\tau)} + \frac{B(\tau-1)}{\gamma(\tau-1)}. \tag{III.11}$$

When $\gamma\delta t = -1/2$,

$$A^{\tau} \approx -3\frac{B(\tau)}{\gamma(\tau)} + 2\frac{B(\tau-1)}{\gamma(\tau-1)}. \tag{III.12}$$

As $(\gamma\delta t)$ becomes small, the value of A^{τ} becomes dominated by an improperly computed time derivative.

Applied to the simple problem of Fig. III.1, the asymptotic formula gives the final relaxed state $A = 0$. Since the explicit and centered formulae are unstable practically for $\delta t > \frac{-1}{\gamma}$ and $\delta t > \frac{-2}{\gamma}$ respectively, the asymptotic formula should be used whenever δt exceeds these values. The maximum error made by using the centered formula for normal equations and the asymptotic formula for the stiff equations occurs at the switchover value for the timestep. Using an explicit-asymptotic combination formula, the maximum error is e^{-1}. A centered-asymptotic combination has an error of e^{-2}.

The implicit formula is always stable, so the switchover point could be taken at any value of δt. It is useful to determine where the two formulae, implicit and asymptotic, are most accurate. From Eq. (III.5), the error made in using the implicit formula for one timestep is

$$\text{Implicit Error} = \frac{1}{1-\gamma\delta t} - e^{\gamma\delta t}. \tag{III.13}$$

The corresponding error using the asymptotic formula is

$$\text{Asymptotic Error} = e^{\gamma\delta t}, \tag{III.14}$$

since the asymptotic solution is zero. These errors are equal when $-\gamma\delta t \cong 1.679$. For timesteps smaller than $\delta t \approx \frac{-1.679}{\gamma}$, the implicit formula is more accurate. For longer timesteps, the asymptotic formula is more accurate. The implicit-asymptotic combination formula for worst error is $e^{-1.679}$.

Since the worst error of the centered-asymptotic combination is smaller than that of the implicit or the implicit-asymptotic solution, there really is little reason to use a fully implicit technique. The asymptotic approximation is most accurate and stable for $-\gamma\delta t \gtrsim 2$ and so should be considered the algorithm of choice for long timesteps. In Section IV these arguments are applied to the solution of the coupled ordinary differential equations describing chemical rate equations. Treating stiff sound waves by an asymptotic slow-flow algorithm is discussed in Section V.

III.B. Terms with Spatial Derivatives

The remaining three types of terms in Table III.1 involve spatial as well as temporal derivatives and hence require the solution of partial differential equations. The discussion will therefore proceed in terms of Fourier analyses of idealized, constant-coefficient, periodic problems. Since the individual equations are linear, each allowed harmonic e^{ikx} of the system can be treated independently. The finite-difference errors are thus analyzed both in terms of phase errors of translation, sometimes called numerical dispersion, and amplitude errors of harmonics arising from excessive numerical smoothing or numerical instability.

A third type of error, the Gibbs phenomenon or Gibbs error, arises when even the simplest wave or convective problem is solved numerically on a finite grid [60]. This effect is illustrated here by the example of a square wave of density $\rho = 1$ and width 20 cells on the computational grid be uniformly translated to the right. The grid has a total of 100 cells and the boundary conditions are periodic. Suppose further that the square wave is being advanced by one of the "exponentially accurate" spectral methods [4], so only the Gibbs error remains.

Figure III.2 shows the numerical resolution obtained for the density step function which has values from 1.0 to 0.0 when it has travelled to 19.5 cm in a 100 cm periodic system. The dots are the known density values at the grid points; they are the only information known from a finite difference solution about the continuous profile. Using the lowest 100 Fourier harmonics, the solid curve is synthesized as the smoothest continuous curve through all the known values. The Gibbs error arises because the higher harmonics are not included in the calculation. It appears as undershoots and overshoots which are worse in the vicinity of large gradients and discontinuities and it becomes apparent as soon as the profile is convected a fraction of a cell from its initial location. Fluctuations such as these of 10-15% can lead to incorrect or unphysical results in the other parts of a detailed calculation.

III.C. Diffusion Equations and Dissipative Effects

The first example of a partial differential term in the coupled equations is the second term in Table III.1, a simple diffusion equation

$$\frac{\partial A(x,t)}{\partial t} = \nu \frac{\partial^2 A(x,t)}{\partial x^2}. \tag{III.15}$$

The coefficient ν is a positive diffusion coefficient which in this discussion is held constant in space and time. In analogy with Eq. (III.1), a spatially and temporally varying source term in the form of $B(x, t)$ might be added to the right hand side of Eq. (III.15). For simplicity in the analysis presented below, this term has not been included.

Then in analogy with Eq. (III.3), Eq. (III.15) can be written in the following simple finite difference form,

$$\frac{A_i^\tau - A_i^{\tau-1}}{\delta t} = \frac{\nu f}{\delta x^2}\left[A_{i+1}^\tau - 2A_i^\tau + A_{i-1}^\tau\right] + \frac{\nu(1-f)}{\delta x^2}\left[A_{i+1}^{\tau-1} - 2A_i^{\tau-1} + A_{i-1}^{\tau-1}\right] \tag{III.16}$$

where now subscript i labels the spatial cell. Again, $f = 0$ gives the usual explicit scheme, $f = 1/2$ the most accurate centered scheme, and $f = 1$ the more stable implicit scheme.

When the spatial variation e^{ikx} is assumed, where $i = \sqrt{-1}$, the spatial differences in square brackets can be replaced by the expression $[-2A^\tau(k)\ (1 - \cos k\delta x)]$. Equation (III.16) then becomes

$$\frac{A^\tau(k) - A^{\tau-1}(k)}{\delta t} = -\frac{2\nu f}{\delta x^2}(1-\cos k\delta x)\, A^\tau(k) - \frac{2\nu(1-f)}{\delta x^2}(1-\cos k\delta x)\, A^{\tau-1}(k) \tag{III.17}$$

which can be solved explicitly for $A^\tau(k)$ in terms of $A^{\tau-1}(k)$. The ratio $A^\tau(k)/A^{\tau-1}(k)$ is called the amplication factor ($\mathcal{A}$) and is less than unity for realistic diffusion. In terms of the amplification factor, the general finite difference solution can be written as

$$A^{\tau}/A^{\tau-1} = \frac{\left[1 - \frac{2\nu\delta t}{\delta x^2}\ (1-f)\ \ (1-\cos k\delta x)\right]}{\left[1 + \frac{2\nu\delta t}{\delta x^2}\ f\ (1-\cos k\delta x)\right]}. \tag{III.18}$$

In the time interval δt, the analytic solution to Eq. (15) decays by an amount

$$(A^{\tau}/A^{\tau-1})^{T} = e^{-\nu k^2 \delta t}, \tag{III.19}$$

where here the superscript T designates the theoretical solution. Since the numerical algorithms are best compared in terms of the non-dimensional parameters $\delta \equiv \frac{2\nu\delta t}{\delta x^2}$ and $k\delta x$, the result Eq. (III.19) may be rewritten as

$$\mathcal{A}_k^{T} = e^{-\frac{1}{2}(k\delta x)^2}, \tag{III.20}$$

which is the $(1/\delta)^{\text{th}}$ root of Eq. (III.19) and expresses the amplification factor per unit time rather than per timestep. The exponential factor $1/\delta$ is included in the definition of the amplication factor so that comparisons of various solutions may be made after a given amount of time even though different length timesteps have been used. The numerical solution indicated by the superscript N, then becomes

$$\mathcal{A}_k^{N} = \left[\frac{1 - \delta\ (1-f)\ (1-\cos k\delta x)}{1 + \delta\ f\ \ (1-\cos k\delta x)}\right]^{1/\delta}. \tag{III.21}$$

The three panels of Fig. III.3 show the analytically derived curve for amplication factor as a function of harmonic wavelength expressed as $k\delta x$ for various values of δ. The far right of each panel is the shortest wavelength that can be represented, 2 cells per wavelength. Infinite wavelengths are at the left. The reflection points of the explicit "E" solution at amplification factor equal to zero in the $\delta = 1.0$ panel and of the "E" and centered "C" solution in the $\delta = 1.5$ panel represent the portion of the spectrum at short wavelengths where the mode amplitude has changed sign because the timestep is too long. These reflection points are again the limit of practical, if not mathematical, stability because negative values of positive definite quantities become possible. For the right hand panel, $\delta = 1.5$, the short wavelength portion of the spec-

trum computed using the explicit algorithm is completely unstable: the amplitude is greater than unity and the sign is wrong. For $k\delta x \gtrsim \frac{2\pi}{3}$, the centered algorithm is practically, although not absolutely, unstable. The mode amplitudes of these short wavelengths decrease rapidly from one timestep to the next, but their sign oscillates.

In all of these comparisons, the implicit algorithm is stable and behaves in a physically reasonable way at short wavelengths. In the regimes where the other algorithms are also stable, the implicit algorithm is somewhat less accurate. Furthermore, parabolic diffusion equations really are not subject to the phase errors of translation as are convection and hyperbolic wave equations. Therefore short wavelengths, where numerical errors are worst, decay quickly and the solution becomes smoother as time progresses. All of these considerations indicate that implicit diffusion algorithms should be used wherever practical. Unfortunately complications such as non-linearity, spatial dependence of diffusion coefficients, and anisotropy often conspire to make the implicit algorithm expensive and complicated to use. An asymptotic solution of the diffusion equation is also possible although guaranteeing global conservation may be difficult. Unfortunately these methods are generally problem dependent and often not easily generalized.

III.D. Wave-Like Equations

The third type of term in Table III.1 represents the propagation of waves,

$$\frac{\partial^2 A}{\partial t^2} = v_w^2 \frac{\partial^2 A}{\partial x^2}, \tag{III.22}$$

where v_w represents, for example, the speed of sound in a material. This same physical phenomenon can also appear as two coupled first-order equations

$$\frac{\partial A}{\partial t} = - v_w \frac{\partial B}{\partial x} \text{ and } \frac{\partial B}{\partial t} = - v_w \frac{\partial A}{\partial x}. \tag{III.23}$$

Wave equations have oscillatory solutions which we shall assume vary as

$$A(x, t) = A_k \, e^{ikx} e^{-i\omega t} \tag{III.24a}$$

$$B(x, t) = B_k\, e^{ikx}\, e^{-i\omega t} \tag{III.24b}$$

in the following analyses. The analytical solution is

$$\omega = v_w k, \tag{III.25}$$

but each spatial Fourier harmonic will propagate at a different phase speed in the numerical finite difference solution. The expressions

$$\frac{A_l^\tau - A_l^{\tau-1}}{\delta t} = -v_w \frac{B_{l+1}^{\tau-1}{}_2 - B_{l-1}^{\tau-1}{}_2}{\delta x} \tag{III.26a}$$

$$\frac{B_{l+1/2}^\tau - B_{l+1}^{\tau-1}{}_2}{\delta t} = -v_w \frac{A_{l+1}^\tau - A_l^\tau}{\delta x} \tag{III.26b}$$

are an explicit, staggered-leapfrog formulation designed to maintain mode amplitudes as long as the algorithm is numerically stable. This algorithm is reversible, but reversibility does not guarantee stability. It does mean that stable waves will propagate undamped although perhaps at the wrong phase velocity.

Substituting Eqs. (III.24) into Eqs. (III.26) result in the following numerical dispersion relation

$$\sin\frac{\omega\delta t}{2} = \frac{v_w\delta t}{\delta x}\sin\frac{k\delta x}{2} \equiv \epsilon \sin\frac{k\delta x}{2}, \tag{III.27}$$

where here we have let ϵ refer to the coefficient $v_w\delta t/\delta x$. This equation is the explicit algorithm in terms of the time integration and clearly approaches the analytic limit in Eq. (III.25) when the mode under consideration is many computational cells long. As long as $\epsilon \leqslant 1$, we can always find a real ω for any choice of $k\delta x$ and thus the solution is stable. When ϵ exceeds unity, $\sin \omega\delta t/2 > 1$ for modes with $k\delta x/2$ near $\pi/2$. These modes are unstable because a complex value of ω is needed to satisfy the dispersion relation. Here, as earlier, there are practical reasons for choosing δt roughly a factor of two smaller than this mathematical limit.

Figure III.4 displays this explicit dispersion relation for four different values of ϵ. The mathematical stability boundary for this algorithm is $\epsilon = 1$ where the theoretical and explicit dispersion relations agree exactly (line labelled T, E in the upper right hand panel). As ϵ is

increased above unity (the two lower panels), there is a maximum stable value of $k\delta x/2$ for which $\epsilon \sin k\delta x/2 = 1$. For shorter wavelengths, the modes are unstable as indicated by the termination of the explicit algorithm dispersion curve. All curves plotted show $\frac{\omega\delta t}{2\epsilon} \equiv \frac{\omega\delta x}{2c}$ plotted versus $\frac{k\delta x}{2}$. This normalization converts the theoretical dispersion curve to a universal straight line exactly as was done previously for the diffusion equations.

Figure III.4 also shows dispersion curves for a reversible implicit algorithm based on a grid staggered in space but not in time.

$$\frac{A_l^\tau - A_l^{\tau-1}}{\delta t} = -\frac{v_w}{2}\left[\frac{B_{l+1}^{\tau-1}{}_2 + B_{l+1/2}^{\tau} - B_{l-1/2}^{\tau} - B_{l-1}^{\tau-1}{}_2}{\delta x}\right], \tag{III.28}$$

$$\frac{B_{l+1/2}^{\tau} - B_{l+1}^{\tau-1}{}_2}{\delta t} = -\frac{v_w}{2}\left[\frac{A_{l+1}^{\tau} + A_{l+1}^{\tau-1} - A_l^{\tau} - A_l^{\tau-1}}{\delta x}\right].$$

Again substituting the $e^{ikx}\, e^{-i\omega t}$ spatial and time dependence gives the following numerical dispersion relation

$$\tan\frac{\omega\delta t}{2} = \epsilon \sin\frac{k\delta x}{2} \tag{III.29}$$

for the reversible implicit algorithm. This method is always stable because a real ω can always be found regardless of the values of $k\delta x$ and ϵ. As can be seen in the figure, the implicitly determined value of ω always falls below both the analytic value and the explicit values when the latter are stable. The explicit reversible algorithm is always more accurate than the implicit algorithm as long as the former is stable.

When ϵ is very large, as in the lower right hand panel, almost all of the waves travel more than a cell per timestep and hence are unstable when integrated explicitly. The maximum stable wave number k_{max} satisfies

$$k_{max}\,\delta x/2 \sim 1/\epsilon << 1 \tag{III.30}$$

and the maximum value which the implicitly determined frequency ω can take is

$$\omega_{max} \approx \pi/\delta t. \tag{III.31}$$

Thus in the case of wave-like phenomena, the stability condition for the explicit method is again the accuracy condition for the implicit method. Asymptotic treatments are difficult to formulate, although certain kinds of wave-like phenomena can be treated by a WKB approximation in which the phase changes rapidly but the amplitudes and rates of change of phase do not. Multiple timescale analyses are also examples of asymptotic formulations which may be appended to detailed models in the form of subscale phenomenologies.

In the case of diffusion terms, the phases were ignored although considerable attention was paid to the mode amplitudes. In the case of hyperbolic wave equations, the discussion focussed on the phases, and the mode amplitudes were held fixed by construction. Since the modes which are most in error, i.e. the short wavelengths, do not decay in this latter case as they did in the former, the use of centered implicit algorithms for timesteps much longer than the explicit stability condition must be undertaken with caution. Of course, when physical damping is also present, the short wavelengths will decay and are not a problem. Often, however, the waves are only weakly damped and the short wavelength components propagate, undamped, at the wrong speed. When it is feasible, such situations are best treated with a Fourier or spectral method [4] which minimizes phase and amplitude errors.

In any case, no matter which algorithm is used, the Gibbs errors at discontinuities and sharp gradients cannot be entirely avoided. In the case of a sharply rising front in a wave equation, the discontinuity breaks up into an expanding sea of ripples. The ever-present problem of Gibbs errors is discussed further in Section III.E and V.A.

III.E. Convective and Continuity Equations

The continuity equation

$$\frac{\partial \rho(x, t)}{\partial t} = - \frac{\partial (\rho(x, t)\, v\, (x, t))}{\partial x} \tag{III.32}$$

combines the headaches of both the diffusion and wave equations because the solution is sensitive to both phase and amplitude errors. Extensive discussions have been published [5,6] on

the techniques and problems which arise in the numerical solution of continuity equations. These are summarized in the paragraphs which follow and are discussed in much more detail in Section V.

Figure III.5 summarizes the results obtained using several of the traditional methods for solving Eq. (III.32) for a square wave propagation problem. The grid is uniform and periodic and the velocity is a constant. The problem posed is the convection of a square wave of density $\rho = 2.0$ on top of a uniform $\rho = 0.5$ background. The timestep is taken to be $\delta t = 0.2$ so the fluid moves 2/10 of a cell per timestep. Before the first cycle at $t = 0$, the computed and analytic solutions are identical. As time progresses the computed solutions, indicated as data points, disperse and decay. The top two panels were computed using the common first-order scheme called one-sided or donor-cell differencing. The diffusion is so large that dispersive effects are completely overshadowed. The initially sharp edges of the density profile, which should propagate as sharp edges, smooth out rapidly until by cycle 800 roughly half the material has numerically diffused out of the square wave. This has occurred even though the square wave is quite large and well resolved. In many three-dimensional calculations, a resolution of 20×20×20 is all that can be afforded. Thus the effect of numerical diffusion is even less severe in the top two panels of Fig. III.5 than in some practical multi-dimensional donor-cell calculations.

The second and third set of panels show two square wave calculations performed using the Lax-Wendroff [7] and Leapfrog [8] algorithms respectively. In these cases the numerical diffusion is second-order, whereas it was first order in $\frac{v\delta t}{\delta x}$ in the donor cell calculation of the top panel. Thus the amplitude errors resulting from numerical diffusion are less severe than dispersion errors when the diffusion is second order in $\frac{v\delta t}{\delta x}$. The characteristic ripples are seen near the top and bottom of discontinuities. Initially they appear at the shortest wavelength and look like Gibb's errors. Since the diffusion is most effective on short wavelengths, the scale of the apparent dispersion becomes longer. In both second-order algorithms, much less of the

material originally in the square wave at $t = 0$ has diffused out at $t = 160$ than was the case using the first order algorithm. Nevertheless, the pronounced undershoots and overshoots pose problems for coupled reactive flow simulations and these problems are as serious as those caused by excess numerical diffusion.

The last two panels show a solution of the same square-wave problem using one of the Flux-Corrected Transport (FCT) algorithms [9]. Flux-Corrected Transport is a nonlinear algorithm which combines strong low-order smoothing to remove Gibbs oscillations with much weaker second-order smoothing needed for numerical stability of the explicit integrations. This FCT approach is the forerunner of a new family of methods called "monotonic" or "monotone" algorithms [9,10,11]. More specific and detailed discussions of monotone algorithms and fully Lagrangian methods which are relatively non-diffusive are given in Section V.

Table III.1
Types of Terms in the Conservation Equations

$\frac{\partial A}{\partial t} = \gamma A + B$	Source, Sink, Coupling, Chemical Kinetics
$\frac{\partial A}{\partial t} = \nu \frac{\partial^2 A}{\partial x^2}$	Diffusion and Dissapative Effects
$\frac{\partial^2 A}{\partial t^2} = \mathrm{v}_w^2 \frac{\partial^2 A}{\partial x^2}$	Wave-Like Equations
$\frac{\partial A}{\partial t} = \frac{\partial A \mathrm{v}}{\partial x}$	Convective and Continuity Equations

IV. CHEMICAL KINETICS CALCULATIONS

The coupled, non-linear, ordinary differential equations which describe the chemical interactions are taken from that part of Eq. (II.2), which represent the production and loss of reacting species:

$$\frac{dn_j}{dt} = Q_j - L_j n_j, \quad j = 1, \ldots, M, \tag{IV.1}$$

where M is the total number of species present. The functional dependences of the terms

$$\begin{aligned} Q_j &= Q_j(\{n_k(t)\}) \\ L_j &= L_j(\{n_k(t)\}), \end{aligned} \tag{IV.2}$$

emphasize the strong coupling between the various species. In general Eq. (IV.1) is composed of a sum of terms which have the form for Q_j,

$$q_1[n_k], \; q_2[n_k][n_l], \text{ or } q_3[n_k][n_l][n_m],$$

and for L_j

$$-l_1[n_j], \; l_2[n_j][n_k], \text{ or } l_3[n_j][n_k][n_l],$$

where the q's and l's are chemical rate constants, their subscripts refer to unimolecular, bimolecular, and termolecular reactions, and the subscripts j, k, l, and m represent species. A substantial amount of information about reactive systems can be obtained from the solution of these equations alone. We know, for example, that models of carefully controlled shock tube and vertical tube reactor experiments need not include any diffusive transport or convective effects to yield excellent approximations of reality. These types of experiments and the calculations which describe them provide an excellent way to study complicated chemical kinetic reaction schemes.

The solution of the chemical kinetics equations in a detailed model is usually the most expensive part of a reactive flow problem. In typical flame or detonation calculations, solution

of the chemistry equations may take an order of magnitude longer than the solution of the convective or diffusive transport terms. The computational cost increases further with the number of species and the dimensionality of the problem. The cost also depends strongly on the form of the temperature dependence of the chemical reaction rates which comprise $\{Q_j\}$ and $\{L_j\}$. If these forms are exponential and involve fractional powers, they are expensive to evaluate numerically. In all cases we require efficient, accurate algorithms to solve Eq. (IV.1).

Some of the numerical methods which have been developed to solve Eq. (IV.1) are briefly described in this section. Next several examples of detailed models for specific experiments as well as the results of several independent comparative modelling studies are given. Later in this paper, in Sections VIII and IX, we show examples of how the information in these equations is used in the solution of the full set of coupled Eqs. (II.1)-(II.12).

IV.A. Solution of Ordinary Differential Equations

Equation (IV.1) is a complicated form of Eq. (III.1). The equation may be stiff when it is used to represent chemical kinetic systems when there are large differences in the time constants associated with different chemical reactions. Stiffness may occur for different species, in different locations, at different times or simultaneously throughout the course of an integration. Regardless of how complex the system, the equations to be solved describe species number densities which are always positive and usually tend to relax to a stable equilibrium. There are also a number of physical conservation conditions which are maintained, such as the total number of all of the atoms or of a specific type of atom in the system.

Classical methods for solving ordinary differential equations range from the simplest Euler method to the fairly complex multi-step predictor-corrector Adams-Moulton methods. Many excellent reviews [e.g., see 12, 13] have been written on these so the details of the heirachy of successively more sophisticated methods will not be discussed here. All of these methods conserve mass to the limits of numerical roundoff errors. However, they are not stable for arbi-

trary step sizes and thus do not handle stiff equations adequately. Methods are required which can account for the effects of strong coupling and which are stable.

The Implicit Runge-Kutta [14], Gear [15], and Kregel [16] methods can in principle handle the stiffness problem. The first two methods allow the order of accuracy to be selected; they are conservative; and they are stable for large timesteps. However, they all have several major computational drawbacks. First, they are global implicit methods of the type described in more detail in Section VII. Solving them requires the inversion of matrices incorporating elements of the Jacobian, which can be a costly operation when many species are involved. Second, such higher-order solutions require storage of information from a previous timestep. This may produce data storage problems. These two problems complicate the use of these sophisticated high-order methods when they are used in reactive flow problems. For the solution of Eq. (IV.1) alone, however, they are often excellent.

Throughout the previous discussion, we have mentioned several criteria that are desirable in a integration method for ordinary differential equations. To summarize, the method must be efficient, accurate, conservative, stable and not require storage of large quantities of data from one time-step to another. Several hybrid techniques [e.g., 17,18] have been developed to attempt to reconcile these often conflicting demands.

As an example of such a hybrid technique, we consider the selected asymptotic integration method [17], which determines which equations satisfy an appropriately chosen stiffness criterion. The non-stiff equations are solved by an explicit Euler method, while a very stable asymptotic method is applied to the stiff equations. In a simplified form, the solution of Eqs. IV.1 may be written for normal equations as

$$n(t+\delta t) = n(t) + \delta t\left[Q(t) - \frac{n(t)}{\tau(t)}\right], \tag{IV.5}$$

and for stiff equations as

$$\frac{n(t+\delta t) - n(t)}{\delta t} = \frac{Q(t) + Q(t+\delta t)}{2} - \frac{n(t) + n(t+\delta t)}{\tau(t) + \tau(t+\delta t)}, \tag{IV.6}$$

where $n(t + \delta t)$ is solved for explicitly and where

$$\tau = \frac{1}{L}. \tag{IV.7}$$

Figure (IV.1) shows qualitatively the types of phase errors which this type of solution can introduce. As described in Section III, an asymptotic method may actually be more accurate for larger timesteps. Thus the timestep must be carefully monitored to insure accuracy, convergence, and adequate conservation.

The selected asymptotic integration method has been described because it is particularly effective in reactive flow problems. The overhead is low both because it is self-starting and because it does not require any matrix inversion. Species densities at only one time level are needed. Accuracy may be controlled by predetermined convergence parameters which control the stiffness criterion, the timestep, and thus effectively the degree of conservation. The method is stable even for large timesteps and it is easily vectorized for use in parallel processing computers.

Another equation which often has to be solved in conjunction with Eq. (IV.1) is that for the time rate of temperature change due to the chemical energy released. The internal energy, ϵ, of a system of molecular species at combustion temperatures cannot be related simply to the temperature by a formula such as

$$\epsilon = \frac{f}{2} kT, \tag{IV.9}$$

where f is the number of degrees of freedom. Instead we need to use Eq. (II.8),

$$\epsilon = H(T, \{n_j\}) - P, \tag{II.8}$$

where H is the enthalpy of the system. Knowing the form of the enthalpy, we can find an expression for $\partial T/\partial t$. Since the expression for the temperature derivative involves all of the $\partial n_j/\partial t$ as well as expressions of the form $\partial h_i/\partial t$ which may be expressed as powers of T, solving for T may be very expensive computationally.

As is clear from Eq. (II.8) as written above, the enthalpy may also involve complicated sums over excited states of the molecule. However, when each of the species is in local thermodynamic equilibrium, the individual $h_j(T)$ can be evaluated as a function of temperature and fit to a polynomical expansion. This has been done by many researchers for the data in the JANAF tables [19] and by Gordon and McBride [20].

By using such tabulated values of $h_j(T)$ and h_{oj}, the tedious temperature integration can sometimes be avoided completely. During each chemical timestep the total internal energy of the system does not change but may be redistributed among chemical states. We may then solve Eq. (II.8)′ iteratively for a new temperature which is consistent with the new number densities calculated. After each chemical timestep, the internal energy, ϵ, is updated by a formula of the type

$$\epsilon(t + \Delta t) = \epsilon(t) + \sum_j (n_j(t + \Delta t) - n_j(t))\, h_{oj}(T). \tag{IV.7}$$

A simple Newton-Raphson iteration technique is adequate. When incorporated in integration programs, it converges in one or two iterations per timestep.

Thus far we have concentrated on the problems which arise when solving ordinary differential equations and we have listed a number of techniques and algorithms to help avoid them. In the remainder of this section we will give a number of examples of their application to real physical systems.

IV.B. Examples of Chemical Kinetics Calculations

The solution to Eq. (IV.1) models the time evolution of species densities in a homogeneous, premixed system. It is an idealized equation, and may be solved with some subset of the restrictions: constant temperature, constant pressure, and constant volume. From the primary quantities, the set $\{n_j(t)\}$, a number of quantities can be derived which may be compared directly with data. These include chemical induction times, emission intensities from excited states of reacting species, and bulk quantities such as overall activation energy and total energy

release. The solution of Eq (IV.1) can also be subjected to analyses which estimate, for a given temperature and pressure, which reactions may be eliminated from the overall scheme or which must be measured much more carefully.

IV.B.1. Shock Tube Experiments

Shock tube studies of chemically reacting systems are perhaps the most commonly used experiments to which Eq. (IV.1) can be applied without incorporating the added complication of coupled hydrodynamics. Figure IV.2 is a schematic which shows the idealized incident and reflected shock waves which would be calculated from the Rankine-Hugoniot equations for the bursting diaphragm problem. The fluid elements in the shock-heated regions Δx_i and Δx_r have been at the elevated temperatures T_i and T_r for times between 0 and τ_i and 0 and τ_r, respectively. Thus, for example, each fluid element starting from just behind the shock front has been at T_i for a successively longer time. In this sense the x coordinate can be considered as a time coordinate and by measuring species concentrations along Δx_i, the time evolution of $\{n_j\}$ is also measured.

There are, however, a number of physical effects which alter the ideal picture. First, Fig. IV.2 is a reasonable approximation as long as boundary layer or damping effects are negligible and thus do not disturb the shocked region. Also, the reacting gas must be dilute enough so that no significant amount of the chemical energy released is fed back into the hydrodynamic flow. It is further assumed that the effects of any initial transients due to the diaphragm bursting contribute a negligible amount of energy to the system and will not significantly affect the chemistry to be studied.

As an example of chemical modeling applied to shock tube measurements, we mention the work of Olson and Gardner [21]. Using data from a set of shock tube experiments on methane oxidation, they were able to test eight different proposed mechanisms for methane combustion. The tests ran over a fairly wide range of temperatures (1600-2500 K), pressures

(0.15 to 10 atm), and stoichiometries. Their conclusion, that C_2H_6 and C_2 hydrocarbon radicals were a necessary component of the model, was a direct result of the series of simulations that they performed. Similar work for methane-ethane mixtures has been done by Westbrook [22] to study explosivity of vapors from liquid natural gas mixtures.

Recent work of Tabayashi and Bauer [23] used a combination of incident shock wave measurements and numerical modelling to study the initiation mechanisms in methane combustion. They were able to relate the spatial gradient of the total density, $d\rho/dx$, in the region Δx_i of Fig. IV.2 to the energy release due to the reactions. This expression involved species densities directly as well as terms such as dn_j/dt in Eq. (IV.1). By combining this relation with a postulated chemical mechanism, they used the model to study the importance of selected chemical rates. Model calculations of $d\rho/dx$ were then compared to experimental results.

As a final example of the use of chemical kinetics calculation to model shock tube measurements, we cite the recent work of Shaub and Lin [24]. This study used the methodology developed by Shaub and Bauer [25] for deducing chemical reaction rate schemes which give the approximate bulk properties of systems not yet quantitatively characterized by experiments. The method involves writing out all possible combinations of chemical reactions among an allowed number of species. Then most of them are judiciously excluded, and for those remaining, reaction rates are estimated. Species densities and ignition delay times were calculated using the model they developed for diborane oxidation and compared to experiments. Without resorting to ad hoc parameter adjustment, Shaub and Bauer obtained excellent agreement with experimental data. Thus even though the kinetics scheme they used is extremely complicated and admittedly a first compilation, Shaub and Lin were able to model correctly the overall energy release as a function of time. Although their approach might serve as a useful guide in the absence of avalable experimental diagnostics, the method certainly needs more work to test its generality.

IV.B.2. Vertical Tube Reactor

In the vertical tube reactor [26], thoroughly mixed reactants at room temperature enter a tube from the bottom and are driven upwards at velocities of about 5-10 cm/sec. Heating the tube from the walls increases the gas temprature. In the simplest mode of operation, a steady state flame is established in which the flow velocity is balanced by the flame speed. The use of a temperature feedback control allows the location of the flame to be stablized to $\pm .5$ mm for many hours. In addition, these low temperature flames release very little heat so that the resulting gradients in temperature and pressure are extremely small. Thus, kinetic models of the combustion which ignore the fluid dynamic or diffusive transport terms are an excellent approximation.

The vertical tube reactor has been used primarily to study the low temperature oxidation of hydrocarbons [26,27]. One such study was the search for the source of chemiluminescent formaldehyde which occurs in the oxidation of di-tert-butyl peroxide (DTBP) [28]. A reaction mechanism has been proposed for DTBP oxidation and it has been tested by comparing model calculations of the product distributions to gas chromatography and mass spectrometer measurements. There are two types of reactions which may be responsible for the excited formaldehyde state, H_2CO^*, either the reaction of two methyl peroxy rad cals

$$CH_3O_2 + CH_3O_2 \rightarrow CH_2OH + H_2CO^* + O_2,$$

or hydrogen abstraction from a methoxy radical by another radical,

$$CH_3O + CH_3O \rightarrow CH_3OH + H_2CO^*$$
$$CH_3O + OH \rightarrow H_2CO^* + H_2O$$
$$CH_3O + CH_3 \rightarrow H_2CO^* + CH_4.$$

These reactions, which involve either methyl peroxy (CH_3O_2) or methoxy (CH_3O) radicals, would result in increased luminosity if the amounts of these radicals were increased. Modeling of the time-dependent chemical kinetics reaction mechanism using sets of equations such as Eq. (IV.1) has determined how much radical forming dopant must be added and where to add it.

Experiments based on these designs have been successfully carried out and showed that methoxy radical abstraction reactions were *not* the source of excited formaldehyde.

In this section we have briefly mentioned just a few of the modelling studies from the vast literature of those performed using a set of equations such as Eq. (IV.1). These studies have shown that extremely valuable kinetic information about the overall consistency of complicated reaction schemes may be derived. By using these studies in conjunction with experimental data, we can test the validity of a proposed mechanism and determine which reaction rates and chemical species must be included. Deficiencies in kinetic models may become obvious when the rate scheme is either tested against independent sets of data or is applied in new regimes of pressure or temperature. In Section IX we describe several attempts to use combined chemical and hydrodynamic models to test the reaction rate scheme.

V. GENERAL HYDRODYNAMIC CONSIDERATIONS

This section discusses some of the basic physical and numerical considerations which arise when dealing with the disparate time and space scales in reactive flow hydrodynamics. The Lagrangian and Eulerian approaches for solving the continuity equation are discussed, and we will show that neither approach is a panacea. Next we describe the fundamental differences between numerical methods used to study supersonic and subsonic flows. The discussion of general hydrodynamic considerations closes with an analysis of techniques for dealing with geometric complexity. Multi-dimensional generalizations in both Eulerian and Lagrangian formulations are described briefly.

V.A. The Eulerian and Lagrangian Approaches

Equation (II.1) expresses the conservation of mass of a system. It may also be written as

$$\frac{\partial \rho}{\partial t} + \underline{v} \cdot \underline{\nabla} \rho = -\rho \underline{\nabla} \cdot \underline{v} \tag{V.1}$$

where $\underline{v} \cdot \underline{\nabla} \rho$ and $\rho \underline{\nabla} \cdot \underline{v}$ represent convection and compression, respectively. The time derivative $\partial \rho / \partial t$ is the Eulerian derivative: it represents the time rate of change of density in a fixed volume of space. We may also write Eq. (V.1) as

$$\frac{d\rho}{dt} \equiv \frac{\partial \rho}{\partial t} + \underline{v} \cdot \underline{\nabla} \rho = -\rho \underline{\nabla} \cdot \underline{v}, \tag{V.2}$$

where the term $d\rho/dt$ is the Lagrangian derivative. Eq. (V.2) expresses the local density change in an element of fluid moving with the flow. Thus in an Eulerian finite difference scheme, the spatial grid points are kept fixed and the fluid moves across them. In a Lagrangian scheme, the grid points are allowed to move with the fluid.

V.A.1 The Eulerian Approach — Dealing with Numerical Diffusion

Accurate resolution of steep gradients is extremely important. Because flame speeds depend on steep species gradients, so do the local energy release rates. Unless Eulerian calcula-

tions have very finely resolved meshes, the continual motion of fluid through an Eulerian grid ensures that there is a substantial amount of numerical diffusion. The numerical diffusion arises as a consequence of the requirements imposed by the numerical methods which keep the solutions both stable and positive.

Figure V.1 shows qualitatively how numerical diffusion arises in the simplest Eulerian convection algorithm, the first order "unwind" or "donor cell" algorithm. The correct advection (dashed line) of a species interface initially at $x = 0$ at time $t = 0$ is compared to that given by the donor cell algorithm (solid profile) for three timesteps of duration δt. The uniform velocity from the left, v, the timestep, δt, and the spatial step, δx, have been chosen in this example such that $v\delta t/\delta x = 1/3$. This means that the correct species discontinuity from $\rho = \rho_o$ to $\rho = 0$ moves from left to right at one third of a cell per timestep.

The numerical solution is found from the simple finite difference formula

$$\rho_i^{n+1} = \rho_i^n - \frac{v\delta t}{\delta x}(\rho_i^n - \rho_{i-1}^n), \tag{V.3}$$

where the superscript n refers to the timestep number and, as throughout this section, the subscript i refers to the cell number. When the velocity is negative, the formula is biased from the right, or "upwind", side,

$$\rho_i^{n+1} = \rho_i^n - \frac{v\delta t}{\delta x}(\rho_{i+1}^n - \rho_i^n). \tag{V.3'}$$

In either case, as long as $|v\delta t/\delta x| \leqslant 1$ in each cell, the new density values $\{\rho_i^{n+1}\}$ at $t = (n + 1)\delta t$ are all positive as long as the density values at time $t = n\delta t$, i.e. the $\{\rho_i^n\}$, are all positive. The price for this guaranteed positivity is the rather severe unphysical spreading of the density discontinuity which should be located at $x = vt$. As we will see, this unphysical spreading is quite rightly called "numerical diffusion" because the added term needed to stabilize and keep positive the numerical solutions appears in the form of a three-point finite-difference diffusion operator.

V.A.2 An Analysis of Numerical Diffusion: Positivity and Stability

From the moving fluid frame of reference in the example of Fig. V.1, the crumbling away of the sharp discontinuity looks like the physical process of diffusion. However, it arises from a purely numerical source. This numerical diffusion occurs because material, which has just entered a cell and is still near one boundary, is smeared over the whole cell. In any attempt to reduce this diffusion, higher-order approximations to the convective derivatives are required.

Consider the usual three point explicit finite difference formula for advancing $\{\rho_i^n\}$ one timestep to $\{\rho_i^{n+1}\}$,

$$\rho_i^{n+1} = a_i \rho_{i-1}^n + b_i \rho_i^n + c_i \rho_{i+1}^n. \tag{V.4}$$

This general form certainly contains the contribution from Eqs. (V.3) and (V.3') above and will also allow us to investigate second-order accurate algorithms with reduced numerical diffusion. As before, let δx be constant from cell to cell and let δt be constant also. Then Eq. (V.4) can be rewritten in conservation form as

$$\begin{aligned}\rho_i^{n+1} = \rho_i^n - \frac{1}{2}[&\epsilon_{i+1/2}(\rho_{i+1}^n + \rho_i^n) - \epsilon_{i-1/2}(\rho_i^n + \rho_{i-1}^n)] \\ &+ [\nu_{i+1/2}\,(\rho_{i+1}^n - \rho_i^n) - \nu_{i-1/2}\,(\rho_i^n - \rho_{i-1}^n)],\end{aligned} \tag{V.5}$$

where here the parameters ϵ and ν will be defined below. When mass conservation is required of Eq. (V.4) to constrain the coefficients $\{a_i\}$, $\{b_i\}$, $\{c_i\}$, we obtain

$$a_{i+1} + b_i + c_{i-1} = 1. \tag{V.6}$$

Positivity of $\{\rho_i^{n+1}\}$ for all possible sequences $\{\rho_i^n\}$ requires that $\{a_i\}$, $\{b_i\}$, $\{c_i\}$ be non-negative for all i.

Identifying terms between Eqs. (V.4) and (V.5) gives the relations

$$\begin{aligned} a_i &\equiv \nu_{i-1/2} + \frac{1}{2}\epsilon_{i-1/2}, \\ b_i &\equiv 1 - \frac{1}{2}\epsilon_{i+1/2} + \frac{1}{2}\epsilon_{i-1/2} - \nu_{i+1/2} - \nu_{i-1/2}, \\ c_i &\equiv \nu_{i+1/2} - \frac{1}{2}\epsilon_{i+1/2}, \end{aligned} \tag{V.7}$$

where $\{\epsilon_{i+1/2} \equiv v_{i+1/2}\delta t/\delta x\}$ and $\{\nu_{i+1/2}\}$ are non-dimensional coefficients of the density average and density difference terms and appear as a natural consequence of considering only adjacent grid points. If the $\{\nu_{i+1/2}\}$ are all positive and sufficiently large, they can ensure that the $\{\rho_i^{n+1}\}$ are positive. The positivity condition derived from Eq. (V.7) is then

$$\nu_{i+1/2} \geqslant \frac{1}{2}\,|\epsilon_{i+1/2}|, \text{ for all } i. \tag{V.8}$$

Thus we see that the condition in Eq. (V.8) for linear positivity in Eulerian convection leads to the strong "numerical diffusion"

$$\rho_i^{n+1} = \rho_i^n + \nu_{i+1/2}\,(\rho_{i+1}^n - \rho_i^n) - \nu_{i-1/2}\,(\rho_i^n - \rho_{i-1}^n) \tag{V.9}$$

where $\nu_{i+1/2} \geqslant \frac{1}{2}\,|\epsilon_{i+1/2}|$. This is first order numerical diffusion and rapidly smears the initially sharp discontinuity. If algorithms are used which have $\nu_{i+1/2} < \frac{1}{2}\,|\epsilon_{i+1/2}|$, positivity is not necessarily destroyed but can no longer be guaranteed. In practice the positivity condition is almost always violated by strong shocks and discontinuities unless the inequality stated in Eq. (V.8) holds. Nevertheless, the numerical diffusion implied by Eq. (V.8) is unacceptable, so some remedy must be sought.

Finite difference schemes which are higher than first order sacrifice assured positivity to reduce the numerical diffusion. The diffusion cannot be zero, however, because the explicit three-point formula, Eq. (V.5), has a numerical stability problem. Rather than using the discontinuity analysis of Fig. V.1, stability is better analyzed by studying test functions of the form

$$\rho_i^n \equiv \rho^n e^{\underline{i}i\beta}, \tag{V.10}$$

where $\beta \equiv k\delta x = 2\pi\delta x/\lambda$ and $\underline{i}$ indicates $\sqrt{-1}$. Substituting this solution into Eq. (V.5), with the fluid velocity taken constant everywhere, gives

$$\rho_0^{n+1} = \rho_0^n\,[1 - 2\nu(1 - \cos\beta) - \underline{i}\epsilon\,\sin\beta], \tag{V.11}$$

where we assume $\{\nu_{i+1/2}\} = \nu$ and $\{\epsilon_{i+1/2}\} = \epsilon$. Since the exact soluton to this linear problem is $\rho_o^{n+1}\Big|_{exact} = \rho_o^n e^{-ik\nu\delta t}$, the difference between this simple result and Eq. (V.11) constitutes the numerical error generated each timestep.

If $|\rho_o^{n+1}/\rho_o^n| \equiv A$, the amplification factor of the finite difference algorithm, linear stability is always assured provided $|A|^2 \leqslant 1$. From Eq. (V.11),

$$|A|^2 = 1 - (4\nu - 2\epsilon^2)(1 - \cos\beta) + (4\nu^2 - \epsilon^2)(1 - \cos\beta)^2, \tag{V.12}$$

which must be less than unity for all permissible values of β between 0 and π. In general, then, $\nu > \frac{1}{2}\epsilon^2$ ensures stability of the linear convection algorithm for any Fourier harmonic of the disturbance provided that δt is chosen so that $|\epsilon| \leqslant 1$. When $\nu > 1/2$, it is also easy to see that there are combinations of ϵ and β where $|A|^2$ exceeds unity (for example, $\epsilon = 0$ with $\beta = \pi$ ensures $|A|^2 > 1$). Thus the range of acceptable diffusion coefficients is quite closely prescribed:

$$\frac{1}{2} \geqslant \nu \geqslant \frac{1}{2}|\epsilon| \geqslant \frac{1}{2}\epsilon^2, \tag{V.13}$$

with the additional constraint $|\epsilon| \leqslant 1$ as noted above.

Even the minimal numerical diffusion required for linear stability, $\nu = \frac{1}{2}\epsilon^2$, may be quite substantial when compared to the physically correct diffusion effects such as thermal conduction, molecular diffusion, or viscosity. Figure V.2 shows the first few timesteps from the same test problem as Fig. V.1, but using $\nu = \frac{1}{2}\epsilon^2$ rather than the $\nu = \frac{1}{2}\epsilon$ required for positivity. The spreading of the profile is only 1/3 as great in this marginally stabilized case as in the previous case where positivity is assured, but a numerical precursor still reaches a full two cells beyond the correct discontinuity location. Furthermore, the overshoot between $x = -\delta x$ and $x = 0$ observed in Fig. V.2 is a natural consequence of underdamping the solution. This loss of monotonicity is equivalent to violation of positivity. When the convection algorithm is stable but not positive, the numerical diffusion is not large enough to mask either numerical

dispersion errors or the Gibbs phenomenon discussed in Section III.

The requirements for positivity and accuracy would then seem to be mutually exclusive from the arguments given above. The Flux Corrected Transport (FCT) algorithms [6,9] and other nonlinear monotone techniques were invented to circumvent this dilemma by using the more accurate $\frac{1}{2}\epsilon^2$ limit where monotonicity (i.e., positivity) is not threatened and by using the stronger $\frac{1}{2}|\epsilon|$ diffusion when it is required to assure monotonicity of the solution. Thus these monotonic algorithms have opened up a new approach to calculating convection accurately.

To prevent negative density values which could arise intermittantly from Gibbs errors, a minimum amount of dissipation must be added to the convection to assure positivity as well as stability at each individual timestep. We write this minimal dissipation as

$$\nu \approx \frac{|\epsilon|}{2}(c + |\epsilon|), \tag{V.14}$$

where here c is a "clipping" factor, $0 \leqslant c \leqslant 1$, describing how much and how often an extra amount of diffusion, an amount over the stability limit, must be added to ensure positivity. In the vicinity of shocks, $c \approx 1$, and in smooth monotonic regions away from local maxima and minima, $c \approx 0$.

The least damped flow which a simple Eulerian scheme can propagate can be expressed in terms of a flow Reynolds number calculated as if the unavoidable numerical diffusion were actually physical viscosity. Substituting Eq. (V.14) into Eq. (V.12) gives

$$\begin{aligned} |\mathscr{A}|^2 &\approx 1 - 2|\epsilon|c\,(1 - \cos\beta) + \epsilon^2[(c+\epsilon)^2 - 1](1 - \cos\beta)^2 \\ &\approx [1 - |\epsilon|c\,(1 - \cos\beta)]^2. \end{aligned} \tag{V.15}$$

The amplification factor, $\mathscr{A}$, can also be identified with the exponential damping rate of the numerically computed solution,

$$\mathscr{A} \approx e^{-\gamma\delta t} \approx 1 - \gamma\delta t. \tag{V.16}$$

From Eq. (V.16) and Eq. (V.15), we can make the identification

$$\gamma\delta t \approx |\epsilon| c(1-\cos\beta) \approx \frac{|\epsilon|}{2} c\, k^2 \delta x^2. \tag{V.17}$$

Here the characteristic length scale of the disturbance is designated by $L \equiv 1/k$. The Reynolds number, $R_e \equiv \frac{Lv}{\nu}$, is the ratio of a dissipation time for structures of size L relative to the convection time across a distance L. Letting R_{end} be the effective dissipation Reynolds number due to numerical diffusion, we have

$$R_{end} \approx \frac{1/\gamma}{L/v} \approx \frac{2L}{c\delta x}. \tag{V.18}$$

which is seen to be independent of the timestep.

Equation (V.18) gives the so called "cell Reynolds number" for an Eulerian flow computation. It is roughly $2/c$ times the number of computational cells within a structure of characteristic size L. Thus one sees immediately that the full linear positivity condition ($c = 1$) is the source of the misconception that the highest Reynold's number flow which can be calculated by an Eulerian method is roughly twice the number of cells across the system. To provide the incompressible flow equivalent of positivity everywhere, even the most accurate spectral simulations use a "real" viscosity chosen to guarantee positivity numerically. Clearly the monotonic schemes, such as FCT, which vary c locally and nonlinearly from cell to cell to maintain positivity, require less overall dissipation and hence are potentially more accurate for simulating high Reynolds number flows. If the average value of the clipping factor c is 1/10, the cell Reynolds number is 2×10^3 on a finite-difference representation of a physical system with 100 cells in each direction. In fact, the clipping factor generally decreases in time as short wavelength structures are smoothed out until a balance is reached between the physical generation and the numerical destruction of short wavelengths due to the nonlinear flux-correction process.

When short wavelength components of a profile are not dominant, the long wavelengths can be calculated much less dissipatively than is implied by the usual $R_{end} \approx 2L/\delta x$ limit. In

these cases positivity is not a major problem and small values of the clipping factor suffice. When short wavelengths are present at large amplitude, the local application of nonlinear monotonicity algorithms still allows the longer wavelengths to proceed at higher Reynolds number. Then strong smoothing is only applied in a small region and hence is applied preferentially to short wavelengths.

Clearly two concepts of cell Reynolds number are needed, one related to resolution and one related to algorithm damping a long wavelength. When short wavelength structures are absent or can be neglected, the longer, slowly decaying wavelengths can be calculated accurately in much higher Reynolds number flows than the usual numerical cell Reynolds number limitation suggests. Short wavelength structures still exist in the calculation for a finite length of time, but they are not excited. When the flow continually generates many dominant short wavelength structures, the clipping factor c may approach unity. Then the two different numerical Reynolds numbers approach the low value usually quoted.

V.A.3 The Lagrangian Approach

The most appealing properties of Lagrangian methods arise because the convective derivative no longer appears explicitly in the problem and the calculation is done in the frame of reference of the moving fluid. Since each Lagrangian cell moves along with the fluid, it does not trade material with neighboring cells due to convection. Thus the mass in each cell is fixed, and the density in each cell varies inversely as the cell volume. In the absence of molecular diffusion, the total mass of molecules of each species also remains fixed in the Lagrangian cell. Thus species penetration at reactive interfaces is free of numerical diffusion. Lagrangian calculations are able to sustain high Reynolds number flows for long times relative to their Eulerian counterparts and they make the treatment of interfaces, free surfaces, and moving boundaries more natural. Why, then, use Eulerian methods at all?

Lagrangian methods do have some extremely severe problems. The foremost problem

occurs in multi-dimensional calculations when the convection of the grid with the flow leads to large grid deformations and a corresponding decrease in numerical accuracy. Regridding and remapping techniques introduce numerical diffusion into the problem just as if a simpler Eulerian calculation were performed initially. Methods have been proposed by, for example, Noh [29], Chan [30], and Lund [31] who suggest combinations of Eulerian and Langrangian calculations to reduce the numerical diffusion associated with regridding. However, any relocation of grid points necessarily re-introduces numerical diffusion through interpolation.

A second problem arises because a high order of accuracy, particularly of spatial derivative terms, is difficult to achieve in Lagrangian calculations. When the computational grid moves, uniform spacing is not generally possible. To construct high order derivatives in a time varying, nonuniform mesh is difficult and first order algorithms are hard to avoid. One problem, maintaining positivity, is replaced by another: the introduction of first order aspects into the calculation.

The third problem is that Lagrangian representations of a compressible fluid still have unavoidable Eulerian features [5]. Consider a simplified form of Eq. (II.3), the energy conservation equation,

$$\frac{\partial E}{\partial t} = -\underline{\nabla} \cdot E\underline{v} - \underline{\nabla} \cdot P\underline{v} \tag{V.19}$$

where

$$E = \frac{P}{\gamma - 1} + \frac{1}{2}\rho v^2. \tag{V.20}$$

Then if we define a new velocity

$$\underline{v}^* = \frac{(E + P)}{E}\,\underline{v}, \tag{V.21}$$

which is always parallel to $\underline{v}$, Eq. (V.3) can be written in the form

$$\frac{\partial E}{\partial t} = -\underline{\nabla} \cdot E\,\underline{v}^* \tag{V.22}$$

which is identical in form to Eq. (II.1). However, $\underline{v} \neq \underline{v}^*$. A grid moving at velocity $\underline{v}$ is Lagrangian for mass but not energy, and a grid moving at $\underline{v}^*$ is Lagrangian for energy but not mass. Since we are often required to solve the full set of equations simultaneously, as in shock or detonation problems, we cannot always avoid the Eulerian aspects of the problem. Thus we are effectively forced to solve many complicated flow problems on an Eulerian grid whether we want to or not.

In addition, Lagrangian calculations in multi-dimensions are very complicated and can be much more expensive per grid point than Eulerian computations. Another problem is that inexpensive direct solution algorithms of elliptic equations cannot be applied. Finally, adaptive gridding is just as important in Lagrangian simulations of flame propagation as it is in Eulerian calculations and is more difficult to implement. We return to these gridding difficulties below in Section V.C. Thus we must debate these various advantages and disadvantages for a particular problem before we choose whether to use an Eulerian or Lagrangian method.

V.B. Calculation of Supersonic and Subsonic Flows

Modelling combustion systems requires the description of flows which are subsonic, such as flames, and flows which are supersonic, such as shocks and detonations. In the best of all possible worlds, we would be able to handle both regimes of flow coupled to chemical reactions and transport effects with one all-inclusive algorithm. Much work has gone into generating such algorithms [32,33] in multi-dimensions as well as one dimension, but a price is paid for the generality. In order to handle implicit sound waves, the problem is usually cast into pressure equation form where a non-physical numerical viscosity is added to stabilize shocks. Improper or fluctuating jump conditions result when shock thicknesses are restricted numerically to a couple of cells. Thus poor resolution and unnecessarily thick shock fronts result in the tradeoff for being able to take long timesteps when the flow is slow and shocks are absent. In addition, implicit algorithms by themselves can transmit non-physical pressure pulses ahead

of the shock with infinite speed.

Conversely, numerical artifices for dealing with nonlinear flows (shocks) degrade the algorithm's performance on slower flows. When the flow velocity is small compared to the speed of sound, the excess numerical damping, which stabilizes nonlinear effects in implicit solutions of the fluid equations, usually appears as a rapid damping of oscillatory sound waves and other local flows. The remnants of the complicated high-velocity flows of supersonic situations appear in subsonic calculations as unnecessary numerical damping. Thus we will describe ways to handle the subsonic and supersonic limits separately. The methods are somewhat limited in generality, but offer advantages in accuracy, speed, and simplicity over the existing global or composite implicit algorithms.

V.B.1. Supersonic Flows

Let us first consider supersonic flows. Finite difference calculations of the energy flow associated with shocks suffer from the effects of numerical diffusion because it is not possible to represent exactly structures such as discontinuities which are thinner than a cell. Since the flow is at or above the sound speed, the Courant condition, $c_s \delta t/\delta x \leqslant 1$, places a restriction on the relation between the computational timestep, δt, and the grid spacing, δx. This condition is about equal to limiting the flow speed to one cell per timestep. Thus there is no obvious benefit from a Lagrangian formulation in the vicinity of a shock. There is also no obvious advantage gained by using an implicit algorithm of the type described above or in Section V.B2 below unless approach to a steady state solution is desired.

There are a number of specialized techniques for performing transient one-dimensional calculations which include gas dynamic shocks. The stardard test for these techniques is the nonlinear Riemann problem, in which one is concerned with the evolution of a simple, arbitrary fluid discontinuity. For example, the discontinuity might be in the pressure, a situation which occurs in the standard shock diaphragm problem discussed in Sections IV and VIII. In

the method of characteristics and in several finite difference methods including Godunov's widely used generalization [34] of donor cell differencing, a Riemann problem is solved cell by cell or region by region in the flow. Integration is performed by analytically extrapolating the flow forward in time.

Glimm's method [35,36] and more recent variations [37] attempt to avoid both the diffusion inherent in Eulerian donor-cell algorithms and the potential complexity of following characteristics in multi-dimensions. These methods discretize the location of discontinuities in the flow, but allow the heights of the discontinuities to be accurately retained. This is just the opposite of the more standard procedures in which the locations of characteristics are followed accurately and then approximate heights of the discontinuities are used to interpolate back onto an Eulerian or Lagrangian grid. Such a change of perspective was suggested by numerical diffusion considerations at surfaces such as a contact discontinuity or a reactive species interface. The price paid for precise shocks is an imprecise knowledge of their location. The random or pseudo-random manner in which fluid values are assigned to the spatial grid leads to errors as large as those encountered in the more direct but diffusive formulations. Mass conservation, momentum conservation, and energy conservation integrals cannot be guaranteed, for example. A form of uncertainty principle, as briefly mentioned earlier, seems to be operating where various types of errors can be traded off against each other but not reduced simultaneously. This uncertainty is clearly just a re-expression of the necessarily finite resolution every digital computation suffers.

Both the normal (Godunov) and the inverted Riemann (Glimm) approaches toward numerical solution of gas dynamic shock problems suffer additional disadvantages. In multi-dimensions and in non-Cartesian one-dimensional geometries, the general Riemann solution for assigning and following the system characteristics does not exist. Therefore, a further set of approximations must be made. To convert the general problem back to locally solvable Riemann problems, the entire problem must be timestep split so that

$$\frac{df}{dt} = \frac{df_x^R}{dt} + \frac{df_y^R}{dt} + g(f), \tag{V.23}$$

where df_x^R/dt and df_y^R/dt represent terms contributing to a solvable one-dimensional Riemann problem in the x- and y-directions, respectively. The remaining term, $g(f)$, must contain all effects not representable as local Riemann problems, including those geometric effects which arise even in one-dimensional cylindrical and spherical coordinate systems.

Riemann problems can be expensive to solve numerically, whether in the normal or the inverted form. The general analytic solution of a particular specialized problem is of little use in improving the overall accuracy of an algorithm which must solve much more general problems. Therefore one ought to have a good reason for adopting a technique which is constrained to sets of equations of the rather specific Riemann form. However, it is only human nature to pay careful attention to the parts we can solve analytically, df_x^R/dt and df_y^R/dt, while paying rather little heed to the "correction" term, $g(f)$. Thus, while many methods may be excellent for a specific, one-dimensional Riemann test problem, they cannot be applied with reasonable accuracy to more complicated and realistic flows. To date, Glimm's method is one that seems to fall into this category.

There is another concern over the applicability of techniques based on the nonlinear Riemann solution, and this is the importance of energy conservation in chemically reacting flows. The normal techniques based on the Riemann solution sometimes have trouble guaranteeing the exact conservation of global mass, momentum, or energy integrals, and the inverted Riemann techniques find it impossible. In the latter case, the random fluctuations in the progression of a shock followed by a reaction zone, for example, have the potential for losing or tapping vast reservoirs of nonphysical numerical energy. It has been our experience that numerical errors always congregate and grow in the close vicinity of physical inconsistencies and discontinuities of the numerical techniques.

We have found that exact energy conservation is required in the vicinity of a detonating

shock in order to avoid large errors. Small inaccuracies of 5-10% in the temperature behind the shock can lead to errors of 100-200% in the profiles because chemical induction times are such sensitive functions of temperature (Section VIII). Oscillations in temperature, even if the average value is correct, may give patches in the shocked flow where ignition takes place before any of the surrounding fluid has ignited. A smoothly propagating detonation is thus impossible in a calculational approach which displays oscillations at the top of a shock or the width of the reaction zone.

Flux Corrected Transport techniques were developed to treat problems where extremely sharp shocks must be represented without numerical oscillations appearing just behind the shock. Because the method used to solve the equations is conservative, the discontinuity is accurately represented. Further, because there is no added viscosity, shocks of 1 or 2 cell thickness result. This is the sharpest transition which can propagate smoothly across an Eulerian grid. In practical applications FCT reduces the resolution needed to perform most calculations by about a factor of two or more in each direction when compared to standard donor-cell and Godunov calculations. The ability of FCT algorithms to treat simple shocks and other gas dynamic discontinuities so well arises because positivity, or more generally monotonicity, is maintained individually in each conservation equation.

A number of monotonic convection algorithms have been proposed and tested in recent years which are extensions, adaptations or variations of the basic positivity concepts embodied in FCT. Harten [11] has developed an "artificial compression method" and Van Leer [10] has applied monotonicity to a number of finite difference algorithms including those based on solving a Riemann problem (e.g., [34]). Recently Forester [38] and Zalesak [39] have considered higher order formulations. The excellent shocked-flow properties of the FCT algorithm has led to its use in both one-dimensional reactive flow calculations [40,41] and also in equivalent two- and three-dimensional models [42]. These are discussed in Sections VIII and X.

There are limitations to the applicability of the best energy conserving formulations. All

finite difference algorithms have significant truncation errors, particularly near steep gradients. Since the velocity is driven by the pressure gradient and the pressure is derived from the fluid energy density,

$$P = (\gamma - 1)\left[E - \frac{1}{2}\rho v^2\right], \tag{V.24}$$

the potential for difference-of-large-number errors exists. The energy density $\mathscr{E}$ is determined from one continuity equation, whereas $\frac{1}{2}\rho v^2$ is determined from two others. Inconsistencies in the truncation errors among these three equations are greatly magnified in the pressure when the local fluid kinetic energy density is much larger than the thermal energy density.

In chemically reactive flow calculations, the globally conserved quantity is $E = \epsilon + \frac{1}{2}\rho v^2 + \sum_j n_j h_{oj}$, the total energy density including the chemical energy of formation of each species. The quantity E is generally larger in magnitude than E. Thus difference-of-large-number errors could cause a problem in evaluating P from a conservative, finite difference treatment for the convective integration of E. In practice, we transform the energy equation to solve for E, and then to treat the energy changes due to chemistry in a separate computation based on the changing number densities,

$$\Delta E_i = \sum_j \Delta n_{ji}\, h_{oji}, \tag{V.25}$$

in order to avoid these difference of large number inconsistencies. This problem will occur to a greater or lesser extent in all reactive flow calculations based on strict local energy conservation. Complete consistency between the convection of E, $\mathscr{E}$, and $\{n_j\}$ is not generally possible unless species density positivity is sacrificed or the numerical diffusion is very large.

The importance of choosing the right form of the energy equation to solve is best illustrated by an extreme example. To be strictly correct, the rest mass energy density, $\sum_j n_j m_j C^2$, should be added to $\mathscr{E}$ and E, where C is the speed of light. In this case, normal atmospheric

pressure, $\sim 10^6$ ergs/cc would only appear in the twelfth decimal place and the calculation would lose all accuracy. In the same sense, the term $\sum_j n_j h_{oj}$ does not need to be included when the timestep is very short because the change in temperature is required to be small during a timestep for overall accuracy and each of the species number densities n_j is being convected separately. Typical chemical energies are measured in electron volts, while thermal energies are typically only a tenth to a fortieth as large.

The explicit, energy conserving, reactive flow algorithms can be used effectively for many subsonic problems, but the Courant timestep limitation becomes a burden when the flow is slow enough. Many tests performed with FCT algorithms [6,9] show that sound can propagate stably at about one cell per timestep whereas the flow becomes ragged when the distance travelled per timestep exceeds a half cell. In practice, we always leave a factor of two leeway on the flow rate condition to permit velocity changes during a timestep: the timestep is chosen so the farthest that the fluid travels in any cell is about one quarter of a cell per timestep. Thus flows as slow as Mach $\sim$ 0.25 can be integrated stably and accurately with no appreciable extra cost using an explicit algorithm. Since the complications involved for solving even the simplest implicit algorithms cost at least a factor of three more in calculation time than for solving an explicit algorithm, any flow which reaches velocities of about a tenth of the speed of sound can probably be integrated cost effectively using an explicit algorithm. Nevertheless, there is a large class of problems in which slower flows must be treated more efficiently, and these are discussed next.

V.B.2 Subsonic Flows

In many flame systems, as in the gedanken flame experiment discussed in Section II, the local sound speed is several orders of magnitude faster than the flame speed and other characteristic velocities arising in the fluid flow. Either an implicit or an asymptotic approach to the fast acoustic waves is required in these cases to keep the computational expense within reasonable bounds. In these situations, the internal energy at any instant is dominated by the thermal

component, since the kinetic energy is quadratically small. Thus difference-of-large-number errors can easily be kept small. Furthermore, a pressure formulation of the energy equation becomes practical because shocks are no longer a consideration.

Other problems appear because of the greatly extended timescales. In the explicit calculations with short timesteps determined by the Courant condition, diffusive transport phenomena are generally small effects and do not govern the very fast timescale phenomena. When the timescales encompass phenomena such as flames and reaction waves, the diffusive transport of material and energy can govern the system evolution and therefore must be calculated accurately. Numerical diffusion becomes a much more serious issue because steep gradients have to be maintained computationally for a much greater period of time. Thus calculations of subsonic phenomena such as flame propagation can take better advantage of Lagrangian techniques than can strongly shocked flows.

Any pressure fluctuation from thermal conduction or chemical energy release induces a local flow of fluid which reduces the pressure deviation. The result of this tendency on long timescales is to approach a constant pressure configuration. In a gravitational field, the pressure exhibits a hydrostatic vertical stratification. In a continually flowing fluid, the pressure exhibits small fluctuations consistent with the motion, but is essentially constant. Through a candle flame, for example, the pressure is constant to better than 0.1%. This means that the local density and temperature, which vary much more strongly than pressure, are inversely related. Two distinct ways to tackle the problem of calculating subsonic flows are discussed below: the various implicit approaches and the asymptotic slow-flow approach.

When finite pressure fluctuations are important and the sound waves are of relatively long wavelength, an implicit treatment of the pressure equation,

$$\frac{\partial P}{\partial t} + \underline{v} \cdot \underline{\nabla} P = -\gamma P \underline{\nabla} \cdot \underline{v} + (\gamma - 1) \underline{\nabla} \cdot (\lambda \underline{\nabla} T) + \left.\frac{\partial P}{\partial t}\right|_{chem}, \qquad \text{(V.26)}$$

can be effective. We note that variations in the pressure appear explicitly except for the coefficient γP multiplying the velocity divergence term. Thus, $\underline{\nabla} \cdot \underline{v} \approx 0$ when the pressure is nearly constant.

In global implicit approaches, the complete set of nonlinear coupled equations describing the physical system is cast into a simple finite difference form. The spatial and temporal derivatives are discretized and the nonlinear terms are linearized locally about the solutions obtained numerically at the previous timestep [43,44,45]. A single implicit equation results from taking the divergence of the momentum equation and using the continuity or energy equation for the mass or energy flux terms. This approach requires use of linear finite difference approximations to the convective derivatives in order to effect an analytic substitution of one equation into another. A rigorously correct treatment requires iteration, and large matrices must be inverted at each timestep to guarantee stability. In one spatial dimension the problem usually appears as a block tridiagonal matrix with M independent physical variables to be specified at N_x grid points. Then an MN_x by MN_x matrix must be inverted at each iteration of each timestep when the chemistry as well as the fluid dynamics is treated implicitly. The blocks on or adjacent to the matrix diagonal are $M \times M$ in size so the overall matrix is quite sparse. In fact, these are often called block implicit algorithms. Nevertheless, an enormous amount of computational work goes into advancing the solution even a single timestep. Multi-dimensional problems, in this approach, lead to matrices which are MN_xN_y by MN_xN_y in two dimensions and $MN_x\ N_yN_z$ by $MN_x\ N_yN_z$ in three dimensions.

When the implicit methods deal only with fluid dynamics, they are relatively inexpensive. They do not, however, appear to permit use of a nonlinear, monotonic transport algorithm. First order numerical diffusion is required to maintain positivity. To recover an equivalent accuracy in an implicit Eulerian calculation involves at least doubling the number of grid points in each spatial dimensin when the mass transport is convectively dominated. Thus the implicit approach costs more by about a factor of 8 in two dimensions an 16 in three when monotonic

transport algorithms cannot be used. This disadvantage is counterbalanced by the ability to take much longer timesteps. McDonald [46] has compiled an excellent review which focusses entirely on implicit methods.

Many variations of implicit algorithms have been discussed in the literature [e.g., 33,47,48]. In these approaches, an equation is derived for the advanced pressure which is solved as an iteration between momentum and reduced energy equations. This approach, attributed to Hirt and Cook [49], appears in the ICE and RICE algorithms. Ramshaw and Trapp [50], however, appear to exclude their equation of state from the implicit, pressure-determining iteration. Furthermore, Westbrook [47] shows that this sort of biased inconsistency can lead to moderately large errors when incorporated in an energy-coupled, reactive flow calculation of a premixed flame.

The slow flow approach of Jones and Boris [51] is an asymptotic rather than an implicit technique. It works best in the limit where the sound speed is very large and the pressure is essentially constant. This algorithm can also be derived from a reactive flow generalization of Ramshaw and Trapp's formulation. It includes chemical and other divergence source terms and allows for an average pressure increase such as occurs in closed vessels. Since they were not concerned with numerical diffusion at a flame front moving through the fluid, but rather with treating sharp interfaces which are nearly stationary in the Lagrangian sense, Ramshaw and Trapp selected the donor-acceptor algorithm, a technique also employed by Noh [52] and Chorin [53]. Rehm and Baum [54] have derived the system of slow flow equations from a more general perspective than Jones and Boris, although they have not yet explicitly considered the chemical reaction terms. Their method presents a systematic expansion procedure where the only effects of compression which are allowed are the asymptotic long-time changes in density which result from local heating and cooling.

To lowest order, the slow flow algorithm has been implemented in cylindrical geometry by Jones [51]. A complete detailed reactive flow model has been formulated where chemical

kinetics and diffusive transport contribute to the lowest order asymptotic determination of the velocity diverence from Eq. (V.26),

$$\underline{\nabla} \cdot \underline{v} \approx \frac{1}{\gamma P}\left[(\gamma - 1)\underline{\nabla} \cdot \lambda \underline{\nabla} T + \frac{\partial P}{\partial t_{chem}} - <\frac{dP}{dt}>\right]. \tag{V.27}$$

Here $<\frac{dP}{dt}>$ indicates the average pressure change in the system from external addition of energy or compression. The curl of the velocity is still advanced by a time-dependent partial differential equation,

$$\frac{\partial \underline{\xi}}{\partial t} + \underline{v} \cdot \underline{\nabla \xi} + \underline{\xi \nabla} \cdot \underline{v} = \frac{-\nabla \rho \times \nabla P}{\rho^2} \tag{V.28}$$

where the vorticity is $\underline{\xi} = \underline{\nabla} \times \underline{v}$. The solutions to these equations no longer encompass compressional sound waves. Strong compressions and rarefactions driven by chemistry and conduction are allowed as long as they evolve slowly compared to sound waves.

There is an important advantage of this type of method: the way in which Eq. (V.28) is advanced has been left unspecified, so that no compromise of positivity is required to implement an implicit algorithm and the best finite difference techniques available may be used for convection. Both Eulerian and Lagrangian finite difference techniques can be used, although Jones and Boris have used an Eulerian FCT algorithm.

There are also several complications which must be dealt with in any calculation using the slow flow approximation. A net addition of heat to the system through chemistry, thermal conduction, or external sources changes the average pressure with time. In a closed container, this average heating, $<dP/dt>$, cannot lead to a velocity divergence and therefore is subtracted from Eq. (V.27) to get the correct value of $\underline{\nabla} \cdot \underline{v}$. Another result of this average is that the pressure is essentially constant in space but not in time. Furthermore, pressure appears in Eq. (V.28) as part of the vorticity source term. Properties of buoyant flames can be calculated by using the average hydrostatic equilibrium pressure gradient which changes slowly with the average temperature. In certain types of self-consistent fluid dynamic problems we must solve Eq.

(V.27) to first order as well as zeroth order to reproduce accurately the kinetic vorticity generation. This can still be done without jeopardizing flexibility in the choice of convective transport algorithms.

In one-dimensional systems it is often as easy to set up the centered or fully forward differenced implicit equations for mass, momentum and adiabatic energy conservation as it is to use the slow flow formulation. Since the chemical species and diffusion velocities are not part of the implicit formulation, this is not a block or global implicit algorithm and hence need not be prohibitively expensive. Furthermore, such a generalization of the slow flow algorithm allows the accurate treatment of adiabatic sound waves when the timestep is small enough. We next consider briefly the use of suitable hydrodynamics algorithms in multi-dimensions, for which all algorithms are more difficult to implement.

V.C. Geometric Complexity in Reactive Flows

In this section four aspects of geometric complexity are considered briefly: representation, spatial gridding techniques, fluid dynamics algorithms, and auxiliary calculations. Of course an overall concern is computational cost. Even if all the multi-dimensional generalizations of successful one-dimensional techniques were available and easy to apply, multi-dimensional calculations could be prohibitive because the computing costs escalate so quickly. A one percent resolution requires roughly 100 computational cells in one dimension, $\sim 10^4$ cells in two dimensions, and $\sim 10^6$ cells in three dimensions. The intrinsically greater difficulty of geometrically complex flows and structures compounds the problem.

Thus some effort has gone into trying to find ways to represent multi-dimensional problems within a one-dimensional calculation. Variable metric techniques [9,55] allow an essentially channelled one-dimensional calculation to represent multi-dimensional flow effects. Cartesian, cylindrical, and spherical geometries as well as variable cross-section tubes are also modelled in this way. Moveable end walls may be used in one-dimensional simulations of internal combustion engines to simulate a piston within a cylinder. Of course, a simulation of phenomena such as swirl, vorticity, shear, convective mixing and instability requires a multi-dimensional model.

V.C.1 Problem Representation

We are faced with the first difficulty arising from geometric complexity when we ask how to best set up a computational grid to use in multi-dimensional flow calculations. In two-dimensional calculations, quadrilateral and triangular Lagrangian finite difference algorithms have been used [30,56,57]. They have not yet, however, been applied to chemically reacting flows. Lagrangian computations have even been performed in three dimensions [58], but again not yet for the reactive case.

The major problem in Eulerian calculations is numerical diffusion, which is decreased

when the resolution is increased. However, even a Lagrangian grid of quadrilaterals has serious problems due to distortion by grid stretching [56,57]. This grid distortion problem is generally handled by grid re-mapping, [30,31,58,59] which itself is a numerically diffusive process. Intermittant re-mapping of a distorted Lagrangian grid can reduce numerical diffusion below Eulerian limits when the number of timesteps between remap operations becomes large enough. However, when short wavelength shear flows are excited, such as occur in reactively driven or turbulent flows, even this potential improvement is of limited use.

The distortion problem for Lagrangian grids can be handled adequately by using a finite difference mesh of triangles rather than rectangles (tetrahedrons in three dimensions). This technique, which has been used in many finite element representations, was adapted to finite differences of incompressible flow [56,57]. The noticeable improvements in performance arise for two reasons. First, the variable number of triangles permitted at each vertex allows smooth representation of much more complicated shapes than can be treated smoothly by an equal number of rectangular cells. Second, since the number of lines meeting at a vertex is not fixed, it can be varied during a calculation by an automatic grid reconnection procedure to prevent severe grid distortions.

While this approach may not be the only method of dealing with severe grid distortions, it is the least numerically diffusive technique employed so far. Fritts [57] has recently employed Lagrangian triangular grid techniques in studying nonlinear aspects of free-surface waves including strongly sheared flows. Ten to fifteen full cycles of the waves can be integrated accurately without significant numerical diffusion or other deterioration of the solution, and the procedure for reconnecting triangle vertices and effectively re-gridding in the presence of strong shear is also reversible and nondissipative. There is another advantage to using triangular cells. The nonlinear mesh-separation instabilities, which plague low-dissipation rectangular cell techniques, seem to be essentially absent or damped with triangular finite difference cells. Drawbacks to the triangular grid approach center around the complexity of the programming

required. The arithmetic operations also seem to hinge strongly on linked lists, random access, and sequential processing making parallel processing less advantageous than for simpler grid structures.

V.C.2 Gridding

In Eulerian calculations adaptive gridding is often used to reduce numerical diffusion by introducing additional computational zones. Therefore, the resolution is increased where gradients of important quantities become steep. In Section VII adaptive gridding is discussed in some detail as a means of solving multiple space scale problems.

V.C.3 Fluid Dynamic Algorithms

The block implicit approach, applied in an alternating direction implicit (ADI) framework [43-46], is one way to calculate subsonic multi-dimensional flows. In this method, calculations are performed for one direction evaluating the properties of the other direction at values from the previous timestep. A number of iterations on this procedure are required to couple the whole calculation accurately. The addition of chemical reactions and molecular diffusion strongly complicates this approach because the matrices which form each block can then become large.

The slow flow algorithm discussed earlier was actually designed to take advantage of the improvements allowed by monotonic algorithms. Thus maximum resolution and minimum numerical diffusion can still be achieved in an Eulerian representation. In two dimensions only one independent vorticity component need be carried; in three dimensions there are two Although obtaining the velocity field from the curl and divergence involves solving Poisson equations which implicitly couple the entire spatial mesh, these are linear, scalar equations for which a number of relatively efficient solution techniques exist. These governing Poisson equations are simpler than the iterated, block tridiagonal equations which arise using the implicit approach. Furthermore, the increase in numerical resolution afforded by the application of

monotone methods allows comparably accurate solutions with many fewer cells, and hence with reduced computational cost.

V.C.4 Auxiliary Equations

Because we do not have the computer memory available to model an infinitely large region of space or to resolve most boundary layers near a solid wall, the application of boundary conditions to reactive flow computations is an economically important issue. It is also a technically complicated issue because there is more latitude for conceptual and programming error in treating boundary conditions than there is in almost any other aspect of setting up a detailed computational reactive flow model. We must determine the correct conditions to apply, how to implement them numerically, and also whether the numerical model allows unwanted interactions between the boundary condition equations and the equations describing the inside of the region.

Here we will consider generically only three types of boundary conditions:

1. Ideal (or non-) boundary conditions,
2. Wave transmission (or radiation) boundary conditions, and
3. Continuitive (or outflow) boundary conditions.

Because boundary conditions are problem-specific, little of a general applicable nature has been written about them compared to the discussions of the numerical techniques which have been published. However, in the review of the APACHE code [49] and in Turkel's review [61], relatively thorough discussions are given of how to apply boundary conditions at the edge of a region in a finite difference representation.

The easiest and perhaps the only way to treat boundary conditions accurately is to get rid of them. This can be done in problems where a symmetry condition exists, since then all boundary points can be treated as interior points. To simplify programming, code designers generally inlclude one or more layers of "ghost" or "guard" cells at the edge of the

computational region. When values of the physical variables on the boundary cannot be determined by direct application of the finite difference equations, (i.e., some pieces of information required are determined by a fluid element off the edge of the mesh), modified boundary formulae for the guard cells are developed which depend only on the information from the interior. This requires using a one-sided formulation for the extrapolation unless a symmetry condition is available to define the ghost values in terms of the newly computed interior cell values.

The simplest of these "non-boundary" conditions arise in cases where some aspect of the boundary can be approximated as a smooth hard wall. Periodic situations, as arise in the consideration of circular systems (stacks of turbine blades, for example), cylinderical systems, or spherical systems, are easy to handle numerically. When flow is directed normal to a wall at cell $i = 1$, physical conditions at $i = 0$ beyond the boundary may be approximated in terms of conditions at $i = 2$. For example,

$$\rho(0) = \rho(2),$$
$$P(0) = P(2),$$
$$V_\perp(0) = -V_\perp(2), \quad (V_\perp(1) = 0) \quad \text{and}$$
$$V_\parallel(0) = V_\parallel(2) \quad \text{(free slip)}.$$

It is also possible to place a fictitious wall halfway between cells. For example, a solid wall at $i = 1/2$ has

$$\rho(0) = \rho(1),$$
$$P(0) = P(1),$$
$$V_\perp(0) = -V_\perp(1), \quad \text{and}$$
$$V_\parallel(0) = -V_\parallel(1) \quad \text{(zero tangential velocity)}.$$

More complicated and therefore uncertain boundary conditions lead to more complex formulae for values at the guard cells. In many cases, a localized phenomenon is being simulated which produces a growing disturbance that propagates away from the region of generation and interaction. In this case we could allow the computational cells to increase in size as they get farther from the interaction. Thus, the computational domain is very large and there is no

corresponding increase in computer storage. The cell stretching should be limited to 5-20% per cell to limit inaccuracies which arise as a result of the varying cell size.

It should be noted that when higher order algorithms are used inside the computational region, it is often more difficult to apply complicated boundary conditions. In low order local algorithms, errors cannot propagate far from the boundaries very quickly and in general the solutions are heavily smoothed. High order methods, such as spectral or pseudo-spectral expansion techniques, may cause more problems because of the highly non-local nature of the techniques being employed. Monotonic convection algorithms are generally advantageous near complicated boundaries because they are stable and as easy to apply as low order methods.

The application of boundary conditions becomes progressively more difficult as we consider the four types of terms of Section III. Source, sink, and coupling terms are local; hence interior points and boundary points behave similarly. Diffusive effects are easy to represent at simple boundaries even when we use an implicit formulation. The value of the quantity being diffused (for example, temperature) can be set on the boundary or the flux can be specified.

Treating wave and convection effects can be much more difficult. Since waves often propagate with very weak damping, smoothing through numerical diffusion cannot be relied on to mask errors in boundary conditions in the way it can be used when modelling diffusive phenomena. In linear and nearly linear problems, it is sometimes possible to isolate analytically the ingoing and outgoing wave systems at the boundary. When this can be done, non-reflective conditions, sometimes called the radiative boundary condition, can be applied by zeroing the incoming wave system and analytically extrapolating the outgoing waves. As a less efficient but more general alternative, a so-called damping or sponge zone may be established in the first few layers of cells adjacent to the boundary. When fluid flow is involved, this region is often called a Rayleigh viscous zone. As a disturbance propagates into the dissipation region, it encounters a medium of increasingly greater damping until the wave can no longer propagate. There will be some signal reflection off the gradient in the damping coefficient Thus the optimum

absorptive boundary is obtained when the spatial variation of the boundary damping coefficient is gradual enough that the outgoing waves reach far into the damping region. These waves then become trapped before the unphysically reflected wave component becomes appreciable. This technique has been used for electromagnetic waves and gravity waves. Although absorption is not perfect, four or five cells are enough to reduce the spuriously reflected wave amplitude by more than an order of magnitude relative to the original wave. Ten cells should be enough to guarantee 99% absorption.

The most difficult boundary condition has always been the continuitive boundary condition for describing the fluid flowing off of a mesh. The one or two lines of ghost cells at the boundary of the region of computation have to represent an infinite outside world whose exact response to what goes on inside the computational region is known only approximately. The problem is again to avoid non-physical reflections and interactions of outward moving flow structures off the boundary and back into the fluid. In all but the simplest linear problems, the continuitive algorithm finally implemented is approximate because inward and outward propagating waves and pulses will be indistinguishable locally for the nonlinear fluid dynamic equations. Monotonic convection algorithms allow extrapolation of the fluid flow parameters off the edge of the system by setting the ghost cell values equal to those just inside the mesh. When two-dimensional or three-dimensional flows are being considered, the extrapolation should be done along the fluid flow lines. In linear convection algorithms which do not have positivety guaranteed, such as extrapolation is often unstable. However, by breaking the fluid disturbance into its constituent characterstics and extrapolating each of these out to the guard cells, a stable if approximate outflow algorithm is obtained for all but the most finicky convection algorithms.

In many fluid dynamic and heat transport calculations, the solution of general elliptic or parabolic equations is required in order to represent physical processes other than convective fluid flow. Whether implicit algorithms or slow flow algorithms are used, Poisson-like equations appear defining quantities such as pressures or velocity potentials. In most situations, the result

of any small scale transport process appears as a diffusive behavior on the macroscale. When the small scale transport is very fast (e.g., photons travel at the speed of light in radiation transport), the derivative macroscopic diffusion equation can be stiff, and thus some form of nonlocal implicit or asymptotic formulation may be required.

We conclude this section with a brief discussion of solution techniques applicable to the elliptic implicit equations which arise in the stiff multi-dimensional hydrodynamic and heat transport portions of the reactive flow calculation. Iteration techniques are useful and easy to program, but they are computationally expensive relative to more direct solution methods. When the finite difference coefficients are constant in any dimension, either Fourier transform or folding techniques can reduce the effective dimensionality of the problem. When the dimensionality is or has been reduced to unity, a direct solution is possible using fast tridiagonal algorithms. Eulerian representations often allow the use of such direct solutions, which are exact and very efficient [62].

When the coefficients of the elliptic equation are variable, due either to physical or geometric reasons, direct solutions are still possible but generally become more expensive because a massive matrix must be inverted. Sometimes iterations are even employed to speed up the solution, as in the incomplete Cholesky-Conjugate Gradient methods [63] and their variants. The efficiency is higher for a given required accuracy than using methods based on ADI or over-relaxation iteration, but many iterations are still needed in some situations. A new direct method, SEVP [64], has recently been published which is based on an error sweepout technique. This has been applied to a number of difficult problems in weather modelling and in combustion [50]. Unfortunately, no generalization of efficient, accurate direct solutions of Hochney [62] or Buneman [65] to the general coefficient (rectangular grid) elliptic equation has yet been discovered. In the simplest case, solution of a 5-point Poisson equation approximation on a rectangular grid, the regular structure of the sparse matrix is retained when the zones are non-uniform in size, but the direct solution techniques will not work because the coefficients

are now variable. Therefore, a search is on to find an algorithm for inverting the two-dimensional 5-point Poisson operator in $\mathcal{O}(N \log_2 N)$ operations where $N = N_X \times N_Y$ is the number of distinct potential values being sought. Direct inversion of the sparse matrix requires $\mathcal{O}(N^3)$ operations, but consideration of the block nature of the sparsity pattern allows this to be reduced to $\mathcal{O}(N^2)$. On a 100×100 mesh, the determination of an $(N \log_2 N)$ solution would reduce the solution time by a factor of about 15.

VI. DIFFUSIVE TRANSPORT PROCESSES

The term "diffusive transport processes" refers to molecular diffusion, thermal conductivity, viscosity, and thermal diffusion. These are the parts of Eqs. (II.1)-(II.5) which are represented by the expressions

$$\frac{\partial n_j}{\partial t} = -\underline{\nabla}\cdot n_j \underline{V}_j \,, \quad \text{species diffusion,} \tag{VI.1}$$

$$\frac{\partial (\rho \underline{\mathrm{v}})}{\partial t} = \underline{\nabla}\cdot \eta(\underline{\nabla}\,\underline{\mathrm{v}} + (\underline{\nabla}\,\underline{\mathrm{v}})^T) \,, \quad \text{viscosity, and} \tag{VI.2}$$

$$\frac{\partial E}{\partial t} = \underline{\nabla}\cdot(-\lambda \underline{\nabla} T + \sum_j h_j n_j \underline{V}_j + k_B T \sum_{j,k} \frac{n_j}{N} \frac{D_j^T}{D_{jk}} (\underline{V}_j - \underline{V}_k)), \quad \text{thermal conductivity,} \tag{VI.3}$$

where the individual variables are defined in Section II and in the Glossary. Transport processes are crucial to the description of flame ignition and propagation since they are the mechanism by which heat and reactive species are transported ahead to the unburned gas. These processes are less important to the overall behavior of well established shocks and detonations because the characteristic timescales for transport processes are much longer than those needed to characterize processes moving at faster than the sound speed.

This section first describes an iterative algorithm for solving for the diffusion velocities, $\{V_j\}$, which avoids the cost of performing matrix inversions. It then summarizes appropriate formulae for evaluating λ, η, D_{jk}, and D_j^T in multi-component systems of neutral gases.

VI.A. Iteration Procedure for Diffusion Velocities

The difficulties of dealing with disparate time and space scales are further complicated when there are large numbers of reacting species. If the cost of a calculation merely scaled as the number of species, M, the problem would be tractable. However, whenever a matrix of size $M \times M$ must be inverted, the operation count scales as M^3. Section IV discussed this problem in terms of the solution of the coupled ordinary differential equations describing complex chemical reaction rate schemes. The solution suggested was to use a combination of

asymptotics for stiff equations and a second order methods for normal equations, thus avoiding the cost of matrix inversion associated with the global implicit methods while maintaining the accuracy of the calculation.

The problem of matrix inversion occurs again when solving Eqs. (II.11) and (II.12), written here as

$$\underline{S}_j = \sum_{\substack{k=1 \\ k \neq j}}^{M} W_{jk} \, (\underline{V}_k - \underline{V}_j), \tag{VI.8}$$

where

$$\underline{S}_j = \underline{\nabla}\left(\frac{n_j}{N}\right) - X_j \frac{\nabla P}{P} - \sum_k Y_{jk} \frac{\nabla T}{T}, \tag{VI.9}$$

in which the diffusive transport coefficients appear in W_{jk} and Y_{jk}. Because the straightforward inversion of Eq. (VI.8) to find $\{\underline{V}_j\}$ requires $\sim M^3$ arithmetic operations for each spatial direction, a more efficient method must be found when there are more than four or five species involved. Here the problem is one of avoiding computational expense, not numerical difficulty.

The most efficient algorithm we have found [51,66] requires $\sim M^2$ operations and is based on a special initial guess. When both Eqs. (VI.8) and (VI.9) are summed over all species, we find that

$$\sum_{j=1}^{M} S_j = 0 \tag{VI.10}$$

where the notation indicating spatial direction has been dropped. Since $\{S_j\}$ sums to zero, the matrix **W** is singular as defined in Eq. (VI.8) and the M different diffusion velocities cannot all be independent. The extra equation needed is the contraint

$$\sum_{j=1}^{M} \rho_j V_j = 0 \, . \tag{VI.11}$$

We will use the fact that once a particular set of solutions $\{V_j^p\}$ is known for Eq. (VI.8), any constant velocity may be added giving another equally correct solution $\{V_j^p + \delta V\}$ for $j = 1, \ldots M$. This as yet undetermined constant, δV, may then be used to enforce the con-

straint Eq. (VI.11).

Let the diffusion coefficient D_{js}, describe diffusion of species j through the background provided by the sum of all other species. Then the zeroth order and starting approximation for the j th diffusion velocity, V_j^0, may be written as

$$V_j^0 \equiv - \frac{\rho - \rho_j}{\rho} \frac{N^2 D_{js}}{(N - n_j) n_j} S_j . \tag{VI.12}$$

Higher order terms arise as corrections to the lowest order solution to the diffusion velocity,

$$V_j \equiv V_j^0 + \delta V_j . \tag{VI.13}$$

The equations for $\{\delta V_j\}$ are found by substituting Eq. (VI.13) into Eq. (VI.8), from which one finds

$$\delta S_j \equiv \sum_{k=1}^{M} A_{jk} S_k = \sum_{k=1}^{M} W_{jk} (\delta V_k - \delta V_j) . \tag{VI.14}$$

Now $\{D_{js}\}$ has been defined to be

$$\frac{D_{js}}{(N-n_j)} \sum_{k \neq j} \frac{n_k}{D_{jk}} \equiv 1 \tag{VI.15}$$

and the matix elements of A are given by

$$A_{jk} \equiv \frac{\rho_j}{\rho} \delta_{jk} + \frac{n_j}{D_{jk}} \frac{(\rho - \rho_k)}{\rho} \frac{D_{ks}}{(N-n_k)} (1-\delta_{jk}) . \tag{VI.16}$$

Equation (VI.14) defines a linear system of equations which can be solved for the $\{\delta V_j\}$. The right hand side of Eq. (VI.14) vanishes when summed on j. It is easy to see that the choice of A_{jk} here is not unique. Since Eq. (VI.11) is true, each row of the matrix A can have an arbitrary constant added according to

$$\tilde{A}_{jk} \equiv A_{jk} - C_j \tag{VI.17}$$

without changing Eq. (VI.14). Such constants leave $\{\delta V_j\}$ unchanged. The general form of the complete solution (assuming convergence of the sum) is

$$V_j = \frac{-(\rho - \rho_j)}{\rho} \frac{N^2 D_{js}}{(N-n_j) n_j} [\delta_{jk} + A_{jk} + A_{jl} A_{lk} + \ldots] S_k \tag{VI.18}$$

where the matrix in square brackets is just the formal expansion of $[1-A]^{-1}$.

Numerical evaluation of Eq. (VI.18) can take advantage of the fact that none of the indicated matrix multiplications actually have to be performed. Since $\{S_j\}$ is known, we multiply from the right first. Each additional power of A is obtained by multiplying a vector, rather than a matrix, by A. This expansion gives an $O(M^2)$ algorithm. In practice we have found it convenient to take $C_j = 0$ in Eq. (VI.17) and we recommend truncating the expansion in Eq. (VI.18) after the A^2 term. At least the first correction A_{jk} needs to be included to get the correct sign for all the diffusion fluxes. The quadratic term adds significant extra accuracy and further iteration is unnecessary. The errors remaining are at most a few percent.

The fast convergence observed seems to result from the initial approximation in Eqs. (VI.12) and (VI.15). The factor $(\rho-\rho_j)/\rho$ in Eq. (VI.18) is crucial. When there are only two species, i.e., $N = n_1 + n_2$, this factor becomes ρ_j/ρ as required to give the exact two species result. Note that terminating the expansion of Eq. (VI.18) at the δ_{jk} term does not give Fickian diffusion. The effective diffusion coefficient differs from Fickian by the factor $(\rho-\rho_j)/\rho$. Furthermore, Fickian diffusion need not even give the correct sign for the diffusive flux.

VI.B. Evaluation of Diffusive Transport Coefficients

In this section a number of extremely useful equations for diffusive transport coefficients have been taken with some modification from the summary by Picone [67]. The forms given are for mixtures of neutral gases. Their derivations are based on or are advancements of the fundamental work of Chapman and Cowling [68] and Hirschfelder, Curtis, and Bird [3]. Throughout we have chosen representations of the coefficients which are easily used in reactive flow models and do not require the expensive inversion of matrices.

VI.B.1 Viscosity

The most convenient form for the viscosity of a gas mixture, has been given by Wilke

[69]

$$\eta = \sum_j \eta_j \left[1 + \frac{\sqrt{2}}{4 n_j} \sum_{k \neq j} n_k \, \phi_{jk} \right]^{-1} . \tag{VI.19}$$

where μ_j is the viscosity of the pure component j and to first order

$$\phi_{jk} = \frac{\left[1 + \left(\frac{\eta_j}{\eta_k} \right)^{1/2} \left(\frac{M_k}{M_j} \right)^{1/4} \right]^2}{\left[1 + \left(\frac{M_j}{M_k} \right) \right]^{1/2}} \tag{VI.20a}$$

and $\{M_j\}$ are the atomic masses of the species. The species viscosities may be written [3, Chapt. 8]

$$\eta_j = \frac{2.67 \times 10^{-5} \sqrt{M_j T}}{\sigma_j^2 \, \Omega_{2,2}} \left(\frac{g}{\text{cm-sec}} \right) \tag{VI.21}$$

where σ_j is the molecular collision diameter and $\Omega_{2,2}$ is a collision integral normalized to its rigid sphere value. We note that when $\Omega_{2,2} \approx 1$, Eq. (VI.20) can be reduced to

$$\phi_{jk} = \frac{[1 + (\sigma_k / \sigma_j)]^2}{[1 + (M_j / M_k)]^{1/2}} \tag{VI.20b}$$

Equation (VI.19) differs from the form given by reference [3] in that pure component viscosities are required instead of binary diffusion coefficients.

VI.B.2. Thermal Conductivity

For the mixture thermal conductivity, an extremely useful equation has been given by Mason and Saxena [70],

$$\lambda = \sum_j \lambda_j [1 + \frac{1}{2\sqrt{2} n_j} \sum_{k \neq j} n_k \, \phi_{jk}]^{-1} \tag{VI.22}$$

where ϕ_{jk} has been defined in Eq. (VI.20a). The pure component conductivities may be written in terms of monatomic thermal conductivities with "frozen" internal degrees of freedom,

$$\frac{\lambda_j^0}{\lambda_k^0} = \frac{\eta_j}{\eta_k} \frac{M_k}{M_j} , \tag{VI.23}$$

and the Euken factor [71], E_j,

$$\lambda_j = E_j \lambda_j^0, \tag{VI.24}$$

where

$$E_j = 0.115 + 0.354 \frac{\gamma}{\gamma - 1}, \tag{VI.25}$$

and γ is the ratio of specific heats, $\frac{C_p}{C_v}$. The $\{\lambda_j^0\}$ may be written as

$$\lambda_j^0 = \frac{8.322 \times 10^{-4}}{\sigma_j^2} \sqrt{\frac{T}{M_j}} \frac{1}{\Omega_{2,2}} \left[\frac{erg}{\text{cm-deg-sec}} \right]. \tag{VI.26}$$

where again $\Omega_{2,2} \approx 1$.

The expressions for $\{\lambda_j\}$, Eq. (VI.24), are fine for non-polar molecules and probably adequate for polar modelcules. The origin of the difficulty [71] lies in the evaluation of the Euken factor which is an average over microscopic states. The derivation of E_j assumes that all states have the same diffusion coefficients and does not allow for distortions in the electron density distribution function.

VI.B.3. Binary Diffusion Coefficients

For some pairs of inter-diffusing species, Mason and Marrero [72] give a table of very accurate binary diffusion coefficients which may be put into the form

$$D_{jk} = \frac{A_{jk} T^{B_{jk}}}{N} \left[\frac{\text{cm}^2}{\text{sec}} \right]. \tag{VI.27}$$

When these have been not tabulated or measured, the $\{D_{jk}\}$ may be estimated from

$$D_{jk} = \frac{2.6280 \times 10^{-3}}{P \sigma_{jk}^2 \Omega_{1,1}} \sqrt{\frac{T^3 (M_j + M_k)}{2 M_j M_k}} \tag{VI.28}$$

where

$$\sigma_{jk} = \frac{\sigma_j + \sigma_k}{2}. \tag{VI.29}$$

The function $\Omega_{1,1}$ depends on the molecular parameters of species j and k and ranges in value from 0.4 to 2.7 in the temperature range of interest. Tables of all the Ω's are given in reference [3].

VI.B.4. Thermal Diffusion

Thermal diffusion is a second order effect [3,68] which is only of importance when there are large differences between the atomic masses of the constituent species. The thermal diffusion ratios $\{K_j^T\}$ are defined as

$$K_j^T = \sum_k \frac{n_j n_k}{N^2 D_{jk}} \left(\frac{D_k^T}{\rho_k} - \frac{D_j^T}{\rho_j} \right) \tag{VI.30}$$

and also may be written as [58]

$$K_j^T = \frac{1}{5k_B N^2} \sum_k \left[\frac{M_j M_k}{M_j + M_k} \right] \left[\frac{6C^* - 5}{D_{jk}} \right] \left[\frac{a_k}{\rho_k} - \frac{a_j}{\rho_j} \right] \tag{VI.31}$$

where C^* is a function of collision intergrals and

$$a_j = \lambda_j \left[1 + \frac{1.065}{2\sqrt{2}\, n_j} \sum_{k \neq j} n_k \phi_{jk} \right]^{-1} \tag{VI.32}$$

is the contribution of the j th species to the mixture thermal conductivity assuming that the internal molecular degrees of frredom are frozen. The $\{D_j^T\}$ required in Eq. (II.4) may be found from [58]

$$D_j^T = \frac{n_j}{N} \sum_k D_{jk} K_k^T . \tag{VI.33}$$

Thus the coefficients needed to incorporate the effects of thermal diffusion may be written in terms of the individual species thermal conductivities and the binary diffusion coefficients.

VII. ALGORITHMS FOR COUPLING MODELS OF PHYSICAL PHENOMENA

In the previous sections we separately discussed modelling the chemical kinetics, hydrodynamics, and diffusive transport processes which are cornerstones of detailed modelling of combustion processes. In this section we describe some of the methods and problems associated with coupling the various representations of individual phenomena in a reactive flow calculation. We begin by contrasting fractional step and implicit coupling techniques and then give an example of explicit coupling for shock and detonation calculations. The splitting methods described are then extended to systems of stiff equations by describing the physical basis of the fractional step coupling methods. Detailed examples are given showing how these general concepts are applied. Adaptive gridding is introduced to deal with multiple space-scale difficulties. Finally, the section is concluded with the solution to the gedanken flame experiment proposed in Section III.

VII.A. Dealing with Multiple Timescales

In Section III we used several examples to show the types of general numerical considerations which influence the accuracy and economics of numerical simulations. In practice, not only must we compute all the individual phenomena efficiently and accurately, but we must also ensure that the interactions among the physical effects are accurately represented. When each phenomenon varies slowly during a timestep, it is relatively easy to couple all of the distinct phenomena together by the usual timestep splitting or fractional step approaches [73]. Then the individual terms in the conservation equations are solved separately and sequentially for each timestep. Thus at at time t, for example, the energy is advanced to the time $(t + \delta t)$ by differencing and solving the thermal conduction term. Then this new value of the energy is used as a starting value at time t to advance the energy by, for example, convection to $(t + \delta t)$. This process is continued until all the terms are advanced. This approach works well until some of the phenomena develop characteristic timescales shorter than the fractional timestep used in the calculation. These phenomena have become stiff with respect to the long-time, slow

behavior of the system.

In a coupled, transient, reactive hydrodynamics model, a number of situations occur for which stiff phenomena must be integrated efficiently on timescales much longer than the shortest characteristic times. During the period of ignition delay in a mixture of hot combustion gases, very fast chemical reactions are locally in a quasi-static equilibrium between production and loss effects. Thus the equations being solved are stiff, but the species densities and temperature change slowly. In a slow, constant pressure flame problem, fast sound waves are stiff on timescales of interest in the propagating flame. Other effects related to diffusion and radiation can be stiff as well. When more than one interacting phenomenon is stiff, coupling these effects together by any method which does not resolve the shortest timescales of the problem is potentially subject to error. Whether this error is important or not depends on specific considerations for each system.

Before deciding how to couple the representations of the individual phenomena into a complete simulation model, we must first decide which time and space scales to resolve. Whether or not a particular scale needs to be resolved depends both on the evolution of the solutions and on the characteristic scales and rates of the constituent physical and chemical effects. An example using the simple one-dimensional diffusion equation will help to make this point clear. Consider the evolution equation for a temperature-like variable, $T(x)$, such that

$$\frac{\partial T(x,t)}{\partial t} = \frac{\partial}{\partial x}\left[D\,\frac{\partial T(x,t)}{\partial x}\right] + S(x,t), \qquad \text{(VII.1)}$$

where $S(x,t)$ is an externally determined source or sink of "heat". A finite difference numerical computation of this equation entails choosing a characteristic timestep δt and space step δx. When $\delta t > \frac{\delta x^2}{D}$, the equation is stiff; the diffusion of gradients at the smallest scale resolved in the calculation is faster than the temporal resolution allowed by the timestep. Whether or not the timestep has to be reduced depends entirely on the actual solution at that instant of time, on the source or coupling terms represented by $S(x,t)$ and on any nonlinearities in the

diffusion coefficient D. When S is smooth and well behaved, the profile $T(x, t)$ smoothes out onto scales longer than δx as part of its natural evolution. In these cases the profiles change slowly because they are smooth even though the diffusion coefficient is large. The equation is stiff in the sense that we do not want to compute with $\delta t \sim \delta x^2/D$. We would like to use the much longer computational step, $\delta t \sim L^2/D$, where L is a characteristic scale length of variations in the profile $T(x)$.

In the early stages of a problem where gradients may be steep and the profile may be changing rapidly, short timesteps must be used to calculate the solution accurately. Thus the equation is not stiff during these phases and presents no solution difficulty. If one attempts to use the longer timestep during quick transient phases, the answers obtained are usually wrong. Even in seemingly counter-example cases, the common sense axiom, "You can't simulate physical phenomena whose characteristic times are less than a timestep," applies. Therefore the choice of phenomena which must be resolved accurately has a direct bearing on the cost of a calculation.

Modelling combustion processes requires coupling algorithms which represent many distinct physical phenomena. Since the correct choice of the timestep determines the accuracy and perhaps stability of the solution, the overriding concern is that, for the timestep chosen, one of these processes must not produce a large change in the value of a variable to which another process is sensitive. The chemical reactions must not result in an energy release which increases the total energy in any cell by more than 10-20%. When the chemistry is in a sensitive temperature regime, the hydrodynamics cannot be permitted to change the temperature by too large an amount.

VII.A.1. The Fractional Step and Global Implicit Approaches

Two distinct approaches have evolved for numerically coupling all the pertinent phenomena and their interactions when some or all of the phenomena are stiff. The first of

these approaches, global implicit differencing, has been described in Section V. The Gear method [15] is an example of this approach for pure kinetics problems; the code developed by Lund [31] is an example of a global implicit model in one dimension; and the one developed by Schnack for MHD problems [74] is three-dimensional global implicit.

In one-dimensional magneto-hydrodynamics and plasma physics problems, the global implicit approach has been used for many years [75] and has recently been adapted to detailed reactive flow modelling [31,76]. The "Method of Lines" technique [77] uses forward-differenced implicit solvers of ordinary differential equations (such as Gear) for spatially stiff as well as temporally stiff problems. The fact that these algorithms need to use "artificial" or numerical viscosity to stabilize shocks [33,48,77] indicates that consideration of temporal stiffness alone is not sufficient to produce accurate solutions of important reactive gas dynamic effects.

The second approach is the fractional step method described above. The individual terms, including those which lead to the stiff behavior, are solved as independently and accurately as possible and then coupled together. In this approach, stiffness in the individual governing equations is handled asymptotically rather than implicity. The Selected Asymptotic Integration Method [17] discussed below in Section IV is an example of this approach for kinetics problems with very fast rates. The asymptotic slow flow algorithm [51] for hydrodynamic problems, for which the sound speed is so fast that the pressure is essentially constant, has been discussed in Section V. Timestep splitting techniques can still be used to couple independent stiff phenomena whose individual stability is provided by asymptotic algorithms provided that the overall algorithm ensures that values of the physical variables change slowly over a timestep.

There are tradeoffs between these two approaches. The implicit approach puts maximum strain on the computer and minimal strain on the modeller. For this method, convergence of the computed solutions is easy to test by improving the temporal and spatial resolution. Non-convergence of any particular calculation may be hard to spot since severe numerical damping

has been introduced to maintain numerical stability and positivity. This damping changes the desired profiles quantitatively, although quickly detected qualitative errors are often smoothed out. Solutions may be wrong yet stable.

In contrast, the fractional step approach puts minimal strain on the computer but demands much more of the modeller. The convergence of the computed solutions is usually easy to test with respect to spatial and temporal resolution, but situations do exist where reducing the timestep can make an asymptotic treatment of a stiff phenomenon *less* accurate rather than more accurate. This follows because the technique often exploits the disparity of timescales between fast and slow phenomena. Non-convergence of any particular solution is sometimes easier to spot in the asymptotic approach because the manner in which the solution degrades is usually catastrophic. In kinetics calculations, lack of conservation of mass or atoms signals inaccuracy rather clearly.

The fractional step approach often leads to more modular simulation models than those generated using a global or block implicit approach. Hydrodynamics, transport, equation of state calculations, and chemical kinetics are tied neatly into individual packages. Specialized techniques for enhancing accuracy can be incorporated at each stage and for each physical phenomenon being modelled separately. Since each phenomenon is treated as an independent package, the full spectrum of numerical tricks can be applied.

At this point the pros and cons of the two approaches seem to roughly counterbalance; they have been presented that way purposely. This apparent equity extends to most accuracy criteria as well. If an interesting timescale is not resolved, neither solution method can give detailed profiles of phenomena occurring on that scale. Similarly, to compute spatial gradients accurately, these gradients must be resolved with enough spatial grid points in either type of calculation.

The fact that the fractional step approach demands more prior thought and effort is

counterbalanced by the work that must be done to reduce the computational expense of using the global implicit method. The need to reduce this calculational expense was the motivation for the development of fractional step formulations. For example, solving a set of chemical kinetics equations for M species requires inverting, perhaps repeatedly, a general matrix of size $M \times M$. This involves approximately M^3 operations. In contrast, the selected asymptotic approach (Section IV) to solving the kinetics equations generally scales as M or M^2.

VII.A.2. The Physical Basis of Fractional Step Coupling

As long as the timescales for the coupling mechanisms between two distinct physical phenomena are resolved, the individual phenomena themselves can be treated separately. This means that the stiff phenomena encountered, whether fluid dynamic or chemical kinetic, can be treated as if in a state of dynamic equilibrium for which the lowest order solution is found by setting a time derivative to zero. For chemical kinetics, the production and loss terms in Eq. (IV.1) cancel to lowest order. For fluid dynamics, the divergence of the velocity field is given algebraically rather than resulting from the time integration of a partial differential equation. For diffusion equations, we similarly find that a partial differential equation in time is replaced by a partial differential equation in the spatial variables.

In Section III we demonstrated that for some of the terms in Eqs. (II.1)-(II.12), asymptotic finite difference techniques can be both more efficient and accurate than implicit methods. When physical phenomena are coupled, these same benefits may be gained. Again, the lowest order asymptotic solution is generally more accurate than the corresponding implicit algorithm. The asymptotic solution is also far more stable than the explicit and centered finite difference time integrations because these tend to go unstable when the timestep for coupling is too large. Therefore the fractional step methods, possibly employing asymptotic techniques, follow the true solutions rather faithfully on all the relevant scales. When the spread of timescales is not too large, or when global-integral conditions allow the detailed macroscopic model to "know" the end result of short scale transient phenomena, detailed modelling and the coupling of the

various scales is relatively easy.

Performing these multiple timescale calculations by fractional step methods requires not only that the two scales of interest are separated, but also that there is an intermediate time scale which can safely be used to patch the two solutions of different scale together. At this intermediate scale, one of two conditions must be satisfied to effect a useful simplification. We require that either 1) the macroscopic "outer" solutions and the microscopic "inner" solution should both be accurate, or that 2) essentially nothing of importance to the macroscale occurs on the intermediate scale. In stiff chemical kinetics integrations, as treated in Sections III and IV, both the explicit and asymptotic treatments are sufficiently accurate in the crossover region that stiff phenomena on all scales can be followed accurately. In reactive shock and premixed flame simulations, the second case prevails: neither the macroscopic calculation nor the microscopic calculation is capable of giving information accurately about the intermediate scale but nothing of significance is assumed to happen there. From these considerations another general rule of thumb for detailed modelling emerges: Keep close track on the changes in an detailed structure of the physical variable profiles. Analyzing these changes is necessary because they indicate whether explicitly coupled solutions are being integrated stably, whether asymptotically coupled solutions work, and whether implicitly coupled solutions give the correct answer.

Although we are primarily considering transient, time dependent solutions of the reactive flow equations, it is important to point out that there is an added degree of complexity when one considers the approach to steady state of a dynamic physical system. We would like to take such long timesteps that all the phemonena are stiff and yet the profiles do not change at all. In this particular case a number of specialized techniques have been developed for chemical kinetic, hydrodynamics, and diffusive transport problems based on equilibrium seeking concepts. Global and block implicit techniques are particularly suited to more general problems in this class.

VII. A.3. Explicit Coupling of Fluid Dynamics and Chemical Kinetics

Perhaps the most important example of coupling two phenomena together using timestep splitting is the coupling of hydrodynamic flow and heat release on the explicit timescale. The reactive shock model [40] discussed below in Section VIII is an example of an explicitly coupled reactive flow model in which the fluid motion is frozen while the chemical rate equations are advanced using their own appropriate timestep. This can be done because the need to follow shocks accurately requires the timestep to be smaller than the time it takes for a wave at the local sound speed to cross the computational cells. On this short, explicit timescale, the precise profile of energy release during the timestep is unimportant because in a timestep information cannot propagate out of the immediate region. All of the energy deposited in the system by sources or chemical reactions and all of the energy transported diffusively appears in the energy Eq. (II.4) as local sources and sinks.

Using a new locally elevated pressure, which reflects the additional amount of energy added, the explicit FCT algorithm [6,9] advances all the convective terms in Eqs. (II.1)-(II.4). At the end of a fluid integration step, the new internal energy is found from

$$\epsilon = E - \frac{1}{2}\rho v^2, \tag{VII.2}$$

where E, ρv and ρ have been advanced by the hydrodynamics algorithm. Then the new temperature, which is required for evaluation of chemical reaction rates and diffusion coefficients, is found by iterating an equation of the form

$$\epsilon = h(T,\{n_j\}) - Nk_BT. \tag{VII.3}$$

During a chemical integration step, T is found after the equations are solved for $\{n_j\}$ and it is assumed that the internal energy remains constant for each chemical timestep. This does not mean that the temperature is constant, however. In addition to performing the asymptotic integration of the stiff rate equations discussed in Section IV, the integrator also subcycles the chemistry timestep as necessary to resolve important, short-timescale transients. During these subcycle steps the species densities change and therefore the temperature and reaction rates are

permitted to change.

When only one of a number of competing phenomena which must be coupled is stiff, the explicit approach works well. In fact, straightforward explicit coupling works whenever the quantity being transferred from one form to another, in this case energy, changes by only a small amount per timestep. In the reactive shock model described above, $\sim$20% changes in the local energy density are allowed per timestep whether caused by chemical, hydrodynamic, or diffusive effects. Large changes per timestep in the density of some or all of the species are permitted as long as these changes do not appreciably affect the energy density.

VII. A.4 Asymptotic Coupling of Fluid Dynamics and Chemical Kinetics

Special care is required in coupling the various kinetic, diffusive, wave and convective terms of Eqs. (II.1)-(II.4) when two or more distinct phenomena are stiff at the same time. Since both chemistry and sound waves are usually stiff in the flame propagation problem, such a difficulty arises in coupling the chemical heat release to the fluid dynamics. The overriding principle as given above is always that the macroscopic variables should change by a controlled amount (10-20%) in each timestep. In a flame problem, timescales are much longer than in a shock or detonation problem. Thus diffusive effects are important and may border on being stiff in regimes such as the flame front where fine resolution is needed.

Since the chemical energy released in a flame goes primarily into fluid expansion, there is not as much of a local temperature increase as there would be if fluid dynamic expansion were completely prohibited. Allowing all the heat to appear locally as temperature in a flame calculation results in unrealistic fluctuations in the physical variables. This particular coupling difficulty is overcome by evaluating in each timestep the change in pressure which would occur at constant enthalphy, but not allowing this energy to heat the fluid during the kinetics part of the calculation. Unlike the shock case where the sound speed is slow, the pressure created in flames due to energy release is quickly removed from the vicinity of its generation by fast but

low amplitude sound waves. When the sound speed is smaller or the flame speed is larger, the timestep must be reduced in order to insure that the flame propagates at substantially less than one cell per timestep. The result is to reduce the hydrodynamic stiffness of the problem.

As an example of how this coupling is effected in the detailed model of the flame, we describe the method used by Oran and Boris [78]. This model uses a one-dimensional Lagrangian fluid dynamics module, ADINC [55], which is stable for timesteps much longer than the Courant sound speed timestep limit. ADINC requires consistency between local pressure as computed from the hydrodynamics and the pressure arising out of changes in density and temperature as constrained by the equation of state. The algorithm also assumes that pressure and density are constant within each individual finite-difference cell and that the physics is evolving slowly enough for full communication across that cell to have occurred in a timestep. For very long timesteps, ADINC reproduces the low order slow-flow asymptotic result in one-dimension, but it is capable as well of following smooth, large amplitude sonic pulses.

In a flame calculation, hydrodynamic expansion and diffusive transport relieve the pressure from the flame region as fast as it is generated. Thus the pressure stays effectively constant. Small pressure fluctuations, $\sim O(v^2/c_s^2)$, do exist and are just large enough to drive the flows which reapportion the energy released by chemistry or transported by diffusion hydrodynamically. The chemistry step should be taken at constant pressure, but it may also be taken at constant volume with the temperature held fixed if the profiles only change slowly per timestep.

At the completion of the chemistry integration, the heat release is converted to an effective pressure change at constant volume because the cell volume has been held fixed during the chemical kinetics calculation. This pressure change is then used as an energy source term for the hydrodynamics timestep to get the correct fluid expansion. In practice this is done by modifying the cell entropies used in ADINC to reflect chemical heat release. At this point thermal conduction and diffusion heat fluxes also contribute changes to the entropy.

The hydrodynamics algorithm governs the local expansions and compressions of the fluid needed to bring the pressure back to a near constant value which is consistent with boundary conditions and inertial hydrodynamic time-lags. The final temperature is evaluated after the independent calculations are complete because the density in the flame front has decreased at constant pressure.

This asymptotic timestep-split approach to coupling the several terms works here because none of the macroscopic profiles is permitted to change extensively during a timestep. Even though diffusion, chemistry and hydrodynamics may be all independently stiff, the flame front itself is not allowed to move more than a modest fraction of a cell per timestep. This necessary restriction reappears throughout detailed modelling and permits the modeller to be relatively cavalier about when and where many of the intermediate quantities are evaluated. As long as all the stiff effects, whatever they are, are summed in a physically correct manner so that near cancellation of large terms is permitted, the overall macroscopic calculations can be performed on the long timescale. However, when fast transients occur and are important to a description of the flow, the calculation must be performed on this timescale or the results will not be accurate. During a properly resolved fast transient, the governing terms are not stiff because the timesteps have to be short to ensure accuracy.

VII.A.5. Some Other Asymptotic Coupling Applications

There are many cases in which the details of the subscale processes may preclude the direct solution of the macroscopic problem in the macroscale alone. In contrast to the example given above, there are physical phenomena on fast timescales whose "dynamic equilibria" cannot be entirely expressed in terms of approach to a quiescent, slowly varying macroscopic state. Additional information is needed which cannot be entirely derived from the solution of the slow timescale problem. To model these situations on the longer scale, we must either solve the short scale problem analytically or develop a calibrated, phenomenological prescription. The resulting subscale model may then be coupled to the slowly varying macroscopic model at the

point where the subscale physical phenomena are important. We shall describe several examples from this difficult category of reactive flow problems and propose possible ways of approaching them.

Chemical Kinetics: The Thermodynamic Equilibrium Assumption

When complicated systems of chemical or atomic reactions and species are required to describe a system, computations are greatly simplified if we can assume that thermodynamic equilibrium exists. In chemical combustion, this allows us to define an equilibrium enthalpy for the system which summarizes the fact that there is a Boltzmann distribution of states of the molecules. We then define a chemical rate constant which summarizes the possible behavior of an ensemble of molecules of one type which are in a Boltzmann distribution.

This simplifying assumption, however, is not always valid. We often find that a particular rate will appear to vary in form from experiment to experiment because of non-equilibrium conditions within the molecule. An energetic reaction, for example, may leave one of the products in an excited state which thus changes the likelihood that the product will undergo a second reaction. Measurement of this second rate would show anomalous dependences on system parameters which cannot be explained in the context of the given reaction scheme with standard rate formulae. Additional physics and hence degrees of freedom are needed. When the system is mostly out of thermodynamic equilibrium, as in the case of a chemical laser, the individual states of a molecule must be treated as separate species. If just a few states are out of equilibrium, it is possible to include a density dependence or a collisional de-excitation submodel in the macroscopic system to provide the needed information.

Propagation of a Reacting Shock

When the temperature and pressure conditions in a combustible mixture behind a shock front are appropriate, the gas burns right behind the shock because the chemical induction time will be very short. For example, a mixture of hydrogen and oxygen may release substantial

energy in a microsecond or less when heated instantaneously to 2000°K. In a typical case in which a shock is travelling at $\sim 10^5$cm/sec, the very narrow burnfront may be separated from the even narrower shock by less than 1 mm. In treating a macroscopic problem where the shock traverses many meters of distance, it may be necessary to treat this shock-burnfront region as a single gas dynamic discontinuity whose internal structure may be ignored on the macroscale.

One would like to treat the interface as a discontinuity whose jump conditions are known a priori. Then, as with the Rankine-Hugoniot relations for an ideal shock, the downstream and the upstream conditions can be related unambiguously using the macroscopic continuity equations integrated across the jump. Unfortunately, more complex compound reactive flow discontinuities such as a shock followed by a burnfront often require more information than is carried in the macroscopic solution alone. Suppose a stable reaction product is formed only between the shock and the burnfront. Then long after the interface has passed the density of this species will depend on the structure of the discontinuity. Again, additional microscale information is needed.

If we assume that a methodology exists to propagate an arbitrary discontinuity in the macroscopic flow, the two distinct timescales can be separated. This asymptotic multi-timescale separation is valid when the jump conditions across the compound discontinuity vary slowly as functions of the evolving macroscopic upstream and downstream states. Then, given the conditions in front of and behind the discontinuity, a localized short duration shock-burnfront simulation can be performed to calculate the instantaneous rate of progress of the discontinuity and the amount of heat released. These additional quantities can be coupled to the macroscopic calculation. Thus physically correct variations of the upstream and downstream states can be computed on the macroscale allowing the overall coupled calculation to proceed.

Propagation of a Flame Front

Since the flame speed is usually slow compared to the sound speed, flames also present multiple timescale difficulties beyond the simple considerations of the fast kinetics and fluid dynamics in a thin flame zone. In an enclosed chamber there are a number of natural resonant frequencies for sound waves which occur at much higher frequency than we would like to resolve. Again, asymptotic techniques can help in developing a model on the macroscale which contains at least some of the effects of these sound waves. As long as these oscillations are much higher in frequency than other phenomena of interest, it is possible to average over the oscillations so that high frequency phase information is lost. Then the wavelength, frequency, and wave energy, all of which vary slowly, become the relevant macroscopic quantities. Since the reaction rates in the flame are generally increasing functions of temperature, the reactions can be expected to increase more during the pressure peak of the wave than they diminish during the troughs. Thus a net increase in flame speed might be expected from oscillations.

Turbulence

The most difficult multi-scale problems are those for which neither the slow, macroscopic solution nor the high frequency submodel contain useful information about the intermediate timescales, and yet important phenomena are taking place on these intermediate scales. Turbulence, particularly reactive flow turbulence, is such a multiple timescale phenomenon. A discussion of various approaches to the detailed modelling of turbulence is reserved for Section X of this paper.

VII.B. Dealing With Multiple Spacescales: Adaptive Gridding

In Section II we showed how the computational cost of a problem could be related to the area which the calculation has to span in the logarithmic $x - t$ space of Fig. II.2. The larger the span of space or timescales, the more expensive the calculation. Thus, reducing either the number of timesteps used to perform a calculation or the number of spatial grid points used in

the spatial representation is effective in reducing the cost.

VII.B.1 The Current Status of Adaptive Gridding in Reactive Flows

The previous discussions in this section have stressed that any phenomenon which cannot be resolved adequately cannot be calculated accurately. To minimize cost and maintain accuracy in temporally stiff integrations, we want to take longer timesteps only when key variables are changing relatively slowly on the timescales we wish to resolve. Stiff spatial problems, those with localized steep gradients, must be treated in an analogous way. In this case, however, the roles of time and space are interchanged and the numerical method used is called "adaptive gridding." Small cell sizes are only used where the solution shows steep spatial gradients in just the same spirit as short timesteps are used when the solution varies quickly. The result is that the small cell sizes impose short timesteps due to the stability criterion which relates δx and δt.

Refined localized gridding techniques for boundary layers in steady state calculations have been used for many years [79]. More recently, fluid dynamic calculations have been developed in which the locally adapted grid moves with the fluid regions requiring fine resolution. Detailed modelling of coupled chemical kinetic-fluid dynamic systems is an even more recent discipline and requires more general approaches to the multiscale problem than have previously been attempted. In recent efforts at numerical modelling of unsteady flame propagation, adaptive gridding procedures have depended on an ad hoc criterion related to local temperature gradients to determine where the finely spaced zones are required [78,80,81]. Currently more general formalisms are being developed for placing the adaptive grid nodes according to a variational finite element formulation. For example, a variational principle may be established to minimize an error defined for the system of equations being solved. The work to date on this approach has also concentrated on model problems but the results are encouraging [82]. However, the generalization of finite element approaches to a full reactive flow combustion problem seems to be prohibitively expensive.

VII.B.2. Adaptive Gridding in Eulerian and Lagrangian Representations

The methodology of adaptive gridding in the Eulerian and the Lagrangian representations is intrinsically different. In Eulerian calculations, a continuous sliding rezone method can be used where the cell interfaces and the fluid move. Lagrangian calculations require discontinuous injection and removal of cell interfaces.

As an example of an Eulerian case consider the reactive shock model [40] for which a general adaptive gridding procedure was developed which takes advantage of a sliding rezone capability. Thus the calculation automatically follows a shock front for which enhanced resolution is required. The region immediately around the shock front and for predetermined distances on each side is gridded with fine, evenly spaced cells. The fine spacing transitions smoothly into the more coarsely resolved region. As the shock moves along the length of the tube, the finely-spaced region is programmed to move with it and may reflect off the boundary wall. The condition on the acceleration,

$$\left| \frac{\Delta P}{\Delta r} \right| \frac{1}{\bar{\rho}} = \text{maximum},$$

was found to be adequate for locating the shock front, where P is the pressure, r is a generalized position coordinate, and $\bar{\rho}$ is an average mass density. In principle there can be any number of finely-spaced regions.

In a Lagrangian fluid calculation, adaptive gridding is still necessary but the procedure is more complicated than in the Eulerian case. While the Lagrangian framework itself provides some natural concentration of grid points in regions where the fluid is compressing, there are situations such as a flame where fine resolution is required but the fluid is expanding. A fundamental problem exists in that it is not obvious how to arbitrarily concentrate grid points in a Lagrangian calculation and still maintain the non-diffusive advantages of using this representation. For the example of a flame front, the region requiring the fine resolution actually propagates through the fluid rather than with it. Forms of continuous re-gridding applied to

Eulerian calculations involve algorithms which are numerically diffusive, and to some extent the grid always moves through the fluid.

In order to avoid the problems of a diffusive grid in a Lagrangian calculation, a method has been devised for which existing computational cells can be subdivided or merged. The addition or subtraction of one or more cell interfaces can be effected without causing numerical diffusion through any of the already existing interfaces. Criteria are programmed so that this process is done automatically in a way which adapts to the resolution needs of the evolving solution. The bookkeeping for this method is complicated since the number of grid points changes and the location in computer memory of data referring to a given physical point in space also changes as cells are subdivided or removed. This method is currently being used in transient flame simulations [78].

VII.B.3. The Future of Adaptive Gridding

In most finite difference and finite element calculations where a time evolution equation is being solved, the timestep chosen for the calculation, δt, does not vary as a function of position. Each grid point is integrated in lock step and hence the concept of a time level is well defined. However, the timestep is usually small everywhere using a single δt because it usually has to be small someplace on the grid. If each cell could be integrated using a different timestep, the total number of point-steps for the calculation could be reduced. Thus in a flame calculation, small space and time cells could be clustered only along the advancing flame front.

Although having a δt that depends on location reduces the number of point-steps required, a serious premium is paid because of the great computational complexity introduced. One might imagine using an evolving triangular grid in $x-t$ space. Then the variable connectivity of the grid could be used to allow for initiation and termination of cell interfaces as well as the greatly disparate timesteps in adjacent cells. Such an approach would incorporate many of the ideas and algorithms for dealing with relativistic fluids and plasmas developed earlier and

undoubtedly will be tried eventually.

There is another, perhaps simpler, adaptive gridding option which would reduce the total number of point-steps needed for the calculation much further than the variable $\delta t - \delta x$ approach described above. This approach depends intrinsically on there being two distinct space scales and is called "intermittent embedding" of an adaptive grid. Thus a finely gridded region is embedded in the macroscopic calculation at intermittent timesteps. This is done often enough to update the properties of the finely spaced region. These properties (jump conditions, flame speeds, etc.) are then used as interior boundary conditions for the coarsely spaced macroscopic region.

Since the region which requires resolution is only resolved and followed during a small fraction of the time, a method of connecting and disconnecting this portion of the grid must then be developed. Furthermore, when the fine grid for the flame front is disconnected, a method for retaining the discontinuity in the coarsely resolved calculation will have to be found. This latter requirement is clearly problem dependent. Thus, for example, a shock will have different jump and conservation conditions than a flame front.

VII.C. Conclusion to the Gedanken Flame Calculation

Using the information discussed so far in this section and in Section V, we now return to the gedanken flame experiment described in Section II with the idea of modifying the numerical methods in order to reduce the computational cost. The problem is to calculate the propagation of a flame front as it crosses a one meter tube using a one-dimensional geometry and given a fixed, detailed chemical reaction rate scheme.

First, we recognize that we are interested in calculating a flame front moving at less than the local sound speed. Thus either a slow flow approximation or any method which treats pressure implicitly would eliminate the sound speed criterion on the timestep. By using the asymptotic slow flow technique described in Section V, and still assuming a uniform grid spacing, the

number of point-steps is reduced from 10^{14} to 10^{11}. Thus the computational time required is reduced from 3000 to 3 years!

But this is still atrocious, and we must now face the problem of eliminating unnecessary grid points by adaptive gridding algorithms as discussed above. Suppose 100 cells of 1 cm length are used and the region surrounding the flame front is finely gridded with 100 additional cells of 10^{-3} cm length. The timestep is still governed by the smallest cells, but by now only 200 cells are needed rather than 10^5. The saving, about a factor of 500, reduces the computational time to 2×10^8 point-steps, or about two days.

Finally, consider performing this calculation using the possible, but as yet unexploited, technique of adaptive intermittent gridding. Now assume that 100 cells are needed to resolve the flame zone. Further, 100 short timesteps are enough to resolve changes in the flame zone brought about by the relatively slowly changing, outer boundary conditions. During the imbedded calculation, the flame front moves only 10 of the fine zones. This is sufficient to determine flame speed and boundary conditions to be used in the coarsely spaced calculation. The imbedded calculation may be done once in each large cell. Thus a total of $100 + (100 \times 10) = 1100$ seconds of computational time is required for the large scale simulation.

This example has illustrated the importance of using the appropriate algorithm as constrained by considerations of the actual problem that must be resolved. It has further illustrated how much may be accomplished by developing the methods of adaptive gridding. One point that has not been mentioned, however, is that much of the cost of a detailed reactive flow calculation is in the integration of the ordinary differential equations describing the chemical kinetics. Using the latest asymptotic techniques, the picture painted above improves by a factor of two to four. But further improvements in the integration time of ordinary differential equations without sacrificing accuracy is certainly an area where development is needed.

VIII. SUPERSONIC REACTIVE FLOWS

In detailed modelling of supersonic reactive flows, we face a number of difficulties which differ from those encountered in modelling the subsonic reactive flows described below in Section IX. These difficulties arise because we must solve continuity-type equations when discontinuities and sharp gradients are present. We also have found that the fluid dynamics portion of the calculation must be extremely accurate because the chemical reaction rates may vary strongly at high temperatures. Thus errors in the calculated energy release may be very sensitive to relatively small fluctuations in calculated temperatures.

The calculational time-step for the fluid dynamics part of the calculation is usually constrained by the local Courant condition in the vicinity of any shocks which form. This limit is approximately equal to the speed of sound in the material divided by the local cell spacing. Unlike the subsonic flows, we cannot average out small scale sound waves by taking advantage of any of the smoothing effects due to a virtually constant pressure. Generally it is these sound waves and their interactions we wish to follow.

Every numerical technique for treating shocks and discontinuities has its own set of advantages and problems, and most of these center around accuracy and generalizability of the method. Thus some specific problems may be solved with great accuracy by a specialized method, but there are usually severe limitations and unanswered questions regarding one's ability to generalize the method. In order to construct accurate detailed models of supersonic reactive flows, the algorithms employed must be versatile enough to include a broad range of physical and chemical processes. We must be able to solve the complete set of Eqs. (II.1)-(II.12) when discontinuities are present. We must be able to couple complicated finite rate chemistries, diffusive transport, and variable initial conditions, boundary conditions, and equations of state to multi-dimensional equations including the compression and advection terms. To date, finite difference solutions of the conservation equations have proven the most versatile because they are most easily extended to multi-dimensions and most easily generalized to incorporate

diffusive and chemical processes.

In this section, we describe a few of the many calculations reported in the literature. This is by no means meant to represent an exhaustive summary of all the work performed. The first set of examples use a single step reaction rate and prescribed energy release. The section is concluded with a description of a detailed reactive shock model and some calculations which have been made using it. In all of the specific examples discussed in this section, we stress of first testing the method in well-understood limits.

VIII.A. Supersonic Flows with a Model Energy Release

Obtained adequate resolution is a problem that confronts anyone attempting to model supersonic reactive flows numerically. We must balance what our purses allow us to calculate against what we know we could calculate given more resources. Because of this resolution problem, there have been very few research groups actually calculating supersonic reactive flows and most of these groups have restricted their consideration to the fluid dynamic flow with a simple model for energy release. Calculations performed using a model energy release do, in fact, tell us a lot about the way in which added energy interacts with the fluid flow. Such calculations have helped us to understand a number of curious phenomena concerning, for example, the stability of a detonation or the properties of blast waves.

In the remainder of Section VIII, we describe the work of several researchers who have numerically modelled supersonic reactive flows. These are excellent examples of the application of numerical methods in that all of these examples, the authors have gone to great lengths to calibrate and test their models against both analytic theory and other independent calculations. This is the important first step which gives them both confidence in the numerical solution and an understanding of the limits of the model. The authors then extend their calculations to regimes for which there is no analytic solution or no previously attempted calculation.

Perhaps the classic supersonic calculations with a simple energy release were related to the results of the linearized stability analysis performed by Erpenbeck [83] on the steady state solution of a three-dimensional cartesian detonation. Specifically, Erpenbeck's analysis was for an overdriven detonation in a material described by a polytropic-gas equation of state and for a heat release that could be described by one reaction with an Arrhenius type rate. Diffusive transport effects were, of necessity, neglected. Thus the problem was analyzed in terms of several parameters which included a heat release Q, an activation energy, E^*, and the degree of overdrive of the detonation, f, which relates the piston velocity to the Chapman-Jouguet velocity characteristic of the gas. Erpenbeck concluded that the steady state solution was unstable to infinitesimal three-dimensional disturbances over a range of finite transverse wavelengths and *also* to one-dimensional, longitudinal, perturbations. This analysis indicated that the part of the parameter range for which instability can occur could represent a real systems.

Such a stability analysis says nothing about the long term evolution of the unstable flow which it predicts. This kind of information must be obtained from numerical solutions of the time-dependent equations describing the system. Fickett and Wood [84] have studied the one-dimensional problem for several sets of parameters around the predicted stability boundary (Fig. VIII.1). Their calculations use the method of characteristics in which shocks are treated as jump discontinuities and diffusive transport effects are neglected. The geometry is cartesian so that the system may be described as a semi-infinite slab of initially unreacted material which is bounded at one edge by a piston, or a moveable plane. An overdriven shock is generated by moving the piston at a velocity which finally becomes constant at a value greater that the Chapman-Jouguet velocity of the material.

The results of these calculations for fixed Q and varying E^* and f agreed very well with the predictions of the theoretical analysis. The numerical simulations showed that in the stable cases, the time-dependent solution eventually approached the steady solution. In the unstable cases, the driving piston prevented the detonations from dying out, so that oscillations in the

shock front pressure were predicted. These oscillations grew rapidly and reached a peak maximum of about 50% about the stable solution. After a long time into the calculation, the observed fluctuations in the amplitude of the oscillations may have been caused by earlier oscillations which were reflected from the piston and then overtook the shock front. (In real detonation experiments, it has been observed that the oscillations may be so large that the detonation periodically dies out and then re-ignites. In these cases diffusive transport effects might be very important.)

Time-dependent calculations testing the Erpenbeck predictions have also been performed by Mader [85] using a finite difference method. In this extensive study, Mader compared solutions for which he 1) used different numerical methods, 2) varied the equation of state, and 3) varied the dimensionality of the disturbances so that both longitudinal and transverse perturbations were allowed.

Figure VIII.2 shows the results Mader obtained for the parameters ($Q = 50$, $f = 1.6$, $E^* = 50$). The calculations were performed with a one-dimensional Lagrangian code and two-dimensional Eulerian and Lagrangian codes and then compared to the results of Fickett and Wood. The long-time results were, in fact, independent of both methods of solution and of how the pertubation was initiated. In general, Mader's calculations verified the results of Erpenbeck for both longitudinal and transverse perturbations.

After having made these tests of his numerical method, Mader then studied the effects of such perturbations on overdriven detonations in nitromethane and liquid TNT. For these cases, the detonations showed the same stability properties to both transverse and longitudinal perturbations as they did to longitudinal perturbations alone. That is, two-dimensional perturbations in these materials did not grow, but decayed into one-dimensionally perturbed flows. As in the ideal gas case, a sufficient amount of overdrive stabilizes the detonations.

The numerical models developed and tested for detonation stability problems are now

used extensively to study detonations in condensed materials [86]. But the instability calculations themselves are extremely important because they show that real detonations of both condensed and gaseous materials may exhibit this oscillatory behavior which cannot be described by steady-state Chapman-Jouguet theory. Furthermore, as Mader has shown, the details of the chemical kinetics and equations of state are crucial to the stability behavior. Both transverse and longitudinal disturbances have been observed in real gas detonations [87]. The disturbances have been made to disappear by sufficiently increasing the amount of overdrive. Observed longitudinal disturbances may be so large that the detonation dies out and then starts again in a periodic way.

Taki and Fujiwara [88] consider gas phase detonations in two spatial dimensions. They employ a simple induction time model developed by Korobeinikov, et al. [89] to approximate the chemical induction and heat release phases of reacting oxy-hydrogen systems. Two scalar parameters are defined which are convected with the fluid. One of these, the induction time parameter , records at the instantaneous local temperature and density the fraction of a chemical induction time remaining before energy begins to be released. The second parameter records the fractional burnup of the fuel and hence the local heat release after a full induction time for the chemical reaction. Calculations of transverse instability of the detonation front were carried to their full nonlinear limit using an explicit first order method due to Van Leer [90]. Good agreement was obtained with equilibrium triple shock spacings measured by Strehlow, et al. [91] for argon and helium diluted oxy-hydrogen systems.

Another set of detonation calculations with a model energy release has been made by Phillips [92] in an effort to understand fundamental properties of unconfined vapor cloud explosions. The questions of importance here are: 1) how does an explosion develop in a vapor cloud, 2) what are the characteristics of the blast wave which propagates beyond the limit of the vapor cloud, and 3) what are the effects of obstacles which cause asymmetries in the explosions. Quantitative answers to these questions would increase our understanding of and ability

to prevent accidental explosions of flammable materials [93].

In order to begin to address these problems, Phillips developed a one-dimensional spherically symmetrical model based on the FCT algorithms discussed in Section V. A source term was used to describe energy releases which were either instantaneous (at $t = 0$) or representative of a detonation in which all the heat is released when a prescribed ignition temperature was reached. Figure VIII.3 shows comparisons between a test calculation and the self-similar solution by Taylor [94]. The theoretical and calculated pressures are in fact very similar, although the calculated pressure at the detonation front does not reach the theoretical value. This value would be improved substantially by increasing the resolution at the detonation front.

Calculations of the decay of a blast wave after detonation of a vapor cloud are shown in Figs. VIII.4, 5, and 6. The cloud is assumed to be spherical, in a uniform atmosphere, and ignited at the center. The gas is assumed to be a typical hydrocarbon-air mixture which has a final temperature of 1900°K after combustion. Detonation starts immediately on ignition and ends at the edge of the cloud. Spreading of the peak pressures are again observed, as in the test case shown above. The curve in Fig. VIII.4 marked 0.0115 sec shows all the mass in the system moving outwards so that the central pressure and density are reduced. Figure VIII.5 shows that at a later time there is an implosion and the pressure at the center jumps to 4 atmospheres from a minimum of 0.095 atmospheres. The 4 atm value would increase if there were greater resolution allowed at the origin. Figure VIII.6 summarizes the time history of the pressure at the center of the implosion. The early peak at about 0.01 seconds in believed to be spurious and resulting from initial numerical transients.

VIII.B Supersonic Flows with Detailed Chemistry

The transonic flow over a re-entering nose cone is one type of reactive flow problem that has been modelled successfully. In this problem, the mean free path is long but the fluid approximation is still valid. Furthermore, real diffusion effects are large enough so that numer-

ical diffusion is not a problem. Widhopf and Victoria [95] have developed a two-dimensional model which uses the explicit leapfrog/Dufort-Frankel scheme for the partial derivatives. An implicit formulation is used for the seven species, six reaction detailed chemistry. A major conclusion to be drawn from this early success is that fast chemical reactions can be handled independently of the slower timestep hydrodynamics provided variations in energy due to chemical reactions are small.

The model developed by Oran, Young, and Boris [40] was designed to handle the large local energy releases typical of combusion. The model includes the effects of a complex chemical reaction scheme as well as accurate diffusive transport properties. The model was designed to study transient phenomena, the way in which a perturbation on the system alters the steady state, the effects of non-ideality of gases, and the way in which the release of chemical energy alters hydrodynamic flow. This model is based on a number of the numerical algorithms discussed in previous sections. These include

1) Flux-Corrected Transport (Section V) to treat discontinuities accurately with minimal numerical diffusion and no artificial viscosity,
2) A sliding rezone (Section VIII) which inserts finely gridded regions where resolution is required,
3) The Selected Asymptotic Method [17] for solving sets of stiff ordinary differential equations (Section IV),
4) Time-step splitting (Section VII), and
5) The expansion method for diffusion fluxes (Section VI).

Simulations have been performed modelling a shock tube in which a diaphragm is burst at the onset of the calculation. Typical initial conditions are shown in Fig. VIII.7. The calculation is started by assuming that the temperature has equilibrated across a diaphragm which separates regions of differing pressure and composition. The relatively simple H_2–O_2 combustion system has been chosen as the reactive gas mixture and is described by about forty chemical reactions.

Then the model calculates as a function of time and space the evolution of the temperature, and the densities of eight reacting species H_2, O_2, H_2O, H, O, OH, HO_2, H_2O_2 and any inert materials present.

The calculation outlined above was first tested against the results obtained from a solution of the Rankine-Hugoniot equations for an ideal gas in cartesian geometry with no diffusive transport or chemical reactions occuring. Such a solution is given in Table VIII.1, and some comparisons with the calculation are given in Table VIII.2.

The model was then used to study a shock propagating in a reactive medium. Two cases are described below: one in which the chemical energy is released quickly enough to alter the properties of the shock, and another in which the shock is reflected from a rigid wall. At the onset of the calculation, the diaphragm is removed and the helium driver fluid begins to move into the low density region. The five distinct regions described by Table VIII.1 are clearly differentiated at about $\sim 1 \times 10^{-5}$ sec. By then the formation of a shock front, contact discontinuity, and expansion fan are clear. By about 2×10^{-5} sec the fluid flow has settled down and looks very much like the ideal pattern. Until enough time has elapsed so that energy release is substantial, the fluid motion is relatively unaffected by the chemistry.

Figure VIII.8 shows the temperature profile after $\sim 1.34 \times 10^{-4}$ sec. At this time the shock front is located at 40 cm down the tube. The different regions are clearly separated in the calculation and the energy released by chemical reactions has noticeable effects on both the shock speed and the shape of the shocked region. The dashed line marks the corresponding temperature profile for the ideal non-reacting fluid calculation. An increase in the temperature at the back of the shocked region, where most of the chemical reactions have occurred, is clearly visible. The calculation also shows a broadening of the region surrounding the contact discontinuity due to diffusion of the helium driver gas into the reactive mixture. The effect of this temperature decrease is apparent in Figs. VIII.9 and VIII.10.

Figure VIII.9 shows the total densities corresponding to the temperatures shown in Fig. VIII.8. As one might expect, the high temperature regime corresponds to a low density regime in the shocked region. We note that both temperature and total density can vary by as much as a factor of two in the shocked region, whereas the pressure variation is at most about 30%. The calculated fluid velocity has not been shown since it varies at most by 10% from the solutions presented in Table VIII.1.

Figure VIII.10 shows the number density of H_2 and O_2, the chain centers, and the product H_2O as a function of location along the length of the tube at 1.47×10^{-4} sec. If we were looking at a case where the temperature were uniform across the high temperature region (i.e., large amounts of diluent present), we would expect the H_2O peak to be in front of the OH peak. In such a case the spatial difference between the peaks would be analogous to the temporal separation between peak OH formation which precedes the maximum product formation in a homogeneous reacting gas mixture. Looking for this effect in the highly exothermic case we are studying can be misleading: here we have to consider both kinetic and fluid dynamic effects. The high OH densities indicate that combustion is occurring between about 36 and 38 cm. This is in agreement with the high temperatures shown in Fig. VIII.9. The unreacted H_2 and O_2 near 35 cm is in the cool region near the contact discontinuity into which helium has diffused.

The second part of the problem discussed is that of a shock reflected off of a rigid wall. Many shock tube experiments are designed to take advantage of the relatively uniform regime near the wall behind the reflected shock. The temperature and density are further elevated here and the fluid velocity is essentially zero. Thus there is a period of relative calm that can be used to watch reactions develop. We look at the same shock as described above and set the wall at 50 cm.

For this problem the results are presented differently. It is assumed that there is a "hole" 1 cm from the reflection wall, at 49 cm, from which the fluid may be monitored. Figure

VIII.11 shows how the temperature at this location changes as a function of time. When the shock passes 49 cm, the temperature jumps to about 2300°K. The temperature stays at this value until the reflected shock passes over this position again. Then the temperature increases to about 3500°K and the pressures increases by a factor of about three. These increases are consistent with what is expected from a solution of the jump conditions for an ideal shock reflected from a wall. The calculated fluid velocity behind the reflected shock is not exactly zero, but it is several orders of magnitude less than the $\sim 10^5$ cm/sec characteristic of the fluid before it is reflected from the wall. As described above, these finite amplitude sound waves, generated in the process of reflection, decrease in amplitude as this region expands.

Once the reflected shock reaches the low temperature region behind the original contact discontinuity, a large amplitude wave will propagate back to the wall and modify the uniform pressure and temperature region. In the case described above, we have a region of low temperature (60°K), high density material (1.6×10^{-4} g/cm^3) moving into a region of high temperature (2300°K), and lower density (1.0×10^{-4} g/cm^3). For a long shock tube, where the shocked region has spread out over a large distance, there can be a substantial time when the reflected high temperature region persists. Then, except for the small finite amplitude sound waves which are present even in experimental situations, the medium can be considered at rest.

Recently this model has been extended to two-dimensional detonation calculations [96]. In order to avoid the expense of integrating a large number of ordinary differential equations representing the chemical kinetics on every spatial grid point, an induction parameter is defined. This quantity is convected with the fluid and tells how long a fluid element has been heated. When the fluid element has been heated for the chemical induction time of the material, energy is released. This model was used to study detonations in hydrogen-air and methane-air systems and was calibrated against a one-dimensional calculations which used a full detailed chemical reaction scheme.

Table VIII.1. Ideal Shock Solution

Region	1	2	3	4	5
Pressure (dynes/cm^2)	1.056×10^{7}	RAREFACTION	1.951×10^{5}	1.951×10^{5}	1.056×10^{4}
Density (g/cm^3)	1.076×10^{-3}		1.557×10^{-4}	2.314×10^{-5}	5.118×10^{-6}
Velocity (cm/sec)	0.0		1.675×10^{5}	1.675×10^{5}	0.0
Temperature (°K)	300		60.3	1216	300.0
Sound Speed (cm/sec)	1.016×10^{5}		4.571×10^{4}	1.089×10^{5}	5.388×10^{4}
Molecular Weight (amu)	4.0		4.00	12.0	12.0
Gamma	1.667		1.667	1.40	1.40

Shock front velocity	1.051×10^{5} cm/sec
Contact discontinuity velocity	1.675×10^{5}
Rarefaction foot velocity	1.218×10^{5}
Rarefaction front velocity	-1.016×10^{5}
Mach number	4.00

Table VIII.2. Shock Front Position

TIME (sec)	SIMULATION (cm)	ANALYTIC (cm)	DIFFERENCE Δ
0	9.5 ± .025 cm		
1.114×10^{-5}	12.15	11.88	.35
2.2313	14.80	14.43	.37
3.550	17.43	17.07	.36
4.822	20.07	19.80	.27
6.101	22.68	22.52	.16
7.305	25.27	25.09	.22
8.446	27.82	27.52	.30
9.558	30.27	29.89	.58
1.067×10^{-4}	33.09	32.25	.34
1.181	35.71	34.70	.31

$V_{SF} = 2.1336\times10^{5}$ cm/sec

IX. SUBSONIC REACTIVE FLOWS

Subsonic reactive flows, in which characteristic flow velocities of interest are very much less than the speed of sound in the reactive medium, are usually treated computationally by either solving the pressure equation implicitly or treating the pressure as constant. A number of approaches to this problem have been discussed in Section V. In the past few years a number of one-dimensional flame models have been developed. Each one seems to employ a different numerical method or combination of methods at various levels of approximation. Computational efficiency and cost may vary by at least an order of magnitude. And all of the techniques reported appear to give answers which are in reasonable agreement with existing experimental observations.

The work described in this section is not intended as a review of all of the literature on detailed modelling of laminar flames. Instead, as in Section VIII, we have selected a number of examples of calculations which show how a detailed model may be used and what specifically can be unraveled from the reams of computer output obtained. Thus this section has been divided into four parts. First we summarize the work of Kooker [76] who studied a hydrodynamic effect, acoustic oscillations generated by a confined premixed flame. The discussion then proceeds to a number of examples by Heimerl and Coffee [97], Warnatz [98], Tsatsaronis [99], and Westbrook and Dryer [100] who used detailed models to extend knowledge of chemical kinetics. The work of Oran and Boris [78] is discussed as an example of how detailed modelling may be used to study and expand the validity of an analytic model. All of the above-mentioned discussions use one-dimensional models. The status of two-dimensional detailed models is then discussed and examples are given from the work of Kansa [101], Butler and O'Rourke [102] and Jones and Boris [59].

IX.A. Acoustic Oscillations in Confined Flames

It is known that a confining geometry influences the behavior of a combustion system

apart from any chemical effects occurring at the walls. This problem was studied by Kooker [76] using a detailed one-dimensional model of a homogeneous mixture of an O_3-O_2 gas. The calculation simulated a closed chamber heated at one end for a fixed amount of time until a flame was ignited and began to propagate across the system.

Figure IX.1 [76] shows simultaneous profiles of temperature, atomic oxygen mass fraction, and density distributions for a flame propagating in 20 mole % O_3 in O_2. Comparing Figs. IX.1A and B shows that there is a pronounced maximum in the atomic oxygen just downstream of the strongest temperature gradient. This was attributed to the fact that the flame speed is fast compared to the recombination rate of atomic oxygen, and thus a reservoir is formed behind the flamefront. The densities of atomic oxygen are, in fact, many orders of magnitude higher than those that would be computed from an equilibrium thermodynamic calculation. Due to the confinement, the density and temperature increase ahead of the flame. This compression of the reactants results in an increase of the rate of energy release, which causes a steepening of the temperature gradients at the flamefront, and results in a net acceleration of the flame speed.

Figures IX.2A, B, and C show, respectively, the position of the flamefront, the flame velocity (as seen by an inertial observer), and the flame velocity minus the local gas velocity at the "foot" of the flame (an estimate for the fundamental burning velocity) for the time interval of Fig. IX.1. The prediction is a pulsating laminar flame which exhibits significant velocity variation within the range 300-900 cm/sec. The oscillation appears to be a complicated function of several modes whose dominant frequency agrees with that predicted by the acoustic analysis of Jost [103,104].

In this example, the origin of the flame oscillation occurs in the heating phase before ignition. Heat transfer through one boundary excites small amplitude acoustic standing waves in the chamber as the pressure increases are equilibrated. These waves are amplified and driven by the flame as it propagates away from the heated boundary. In the case described, the

ignition time is longer than the acoustic transit time for the system. In other cases, where the ignition time is on the order of the acoustic travel time in the chamber, the onset of oscillations is delayed until the flame propagates some distance into the chamber.

Because of the non-linear coupling between the equations governing conservation of momentum and energy, confined combustion is basically oscillatory. Combustion chamber oscillations are known to occur in systems such as ramjets, turbo-jet afterburners, industrial furnaces, rocket engines, and guns. In practice, the amplitude range of the oscillations may be small due to system losses. Kooker's work does point out that an analysis of any confined or partially confined combustion based on assumptions which preclude oscillatory behavior (e.g., spatially uniform pressure) could lead to predictions with indeterminant errors.

IX.B. Chemical Kinetic Studies

The use of one-dimensional detailed reactive flow models to examine chemical kinetic mechanisms has been demonstrated by the extensive works of Westbrook and Dryer [100], Heimerl and Coffee [97], Warnatz [98], Galant [105], and many others. Model calculations have been compared to measured flame velocities and density profiles of major and minor species behind a flamefront. We will describe some of this work and illustrate how the techniques have been applied to successively more complicated chemical systems.

The simplest chemical system studied with one-dimensional models has been O_3-O_2 [76,106,107]. Above we described Kooker's analysis of the acoustic coupling between energy released in ozone combustion and standing waves in an enclosed chamber. Here we are concerned with the validity and accuracy of the proposed kinetic mechanism and whether it reproduces laminar flame data. Calculations may be compared to the experimental studies of ozone burning which have been performed by Streng and Grosse [108]. From their measurements at one atmosphere of pressure, they derived the empirical expression for the burning velocity,

$$V_b = 563\ X(O_3) - 88.8\ \frac{\text{cm}}{\text{sec}},$$

where $X(O_3)$ is the mole fraction of O_3 initially in the mixture. Measured values of V_b at $X(O_3)$ less than 0.3 were less accurate than those at higher values of $X(O_3)$ and there were no measurements of individual species concentrations.

Figure IX.3 shows a comparison between the measurements and the calculations by Heimerl and Coffee [97] and Warnatz [98]. Each calculation used notably different diffusive transport and chemical rate coefficients, although they predicted very similar flame velocities. Thus even in the simplest realistic scenario, we are faced with ambiguities concerning the correct set of the input data. The O_3-O_2 system is described by three sets of forward and reverse reactions:

$$O_3 + M \rightleftharpoons O + O_2 + M, \qquad k_1,\ k_{-1}$$

$$O + O_3 \rightleftharpoons O_2 + O_2, \qquad k_2,\ k_{-2}$$

$$O + O + M \rightleftharpoons O_2 + M, \qquad k_3,\ k_{-3}$$

where the k_i, k_{-i} refer to the rate of the i^{th} forward and reverse reaction, respectively. Heimerl and Coffee have shown that the difference between their calculation and Warnatz' calculation resides in the authors' choice of k_1 and k_2. Figure IX.4 shows ratios of the values the input parameters used by Heimerl and Coffee to those of Warnatz. The ratio of k_1 values drops from close to unity at 1000°K to about 0.4 at 2400°K, while the ratio of k_2 values rises from about 1.5 to 1.8 over the same temperature range. Further studies indicated that for the case where $X(O_3) = 1.0$, k_1 and k_2 have about an equal effect on the burning velocity, and in going from one model to another, the high temperature values of k_1 and k_2 change in opposite directions. The agreement between calculations of flame speed is the product of a fortuitous cancellation of effects.

There are, however, substantial differences in model predictions of both temperature and atomic oxygen densities for this same value of $X(O_3)$. These are shown in Figs. IX.5. Predicted atomic oxygen densities vary by as much as a factor of two and predicted tempera-

tures by about 350°K. As can be seen from the dashed line, which indicate Heimerl's calculations when Warnatz' values of k_1 and k_2 are used, there are smaller differences which may be attributed either to the sum of the differences in input or perhaps to numerical methods. Thus it becomes quite clear that without more experiments which either vary $X(O_3)$ or which measure the species densities, we cannot differentiate between the two models. Another possible solution might be independent measurements or ab initio calculations of the rate constants.

The homogeneous premixed hydrogen flame constitutes the next level of chemical complexity. In this case the chemical reaction scheme may involve as many as fifty rates. Further, because we are dealing with complex molecules, the diffusive transport coefficients cannot be calculated as accurately as for the ozone flame discussed above. With more reactions, we have in principle even more of a problem with non-uniqueness of the sets of input variables.

Hydrogen-oxygen and hydrogen-air flames have been modelled by Warnatz [98], Oran and Boris [78], Dixon-Lewis, [109], and Stephenson and Taylor [107]. For these flames, there are extensive measurements available of chemical reaction rates and flame data. Figure IX.6 shows a typical propagating flamefront and Fig. IX.7 shows an expansion of the flame region containing steep temperature and density gradients [78]. A typical comparison of calculated and measured flame velocities [98] is shown in Fig. IX.8. As yet no extensive comparison such as Heimerl performed for the ozone system has been made.

Methane and methanol combustion in oxygen and air surpasses hydrogen combustion in complexity. Proposed mechanisms require from thirteen to thirty species and from forty to one hundred and fifty rates, depending on whether or not reactions involving H_2O_2, CH_x with x less than 3, C_2 hydrocarbon or alcohol radicals are included. To the naive but worried modeller, there appears to be enough ambiguity in what must be included and uncertainty in the rate coefficients to guarantee that there will be a difficult uniqueness problem to deal with. Even with these obstacles to face, however, impressive work on modelling homogeneous premixed flames has been carried out by Tsatsaronis [99], Westbrook and Dryer [100] and Creighton and

Lund [110].

Tsatsaronis used a computational procedure developed by Patankar and Spalding [111] and Spalding Stephenson, and Taylor [112] to perform extensive comparisons between calculations and measurements of CH_4-O_2 and CH_4-air flames. These included studies of the effects of varying the equivalence ratio in atmospheric CH_4-air flames, the effects of increasing the temperature of the unburned gas mixture in stoichiometric flames at one atmosphere, the effects of varying the initial pressure, and the temperature and species profiles behind the flame front. The final results presented include a set of chemical rate coefficients which contain only thirteen species and twenty-nine pairs of forward and reverse reaction rates. Tsatsaronis indicated that he had to adjust six of these pairs in order to obtain a set which best fit all of the available data.

Figures IX.9 shows typical results of these comparisons. The experimental data was taken from Andrews and Bradley [113] who summarize the results of many investigators and give detailed citations to the data. In addition to data of the type shown in these figures, there have recently been a series of stabilized burner measurements by Peeters and Mahnan [114], Dixon-Lewis and Williams [109] and Fristrom, Grunfelder, and Favin [115] who obtained temperature and species profiles. Tsatsaronis' comparisons of calculations to the data of Peeters and Mahnan are shown in Figs. IX.10.

Similar studies have been performed by Creighton and Lund [110] using a modified form of the rate scheme proposed by Westbrook and Dryer [100]. These tests used several more species and several fewer reaction rates and focused on defining the sensitivity of observables to changes in input parameters. As in the results shown in Figs. IX.10, Creighton and Lund obtained good agreement to measurements of major species and some of the minor species data after appropriate adjustments of the rate constants or diffusive transport coefficients. For both sets of mechanisms, however, the agreements between measurements and some of the minor species, such as HO_2, CH_3, and CH_2O, were not as good.

The methane studies discussed above are another example in which the chemical rate scheme proposed to fit the data is not unique. Because so many rates and species are involved, it is difficult to use the flame data to test anything but the grossest features of the reaction rate scheme. Furthermore, we must be extremely cautious about applying any mechanism blindly in regimes outside of the pressure, stoichiometry and temperature range which has been validated.

Recently there has been a study by Gelinas [116] who compared measured induction times in methane systems to those predicted by the chemical rate scheme proposed by himself, Westbrook [22], Olson and Gardner [21], and Tsatsaronis. He found in this study that the first three schemes gave reasonable agreement with measurements but that the one proposed by Tsatsaronis gave induction times which are *many* orders of magnitude too large. From this we can only conclude that either the flame data available is insensitive to the short-time behavior of the system or that this behavior is effectively accounted for by different compensating rates in different reaction rate schemes.

Westbrook and Dryer [100] have used the one-dimensional flame model developed by Lund [31] to study methanol oxidation. The reaction rate scheme they propose has twenty-six chemical species and eighty-four elementary reactions and so is even more complicated and perhaps more ambiguous than that proposed by Tsatsaronis for methane. The proposed mechanism was first tested against shock tube and turbulent flow reactor data and thereby tuned to include important reactions involving CH_3OH and CH_2OH. Within the temperature range 1000-2180°K, fuel-air equivalence ratios of 0.05-3.0, and pressures of 1-5 atm, the reaction rate scheme gave excellent agreement with experiment.

Westbrook and Dryer then proceeded to study the dependence of laminar flame speeds and structure on the pressure, equivalence ratio, and unburned gas temperature, comparing these results when possible to available measurements. A typical example is shown in Fig. IX.11, which compares the species concentrations data taken by Akrich, Vovelle, and

Delbourgo [117] to model calculations. In general, however, there is not a plethora of data available and the many calculations thus serve as a prediction of what will be seen when the measurements are performed.

It has been noted by many authors that the major test of a proposed kinetic mechanism is not whether it predicts major species concentrations and bulk trends well, but how well it predicts the minor species and radicals. We must also realize that much of the work described above is really not prediction, but postdiction used to test input parameters over a range of pressures and temperatures. All of this is valuable and in effect gives us models and information that can be used with the same caution we use most empirical models. When the physical situation changes, they will need to be modified or extended to incorporate more of the fundamental processes. It is thus our recommendation that flame calculations not be used to deduce empirical chemical rates schemes. Instead, they should be used to test whether rates schemes derived from kinetics experiments and models (Section IV) do give reasonable predictions of flame data.

IX.C. A Comparison with Theory

We now consider one example of the use of detailed modelling in conjunction with theoretical analysis [78] to study ignition caused by heat addition to a combustible gas. The theoretical model defines four parameters:

E_o, the total energy deposited,

τ_o, the time interval for deposition of E_o

R_o, the initial radius of the gaussian in which E_o is deposited, and

$\tau_c(T)$ the chemical induction time as a function of temperature, T.

We assume a homogeneous premixed gas, one-dimensional spherical geometry, linear energy deposition with time, and constant γ. The continuity equation is written

$$\frac{1}{\rho}\frac{d\rho}{dt} = -\underline{\nabla}\cdot\underline{v} \tag{IX.1}$$

and the slow flow equation described in Section V gives

$$\frac{dP}{dt} \approx 0 = -\gamma P\underline{\nabla}\cdot\underline{v} + \underline{\nabla}\cdot\gamma Nk_B\kappa\underline{\nabla}T + S(t)e^{-k^2(t)r^2}. \tag{IX.2}$$

Here k_B is Boltzmann's constant and κ is a function of the mixture thermal conductivity, λ,

$$\kappa \equiv \frac{\gamma-1}{\gamma Nk_B}\lambda(T). \tag{IX.3}$$

The last term on the right hand side of Eq. (IX.2) is the source term. Proper choice of $S(t)$ ensures that a given amount of energy, E_o, is deposited in a certain volume, $\frac{4\pi}{3}R_o^3$, in a time τ_o. It is the choice of this Gaussian profile which allows us to obtain a "closed" form similarity solution given below in spherical coordinates.

Using the assumption that $dP/dt \approx 0$, an algebraic equation is written for $\underline{\nabla}\cdot\underline{v}$ from Eq. (IX.2) which combines with Eq. (IX.3) and the ideal gas law to give

$$\frac{1}{T}\frac{dT}{dt} = \frac{S(t)}{P_\infty}e^{-k^2(t)r^2} + \underline{\nabla}\cdot\frac{\kappa}{T}\underline{\nabla}T \tag{IX.4}$$

where P_∞ is the background pressure. The solution is then

$$T(r,\ t) = T_\infty\, e^{A(t)e^{-k^2(t)r^2}} \tag{IX.5}$$

and

$$\rho(r,\ t) = \rho_\infty\, e^{-A(t)e^{-k^2(t)r^2}} \tag{IX.6}$$

where T_∞ and ρ_∞ are the background temperature and pressure, respectively. Thus the non-linear slow-flow equations including expansions and contractions of the flow have been converted into a single equation which is linear in the logarithm of the temperature.

Assuming that

$$v(r,t) \approx v_1(t)r \tag{IX.7}$$

and demanding energy conservation allows us to write two coupled ordinary differential equations for $k(t)$ and $A(t)$,

$$\frac{dk}{dt} = -kv_1 - 2\kappa k^3 \tag{IX.8}$$

$$\frac{dA}{dt} = \frac{S(t)}{\gamma P} - 6\kappa k^2 A \tag{IX.9}$$

where

$$v_1 = \frac{S}{3\gamma P_\infty}\frac{F'(0) - F'(A)}{F(A)} + 2\kappa k^2 \frac{AF'(A) - F(A)}{F(A)}. \tag{IX.10}$$

and

$$F(A(t)) \equiv \int_0^\infty 4\pi x^2 \left[1 - e^{-At \cdot x^2}\right] dx. \tag{IX.11}$$

The model requires a curve of chemical induction time as a function of temperature in order to define the induction parameter,

$$I(t) = \int_0^t \frac{dt'}{\tau_c(T(r, t'))}. \tag{IX.12}$$

Ignition "occurs" when $I(t) = 1$ in this model, an exact result in the limit of constant temperature near the center of the heated region.

Typical results for a mixture of H_2:O_2:N_2 / 2:1:10 are shown in Fig. IX.12. The left hand portion of the figure shows the time variation of the nonlinear amplitude, A, and the characteristic radius, R_c. The right hand portion shows the central temperature, $T(r = 0)$ and the induction parameter, I, also as a function of time. The "*" marks the time for which ignition is predicted by the model, substantially later than the time at which the energy deposition has ceased. This particular choice of $E_o = 3.3 \times 10^4$ ergs is in fact the minimum ignition energy predicted by the theory.

The similarity solution described above was used in conjunction with a detailed simulation to test ignition predictions typical of those shown in Fig. IX.12. The full set of conservation equations was solved using the ADINC algorithm [55] which solves implicitly for the pressure.

The chemical rate scheme consisted of about fifty rates and ten species. A full set of diffusive transport coefficients was included. The detailed model was then configured to run in spherical symmetry with an open boundary and a Gaussian energy deposition.

Figure IX.13 shows the results of a series of calculations performed with the detailed model. Ignition is clearly indicated for ignition energies of at least 3.3×10^4 ergs, which agrees well with the theory. This type of combined calculation gives us confidence in both the analytical model and the detailed simulation until we reach a range of parameters which invalidates one of the models. This problem and the importance of molecular diffusion in certain parameter regimes has been discussed by Oran and Boris [78].

IX.D. Two-Dimensional Subsonic Reactive Flow Calculations

Although the technology exists to solve Eqs. (II.1)-(II.12) in more than one dimension, the added computational and storage costs preclude the level of detail that has been included in the calculations described above. Thus two-dimensional models have generally been used to study hydrodynamic or geometric effects and have included very limited representations of the chemical reactions. Below we briefly describe the results of Kansa [101] who studied the effects of buoyancy on burning, the results of Butler and O'Rourke [102] who worked at flame propagation in unusual geometries, and the work of Jones and Boris [51] who included a simple but realistic model for chemical kinetics.

Consider a large, hot spherical droplet of fuel. As the gas molecules evaporate, they diffuse into the surrounding air and react irreversibly with energy release. In an open chamber without a gravity term to differentiate "up" from "down", the problem may be approximated by a one-dimensional model. In two dimensions, there are distortions in the flow which develop as the calculation approaches a steady state.

Kansa [101] has used a two-dimensional model with an idealized one-step chemical scheme to study this burning wick problem with and without the effects of gravity. The

numerical technique applied was based on the RICE [33], method for which modifications were made by Kansa to allow the iterations on large matrices to converge more quickly. Kansa concluded that without the buoyancy term the typical hydrocarbon-air flame studied is quenched by its own combustion products. When buoyancy is included, however, the flow field is distorted and an upward buoyant convection of the hot gases develops. Thus the gravity term generates an asymmetric flow field in which oxidation occurs and products are moved up and out of the burning region. A shear flow is set up near the combustion zone at which the oxidant and fuel mix. These results were in qualitative agreement to the temperature contours and flow field measured experimentally by Hertzberg et al. [118].

Butler and O'Rourke [102] used the RICE code to study burning in two cylindrical chambers connected at the bottom by a third chamber. Intially these chambers were completely filled with reactant at uniform temperature and pressure. Then a fixed amount of energy was deposited about the symmetry axis and near the wall of one of the large chambers. This energy was enough to ignite a flame which propagated through the system.

In order to avoid having to worry about resolution at the flame front, a "turbulent diffusivity" was defined which was at least as large as the numerical diffusion and much larger than laminar diffusion effects. Thus, in an ad hoc way, they "modelled" a turbulent flame whose propagation velocity is greater than that of a laminar flame. By defining the problem in this way, they avoided the need for the complicated adaptive gridding algorithms required to resolve a flame front. In the limit of a laminar flame, the answers obtained would be totally dominated by numerical diffusion.

The results of the calculations showed that as the flame in the first chamber was ignited and began to propagate, a compression wave was generated ahead of it in the other large chamber. At later times, the flame front had advanced rapidly and velocities at the inlet were large. A large vortex formed as the flame collided with the right hand wall. Eventually the gases in the small chamber expanded to the point where velocities in the inlet reversed

direction. The series of velocity vector and reactant density contour plots in Fig. IX.14 show a time-sequence of this calculation.

To our knowledge, the model of Jones and Boris [51] is perhaps the only two-dimensional time-dependent subsonic reactive flow model currently set up with a realistic chemical reaction scheme and the complete set of diffusive transport coefficients. The added flexibility derives in part from their use of the asymptotic techniques described in this paper. A number of benchmarks of the model and each of its constituent algorithms have been reported. To do this they used both analytic solutions and one-dimensional flame calculations of the types described above.

A typical test is represented by the results shown in Fig. IX.15. A flame was initiated in a homogeneous premixed gas by assuming that the temperature is constant and high out to R_o, where it drops suddenly to 300°K. This one-dimensional model thus assumed spherical symmetry with a hot spot from $r = 0$ to $r = R_o$ in a volume $\frac{4}{3}\pi R_{\max}^3$. The two-dimensional model assumed a hot, spherical spot of the same size in a cylindrical volume made equal to $\frac{4}{3}\pi R_{\max}^3$.

Figure IX.15 shows the central temperature as a function of time. The initial temperature increase is a result of energy release due to burning in the hot sphere. Once the flame is initiated and has propagated past the initial hot spot, the temperature at the center decreases due to adiabatic expansion and thermal diffusion of excess heat out of this region. However, because the chamber is closed, the pressure is constantly increasing due to the constant release of energy. A point is finally reached ($\sim 10^{-2}$sec) where all of the unburned material ahead of the flame ignites. The differences in the one-and two-dimensional calculations at 10^{-2} sec may be attributed to the fact that the geometry of the chambers in each calculation is slightly different and that the resolution of the one-dimensional model is better.

X. REACTIVE FLOWS WITH TURBULENCE

Our understanding and eventual ability to predict the complicated interactions occurring in turbulent reactive flow problems is imperative for many combustion modelling applications. The goal of this section is to first describe the fundamental physical processes we must model if we wish to simulate reactive flow turbulence and then show how detailed modelling of these phenomena may be used to help construct practical phenomenological turbulence models for reactive flows. The presence of turbulence alters mixing and reaction times and heat and mass transfer rates which in turn modify the local and global dynamic properties of the system. Because turbulence is so important, we need reasonably accurate models to use in reactive flow hydrodynamics codes. The general views of the turbulence community of what these models should be are well-represented in the many references given at the end of this paper. It is our belief that none of these models includes enough of the physics of expanding, variable density, transient, multi-scale reactive flows to provide a reliable predictive model representing turbulence in a general code. Thus we concentrate on a complementary representational framework for modelling turbulence dynamically which we hope will suggest new ways of approaching these old problems.

If the full set of conservation equations for mass, momentum, and energy in multispecies flow could be solved exactly for a large enough range of time and space scales, turbulence and turbulent mixing phenomena would be contained explicitly in the solutions. Unfortunately, even the fastest and largest computers are neither fast nor large enough to solve a typical problem involving turbulence from first principles even though the fundamental mathematical model is adequate. The basic problem in doing the computation arises from the vast disparity in time and space scales among the fundamental physical processes. For example, consider a system in which the mean free path λ, the characteristic scale length of diffusive mixing in reacting shocks, is six orders of magnitude smaller than the macroscopic convection length, L. A three-dimensional model resolving both scales would need $\sim 10^6$ computational cells in each

spatial dimension, or a total of $\sim 10^{18}$ grid points. Perhaps it might be possible to use 10^6 grid points, but certainly not twelve orders of magnitude more. In trying to represent all of the macroscopic, turbulent mixing, and characteristic molecular dissipation scales in a single calculation, we are confronted with perhaps the most perplexing multiple time-scale and multiple space-scale problem in the detailed modelling of reactive flows. We must develop some practical algorithm to encompass these widely disparate scales in the same calculation.

In modelling turbulence phenomena, it has been the rule to try to develop separate equations which describe the subgrid scale mixing and reactions. These are then coupled to the coarsely resolved macroscopic fluid dynamics calculations we know how to perform. Here the proper separation and recoupling procedures for subgrid turbulent mixing and macroscopic flow are not nearly as obvious as the analogous problem of coupling a detailed chemical kinetics reaction scheme to a laminar hydrodynamics calculation [40,66]. It is not even clear how to represent some of the important transient mixing phenomena qualitatively let alone arrive at quantitative estimates of their effect.

We first discuss the fluid dynamic origins of turbulent mixing in order to obtain an intuitive picture of the range of phenomena which must be represented. We then use this information to develop a list of resulting requirements which we would like an ideal turbulent mixing submodel to have. We next consider first-principle, ab initio calculations which can provide information about the dynamic characteristics and spectral evolution at length scales smaller than can be resolved with a macroscopic fluid dynamics model. Ab initio calculations are often extremely expensive, but must be performed to provide detailed understanding of microscale processes and of transition to turbulence. Purely phenomenological turbulence models cannot be expected to tell us anything fundamental about turbulence or turbulent mixing. The basic physical processes must be built into the phenomenology; they cannot be derived from it. Thus a series of idealized ab initio calculations may be used, for example, to delineate the hydrodynamic channels for turbulent energy reapportionment and to provide ways to analyze those

rroperties which must be built into the phenomenological models.

We then describe four types of phenomenological turbulence models. In a phenomenological model we seek to represent but not to resolve all the myriad of individual fluid dynamic degrees of freedom within each macroscopic cell as efficiently as possible. If the basic processes controlling a particular measurable transient or turbulent transport effect are not represented in a phenomenological model, certainly the model cannot predict the occurrence of the effect.

X.A. The Origins of Turbulence

In this section we discuss three aspects of reactive flow mixing which, when considered together, give a consistent picture of turbulent flows. By thinking in terms of these three different aspects and their interactions, we gain an inituitive understanding of reactive turbulence and the ways in which it differs from the classical non-reactive cases. The first aspect deals with the hydrodynamic channels for mixing. It is instructive to adopt the idea that turbulence begins in a laminar macroscopic flow as the onset of a fluid instability. The energy which drives this macroscopic instability then cascades through various hydrodynamic channels and is spread convectively over a broader spectral range. By concentrating on the fluid instabilities and their evolution as a response to changing fluid conditions, turbulent mixing can be viewed as a cascade of systems of distinct instabilities [119]. The second aspect focuses on the idea that turbulent mixing is dependent on the contortion of reactive surfaces which originally separate reactive species. We must first follow and then predict the behavior of these surfaces as they move and stretch with the fluid. Steady increase of the reactive surface area enhances molecular mixing and speeds reactions. The third aspect of the reactive flow mixing problem is the detailed chemical kinetics and chemical energy released by these reactions. Energy release in gaseous flows promotes expansion and, if the flow is sufficiently exothermic, can induce buoyancy. Thus the kinetics feeds back into the hydrodynamic channels and the cycle is closed.

An extensive body of knowledge has been developed in using models of turbulence and

turbulent mixing in constant density non-reacting fluids [120-123]. However, in combustion systems there are interactions which modify or may even obviate these models. One such physical mechanism is the localized change in the rates of heat and mass transport due to the temperature dependence of transport coefficients. Another mechanism arises from the strong density gradients occurring locally in the combustion. Non-linear phenomena such as these determine the turbulent scale lengths and eventual chemical reaction effects. The various scale lengths covered by diffusive mixing, convection, and fluid instabilities are bounded by a dissipative mean free path scale length on one hand and the macroscopic system scale on the other. This is shown schematically in Fig. X.1. Since energy release due to chemical reactions can only occur where the fuel and oxidizer mix molecularly, turbulent combustion is driven by an energy source which fluctuates on the scale of the turbulent mixing lengths. This situation differs markedly from classical turbulent flows.

X.A.1. Dynamic Fluid Instabilities and Hydrodynamic Channels: The First Aspect

There are many examples of possible hydrodynamic channels for turbulent energy reapportionment. Most of these channels involve transient effects for which detailed balance or steady state arguments are inapplicable [124]. They involve the quick onset of a relatively short wavelength fluid instability which results from a slow or parametric variation of the background flow. Thus the configuration changes from one of local hydrodynamic stability to one of instability. At and just beyond the transition point of marginal stability, the growth rates are very slow and the unstable wavelengths relatively long. As the background flow continues to evolve into the unstable regime, maximum growth rates increase and instability spreads over a broader band of the spectrum. The turbulence, which is the non-linear manifestation of these instabilities, arises in bursts on the macroscopic scale and is an intrinsically transient phenomenon. Thus the idea of a steady state cascade of either vorticity or turbulent energy is an artificial concept because so many of the channels underlying the turbulent process are intermittent. New concepts are needed to describe these turbulent bursts.

Marginal stability methods [125-127] can play a very useful role in determining the transient interactions between macroscopic flows and the microscopic instabilities which they induce. In splitter-plate experiments, for example, the Kelvin-Helmholtz instability grows initially at wavelengths characteristic of the entrance flow. For certain experimental designs the instability may be essentially two-dimensional [128,129]. A vortex street begins to develop and vortices coalesce with rapidly stretching braids of interfacial material winding up in the cores. Figure X.2 shows a numerical calculation of such an instability. When the local Reynold's number is high enough, the flow in the vortices becomes Taylor unstable in the third dimension at still shorter wavelength. Thus a one-time situation occurs and then passes.

In splitter-plate experiments there is a constant source of energy and a tendency toward instability. The turbulence grows up to a level where the governing flow remains near marginal stability. If the turbulence decays somewhat, the background flow becomes more unstable until the turbulence builds up again. If the turbulence becomes somewhat too strong, the background flow is broken down and smeared out with the general effect of reducing the growth of instabilities. In the smoother flow the turbulence soon starts to abate. Since there is a decay time associated with the turbulence and an induction time-lag for the instabilities, it is not surprising that intermittency, coherent structures, and bursts of turbulence are the norm rather than the exception.

One of the major physical conditions which distinguishes reactive flow from classical turbulence is the existence of density gradients. These cause the baroclinic generation of vorticity, ξ, through the term

$$\frac{d\xi}{dt} = \frac{\nabla\rho \times \nabla P}{\rho^2} + \ldots ,$$

where ρ and P are the multidimensional fluid density and pressure fields, respectively. Below we consider two of the hydrodynamic channels activated by density gradients. These channels are rather typical of the many multi-scale interactive effects which will have to be understood before we can claim to understand turbulence.

When the mass density ρ is constant, as is assumed in much of the classical turbulence literature, all of the effects potentially depending on the vorticity source term are absent by construction. In the classical picture, the turbulent vorticity spectrum is driven at macroscopic scales, the intermediate wavelengths are populated by cascade and vortex stretching, and the short wavelengths in the spectrum are dissipated viscously (collisionally). In combustion, the localized release of heat in molecularly mixed fuel-oxidizer pockets causes strong transient expansion of the combusting gases. The resulting low density region has scale lengths characteristic of the combustion process and interacts with pressure gradients to generate vorticity in the flow on these same characteristic scales. Vorticity on these scales is efficient at turbulent mixing and can be expected to feed back on itself. The combustion process is in turn enhanced as long as fuel and oxidizer are present. Since the spectrum seems now to be driven at short wavelengths as well as long, plateaus or even peaks might form in the spectrum altering the usual notions of cascade, scaling, and hence modelling.

There are two different channels for turbulent mixing that this fluid expansion activates in chemically reactive flows. These can be understood qualitatively in terms of localized Rayleigh-Taylor growth. The first role, an *active* one, occurs when a pocket of gas is actively expanding due to the heat released from chemical reactions. This case is shown schematically in Fig. X.3. The expansion occurs in a restricted volume because the fuel and oxidizer enter the reaction region separately. A time-varying acceleration accompanying this expansion is felt in the surrounding fluid. A region of strong density gradients undergoing this acceleration will be subject to the Rayleigh-Taylor instability during much of the time the energy is being released. A perturbation, whose wavelength is comparable to the distance the fluid moves while expanding, will e-fold about once from the expansion. A nonlinear analysis of the integrated vorticity generation in this problem and ab initio simulations to calibrate the analysis have been performed in cylindrical geometry [130]. The transient expansion induces persistent vortex filaments whose characteristic mixing time, τ_{mix}, is given in terms of the expansion time, τ_{ex}, by

$$\frac{\tau_{mix}}{\tau_{ex}} \approx \frac{37\ X_f}{[\sqrt{X_f} - 1]^2 \ln X_f} \tag{X.1}$$

where X_f is the volumetric expansion factor from the chemical reactions. For combustion applications, X_f is generally in the range 4 to 10. Thus the corresponding induced mixing progresses only 3% as fast as the driving expansion, but it continues indefinitely. The expansion, however, is an intrinsically transient phenomena.

The second role of density gradients, depicted in Fig. X.4, is *passive*, but is potentially more important than the active role. In the passive role the expansion influences turbulent mixing by providing the density gradient which leads to vorticity generation. Consider a localized fluid vortex rotating at angular frequency ω. The acceleration of the fluid is $R\omega^2$ at radius R. Smaller low-density pockets in this vortex, formed by chemical reaction at an earlier time, are unstable to the Rayleigh-Taylor modes where the local centrifugal fluid acceleration points opposite to the density gradient. The acceleration is provided by the divergence-free rotational flow generated earlier or driven into the system externally.

Because the active generation of vorticity is limited in time to the expansion phase itself, it is reasonable to expect that the amount of vorticity generated by the passive interaction of existing density gradients with large scale vortices is even greater. A very simple analysis indicates that there are several growth times of the Rayleigh-Taylor mode during a single rotation of the vortex when the mode wavelength is comparable to the vortex radius. Since neither the active role nor the passive role of expansion are described by standard incompressible fluid turbulence theories and models, improved models incorporating these and other hydrodynamic channels will have to be developed.

X.A.2. Reactive Interface Dynamics: The Second Aspect

Turbulent mixing can also be viewed as the stretching and convolution of surfaces which originally separate reactive species. These reactive interfaces or surfaces move with the fluid. As the fuel and oxidizer diffuse molecularly, these surfaces continue to lie normal to the

strongest species density gradients. The situation is presented in Fig. X.5. In the upper left-hand panel a cube of fluid 1 cm on a side is shown at time $t = 0$. An interface between reacting species A and B divides the cube into two halves. Subsequent stretching of this reactive surface is controlled by the local fluid velocity.

Motion of the fluid elements making up the reactive surface breaks down into a component normal to the surface which can change the integrated area and components parallel to the surface which cannot. These two distinct situations are illustrated in Fig. X.6. All of these components are important and complement each other in the turbulent mixing process. When nearby points on the surface separate or stretch, the fluid on opposite sides of the surface approaches the surface to keep the flow roughly divergence-free. Any species or temperature gradients normal to the initial surface are enhanced, which in turn increases the diffusive interpenetration of the reactants. This surface stretching process is independent of convective interpenetration of material which also enhances mixing. This latter process, shown on the right of Fig. X.6, is governed by derivatives of the normal velocity parallel to the surface. By increasing the actual area of the reactive surface, the bulk reactivity is also increased. Stretching and interpenetration usually occur simultaneously but for clarity have been illustrated separately in Fig. X.6.

If the turbulent spectrum is dominated by short wavelengths, an originally smooth surface will become very wrinkled at short wavelengths before larger scale convolutions have had a chance to grow. This is illustrated in the upper right hand panel of Fig. X.7. Because the length scale of the turbulent spectrum is close to molecular mixing lengths, the effective volume in which enhanced mixing occurs is much less than what would be calculated knowing the stretched surface area. Adjacent folds of the surface which approach within the molecular diffusion length of each other tend to merge their mixed volumes, as shown in the Fig. X.7. The small surface corrugations rapidly get smoothed over with diffusive "fluff" so the effect of molecular diffusion is to limit the rate of convective growth of the reactive surface area.

In the opposite case, shown in the lower left hand panel of Fig. 7, the dominant wavelengths are long compared to the molecular mixing length. The surface is characterized by relatively smooth, long wavelength bulges which can fill a large volume before any of the mutual interference effects described in the previous paragraph occur. In fact, the area of an ideal Lagrangian surface in an isotropic, homogeneous turbulent velocity field should probably increase exponentially. Molecular mixing now occurs along convolutions which have scales longer than the diffusion length. Eventually, however, overlap of the effective mixed volume occurs as the surface becomes more convoluted. Thus, the molecularly mixed volume is again limited even though the ideal reactive surface area goes to infinity.

X.A.3. Detailed Chemical Kinetics: The Third Aspect

The two aspects of time-dependent turbulent mixing in reactive flows presented above, the hierarchy of instabilities and the evolution of the reactive surface, focus on the nonlinear fluid dynamic interactions and the reactant-mixing effects respectively. These two aspects complement each other and a clear picture from each will be required to gain a proper perspective on turbulent mixing. The third aspect we wish to discuss is detailed chemical kinetics. The essentially one-dimensional profiles of the fuel, oxidizer, and other reactants perpendicular to the reactive surface change not only from convection and molecular diffusion but also from chemical reactions. The fluid dynamic expansion and heat release must self-consistently couple back into the excitation of hydrodynamic channels to complete the picture.

A major concern then is the range of validity of fast chemistry approximations made to simplify the analysis. In some cases the overall reaction rate is governed by the diffusion of hot fuel and oxidizer together through an expanding region of hot products and reactants. In other cases the fuel and oxidizer mix convectively and then molecularly before heating and ignition occurs. These latter situations are generally ignited by a rapidly moving flame front which travels parallel to the reactive interface rather than perpendicular to it. Here finite chemical kinetics clearly plays a crucial role since it determines the flame speed.

We have emphasized the feedback and interactions among of hydrodynamic channels, reactive interface dynamics, and detailed chemical kinetics. These three distinct aspects also suggest independent yet complementary approaches to ab initio computational techniques, which are considered further below.

X.B. Properties of an "Ideal" Subgrid Mixing Model

Accurate yet compact phenomenological turbulence models must be developed to model realistic combustor systems, open flames, and other turbulent reactive flows confidently and efficiently. These computational models must asymptotically decouple the subgrid turbulence and microscopic instability mechanisms from calculations of the macroscopic flow. In this section, the important properties which we would like to see incorporated in an ideal turbulence model are listed and described. The goal is to use these desired properties to guide us in both extracting information from ab initio calculations and constructing phenomenological turbulence models.

X.B.1. Chemistry-Hydrodynamic Coupling and Feedback

Explicit feedback mechanisms must be formulated to describe energy transfer from the mixing and subsequent chemical reactions to the turbulent velocity field and the macroscopic flow. The "laminar" macroscopic flow equations contain phenomenological terms which represent averages over the microscopic dynamics. Examples of these terms are eddy viscosity coefficients, diffusivity coefficients, and average chemical heat release terms which appear as sources in the macroscopic flow equations. These modified Navier-Stokes equations are postulated to include the effects of turbulence. Besides providing these phenomenological terms, the turbulence model must make use of the information provided by the large scale flow dynamics in order to determine the energy which drives the turbulence. The model must be able to follow reactive interfaces on the macroscopic scale.

X.B.2. Modelling Onset and Other Transient Turbulence Phenomena

The model should be able to predict the onset of turbulence in what was initially laminar flow since bursts and other highly transient phenomena seem to be the rule in reactive flow turbulence. The fundamental gradients in density, temperature, and velocity fields in the reacting fluid drive the macroscopic fluid dynamic instabilities which initiate turbulence. Thus these gradients from the macroscopic calculation are bound to be key ingredients in determining the energy that is available to drive the turbulence. Density stratification in a time-dependent fluid dynamics model is essential.

X.B.3. Complicated Reactions and Flow

The ideal turbulence model should allow for detailed calculations or suitable parameterizations of chemical kinetics, of buoyancy effects, and of the other hydrodynamic channels which the physics in a given situation might require. In particular it must be possible to deal with multiscale effects within the subgrid model. If there is a delay as velocity cascades to the short wavelength end of the spectrum, the model must be capable of representing this. Otherwise bursts and intermittency phenomena cannot be calculated.

X.B.4. Lagrangian Framework

An ideal subgrid model probably should be constructed on a Lagrangian hydrodynamics framework moving with the macroscopic flow. This requirement reduces purely numerical diffusion to zero so that realistic turbulence and molecular mixing phenomena will not be masked by numerical smoothing. This requirement also removes from concern the possibility of masking purely local turbulent fluctuations by truncation errors occuring when macroscopic convective derivatives are represented numerically. The time-dependent (hyperbolic) Lagrangian framework should also generalize to three dimensions as well as resolve reactive interfaces dynamically.

X.B.5. Scaling

Breaking the calculation into macroscopic scales and subgrid-scales is an artifice to allow us to model turbulence. The important physics occurs continuously over the whole spectrum from $k = 0$ to k_{diss}, the wave number above which the spectrum is dominated by viscous damping. Thus the macroscopic and subgrid scale spectra of any physical quantity must couple smoothly at k_{cell}, the cell size wave number. If this number changes, as might happen if numerical resolution is halved or doubled, the predictions of the turbulence model coupled to the macroscopic fluid equations must not change.

X.B.6. Efficiency

Of course, the model must be efficient. The number of degrees of freedom required to specify the status of turbulence in each separately resolved subgrid region must be kept to a minimum for the model to be generally useable. The real fluid has essentially an infinite number of degrees of freedom to represent the state of the gas in each small element. We would like to be able to do the job with a minimal number of degrees of freedom

Finding a representation which has all of these ideal properties is not easy. Several alternative approaches are mentioned below. It is obvious that consideration of the dynamic aspects of instability cascade and reactive surface evolution necessitate significant departures in modelling techniques from methods found adequate when fast chemistry or steady state Eulerian models of classical turbulence are assumed.

X.C. Ab Initio Calculations

To assess quantitatively the interaction between energy release and turbulence, it is possible to perform idealized fundamental reactive fluid dynamic calculations taking advantage of today's advanced computer systems. Available algorithms permit us to solve the full set of conservation equations for multi-dimensional multi-species flow on what is generally considered

the hydrodynamic subgrid scale. These time-dependent numerical models consider buoyancy and compressibility effects and include realistic expressions for heat and mass diffusion and chemical reactions. Thus the full spectrum of compressible fluid dynamic effects may be simulated for a small volume with enough grid points to resolve the turbulence and the dissipation scales as well as the necessary macroscopic convective effects.

The ultimate goal of such ab initio calculations is to advance our basic understanding of turbulence and to provide information about the small scale mixing and energy release which can then be used to construct and calibrate phenomenological turbulence models. In constant density, idealized, incompressible turbulence, a number of these ab initio calculations have been successfully performed [4,131-133]. Such calculations can also be made for compressible reactive turbulence, but the computations are somewhat more difficult. This difficulty manifests itself in a number of ways. First, resolution of all scales in complicated macroscopic problems is not generally possible so only very idealized and restricted questions may be asked. Second, an ab initio calculation is performed only for one specific initial condition. Thus statistical information about the "turbulence" must be obtained in transient problems by performing a number of calculations and averaging. Finally, the cost of these detailed, first-principle fluid dynamic calculations is not small.

The results of these detailed ab initio simulations are correspondingly valuable. Any correlation, stress term, fluctuation, conditioned sample, or overlap integral can be determined from the computed flow without interfering with the numerical experiment. Therefore closure assumptions for more phenomenological turbulence models may be tested directly. This calibration procedure is particularly valuable because the detailed computational solution of many important large-scale reactive flow problems is well beyond present technology. It will be necessary to use intermediate phenomenological, i.e., lumped-parameter, models to incorporate all of the scales for practical engineering applications. These models must be carefully calibrated using experimental data and specific ab initio calculations.

The ab initio calculations themselves, not their parameterizations, are the only computations that can teach us something about subgrid scale turbulence. Realistic chemical models can be included on the microscopic scale if a restricted enough system is being treated. Therefore each fluid element, as it undergoes hydrodynamic motions which differ slightly from its neighbors, experiences a correspondingly different chemical history. The lumped-parameter subgrid model must necessarily represent an average behavior in a macroscopic fluid element. These averages can be evaluated directly in idealized situations using large detailed ab initio turbulence simulations.

The probability density functions (PDFs) currently used in multi-moment modelling of turbulence can be measured from detailed simulations as a function of time, configuration, and chemical kinetics. This can even be done in situations where the energetic feedback of the reactions on the hydrodynamics is specifically incorporated. Thus not only can phenomenological models be tested, they can be upgraded as improved phenomenologies are derived from the analyses of the ab initio calculations themselves.

Perhaps most important, ab initio calculations can be used to answer fundamental questions about the turbulent mixing process itself. The active and passive roles of expansion in reactive flow turbulence were discussed above as an illustration of nonlinear fluid dynamic phenomena which enter when sharp density variations and energy-significant reactions characterize the flow. These phenomena are only two examples of many identifiable hydrodynamic channels for turbulent energy reapportionment. Ab initio calculations can be used to isolate these individual channels on selected scales and study their characteristic signature in the flow. Other examples of such channels would be mixing from growth of the Kelvin-Helmholtz instability at shearing interfaces driven by the effects of buoyancy, Taylor instability arising naturally in larger vortices and vortex sheets, and Rayleigh-Taylor instability mixing where the pressure gradients are gravitationally induced. Each of these channels is really a mechanism for taking relatively organized kinetic, potential, or internal energy on one scale and reapportioning it to

other scales. Results from two two-dimensional simulations are presented below to show the kinds of information that may be extracted. Similar calculations are being performed in three-dimensions where necessary or with different initial conditions that focus attention on other hydrodynamic channels.

Results from one such ab initio calculation are shown in Figs. X.8 and 9. A two-dimensional version of the FCT reactive flow model [6,40] was used to solve the time-dependent conservation equations for mass, momentum and energy on a square, doubly periodic domain using an ideal gas equation of state. A three species model kinetics scheme is included to represent the exothermic reaction $A + B \rightarrow C +$ Heat. Each of the three species mass densities (ρ_A, ρ_B, and ρ_C) satisfies its own continuity equation with an added molecular diffusion term. Viscosity is neglected (a von Neuman-like treatment of shock heating is not needed in the FCT formalism). Figures X.8 and 9 show different computer plots of the results for two fluids of different density, which interpenetrate and diffusively mix as the result of an initial velocity field. Using such calculations we hope to measure the variation of mixing rate with density difference. In Fig. X.8, contours at $\rho_a + \alpha(\rho_b - \rho_a)$ are shown where $\alpha = 0.1, 0, 2, \ldots, 0.9$. After 0.3 seconds, the beginning of convective mixing is seen due to an initially impressed random velocity field. At the two later times shown (lower panels), molecular mixing, enhanced by short wavelength convection, leaves only the contours at $\alpha = 0.4$, 0.5, and 0.6. As can be seen from Fig. X.9, molecular mixing rapidly smooths out the jagged interfaces which result from the short wavelength components of the "turbulence" field at the beginning of the calculations. From this calculation we see that ab initio models can be used only in very idealized turbulence problems although these limited problems can be solved.

Another time-dependent two-dimensional ab initio calculation performed on the Kelvin-Helmholtz instability [42] is shown in the four panels of Fig. X.2. Two different fluids initially in relative shear flow abut at a sharp interface at $x = 0$. The fluid on the left moves up and the

fluid on the right moves down. Solid wall boundary conditions are applied to the left and right boundaries at $x = +100$ and $x = -100$ respectively. The vertical boundaries are periodic to accommodate the inflow and outflow systematically. Enough cells are present in the calculation (200×360) to allow representation of relatively short scale lengths such as the interface between species A and B (shown as two contours at the levels 0.4, and 0.6 in the function $\rho_A/(\rho_A + \rho_B)$. Intermediate scale lengths, such as the vortex size which develops, and longer scales characteristic of the system size can thus be easily resolved. The different interactions of these scale lengths, such as the vortex pairing shown in Fig. X.2, can be displayed and studied explicitly in properly posed and analyzed ab initio calculations.

Two additional data curves superimposed on the contour plots of Fig. X.2 are the one-dimensional vertical averages of the species densities at each horizontal location in the calculation. These averages appear as solid bars at $y = 180$ in the upper left hand panel, our initial configuration. Species A, plotted as A's, has a vertically averaged value of $\rho_A/\rho = 1$ on the left of the initial shear interface and zero on the right. Species B has just the reverse initial profile. As the fluid instability progresses, the vertically averaged density shows a gradual transition crossing the shear layer, even though the spatially varying and stretching reactive surface remains sharp. In this way, deterministic, detailed, convective effects in the ab initio calculations can be compared one-for-one with fuzzy, statistical, averaged, diffusive-like effects in a phenomenological model.

Also from Fig. X.2 we can see that the average density at the edge of the turbulent layer displays a rather discontinuous drop reminiscent more of erosion at the edge of a cliff than of gentle interdiffusive penetration of two species. The effective one-dimensional diffusion coefficient must be highly variable in space and time to model the intrinsically two-dimensional mixing which occurs. Such variability may be provided by making the turbulent diffusivity a nonlinear function of the "turbulence" itself. We can also see, particularly in the lower right hand panel, that even though both $<\rho_A/\rho>$ and $<\rho_B/\rho>$ are about 1/2 at $x = 0$, very little

of the fluid is actually mixed. Rather, strips of one or the other pure fluid are interleaved. Reactions between A and B can only occur where they are molecularly mixed. Thus reactions would still be occurring as surface phenomena even though $<\rho_A> \sim <\rho_B>$ in an apparently extensive volume.

This last example makes clear one of the great operational advantages of using detailed ab initio calculations in the construction of phenomenological turbulence models. A crudely resolved macroscopic flow calculation with a subgrid model for turbulence could be compared to an ab initio calculation of the same exact problem. By varying only the resolution and keeping identical the initial conditions, fluid dynamics algorithm, and boundary conditions the transition from a detailed ab initio representation to a cruder phenomenological representation can be studied in detail.

In a complete model of reactive turbulence, all space and time scales between the macroscopic convection and the molecular dissipation scales are potentially important to the fluid and must enter into the description of turbulence. There is no intermediate scale which can be ignored safely in making the asymptotic decoupling between macroscopic and statistically indistinguishable microscopic scales. However, the transition from a discrete representation on a macroscopic mesh to a phenomenological subgrid representation is necessarily discontinuous and therefore likely to be a major source of difficulty.

In the ab initio calculations, the characteristics of and interactions between the various hydrodynamic channels for turbulent reapportionment comprise a local description of the turbulent mixing problem. This local approach risks missing global interactions in and constraints on the flow. These can only be treated by using a complementary phenomenological model coupled with the large scale macroscopic flow. Various options for phenomenological modelling are discussed in the next section.

X.D. Options for Phenomenological Turbulence Modelling

Most of the current phenomenological turbulence modelling techniques are based on the idea that local fluctuations in the macroscopic mean flow decorrelate rapidly in space. Thus the local turbulence details would depend only weakly on turbulent fluctuations a small but macroscopic distance away. Within this context, a local turbulent energy density, a characteristic mixing length, and concentration fluctuations may be defined. Conversely, fluctuating coherent structures on the macroscale must be represented in the fluid dynamics; a local turbulence model cannot be expected to deal with non-local fluid dynamics.

Below we describe four kinds of phenomenological models:

1. Turbulent Energy and Scale Models,
2. Moment Equation Methods,
3. Physically Motivated Phenomenological Models,
4. Localized Spectral Dynamics Model.

These approaches are discussed in terms of the six criteria listed above. The four generic model types described below are certainly not all-inclusive, but they are representative of the major approaches pursued today in reactive turbulence.

X.D.1. Turbulent Energy and Scale Models

Based on the idea that turbulence can be described by local fluctuations, a number of authors have written down evolution equations to propagate the turbulence energy, scale lengths, species overlap integrals, etc. The equations for these subgrid quantities or combinations of them take the same form as those of the mean fluid quantities. The characteristic source and sink terms are functions of both mean flow variables and local turbulence parameters. There is a long history of work in this area, starting with Kolmogorov [134] in 1942 and continuing to date with the three-equation model of Spalding [135].

These one-, two-, and three-equation approaches have been used most successfully for certain classical non-reactive flow problems which primarily involve shear flows with high Reynolds numbers away from boundaries and turbulent boundary layers. The results are often acceptably accurate in describing problems in which the turbulence has already developed. The free parameters which always appear in these models must be optimized or calibrated against experiments. These methods are questionable for the treatment of reactive flows, high Mach number flows, low Reynolds number flows, flows where gravity is important, or intermittant turbulent bursts. The presence of large coherent structures in real mixing situations casts further doubt on the authenticity of many of these models. Nevertheless, since phenomenological models are essentially interpolative, good results are possible whenever good data exist.

X.D.2. Moment Equation Methods

In an attempt to make these turbulent energy and scale models more reliable and rigorous, mathematical approaches have attempted to generalize the intuitive models described above into more formal closure procedures [136-139]. The physical variables are decomposed into a mean part representing the macroscopic flow and a fluctuating part representing the subgrid scale turbulence. Equations for the mean and fluctuating components are derived in terms of successively higher order nonlinear correlations of the fluctuating quantities. The hierarchy of moment equations can only be closed, however, by making an assumption that the unknown higher-order terms can be written as combinations of lower-order quantities. In practice, "the hierarchy of equations is closed by semi-empirical arguments which range from very simple guesses for an exchange coefficient to much more sophisticated hierarchies, in which the ultimate closure is very remote from any physical bases" [124].

These closure approximations, which have been considered in spectral space [140] as well as configuration space, often contain a number of non-dimensional parameters which are

hoped to be universal in the sense of being constant or nearly constant over a wide range of turbulent flows. Of course this multiple-moment approach also suffers the criticism that so many free parameters become potentially available, if the hierarchy is carried far enough, that any functional behavior could be fitted. Nevertheless, for certain non-reactive, incompressible, constant-density flows, satisfactory agreement between the models and selected experiments is obtained.

The extension of the moment methods to reactive flows has used the idea of a probability density function (PDF), [141,142] which attempts to relate time averaged macroscopic quantities to their instantaneous local values. Choice of the PDF is close to arbitrary, although physical significance is being attached to whether delta functions or trapezoids are used [142]. A major conceptual problem lies in the fact that some calculations are extremely sensitive to the form of the PDF.

A related problem concerns the exact order and form of closure. It was originally hoped that by going to higher and higher order models, more accuracy would be obtained. The current feeling is that the simple two- or three-equation models do as well as the higher order models. Higher orders yield more free parameters which can be fit to data. But the resulting models are no more universal because the expansions on which they are based tend to break down whenever the fluctuations in the flow are comparable in magnitude to the primary flow or when coherent structure in the turbulence demands the retention of phase information.

Another point should be mentioned here. The turbulence modelling schemes currently used convert the detailed consequences of microscopic motions, which are thought of as stochastic random phenomena, into absolutely deterministic effects driving flow on the macroscopic scale. Thus in a reacting fluid system which is modelled by a set of laminar fluid equations and a prescription for the effects of turbulence, a given initial configuration will always lead to the same final state. Even though the real fluid system is being described in the model by only a small finite number of degrees of freedom, the answers predicted by the model are

completely deterministic. There are an infinite number of configurations of the real system which would be represented in the model by the same final representation, and each of these real configurations should really lead to a different final state. The variance of these final states within a given finite model representation has to be determined, and is the subject of extensive mathematical and physical research. Distinct classes of solutions seem to exist in simplified physical problems. These solutions depend on whether the problem is ergodic, i.e., whether it gives rise to periodic, quasi-periodic, or non-periodic solutions [119]. Whether this mathematical classification bears corresponding physical significance has not been determined.

It is by no means clear that increased study and development of these mathematical, expansion-based phenomenologies is the way to go. In addition to the problems described above, there are other difficulties as well. The first of these involves modelling turbulent transients (bursts) and turbulence onset. In most physical systems, turbulence arises naturally as a consequence of an unstable macroscopic flow configuration and dies out when the destabilizing situation abates. As mentioned above, specific local evaluation of fluid dynamic stability criteria should be a part of any reliable model, although it does not seem to be included in any of the moment models. In fact, the description of turbulent shear flows in terms of a mean profile in at least some flows (mixing layer and boundary layer) has been shown to be the result of a superposition of nearly deterministic large-scale structures having random phases [124]. The classic experiments by Roshko and others demonstrate this fact clearly [128,129].

Another aspect of these transient-vs-steady-state problems is shown in Fig. X.10. Typical flow streamlines in both the steady state and the transient laminar computations of flow in a simple two-dimensional combustor are illustrated. The lower panel shows realistic macroscopic fluctuating eddies carrying pockets of relatively pure oxidizer to the top of the chamber and relatively pure fuel to the bottom. Any phenomenological turbulence models based on the steady state flow of the top panel cannot describe convection of pockets of pure fuel or oxidizer into the far corners of the chamber, for it would require a flow with material crossing streamlines. Neither will diffusive approximations be able to get the pure fuel or oxidizer there.

Therefore, suitably modified approaches to the modelling are required to correctly treat this problem.

X.D.3. A Physically Motivated Phenomenological Approach

An alternative approach to multi-equation and multi-moment methods involves actually modelling the probability distribution function (PDF) based on certain physical processes we know occur. The models must also provide procedures for deriving the time-averaged fluid quantities. Methods of this type have been developed and tested by a number of authors [143-146]. Their hope is that by building some of the physics into the PDF, the computed mean quantities will be less sensitive to those of its feature which are not known.

Spalding's ESCIMO theory [146] is one example of this type of model currently being developed with more emphasis than most on following the reactive interfaces. Mixtures of different composition form interleaved folds which are born, stretch and die as a function of time. The gradients are smoothed and broadened by molecular diffusion. Only the direction normal to the interface is considered, so multidimensional effects appear as compression and dilation of the gradients in the one spatial dimension which is represented. The internal gradients and structures of the folds are only driven by the macroscopic flow but not derived from it or coupled directly to it. In terms of the reactive surface concepts introduced above, the ESCIMO theory concentrates on the perpendicular diffusive mixing and associated detailed kinetics where the reactive flow is laminar on the small scale. The effects of mutual interference in adjacent folds of the surface are neglected and there is no way of knowing what the size distribution is for these folds at their birth. What we have is a number of small-scale one-dimensional laminar problems which must be related to the macroscopic flow. This has been termed the "demography" problem.

We see, therefore, that the ESCIMO approach is a simplified ab initio model which can teach us something about the local mixing and chemical kinetic aspects of turbulence as well as

being the representational basis of a potentially useful phenomenological model. Studies of the time-history of individual folds may include effects such as complex chemical reactions, molecular diffusion, etc. This is one way to study localized mixing in the microscale under idealized circumstances. The model is limited, however, in its predictive capability by those physical processes which have not been included, as well a by the open-ended question of how the parcels interact with the macroscale. Detailed modelling calculations still require a parameterized, coupled, dynamic model of the subcell turbulence. Such a model should be capable of representing and predicting multiscale phenomena such as occur in instability cascade.

X.D.4. Local Spectral Dynamics

Suppose every computational fluid element has local subscale motions which must be described simply and accurately. Further, suppose these local motions can be described in important respects by a local spectrum of fluctuations. Then an efficient and flexible turbulence model might be developed by modelling the local spectrum,

$$E_k \equiv |\frac{1}{2}\rho V_k^2|, \tag{X.2}$$

in each fluid element using just a few degrees of freedom. Here ρ is the mass density and V_k is the k^{th} wavelength component of the fourier transform of the fluid velocity. We further assume for now that only a scalar spectrum is needed to model the local motions and that the region which has to be modelled is limited as shown in Fig. X.1. For wavenumbers larger than k_{diss}, viscous dissipation, thermal conduction, and molecular diffusion effects dominate and the fluctuation spectra should be predictable given the values at k_{diss}. For wavenumbers smaller than k_{cell}, the macroscopic hydrodynamics equations resolve these scales explicitly.

In between k_{diss} and k_{cell}, some form of discrete representation of the localized turbulence short wavelength spectrum is needed. The best form has not yet been determined. In the figure, three discrete values of the spectrum at k_1, k_2, and k_3 are shown breaking the turbulent interactions regime into three finite width cells or bins. The optimal number of such cells must also be determined. At least three bins are necessary to allow for transient instability onset,

changing turbulent length scales, and multiscale phenomena. More bins will undoubtedly improve flexibility and accuracy of the model. In earlier idealized tests of this approach on the Kelvin-Helmholtz instability, it was necessary to use at least two bins per decade of characteristic scale length.

To advance E_{k_1}, E_{k_2}, E_{k_3}, the localized spectral strengths at k_1, k_2, k_3, a set of ordinary differential equations is written down which are somewhat analogous to the coupled rate equations for chemical kinetics. For each macroscopic cell, there are a series of equations for the form

$$\frac{dE_{k_i}}{dt} = \sum_j \left(Q_{k_i}(\gamma_j) - L_{k_i}(\gamma_j)\right) \tag{X.3}$$

where Q_{k_i} and L_{k_i} are production and loss terms for spectral cell k_i. The $\{\gamma_j\}$ refer to the particular processes which can act as production (Q) or loss (L) terms and they represent the hydrodynamic channels for turbulent energy reapportionment, chemical reactions, diffusion processes, etc. These source and sink terms couple the various wavelength bins in much the same manner as specific chemical reactions or reaction types couple different chemical kinetic species. All the conservation conditions on total momentum and energy in the spectrum apply with the added complication of source and sink terms at both long and short wavelength. Energy dissipated at short wavelengths appears as localized heat in the macroscopic energy equation and as turbulent viscosity in the macroscopic momentum equation.

In this general approach attention is focussed on the interactions between various local coherent flow structures rather than on overall correlations. The simplifications arise from treating the identifiable hydrodynamic channels as separate interactions with characteristic transformations of the "turbulence" spectrum. By way of contrast, the more standard configuration space and spectral space models (e.g Jeandel, Brison and Mathieu [140]) tend to lump all the hydrodynamic channels together and treat the individual correlations instead. The closure problem appears in this spectral dynamics approach through the need to relate the

evolving local spectrum to the macroscopic flow rather than the need to relate higher-order correlations to known lower-order correlations.

In preliminary studies, the obvious anisotropy of some of the hydrodynamic channels will be ignored, and it is hoped that the use of several spectra will not be necessary. Fully calibrated and theoretically understood parameterizations of the reactive surface area evolution as a function of spectral structure will be needed if accurate chemical kinetics models are to be included. By constructing, in effect, a systems model, the specific analytic and phenomenological models developed to understand the reactive flow physics itself can be incorporated rather directly. The works of Libby and Bray [147] and Williams [148], for instance, appear more readily adaptable to the local spectral dynamics formalism than to direct incorporation in more standard models. Further, the complementary results of a complete set of ESCIMO-like Lagrangian reactive flow calculations may also need to be folded in.

Certainly only a careful quantitative analysis of the specific hydrodynamic channels and their interactions can point the way to valid simplifications in this miserable modelling morass. This analysis must provide a represention of the basic fluid instabilities as source and sink terms, probably in terms of instability growth rates derived from separately performed ab initio or microscopic calculations. Considerable success with a variant of this approach has been achieved in a number of plasma physics problems where small-scale micro-instabilities affect macroscopic transport [125,126,149-151]. A similar approach has been postulated for nonreactive flow by Brodkey [152]. However, his source and sink terms did *not* explicitly identify individual hydrodynamic channels or a way of incorporating the effective boundary conditions of the macroscopic gradients on the subscale quantities. Studies of the effect of chemical energy release on the spectrum, E_k, have been made by Eschenroeder [153].

The goal of this local spectral dynamics approach is to use a combination of ab initio calculations and analytical theory to provide insight into the form of the P_k and L_k functions. This complementary approach is appealling physically because it allows all the important aspects

of the six criteria presented above to be met. The model may include the growth and decay of the important hydrodynamic channels and thus potentially allows for onset and transient phenomena. Chemical reactions may be included, at the very least through an enhancement of the spectrum at wavelengths between k_{cell} and k_{diss}. Since we clearly must accept a prediction which is true only on average, the neglect of all but a few of the internal turbulent fluid degrees of freedom in each cell ensures this and provides efficiency. Scaling is ensured through a source term imposed on the equations at k_{cell}. Thus the procedure sketched out above does, at least in principle, meet the six conditions postulated earlier as necessary if not sufficient for a reactive flow turbulence submodel. Undoubtedly many new approaches to representing and then modelling small scale turbulence effects will be developed as well as modifications of the more familiar methods.

XI. CONCLUSION

This paper has presented an introduction to detailed modelling. We have tried to show how detailed modelling is different from both empirical modelling, which is primarily curve fitting to experimental data, and from phenomenological modelling, in which an equation is proposed to model our intuition. However, by describing several flame and detonation calculations, we have shown that even the most detailed of detailed models usually contains empirical or phenomenological components. Such simplified components are necessary because of large disparities in the time or space scales we must represent. Because results obtained from a detailed model may be more comprehensive than those from an analytic theory, they can be used to bridge the gap between theory and experiment. From experimental observation and approximate theoretical models we postulate quantitative physical laws which we expect an effect to obey. These laws are then tested against reality by incorporating them in a detailed model which makes quantitative predicitions for comparison with experimental measurements. Thus perhaps the most fundamental use of detailed modelling is to test our understanding of the controlling physical processes.

A computer simulation using a detailed model is similar to an experiment in that it does not easily give the simple equations relating physical variables which an analytic theory may provide. Instead, each calculation is a unique experiment preformed with one set from an infinity of possible sets of geometric, boundary, and initial conditions. Although detailed modelling may not directly provide the types of analytic relationships which guide our intuition and allow us to make quick estimates, it gives us the flexibility to evaluate the importance of a physical effect by simply turning it off or on or changing its strength. These models may also be used to test the range of validity of theoretical approximations. Any analytic results available are valuable in benchmarking the model. A series of tests which compare analytic results to numerical simulations may calibrate the simulation before it is compared to experiments or used for extrapolation. Conversely, a well-tested detailed model serves as a very useful means

of calibrating unknown parameters and form factors in approximate theories and expressions.

Errors and confusion in modelling arise because the complex set of coupled, non-linear, partial differential equations is not an exact representation of the physical system. Consider, for example, the use of input parameters such as chemical rates or diffusion coefficients. These quantities, used as submodels in the detailed model, must be derived from more fundamental theories, models or experiments. We have seen that they may not be known to any appreciable accuracy and often their values are simply guesses. Or consider the geometry used in a calculation. We have seen that it is often one or two dimensions less than needed to completely describe the real system. Potentially important multi-dimensional effects may then be either crudely approximated or ignored.

However, we limit the representation with which we are dealing both because of cost and computer constraints and because we can often learn a great deal about a system by studying a limited representation of that system. Since the solutions obtained from detailed model calculations more closely approximate reality and have a greater range of validity than those obtained from theoretical analyses, they may be used to test the accuracy of an approximate theory or to calibrate unknown parameters and form factors in these theories. Conversely, we have stressed throughout this paper the need to validate numerical models by comparisons with experimental data and analytical results. Only models whose range of validity is well-understood can be used with confidence for prediction and design.

In addition to errors inherent in the representation itself, there are many types of errors which arise from inexact solution techniques. Large parts of this paper have been devoted to describing methods of reducing or eliminating errors introduced by finite difference methods. We have concentrated on finite difference methods because they are the most versatile and can be made extremely accurate. Most of the difficulties described are associated with obtaining adequate resolution. In modelling shocks, detonations, or flame propagation, time and space scales of interest can span as many as ten orders of magnitude. Thus, to obtain adequate

resolution at steep gradients, we have described a number of methods which rely on asymptotic techniques or adaptive gridding.

Throughout this paper we have pointed to topics where further development of numerical methods would be especially important for solving combustion problems. These include, for example, faster, and yet accurate methods for integrating ordinary differential equations to solve the chemical equations, more general Poisson solvers for multi-dimensional flame calculations, and more general adaptive gridding techniques, such as imbedded adaptive gridding.

Advances in the areas of numerical analysis listed above would be extremely useful, but there are many problems in combustion for which the basic physics and chemistry are not well characterized. Outstanding among these is turbulence, for which a general satisfactory framework for its inclusion in hydrodynamics models has not been developed. Further challenges are posed by the general research areas of radiation transport and heterogeneous processes such as phase changes, droplet dynamics, and soot formation.

All of these phenomena will surely be modelled using many of the techniques we have described. However, new insights into the physics and chemistry as well as new numerical methods will have to be devised before the complete spectrum of reactive flow phenomena can be dealt with anywhere near as well as phenomena in laminar gas phase combustion.

Acknowledgements

The authors would like to thank Drs. Martin Fritts, Steven Zaleszak, Theordore Young, Walter Jones, Marie Flanigan, J. Michael Picone, Teman Burks, Doren Indritz and Walter Shaub of the Naval Research Laboratory for their help with this article. We would like to acknowledge the many helpful discussions with and comments from Dr. C. Westbrook of Lawrence Livermore Laboratories, Drs. D. Kooker, J. Heimerl, and T.P. Coffee of the U.S. Army Ballistics Research Laboratory, Dr. H. Phillips of the British Health and Safety Executive, Dr. E. Kansa of the U.S. Bureau of Mines, and Dr. J. Ramshaw and J. Dukowicz of Los Alamos Scier.tific Laboratory.

We would also like to thank Drs. D. Garvin on the National Bureau of Standards for the information provided in Fig. II.1. We would like to acknowledge Dr. H. Phillips of the Health and Safety Executive and the British Crown Copyright for use of Figs. VIII.3-6, Dr. W. Fickett of Los Alamos Scientific Laboratory and the Physics of Fluids for use of Fig. VIII.1, Dr. C. Mader of Los Alamos Scientific Laboratory and the Combustion Institute for use of Figs. VIII.2, Dr.-Ing. G. Tsatsaronis of the Lehrstuhl für Technische Thermodynamik, Aachen, W. Germany, and the Combustion Institute for use of Figs. IX.10, Dr. J. Warnatz for use of Fig. IX.8, Dr. J. Ramshaw of Los Alamos Scientific Laboratory and the Combustion Institute for the use of Fig. IX.14, Dr. D. Kooker of the U.S. Army Ballistics Research Laboratory and the Combustion Institute for use of Figs. IX. 1 and 2, Dr. J. Heimerl of the U.S. Army Ballistics Research Laboratory for use of Figs. IX.3, 4, 5a, b, and Dr. C. Westbrook of Lawrence Livermore Laboratories for the use of Fig. IX.11.

Finally, we would like to thank Drs. H. Carhart, F. Saalfeld, A. Harvey, A. Schlinder, H. Rabin and Prof. N. Chigier for their help and encouragement and Dr. D. Oran for editing the manuscript. This work has been sponsored by the Naval Research Laboratory through the Office of Naval Research and by the Naval Material Command.

Glossary of Symbols

The symbols defined below are those which are used in more than one main section (Roman numeral I through XI) of this paper. They are defined in the text in the first section in which they are used. Other symbols used in the paper, which are not defined below, are defined for and used only in one section.

$\mathscr{A}$	Amplification factor in a finite difference method.
c_s	Speed of sound
D_j^T	Thermal diffusion coefficient of species j.
D_{jk}	Molecular diffusion coefficient of species j through k.
E	Total energy minus the heats of formation at 0° K.
$\mathscr{E}$	Total energy of the system.
h_j	Temperature dependent enthalpy of species j.
h_{0j}	Heat of formation of species j at 0° K.
H	Total temperature dependent enthalpy of the system.
i	Index referring to spatial points (subscript).
$\underline{i}$	$\sqrt{-1}$
j	Index referring to species (subscript).
k	Index referring to species (subscript).
k_B	Boltzmann's constant.
L_j	Term representing loss of species j.
M	Total number of species present.
M_j	Mass of species j (amu).
n	Index referring to timestep (superscript).
n_j	Number density of species j.
N	Total number density.
P	Pressure.

Q Heat flux.

Q_j Term representing production of species j.

S_j Source term for species j in diffusion velocity matrix.

t Time.

T (1) Temperature, (2) Transpose operation (superscript in a matrix).

v Fluid velocity.

V_j Diffusion velocity of species j.

v_w Characteristic wave velocity

γ Ratio of specific heats: C_p/C_v.

ϵ Internal energy.

η Mixture viscosity coefficient

η_j Viscosity coefficient for species j.

λ Mixture thermal conductivity coefficient

λ_j Thermal conductivity coefficient of species j.

ξ Vorticity.

ρ Mass density.

ρ_j Mass density of species j.

REFERENCES

1. L.D. Landau and E.M Lifshitz, *Fluid Mechanics*, Pergamon Press, New York, 1959.

2. F. Williams, *Combustion Theory*, Addison Wesley, Reading, Mass., 1965.

3. J.O. Hirshfelder, C.F. Curtis, R.B. Bird, *Molecular Theory of Gases and Liquids*, John Wiley and Sons, Inc., New York, 1954.

4. D. Gottlieb and S.A. Orszag, *Numerical Analysis of Spectral Methods: Theory and Applications*, Vol. 26 published for the Society for Industrial and Applied Mathematics, J.W. Arrowsmith, Ltd, Bristol, England, 1977.

5. J.P. Boris, Numerical Solution of the Continuity Equation, *Proceedings of the Second European Conference on Computational Physics*, North Holland Pub. Co., 1976. Also, NRL Memorandum Report 3327, Naval Research Laboratory, Wash., D.C., 20375, 1976.

6. J.P. Boris and D.L. Book, Solution of Continuity Equations by the Method of Flux Corrected Transport, in *Methods in Computational Physics*, **16**, 85-129, Academic Press, New York, 1976.

7. P.D. Lax and B. Wendroff, Systems of Conservation Laws, *Commun. Pure Appl. Math.* **13**, 217-237, 1960.

8. R. Courant, K.O. Friedrichs, and H. Lewy, On the Partial Difference Equations of Mathematical Physics, *Math. Ann.*, **100**, 32; translated by *IBM J. Res. Dev.* **11**, 215-234, 1967.

9. J.P. Boris and D.L. Book, Flux Corrected Transport I: SHASTA—A Fluid Transport Algorithm that Works, *J. Comp. Phys.* **11**, 38-69, 1973; D.L. Book, J.P. Boris, and K.H. Hain, Flux Corrected Transport II: Generalizations of the Method, *J. Comp. Phys.*, **18**, 248-283, 1975; J.P. Boris and D.L. Book, Flux-Corrected Transport III: Minimal-Error FCT

Algorithms, *J. Comp. Phys.* **20**, 397-432, 1976; J.P. Boris, *Flux-Corrected Transport Modules for Solving Generalized Continuity Equations*, Naval Research Laboratory Memorandum Report No. 3237, March, 1976.

10. B. VanLeer, Toward the Ultimate Conservative Difference Scheme, *J. Comp. Phys.* **14**, 361-370, 1974.

11. A. Harten, The Artificial Compression Method for Computation of Shocks and Contact Discontinuities. I. Single Conservation Laws, *Comm. Pure Appl. Math.*, **30**, 611-638, 1977; A. Harten, The Artificial Compression Method for Computation of Shocks and Discontinuities: III. Self-Adjusting Hybrid Schemes, *Math. Comp.*, **32**, 363-389, 1978.

12. A. Ralston, *A First Course in Numerical Analysis*, Chapter 5, McGraw-Hill, New York, 1965.

13. T.R. McCalla, *Introduction to Numerical Methods and Fortran Programming*, John Wiley and Sons, Inc., New York, 1967.

14. J.C. Butcher, Implicit Runge-Kutta Processes, *Math. Comp.* **18**, 50-64, 1964.

15. C.W. Gear, *Numerical Initial Value Problems in Ordinary Differential Equations*, Prentice-Hall, Englewood Cliffs, New Jersey, 1971.

16. M.D. Kregel, A Numerical Integration Method Useful for Studying Ionospheric Phenomena, *J. Atmos. Terr. Phys.* **34**, 1601-1605 1972; T.P. COffee, J.M. Heimerl, and M.D. Kregel, A Numerical Method to Integrate Stiff Systems of Ordinary Differential Equations, Technical Report ARBRL-TR-02206, January 1980, Ballistics Research Laboratory, Aberdeen, Maryland.

17. T.R. Young and J.P. Boris, A Numerical Technique for Solving Stiff Ordinary Differential Equations Associated with the Chemical Kinetics of Reactive-Flow Problems, *J. Phys.*

25. W.M. Shaub and S.H. Bauer, The Reduction of Nitric Oxide During the Combustion of Hydrocarbons, *Combust. Flame* **32**, 35-55, 1978.

26. F.W. Williams and R.S. Sheinson, Vertical Tube Combustion Reactor, U.S. Patent #3,926,562, Dec. 16, 1975. Also Manipulation of Cool and Blue Flames in the Winged Vertical Tube Reactor, *Combust. Sci. and Tech.* **7**, 85-92, 1973.

27. R.S. Sheinson and F.W. Williams, Chemiluminescence Spectra from Cool and Blue Flames: Electronically Excited Formaldehyde, *Combust. Flame* **21**, 221-230, 1973; also F.W. Williams and W.L. Stumpf, Jr., Quantitative Sampling from a Vertical Tube Reactor, *Analytical Chemistry* **44**, 1829-1833, 1972.

28. D. Indritz, Chemiluminescence from Di-t-Butyl Peroxide and the Computer Design of Experiments, Ph.D. Dissertation, Princeton University, 1978; D. Indritz, H. Rabitz, and F.W. Williams, Use of Modeling to Design Experiments. Doping Radicals into Complex Combustion Systems, *J. Phys. Chem.* **81**, 2526-2531, 1977.

29. W. Noh, CEL: A Time-Dependent, Two-Space-Dimensional Coupled Eulerian-Lagrangian Code, *Methods in Computational Physics*, Vol. 3, Academic Press, New York, 1964.

30. R.K-C. Chan, A Generalized Arbitrary Lagrangian-Eulerian (GALE) Method for Incompressible Flows with Sharp Interfaces, Report 73-575-LJ, Science Applications, Inc., P.O. Box 2351, La Jolla, California, 92037.

31. C.M. Lund, HCT—A General Computer Program for Calculating Time-Dependent Phenomena Involving One-Dimensional Hydrodynamics Transport, and Detailed Chemical Kinetics, UCRL-52504, Lawrence Livermore Laboratories, Livermore, California, 1978.

32. F.H. Harlow and A.A. Amsden, A Numerical Fluid Dynamics Method for All Flow Speeds, *J. Comp. Phys.* **8**, 197-214, 1971.

Chem. **81**, 2424-2427, 1977. Also, a more detailed account in T.R. Young, CHEMEQ—A Subroutine for Solving Stiff Ordinary Differential Equations, Naval Research Laboratory Memorandum Report 4091, Naval Research Laboratory, Wash., D.C., 20375, 1979.

18. T.J. Keneshea, A Technique for Solving the General Reaction Rate Equations in the Atmosphere, AFCRL-67-0221, Air Force Geophysical Laboratory, Hanscom AFB, Mass. 01731, April, 1967.

19. D.R. Stull and H. Prophet, *JANAF Thermochemical Tables*, 2nd edition National Standard Reference Data Series, U.S. National Bureau of Standards, No. 37, Gaithersburg, Md., 1971.

20. S. Gordon and B.J. McBride, *Computer Program for Calculation of Complex Chemical Equilibrium Compositions, Rocket Performance, Incident and Reflected Shocks,* and *Chapman-Jouguet Detonations*, NASA SP-273, 1976, National Aeronautics and Space Administration, Wash., D.C.

21. D.B. Olson and W.C. Gardiner, Jr. An Evaluation of Methane Combustion Mechanisms, *J. Phys. Chem.* **81**, 2514-2519, 1977.

22. C.K. Westbrook, An Analytical Study of the Shock Tube Ignition of Mixtures of Methane and Ethane, *Combustion Science and Technology* **20**, 5-17, 1979.

23. K. Tabayashi and S.H. Bauer, The Early Stages of Pyrolysis and Oxidation of Methane, *Combust. Flame* **34**, 63-83, 1979.

24. W.M. Shaub and M.C. Lin, On Characterization of High Temperature Vapors, *Proceedings of the 10th Materials Research Symposium*, 1249-1264, National Bureau of Standards, Gaithersburg, Md., Sept., 1978.

33. W.C. Rivard, O.A. Farmer, and T.D. Butler, RICE: A Computer Program for Multi-component Chemically Reactive Flows at All Speeds, Los Alamos Scientific Laboratory Report LA-5812, Los Alamos Scientific Laboratory, Los Alamos, New Mexico, 1975.

34. S.K. Godunov, A Difference Technique for Numerical Solution of Hydrodynamic Shocks *Mat. Sb.* **47**, 271-306, 1959.

35. J. Glimm, Solutions in the Large for Nonlinear Hyperbolic Systems of Equations, *Comm. Pure Appl. Math.*, **18**, 697-715, 1965.

36. G.A. Sod, A Survey of Several Finite Difference Methods of Systems of Nonlinear Hyperbolic Conservation Laws, *J. Comp. Phys.* **27**, 1-31, 1978.

37. A.J. Chorin, Random Choice Solution of Hyperbolic Systems *J. Comp. Phys.* **22**, 517-534, 1976; *J. Comp. Phys.*, Random Choice Methods with Applications to Reacting Gas Flows, **25**, 253-273, 1977.

38. C.K. Forester, Higher Order Monotonic Convective Difference Schemes, *J. Comp. Phys.* **23**, 1-23, 1977.

39. S.T. Zalesak, Fully Multidimensional Flux-Corrected Transport Algorithms for Fluids, *J. Comp. Phys.* **31**, 335-362, 1979.

40. E.S. Oran, T.R. Young, and J.P. Boris, Application of Time-Dependent Numerical Methods to the Description of Reactive Shocks, *Proceedings of the 17th Symposium (International) on Combustion*, The Combustion Institute, Pittsburgh, Pa, 43-54, 1978.

41. S. Eidelman and A. Burcat, The Mechanism of a Detonation Wave Enhancement in a Two-Phase Combustible Medium, to appear *Proceedings of the 18th Symposium (International) on Combustion,* The Combustion Institute, Pittsburgh, Pa., 1980; S. Eidelman and A. Burcat, The Evolution of a Detonation Wave in a Cloud of Fuel Droplets, to appear in

AIAA Journal, 1980.

42. J.P. Boris, T.P. Coffey, and S. Fisher, The Kelvin-Helmholtz Instability and Turbulent Mixing, NRL Memorandum Report 3135, Naval Research Laboratory, Washington, D.C., 20375, September, 1975.

43. I. Lindemuth and J. Killeen, Alternating Direction Implicit Techniques for Two-Dimensional Magnetohydrodynamic Calculations, *J. Comp. Phys.* **13**, 181-208, 1973.

44. W.R. Briley and H. McDonald, Solution of the Three-Dimensional Compressible Navier Stokes Equations by an Implicit Technique, *Proceedings Fourth International Conference on Numerical Methods in Fluid Dynamics*, 105-110, Springer-Verlag, New York, 1975; H. McDonald and W.R. Briley, Three-Dimensional Supersonic Flow of a Viscous or Inviscid Gas, *J. Comp. Phys.* **19**, 150-178, 1975; W.R. Briley an H. McDonald, Solution of the Multi-Dimensional Compressible Navier-Stokes Equations by a Generalized Implicit Method, *J. Comp. Phys.* **24**, 372-397. 1977; W.R. Briley and H. McDonald, On the Structure and Use of Linearized Block Implicit Schemes, *J. Comp. Phys.* **34**, 54-73, 1980.

45. R.M. Beam and R.F. Warming, An Implicit Finite-Difference Algorithm for Hyperbolic Systems in Conservation-Law Form, *J. Comp. Phys.* **22**, 87-110, 1976; R.F. Warming and R.M. Beam, On the Construction and Application of Implicit Factored Schemes for Conservation Laws, *Symposium on Computational Fluid Dynamics*, SIAM-AMS Proceedings, Vol. 11, 1977; R.M. Beam and R.F. Warming, An Implicit Scheme for the Compressible Navier-Stokes Equations, *AIAA Journal*, 393-402, 1978.

46. H. McDonald, Combustion Modelling in Two and Three Dimensions—Some Numerical Considerations, *Prog. in Energy and Combust. Sci.*, **5**, 97-122, 1979.

47. C.K. Westbrook, A Generalized ICE Method for Chemically Reactive Flows in Combustion Systems, *J. Comp. Phys.* **29**, 67-80, 1978.

48. J.D. Ramshaw and J.K. Dukowicz, APACHE: A Generalized-Mesh Eulerian Computer Code for Multicomponent Chemically Reactive Flows, Report LA-7427, Los Alamos Scientific Laboratory, Los Alamos, New Mexico, 87545. This code uses the tensor viscosity method for differencing the convective term, as described by J.K. Dukowicz and J.D. Ramshaw, *J. Comp. Phys.* **32**, 71-79, 1979.

49. C.W. Hirt, A.A. Amsden, and J.L. Cook, An Arbitrary Lagrangian Eulerian Computing Method for All Flow Speeds, *J. Comp. Phys.* **14**, 227-254, 1974.

50. J.D. Ramshaw and J.A. Trapp, A Numerical Technique for Low-Speed Homogeneous Two-Phase Flow with Sharp Interfaces, *J. Comp. Phys.* **21**, 438-454, 1976.

51. W.W. Jones and J.P. Boris, Flame—A Slow-Flow Combustion Model, NRL Memorandum Report 3970, Naval Research Laboratory, Washington, D.C., 20375, 1979, and W.W. Jones and J.P. Boris, Flame and Reactive Jet Studies Using a Self-Consistent Two-Dimensional Hydrocode, *J. Phys. Chem.* **81**, 2532-2534, 1977.

52. W. Noh and P. Woodward, SLIC (Single Line Interface Calculation *Proceedings of the Fifth International Conference on Fluid Dynamics*, p. 330-340, Springer-Verlag, 1976.

53. A.J. Chorin, Flame Advection and Propagation Algorithms, *J. Comp. Phys.* **35**, 1-11, 1980.

54. R.G. Rehm and Howard R. Baum, The Equations of Motion for Thermally Driven, Bouyant Flows, *J. Research* (National Bureau of Standards) **83**, 297-308, 1978.

55. J.P. Boris, ADINC: An Implicit Lagrangian Hydrodynamics Code, Naval Research Laboratory Memorandum Report 4022, Naval Research Laboratory, Wash., D.C., 20375, 1979.

56. W.P. Crowley, *Proceedings of the Second International Conference in Numerical Methods in Fluid Dynamics*, Springer-Verlag, New York, 1971.

57. M.J. Fritts and J.P. Boris, The Lagrangian Solution of Transient Problems in Hydrodynamics using a Triangular Mesh., *J. Comp. Phys.* **31**, 173-215, 1979; M.J. Fritts, E.W. Miner, and O.M. Griffith, Numerical Calculation of Wave-Structure Interactions, in *Computer Methods in Fluids,* Chapter 1 Penteck Press, 1980; M.J. Fritts, Transient Free Surface Hydrodynamics, NRL Memo Report 3651, 1977, Naval Research Laboratory, Wash, D.C., 20375.

58. J.U. Brackbill, Numerical Magnetohydrodynamics for High-Beta Plasmas, *Methods in Computational Physics* **16**, 1-42, 1976.

59. G.B. Zimmerman, Numerical Simulation of the High Density Approach to Laser Fusion, Lawrence Livermore Laboratory, Preprint UCRL-74811, Livermore, California, 1973.

60. See, for example, C. Lanczos, *Applied Analysis*, Prentice Hall, New Jersey, 1956; also see G. Arfken, *Mathematical Methods for Physicists*, 2nd edition, Academic Press, New York, 1971.

61. E. Turkel, Numerical Methods for Large-Scale Time-Dependent Partial Differential Equations, Report No. 79-20, Institute for Computer Applications in Science and Engineering, NASA Langley Research Center, Hampton, Va.

62. R.W. Hockney, The Potential Calculation and Some Applications, *Methods in Computational Physics* **9**, 135-211, 1970.

63. D.S. Kershaw, The Incomplete Cholesky - Conjugate Gradient Methods for the Iterative Solution of Systems of linear Equations, *J. Comp. Phys.* **26**, 43-65, 1978.

64. R.V. Madala, An Efficient Direct Solver for Separable and Non-Separable Elliptic Equations, *Monthly Weather Review* **106**, 1735-41, 1978.

65. O. Buneman, *A Compact Non-Iterative Poisson Solver*, Stanford University Institute for Plasma Rsearch, Report #294, 1969.

66. J.P. Boris and E.S. Oran, Detailed Modelling of Reactive Flows, *Proceedings of the GAMNI International Conference on Numerical Methods for Engineering, Paris, 1978.*

67. J.M. Picone, Approximate Equations of Multicomponent Mixtures of Neutral Gases, Naval Research Laboratory Memo Report, 1980.

68. S. Chapman and T.G. Cowling, *The Mathematical Theory of Non-Uniform* Gases, Cambridge University Press, Cambridge England, 3rd Ed., 1970.

69. C.R. Wilke, A Viscosity Equation for Gas Mixtures, *J. Chem. Phys.*, **18**, 517-519, 1950.

70. E.A. Mason and S.C. Saxena, Approximate Formula for the Thermal Conductivity of Gas Mixtures, *Phys. Fluids*, 1, 361-369, 1958.

71. J.O. Hirschfelder, Heat Transfer in Chemically Reaching Mixtures, I, *J. Chem. Phys.* **26**, 274-282, 1957; also, Heat Conductivity in Polyatomic Electronically Excited, or Chemically Reaching Mixtures, *6th Symposium (International) on Combustion*, 351-366, Reinhold Pub. Corps., New York, 1957.

72. E.A. Mason and T.R. Marrero, Gaseous Diffusion Coefficients, *Journal of Physical and Chemical Reference Data*, **1**, 3-118, 1972.

73. N.N. Yanenko, *The Method of Fractional Steps*, Springer-Verlag, New York 1971; A.W. Rezzi and H.E. Bailey, A Generalized Hyperbolic Marching Method for Chemically Reacting Three-Dimensional Supersonic Flow Using a Splitting Technique, AIAA *Second Computational Fluid Dynamics Conference*, Hartford, Conn. June 19-20, 1975.

is available from the American Institute of Aeronautics and Astronautics, 1290 6th Avenue, New York, N.Y. 10019, paper no. A752167; R.J. Kee and J.A. Miller, "A Split-Operator, Finite Difference Solution for Axisymmetric Laminar Jet Diffusion Flames," SAND 77-8502, Sandia Livermore Laboratory, April 1977; W.A. Reinhardt, "Parallel Computation of Unsteady, Three Dimensional, Chemically Reacting, Nonequilibrium Flow Using a Time-Split Finite-Volume Method on the Illiac IV," *J. Phys. Chem. 81* (25), 2427-2435, 1977.

74. D. Schnack and J. Kileen, Nonlinear, Two-Dimensional Magnetohydrodynamic Calculations, to appear in *J. Comp. Phys.*, 1980.

75. K. Hain, G. Hain, K.V. Roberts, S.J. Roberts, and W. Koppendörfer, Fully Ionized Pinch Collapse, *Zeitschrift für Naturforschung*, **15**, 1039-1050, 1960; D. Düchs and H.R. Griem, Computer Study of Dynamic Phase of a Small O-Pinch, *Phys. Fluids* **9**, 1099-1110; 1966; D. Düchs, H.P. Fürth, P.H. Rutherford, Radial Transport in Tokamak Discharges, *Plasma Physics and Controlled Nuclear Fusion Research*, Vol. 1, 369-391, 1971, International Atomic Energy Angency, Vienna, 1971.

76. D.E. Kooker, Transient Laminar Flame Propagation in Confined Premixed Gases: Numerical Predictions, *17th Symposium (International) on Combustion*, The Combustion Institute, Pittsburgh, Pa., 1329-1339, 1978; also, Numerical Predictions for Laminar Flame Propagation in Confined Ozone/Oxygen Mixtures: Influence of Initial Temperature and Pressure, *Proc. 17th AIAA Aerospace Sciences Meeting*, Paper 79-0292, 1979, AIAA, New York.

77. J.M. Hyman, "A Method of Lines Approach to the Numerical Solution of Conservation Laws," *Third IMACS International Symposium on Computer Methods for Partial Differential Equations*, LeHigh University, Bethlehem Pa, June 20-22, 1979. also Los Alamos UR 79-837, Los Alamos Scientific Laboratory, Los Alamos, N.M.

78. E.S. Oran and J.P. Boris, Theoretical and Computational Approach to Flame Ignition, *Proc. International Colloquium as Gas Dynamics of Explosions and Reactive Systems*, AIAA, New York, 1979

79. E.g., A.R. Mitchell and J.Y. Thomson, Finite Difference Methods of Solution of the von Mises Boundary Layer Equation with Special Reference to Conditions Near a Singularity, *Z. Angew. Math. Phys.*, **9**, 26-37, 1958.

80. S.B. Margolis, Time-Dependent Solution of a Premixed Laminar Flame, *J. Comp. Phys.*, **27**, 410-427, 1978.

81. H.A. Dwyer and B.R. Sanders, Numerical Modelling of Unsteady Flame Propagations, SAND 77-8275, Sandia Laboratories Report, Livermore, California, 1978; H.A. Dwyer, R.J. Kee, and B.R. Sanders, The Use of Generalized Coordinates and Adaptive Grids for Two-Dimensional Unsteady Flames, *Proceedings of the 7th International Colloquium on Gas Dynamics of Explosions and Reactive Systems*, AIAA, 1979.

82. R. Gelinas, S.K. Doss, K. Miller, A Finite Element Method with Moving Nodes, submitted to *J. Comp. Phys*; also Report No. SAI/PL/F179, Science Applications, Inc., 1811 Santa Rita Road, Pleasanton, California.

83. J.J. Erpenbeck, Stability of Idealized One-Reaction Detonations, *Phys. Fluids*, **7**, 684-706, 1964; also Stability of Idealized One-Reaction Detonations: Zero Activation Energy, *Phys. Fluids*, **8**, 1192-1193, 1965.

84. W. Fickett and W.W. Wood, Flow Calculations for Pulsating One-Dimensional Detonations, *Phys. Fluids*, **9**, 903-917, 1966.

85. C.L. Mader, One- and Two-Dimensional Flow Calculations of the Reaction Zones of Ideal Gas, Nitromethane, and Liquid TNT Detonations, *12th Symposium (International) on Combustion*, 701-710, The Combustion Institute, Pittsburgh, Pa., 1969

86. M.D. Slaughter, B.W. Olinger, J.D. Kersher, C.L. Mader, A.L. Bowman, Interaction of Explosive-Driven Air Shocks with Water and Plexiglas, LA-7454, Los Alamos Scientific Laboratory, P.O. Box 1663, Los Alamos, N.M., 87545, 1978.

87. See, for example *9th Symposium (International) on Combustion*, Academic Press Inc., New York, 1963, which includes: H. Gg. Wagner, Reaction Zone and Stability of Gaseous Detonations, 454-460; N. Manson, C. Brochet, J. Brossard, and Y. Pujol, Vibratory Phenomena and Instability of Self-Sustained Detonations in Gases, 461-469. Also, G.L. Schott, Observations of the Structure of Spinning Detonations, *Phys. Fluids* **8**, 850-865, 1965.

88. S. Taki and T. Fujiwara, Numerical Analysis of a Two-Dimensional Nonsteady Detonations, *Proceedings of the AIAA 9th Fluid and Plasma Dynamics Conference*, 1-9, 1976.

89. V.P. Korobienikov, V.A. Levin, V.V. Markov, and G.G. Chernys Astronautica Acta **17**, Propagation of Blast Waves in a Combustible Gas, 529-537, 1972.

90. B. Van Leer, Stabilization of Difference Schemes for the Equations of Inviscid Compressible Flow by Artificial Diffusion, *J. Comput. Phys.* **3**, 473-486, 1969.

91. R.A. Strehlow, A.A. Adamczyk and R.J. Stiles, Transient Studies of Detonation Waves, *Astronautica Acta* **17**, 509-527, 1972.

92. H. Phillips, Decay of Spherical Detonations and Shocks, Technical Paper No. 7, British Governments Health and Safety Executive, Health and Safety Laboratories, Buxton SK179JN, England, 1977.

93. R.A. Strehlow, Unconfined Vapor Cloud Explosions—an Overview. *14th Symposium (International) on CombustionfR, 1189-1200, 1973; R.A. Strehlow and W.E. Baker, The Characterization and Evaluation of Accidental Explosions, Prog. Energy and Comb. Sci.* **2**, 27-60, 1976.

94. G.I. Taylor, The Dynamics of the Combustion Products behind Plane and Spherical Detonation Fronts in Explosives, *Proc. Roy. Soc.*, **A200**, 235-247, 1949.

95. G.F. Widhopf and K.J. Victoria, On the Solution of the Unsteady Navier-Stokes Equations Including Multi-Component Finite Rate Chemistry, *Computers and Fluids* **1**, 159-184, 1973.

96. E.S. Oran, J.P. Boris, T. Young, M. Flanigan, T. Burks, M. Picone, Numerical Simulations of Detonations in Hydrogen-Air and Methane-Air Mixtures, *18th Symposium (International) on Combustion*, The Combustion Institute, Pittsburgh, Pa., 1980; also simulations of Gas Phase Detonations: Introduction of an Induction Parameter Model, NRL Memo. Report, Naval Research Laboratory, Washington, D.C. 20375; D. Book, J. Boris, A. Kuhl, E. Oran, M. Picone, S. Zalesak, Simulation of Complex Shock Reflections from Wedge in Inert and Reactive Gas Mixtures, to appear in *Proceedings of the 7th International Conference on Numerical Methods in FLuid Dynamics*, Springer-Verlag, New York, 1980.

97. J.M Heimerl and T.P. Coffee, The Detailed Modelling of Premixed, Laminar Steady-State Flames, I. Ozone, to be published in *Combust. Flame*, 1980.

98. J. Warnatz, Calculation of the Structure of Laminar Flat Flames I: Flame Velocity of Freely Propagating Ozone Decomposition Flames, *Ber. Bunsenges Phys. Chem.* **82**, 193-200, 1978. II: Flame Velocity and Structure of Freely Propagating Hydrogen-Oxygen and Hydrogen-Air-Flames, *Ber. Bunsenges Phys. Chem.* **82**, 643-649, 1978. The Structure of Freely Propagating and Burner Stabilized Flames in the $H_2 - CO - O_2$ System, *Ber. Bunsenges. Phys. Chem.* **83**, 950-957, 1979.

99. G. Tsatsaronis, Prediction of Propagating Laminar Flames in Methane, Oxygen, Nitrogen Mixtures, *Comb. Flame* **33**, 217-239, 1978.

100. C.K. Westbrook and F.L. Dryer, A Comprehensive Mechanism for Methanol Oxidation, submitted to *Comb. Sci. and Tech.*, 1979; also UCRL preprint 82434, March, 1979, Lawrence Livermore Laboratory, Livermore, Calif., 94550. C.K. Westbrook and F.L. Dryer, Modelling of Flame Properties of Methanol, *Proc. Alcohol Fuels Technology 3rd Int. Sym*; Asilomar, Calif., 1979; also UCRL preprint 82434, March, 1979, Lawrence Livermore Laboratories, Livermore, Calif., 94550. C.K. Westbrook and F.L. Dryer, Prediction of Laminar Flame Properties of Methanol-Air Mixtures, UCRL preprint 82717, April 1979, Lawrence Livermore Laboratories, Livermore, Ca., 94550; submitted to *Comb. Flame.*

101. E.J. Kansa, An Implicit Nonlinear Algorithm for Solving Transient Multidimensional Chemically Reacting Fluid Flow Problems, Pittsburgh Mining and Safety Research Center, Bureau of Mines, Pittsburgh, Pa.

102. T.D. Butler and P.J. O'Rourke, A Numerical Method for Two-Dimensional Unsteady Reacting Flows, *16th Symposium (International) in Combustion*, The Combustion Institute, Pittsburgh, Pa, 1503-1515, 1976.

103. W. Jost, J. Krug, and L. Sieg, Observations on Disturbed Flames, *4th Symp. (Int.) on Combustion*, p. 535-537, The Combustion Institute, Pittsburgh, Pa., 1953.

104. H. Guenoche, Flame Propagation in Tubes and Closed Vessels, p. 149, *Nonsteady Flame Propagation*, G.H. Markstein (ed.), Macmillan, 1964.

105. S. Galant, Analysis of Inhibition Phenomena in Halogenated Flames, *Proceedings of the 7th International Colloquium on Gas Dynamics of Explosives and Reactive Flows*, AIAA, 1979.

106. S.B. Margolis, Time-Dependent Solution of a Premixed Laminar Flame, *J. Comp. Phys.* **27**, 410-427, 1978.

107. P.L. Stephenson and R.G. Taylor, Laminar Flame Propagation in Hydrogen, Oxygen, Nitrogen Mixtures, *Combust. Flame* **20**, 231-244, 1973.

108. A.G. Streng and A.V. Grosse, The Ozone to Oxygen Flame, *6th Symp. (Int.) on Combustion*, The Combustion Institute, Pittsburgh, Pa., 264-273, 1957.

109. G. Dixon-Lewis and A. Williams, Some Observations on the Combustions of Methane in Premixed Flames, *11th Symposium (International) on Combustion*, The Combustion Institute, Pittsburgh, Pa., 951-958, 1967; G. Dixon-Lewis, Flame Structure and Flame Reaction Kinetics, I. *Proc. R. Soc. London* **A298**, 495-512, 1967; II. ibid II, **A307**, 111-135, 1968; ibid V, **A317**, 235-236, 1970; ibid VI, **A330**, 199-218, 1972; ibid VIII, **A331**, 571-584, 1973; Kinetic Mechanism, Structure and Properties of Premixed Flames in Hydrogen-Nitrogen Mixtures, ibid **292**, A1388, 45-99, 1979.

110. J.R. Creighton and C.M. Lund, Modelling Study of Flame Structure in Low Pressure, Laminar, Pre-mixed Methane Flames, *Proc. 10th Materials Research Symp.*, 1223-1249, National Bureau of Standards, Gaithersburg, Md., 1978.

111. S.V. Patankar and D.B. Spalding, *Heat and Mass Transfer in Boundary Layers*, 2nd Ed., Intertext Books, London, 1970.

112. D.B. Spalding, P.L. Stephenson, R.G. Taylor, A Calculation Procedure for the Prediction of Laminar Flame Speeds, *Comb. Flame* **17**, 55-64, 1971.

113. G.E. Andrews and D. Bradley, The Burning Velocity of Methane-Air Mixtures, *Combust. Flame* **19**, 275-288, 1972; also Determination of Burning Velocity by Double Ignition in a Closed Vessel, *Combust. Flame* **20**, 77-89, 1973.

114. J. Peeters and G. Mahnen, Reaction Mechanisms and Rate Constants of Elementary Steps in Methane-Oxygen Flames, *14th Symposium (International) on Combustion*, The Combustion Institute, Pittsburgh, Pa., 133-146, 1973.

115. R.M. Fristrom, C. Grunfelder, and S. Favin, Methane-Oxygen Flame Structure. II. Characteristic Profiles in a Low-Pressure, Laminar, Lean, Premixed Methane-Oxygen Flame, *J. Phys. Chem.* **64**, 1386-1392, 1960.

116. R.J. Gelinas, Ignition Modelling, SAI Report PL-NII-78-02, Science Applications, Inc., 1811 Santa Reta Road, Pleasanton, Calif., 94566.

117. R. Akrich, C. Vovelle, and Delbourgo, Flame Profiles and Combustion Mechanisms of Methanol-Air Flames Under Reduced Pressure, *Combust. Flame* **32**, 171-179, 1978.

118. M. Herzberg, Report RI8127, U.S. Bureau of Mines; 1976 also, M. Herzberg, K. Cashdollar, C. Litten, and D. Burgess, Report RI8263, U.S. Bureau of Mines, Pittsburgh, Pa., 1978.

119. H.L. Swinney and J.P. Gollub, The Transition to Turbulence Physic Today, 41-49, August, 1978.

120. F.H. Harlow, Turbulence Transport Modelling AIAA Selected Reprint Series, Vol. XIV, AIAA, N.Y., 1973.

121. B.E. Launder and D.B. Spalding, *Mathematical Models of Turbulence*, Academic Press, New York, 1972.

122. W.C. Reynolds and T. Cebeci, Calculation of Turbulent Flows, *Turbulence: Topics in Applied Physics*, Chapt. 5, 193-229, Springer-Verlag, New York, 1978.

123. W.C. Reynolds, Computation of Turbulent Flows, *Annual Reviews of Fluid Mechanics*, **8**, p. 183, 1976.

124. H.W. Liepman, The Rise and Fall of Ideas in Turbulence, *American Scientist*, **67**, 221-228, 1979.

125. J. Boris, J.H. Orens, J. Dawson and R.V. Roberts, Computations on Anomalous Resistance, *Physical Review Letters 25*, (11), 706-710, 14 September 1970.

126. W. Manheimer and J. Boris, Self-Consistent Theory of a Collisionless Resistive Shock, *Physical Review Letters 28*, 11, pp. 659-662, March 1972; also Marginal Stability Analysis: A Simpler Approach to Anomalous Transport, *Comments on Plasma Physics and controlled Fusion*, 3(1), 15-24, Gordon and Breach, New York, 1977.

127. M. Lessen, On the Power Laws for Turbulent Jets, Wakes and Shearing Layers and Their Relationship to the Principle of Marginal Instability, *J. Fluid Mech.*, **88**, 535-540, 1978.

128. A. Roshko, Structure of Turbulent Shear Flows: A New Look, *AIAA Journal*, **14**, 1349-1357, 1976; A. Roshko, Progress and Problems in Understanding Turbulent Shear Flows, (Ed. S.N.B. Murthy), 295-311, Plenum, 1975.

129. F.K. Browand and P.D. Weidman, Large Scales in the Developing Mixing-Layer, *J. Fluid Mech.*, **76**, 127-144, 1976. F.K. Browand and J. Laufer, The Role of Large Scale Structures in the Initial Development of Circular Jets, *Proc. 4th Biennial Symposium on Turbulence in Liquids*, Univ. Missouri-Rolla, 333-344, Science Press, 1975.

130. J. Boris and M. Picone, Beam Generated Vorticity and Convective Channel Mixing, NRL Memo. Report, Naval Research Laboratory, Washington, D.C., 20375, 1980.

131. S.A. Orszag, M. Israeli, Numerical Solution of Viscous Incompressible Flows, *Annual Reviews of Fluid Mechanics*, **6**, 281-318, 1974.

132. D. Kwak and W.C. Reynolds, Three-Dimensional Time Dependent Computation of Turbulent Flow, Rept. TF-5, Mech. Engrg. Dept., Stanford University, 1975.

133. S. Shaanan, J.H. Ferziger, and W.C. Reynolds, Numerical Simulation of Turbulence in the Presence of Shear, Rept. TF-6, Mech. Engrg. Dept., Stanford University, 1975.

134. A.N. Kolmogorov, Equations of Turbulent Motion of an Incompressible Fluid, *Izv. Akad. Nauk. Ser. Phys.* **6**, No. 1/2, 56-58, 142.

135. D.B. Spalding, Concentration Fluctuations in a Round Turbulent Free Jet, *Chem. Eng. Sci.*, **26**, 95-107, 1971.

136. W.S. Lewellan, M.E. Teske, and Coleman duP. Donaldson, Variable Density Flows Computed by a Second Order Closure Description of Turbulence, *AIAA Journal*, **14**, 382-387, 9176.

137. W.S. Lewellen, Use of Invariant Modelling, *Handbook of Turbulence, Vol. 1*, Ed. by Walter Frost and Trevor H. Moulden, Plenum Pub. Co., 1977.

138. C. duP. Donaldson, On the Modelling of the Scalar-Correlations Necessary to Construct a Second-Order Closure Description of Turbulent Flow, *Turbulent Mixing in Nonreactive and Reactive Flows*, Ed. by S.N.B. Murthy, Plenum Press, New York, 1975.

139. E.S. Fishburne, A.K. Varma, and C. duP. Donaldson, Aspects of Turbulent Combustion, Proceedings AIAA 15th Aerospace Sciences Meeting, 24-26, January, 1977.

140. D. Jeandel, J.F. Brison, and J. Mathieu, Modeling Methods in Physical and Spectral Space, *Phys. Fluids* **21**, 169-182, 1978.

141. R. Borghi and D. Dutoya, On the Scale of the Fluctuations in Turbulent Combustion, *Proceedings of the Seventeenth Symposium (International) on Combustion*, 235-244, The Combustion Institute, Pittsburgh, Pa., 1979..

142. K.N.C. Bray, The Interaction Between Turbulence and Combustion, *Proceedings of the Seventeenth Symposium (International) on Combustion*, 223-233, The Combustion Institute, Pittsburgh, Pa., 1979.

143. F.E. Marble, The Coherent Flame Model for Turbulent Chemical Reactions, Project SQUID Technical Report TRW-9-PU, January, 1977.

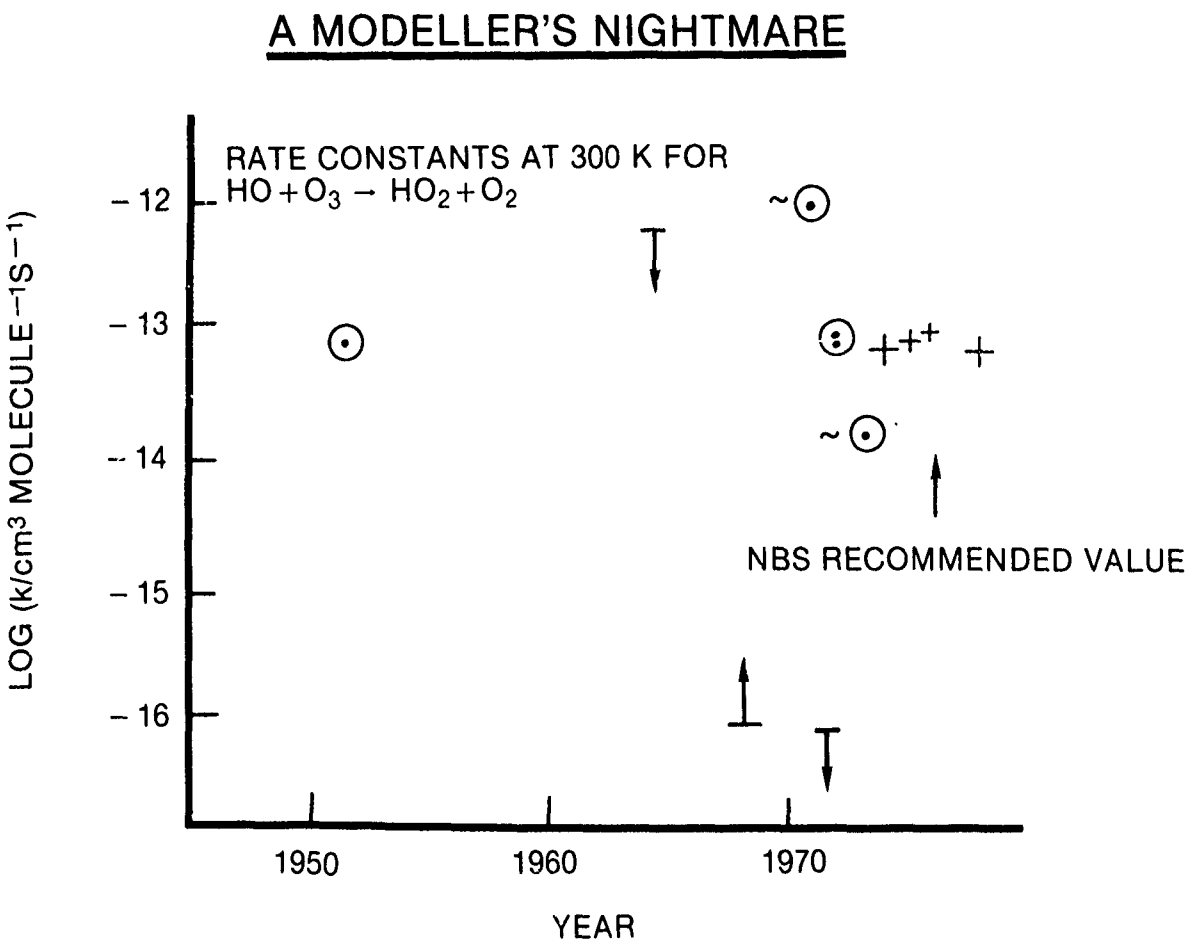

Fig. II.1 – Rate constant for the reaction $HO + O_3 \rightarrow HO_2 + O_2$ shown as a function of the year of its measurement. Measurements are indicated by points, circles, daggers, and horizontal bars. Arrows on top or below the bars indicate measurements which give upper and lower bounds. (Information provided by Dr David Garvin of the U.S. National Bureau of Standards.)

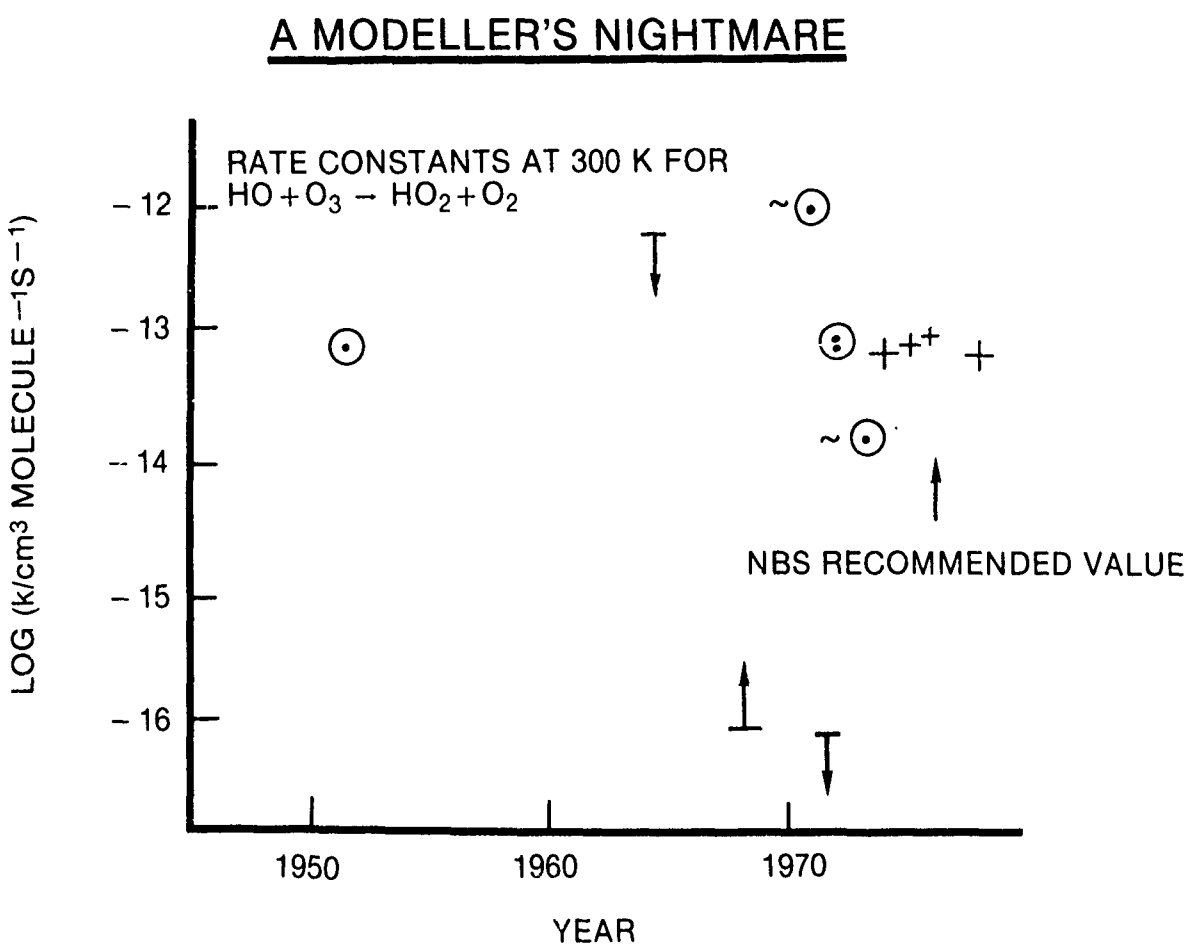

Fig. II.1 — Rate constant for the reaction $HO + O_3 \rightarrow HO_2 + O_2$ shown as a function of the year of its measurement. Measurements are indicated by points, circles, daggers, and horizontal bars. Arrows on top or below the bars indicate measurements which give upper and lower bounds. (Information provided by Dr. David Garvin of the U.S. National Bureau of Standards.)

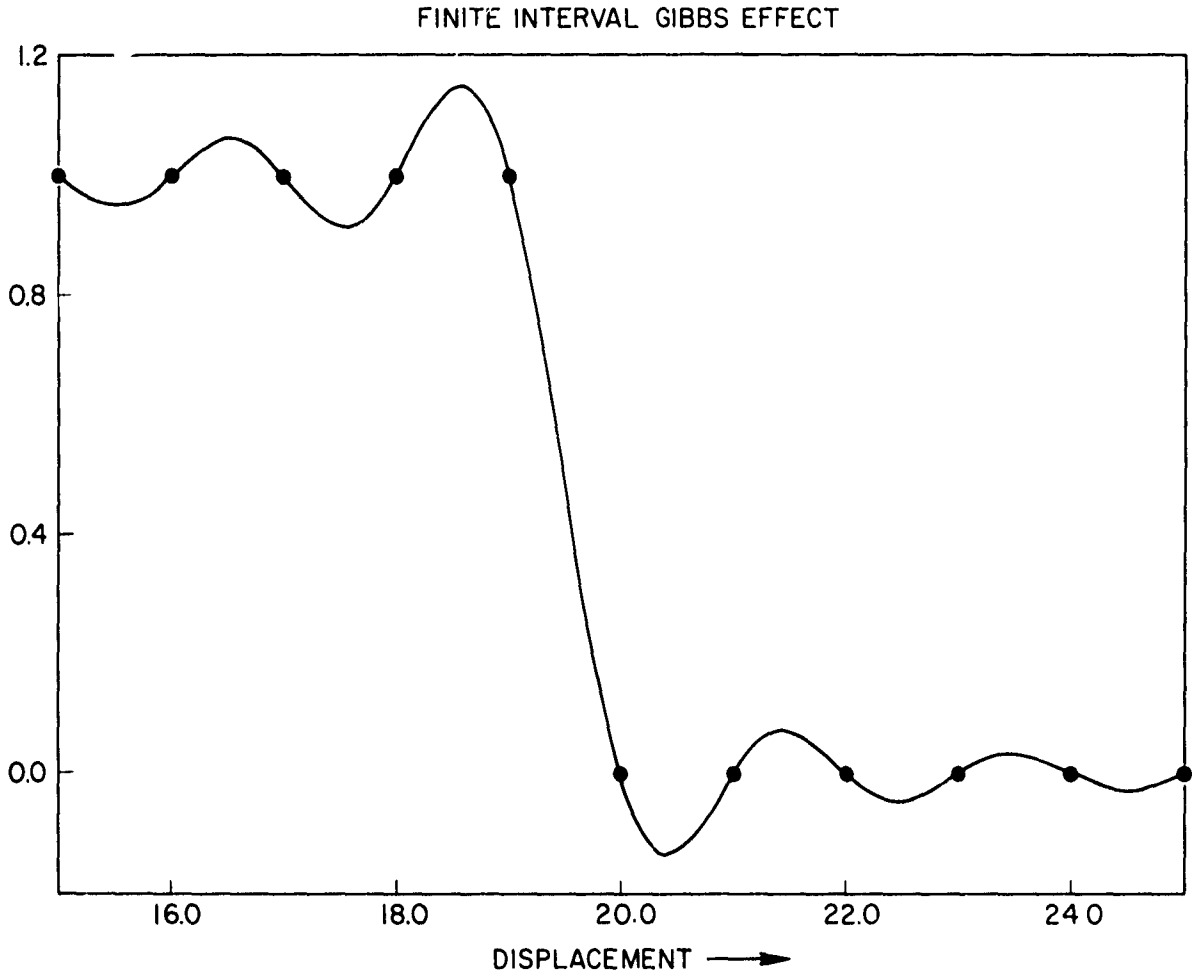

Fig. III.2 — Illustration of the way in which the Gibb's errors appear in a calculation. Grid points are marked by the black dots.

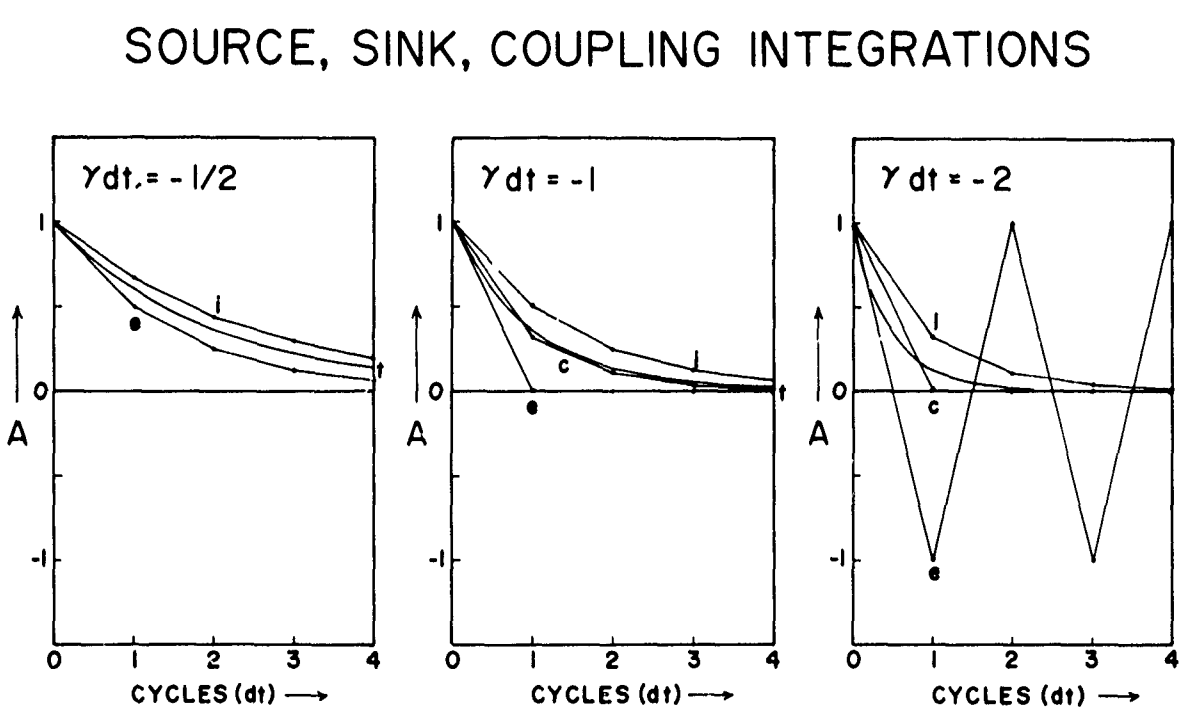

Fig. III.1 — Solutions for the source, sink, and coupling terms when γ in Eq. (III.1) is negative. Note that *t*, *e*, *c*, and *i* indicate the analytical, explicit, centered, and implicit solutions, respectively

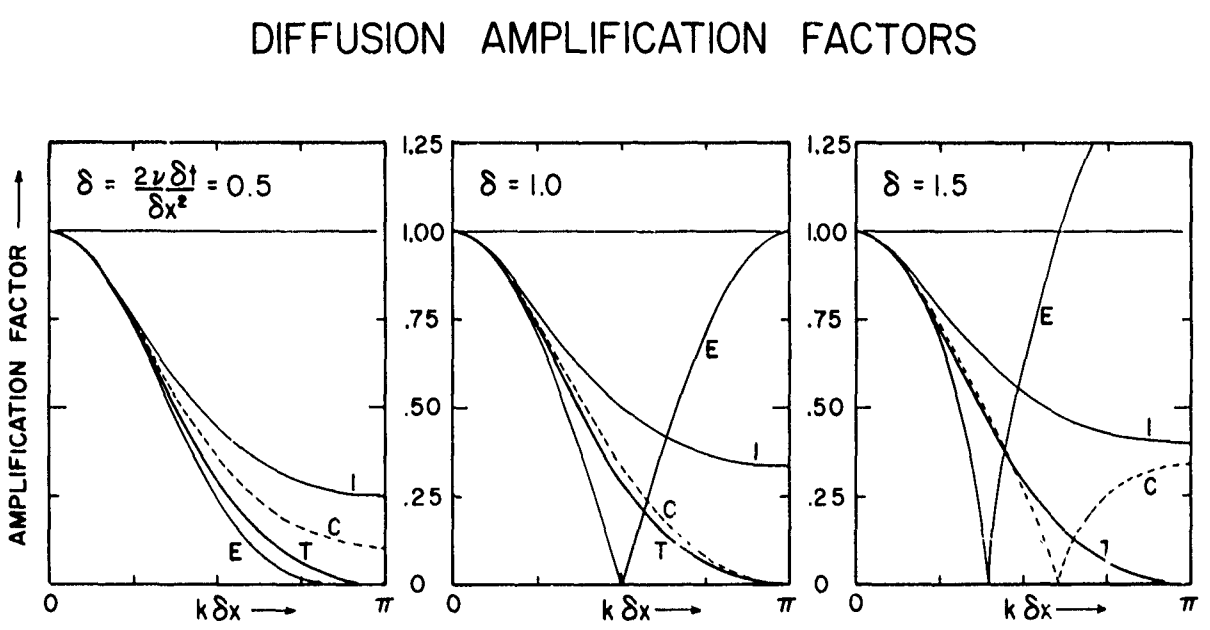

Fig. III.3 – The amplification factor as a function of $k\delta x$ for various values of δ. The *T*, *E*, *C*, and *I* refer to the analytical, explicit, centered, and implicit solutions for the diffusion-like term, respectively.

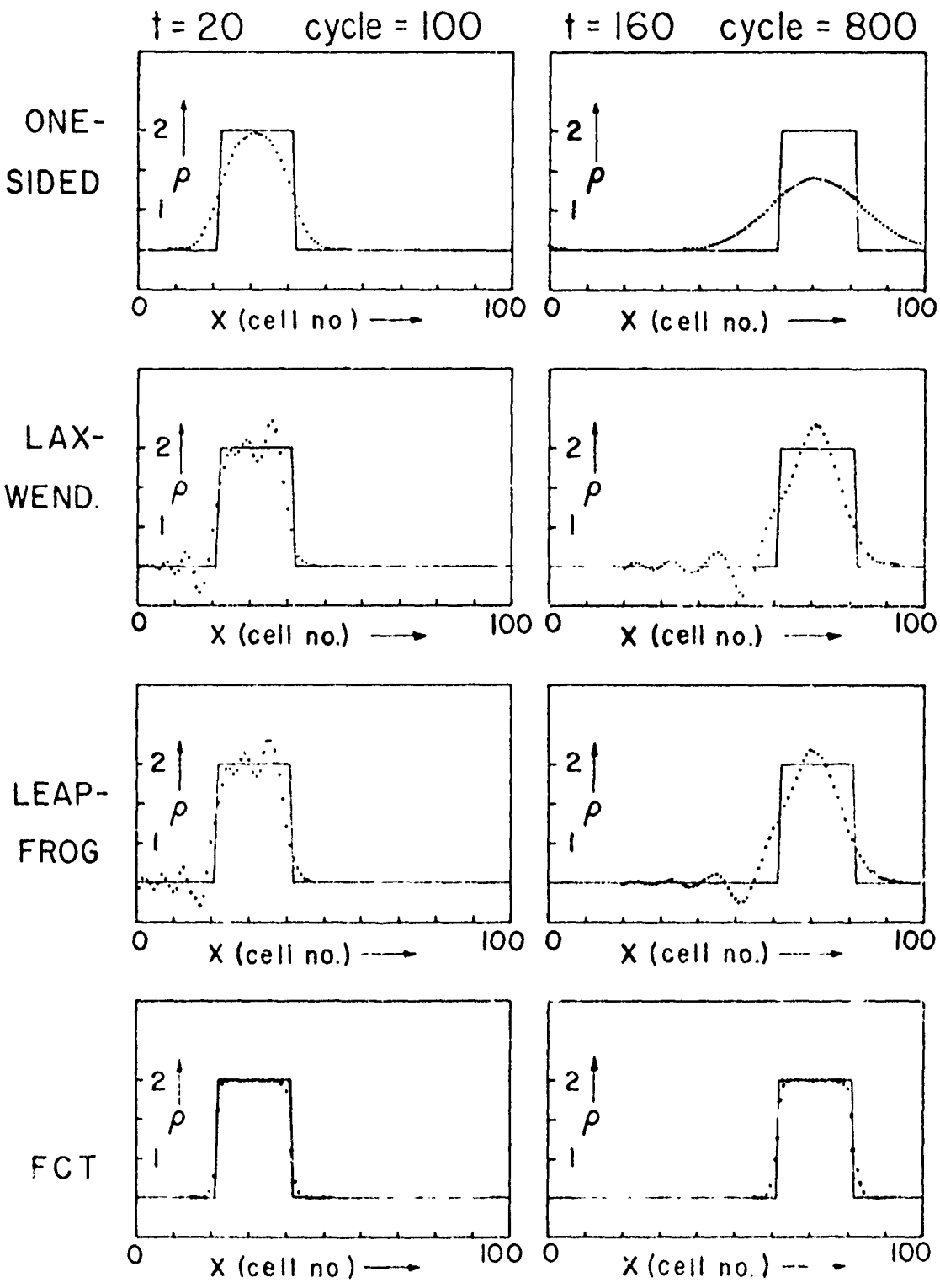

Fig. III 5 — Comparison of four types numerical solutions obtained for the propagation of a square wave The dots indicate the values calculated by the methods listed on the left-hand side

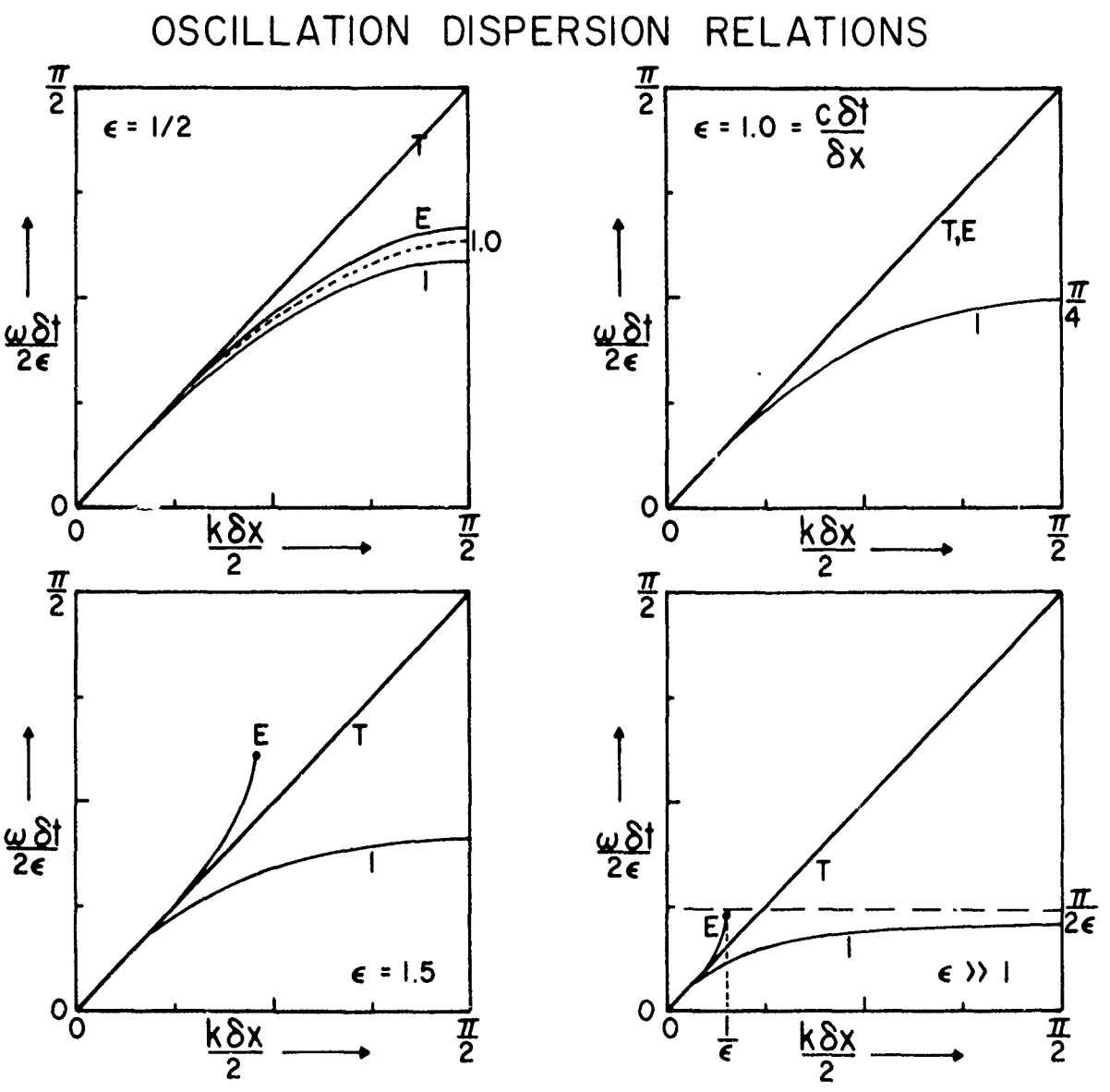

Fig. III.4 — The dispersion relation derived for the solution of wavelike terms for four values of the parameter ϵ (Eq III.27)

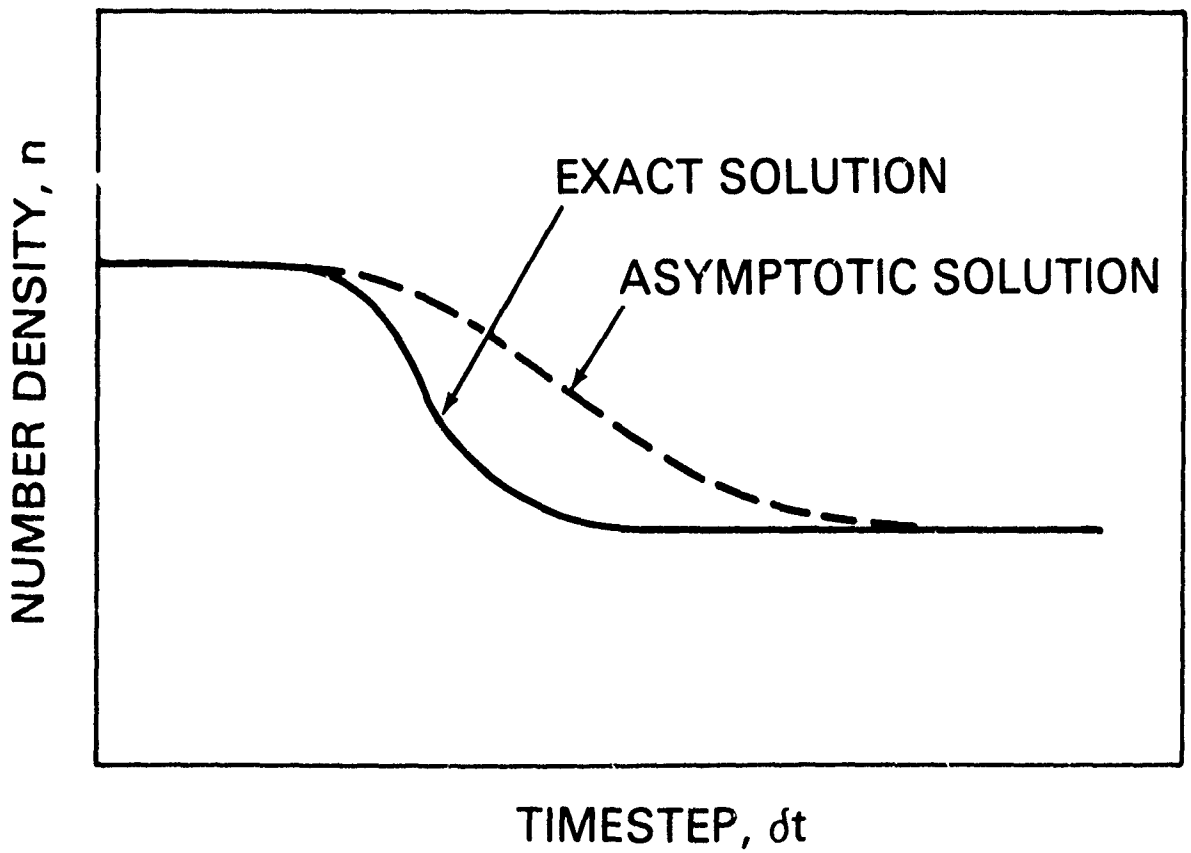

Fig. IV 1 — Schematic diagram showing qualitatively the types of phase errors which may occur in asymptotic solutions of the chemical rate equations Note the increased accuracy for long timesteps.

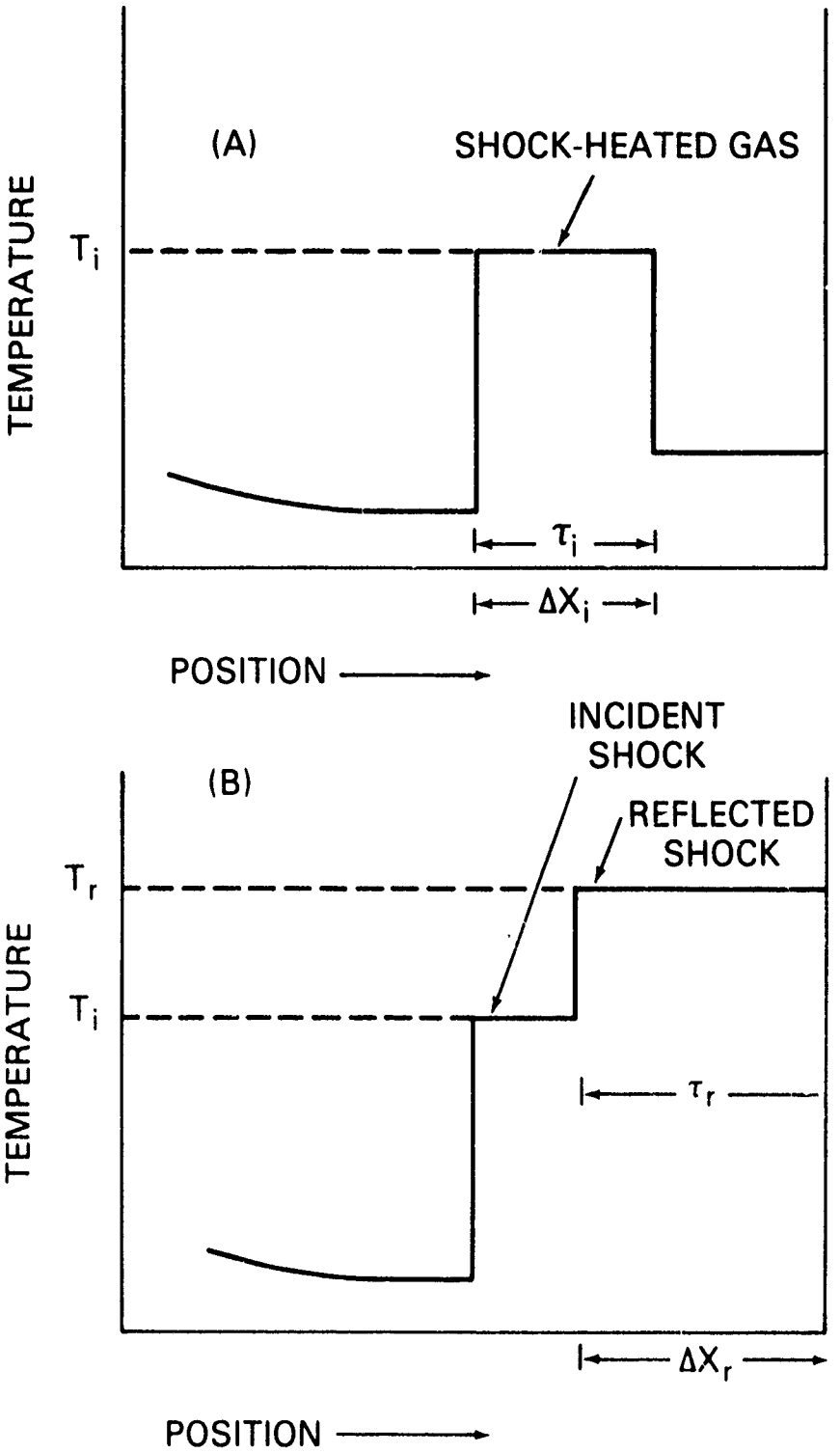

Fig IV 2 — Schematic diagram showing the temperature profiles for incident and reflected shock waves The value of τ_i and τ_r are the maximum lengths of time for heating fluid elements behind the incident and reflected shocks at temperatures T_i and T_r, respectively

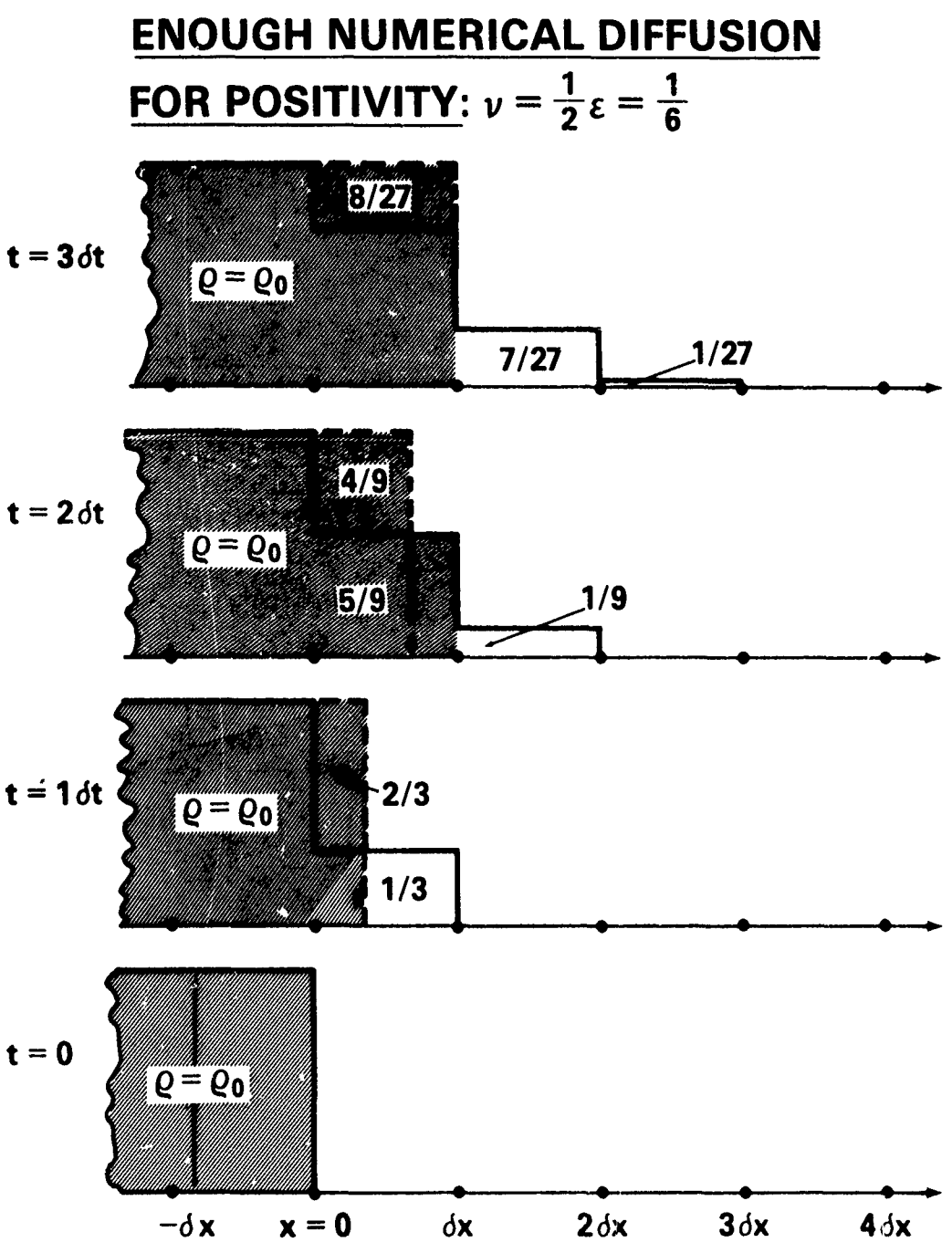

Fig. V.1 — A calculation which illustrates the numerical diffusion which arises when the donor cell finite difference algorithm is used

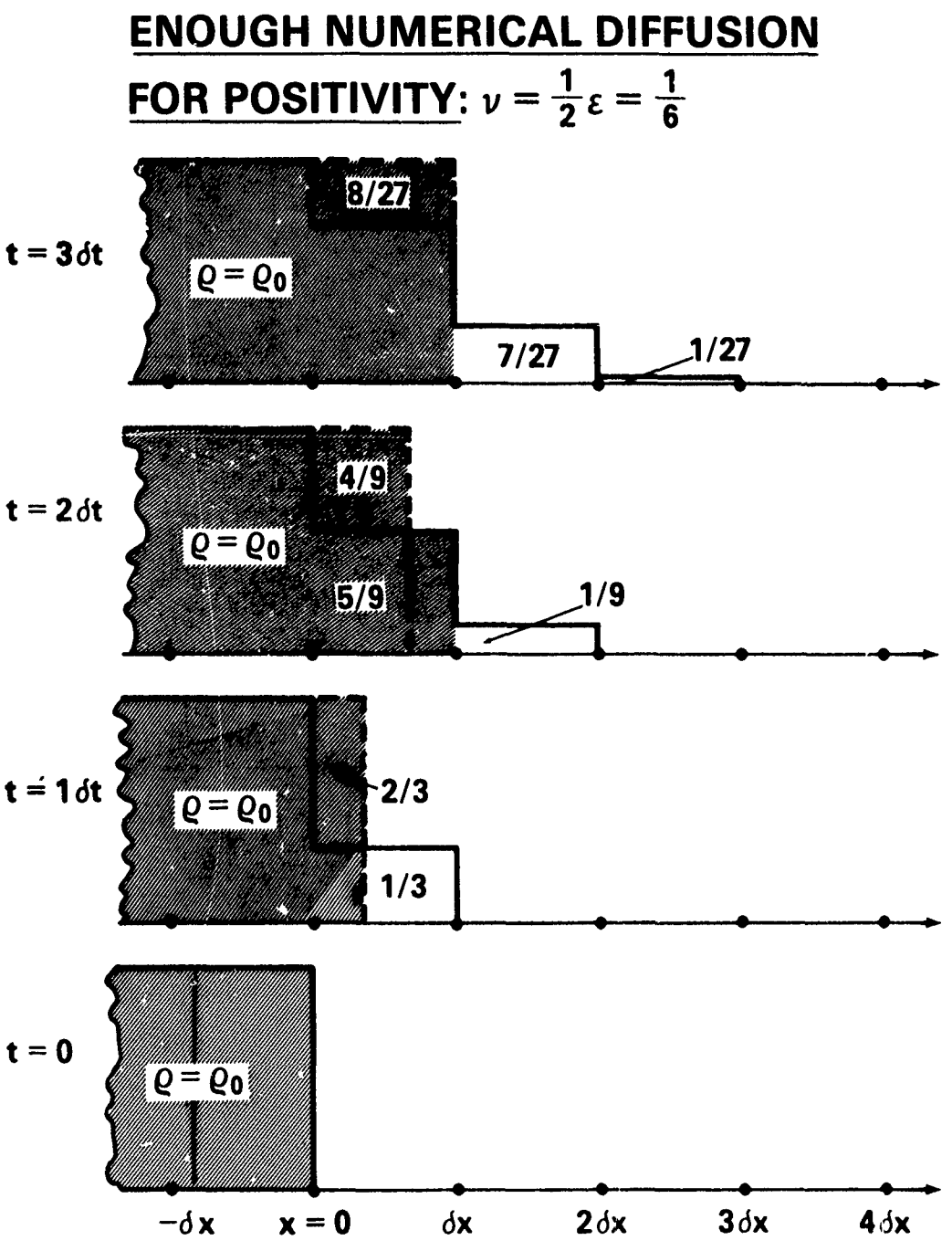

Fig. V.1 — A calculation which illustrates the numerical diffusion which arises when the donor cell finite difference algorithm is used

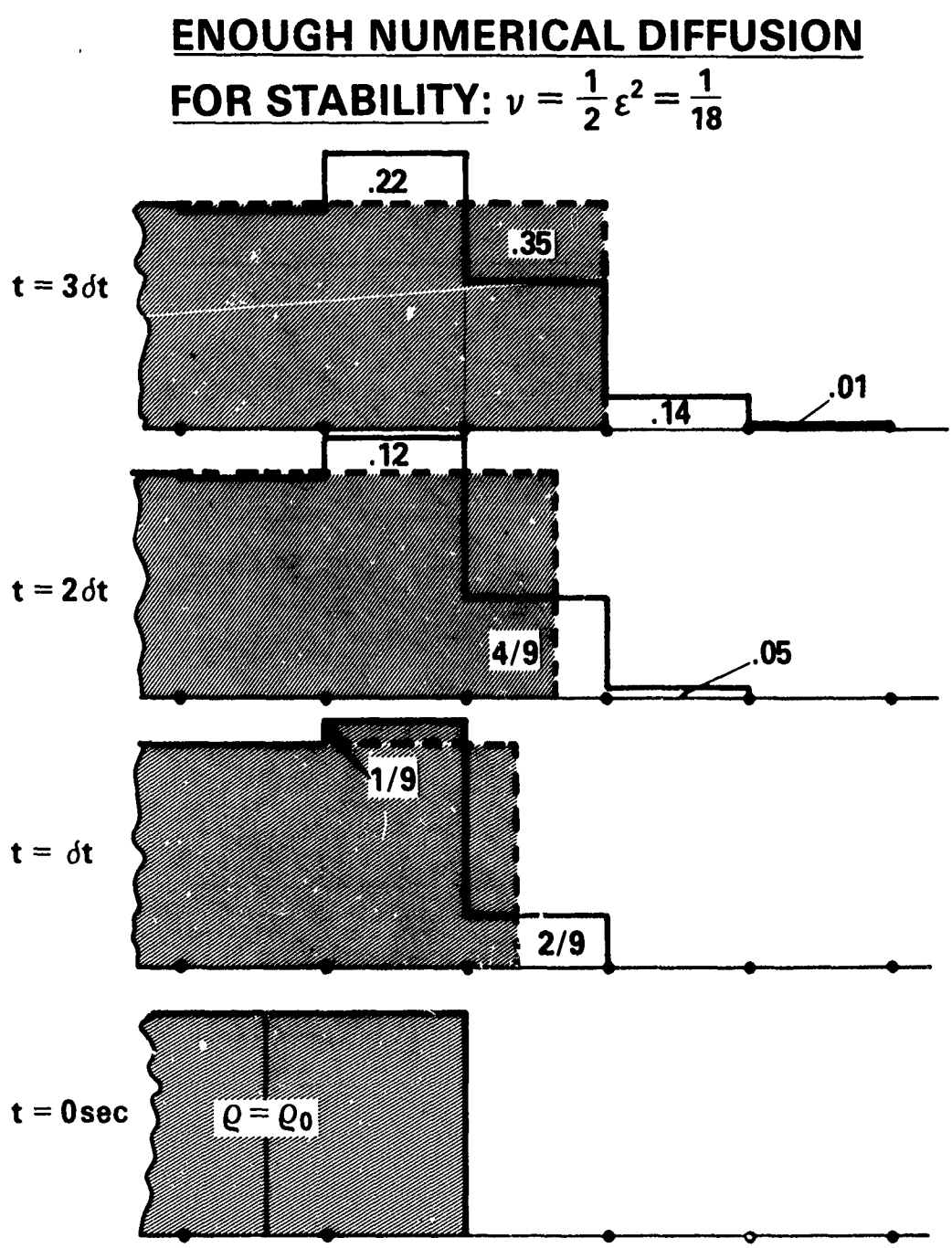

Fig. V.2 — A calculation which illustrates the loss of monotonicity which arises when enough numerical diffusion is left in the calculation to maintain stability.

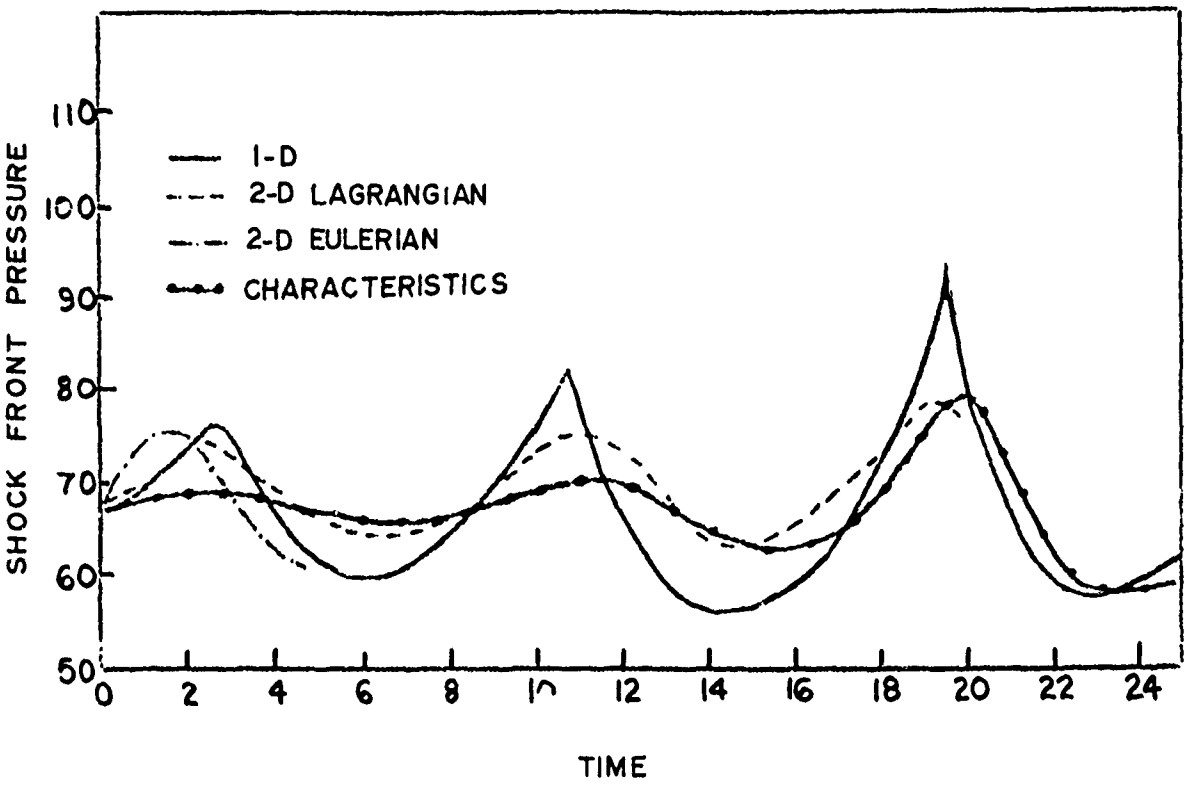

Fig. VIII.2 — Comparisons of the results of solving the detonation oscillation problem [83,84] using four different numerical techniques.

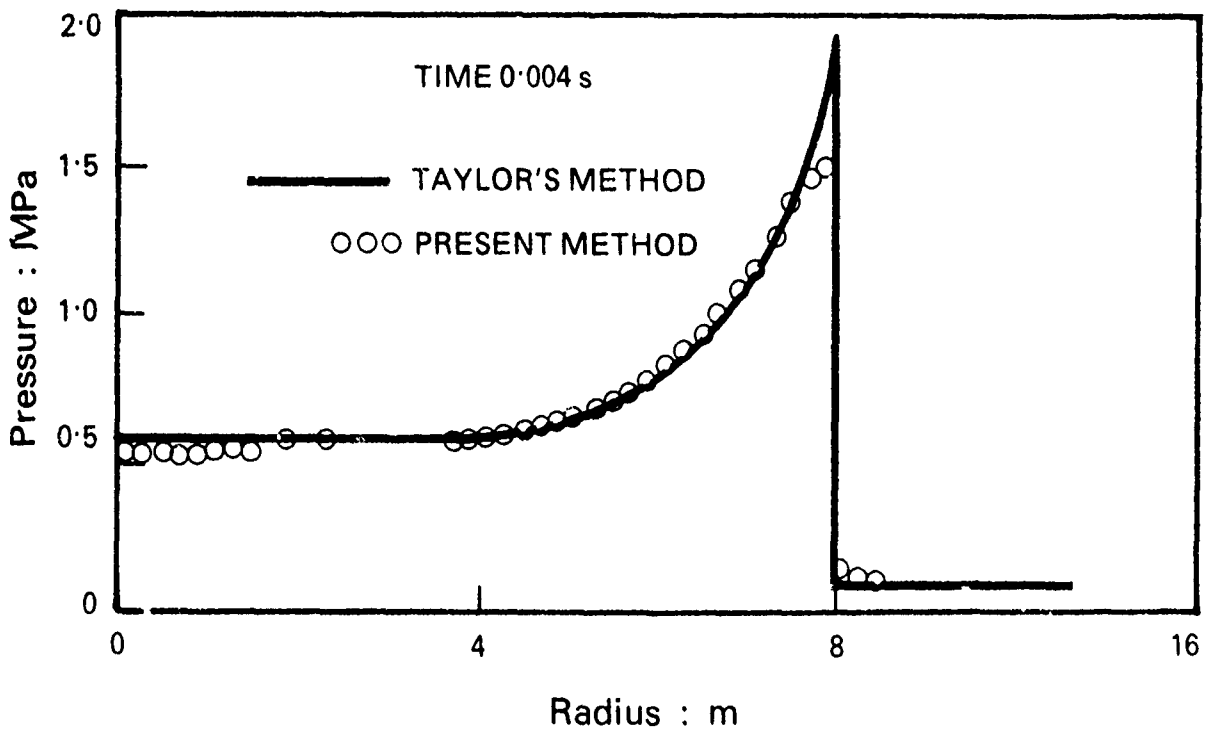

Fig. VIII.3 — Comparison of the self-similar solution to the spherical blast wave problem derived by Taylor [94] to the numerical calculation by Phillips [92].

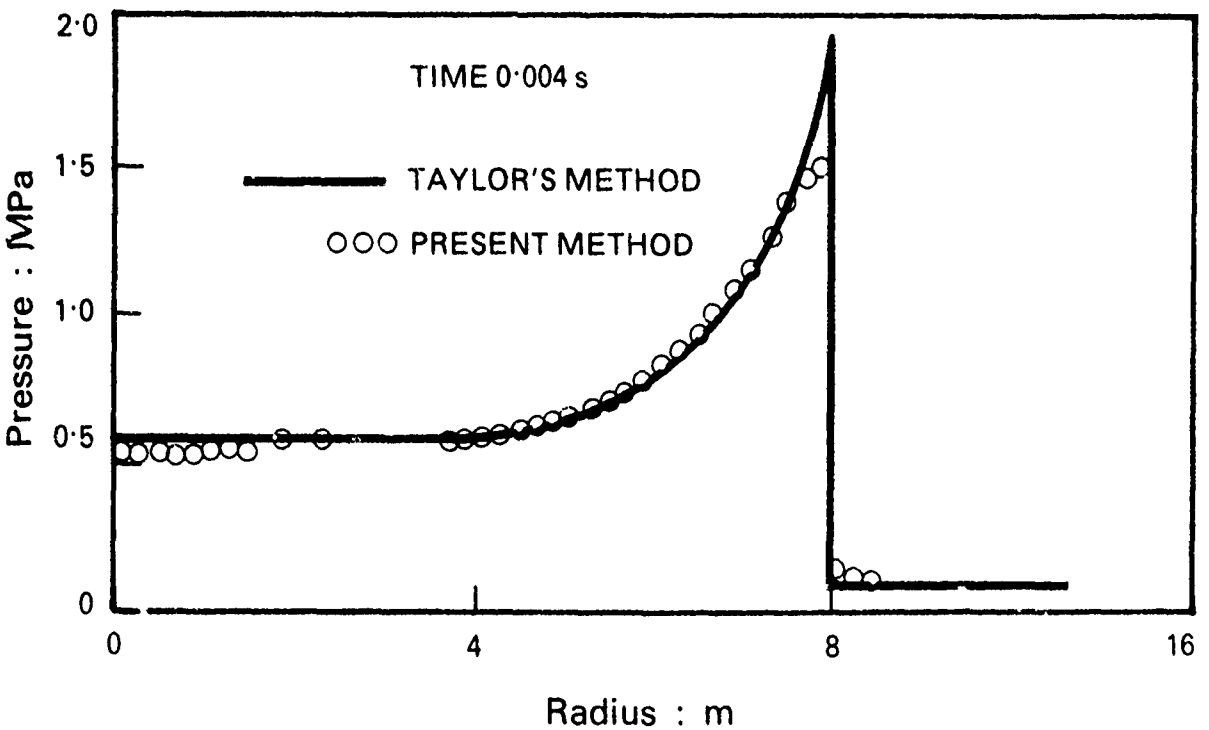

Fig. VIII.3 — Comparison of the self-similar solution to the spherical blast wave problem derived by Taylor [94] to the numerical calculation by Phillips [92].

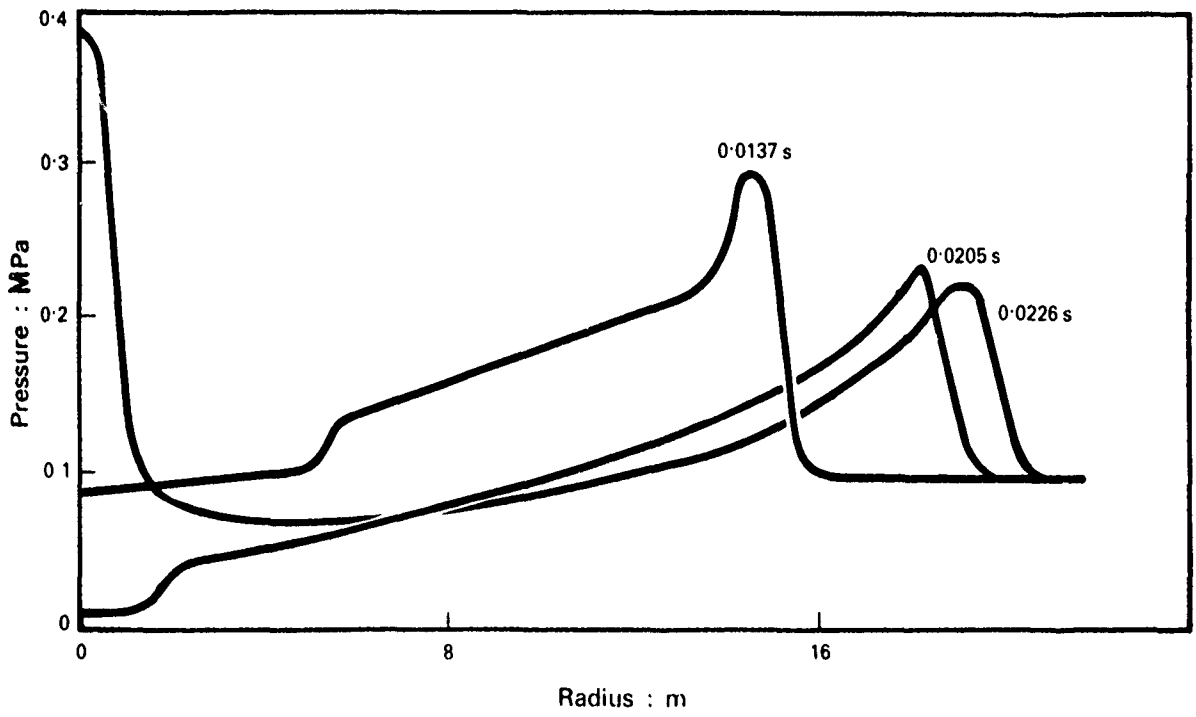

Fig. VIII.5 — Same as VIII.4, but for later times.

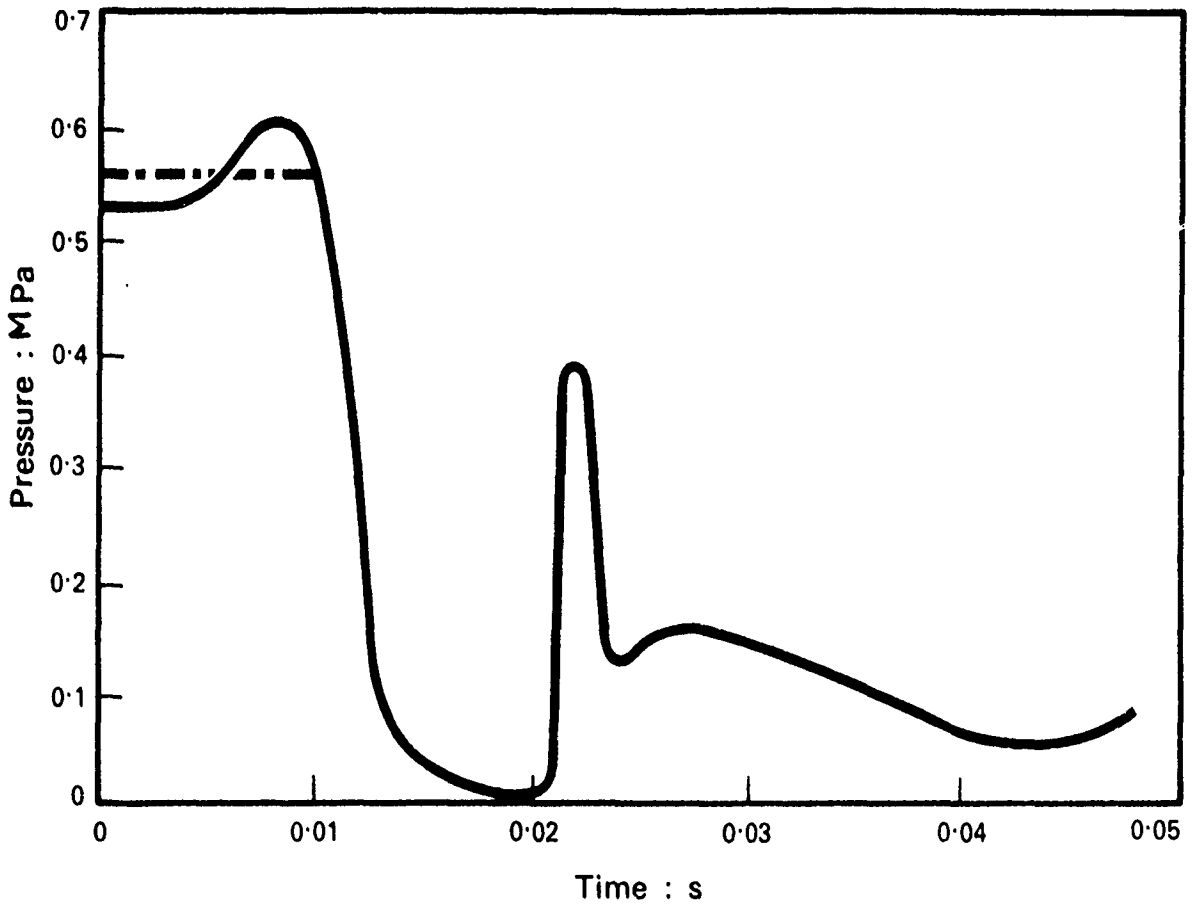

Fig. VIII.6 — Central pressure as a function of time for the decay of the spherical blast shown in Figures VIII.4-6.

REACTIVE SHOCK PROBLEM
INITIAL CONDITIONS

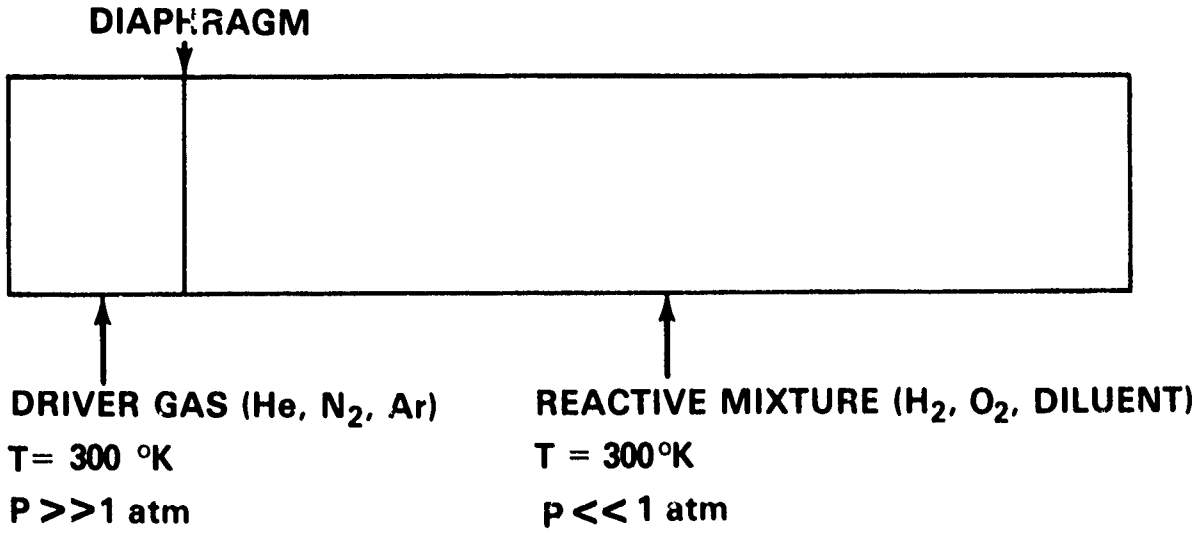

Fig. VIII.7 — Initial density, temperature, and pressure for the reactive shock calculation.

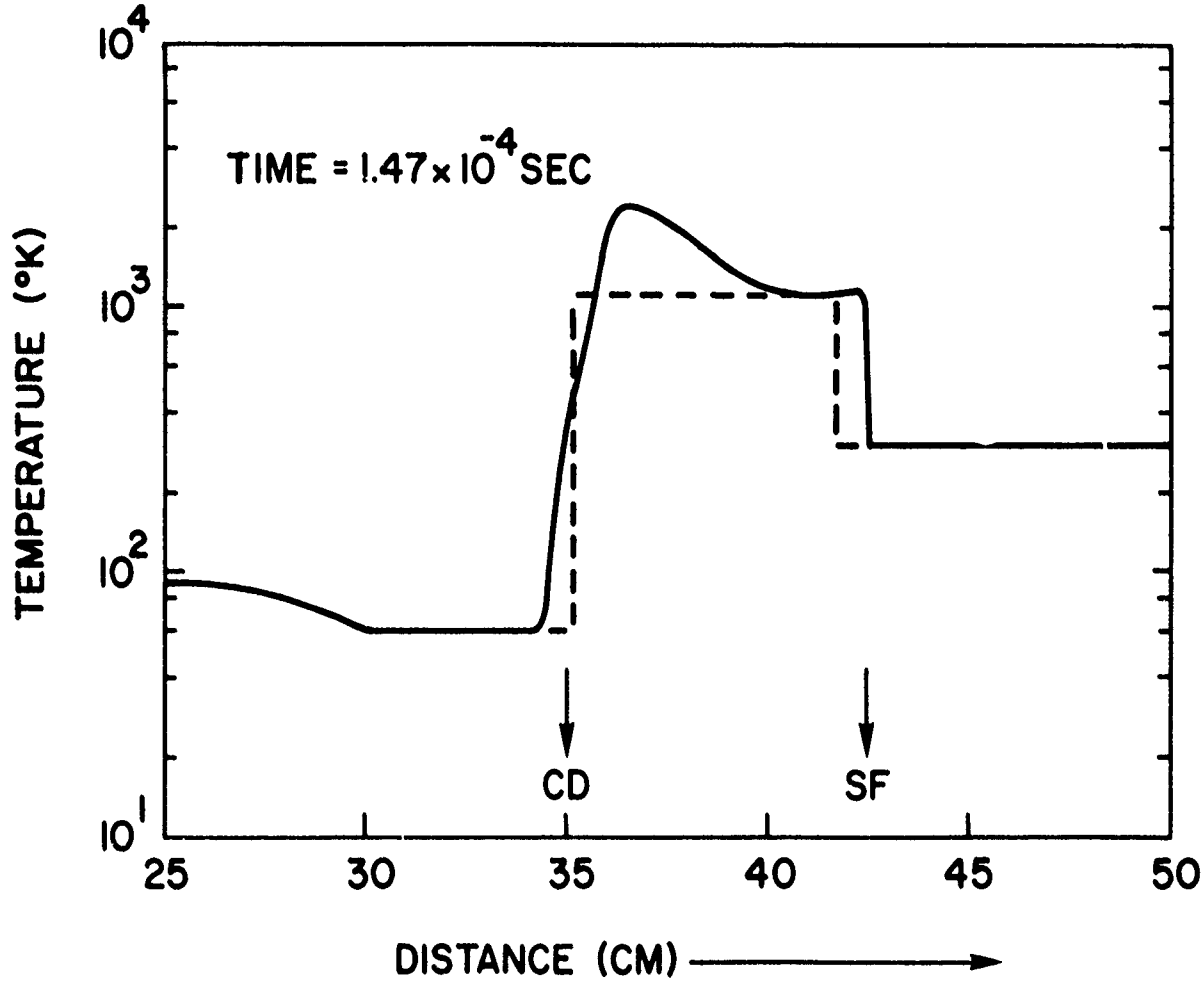

Fig. VIII.8 — Calculated temperature as a function of distance after the shock has traveled 40 cm down the tube. The dashed lines indicate results from the ideal solution. The position of the shock front and contact discontinuity are noted by SF and CD, respectively.

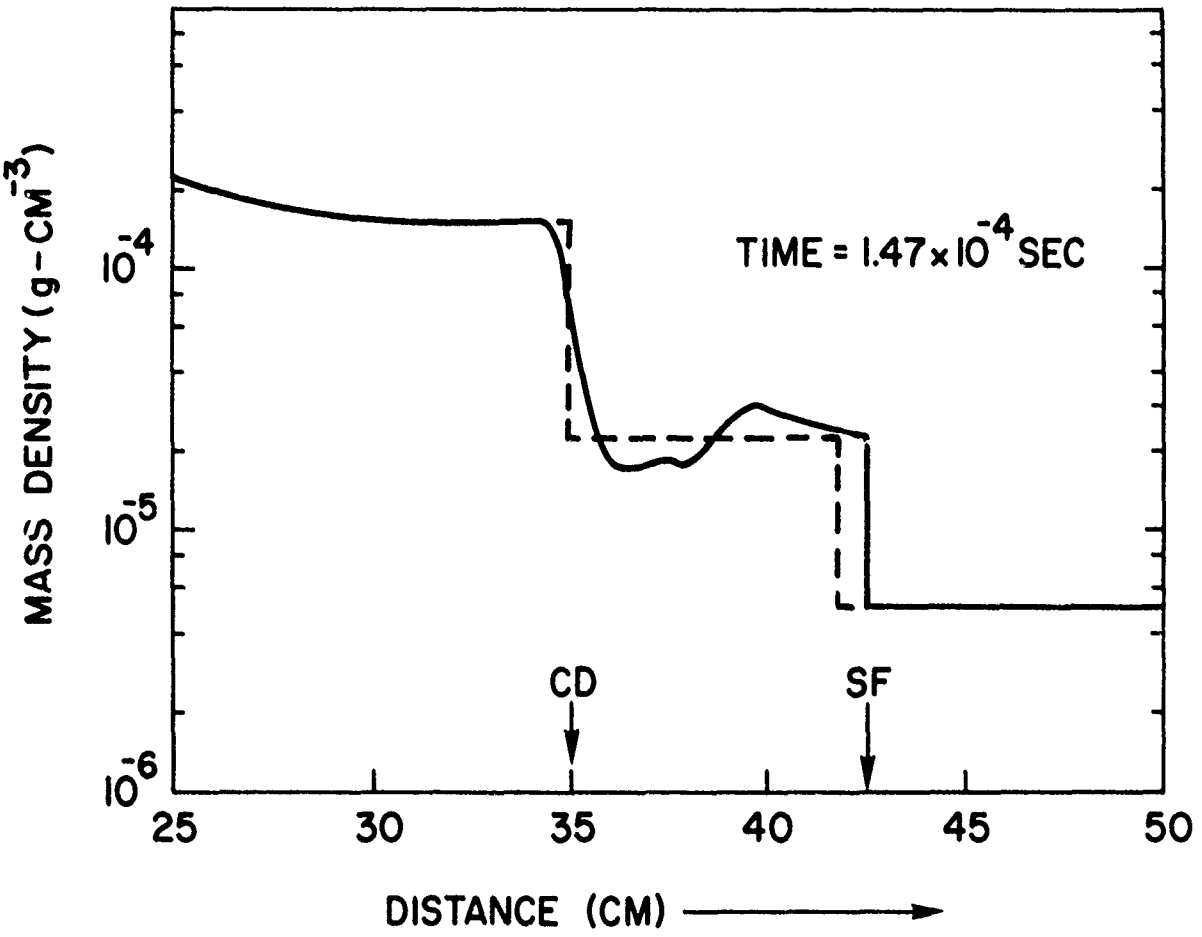

Fig. VIII.9 — Calculated mass density as a function of distance at the time corresponding to Fig. VIII.9a.

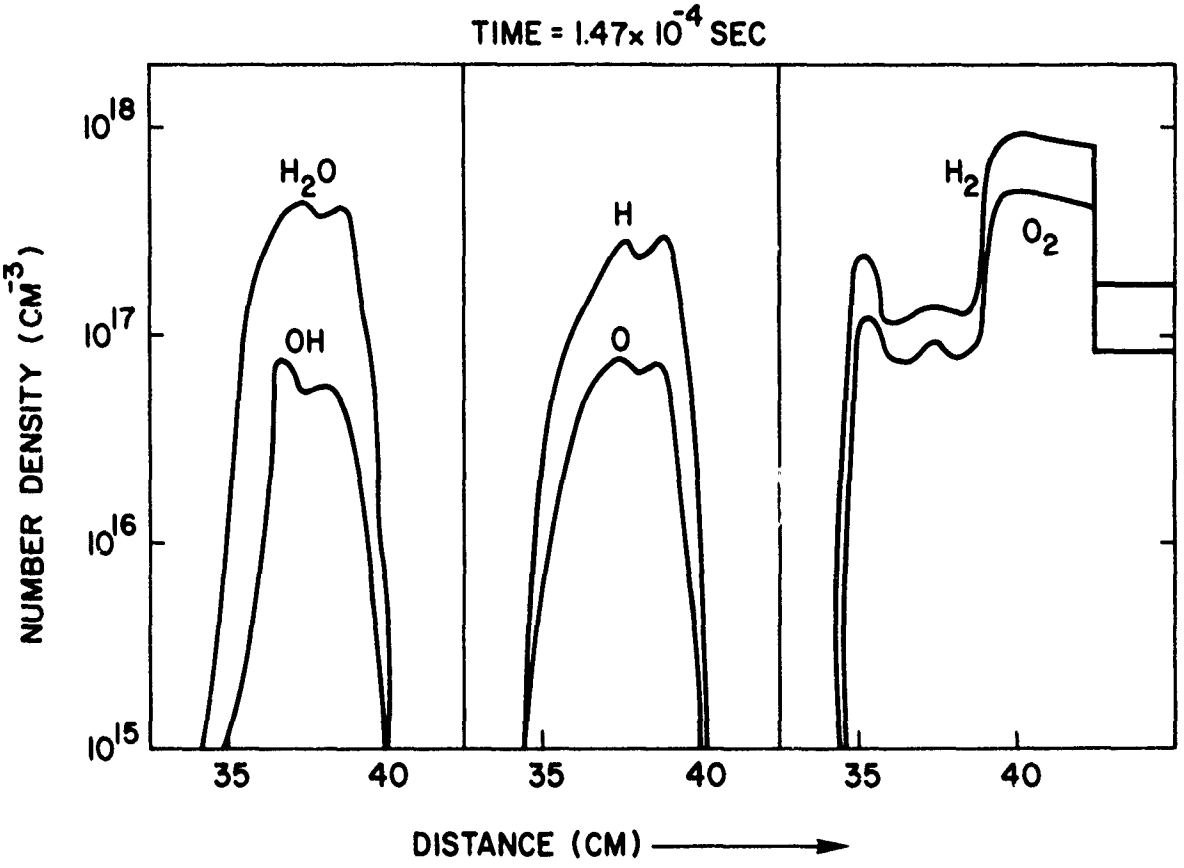

Fig. VIII.10 — Profiles of number density for H_2O, H, O, OH, H_2O, and O_2 as a function of position in the shock tube. These correspond to the temperature profile in Fig. VIII.9.

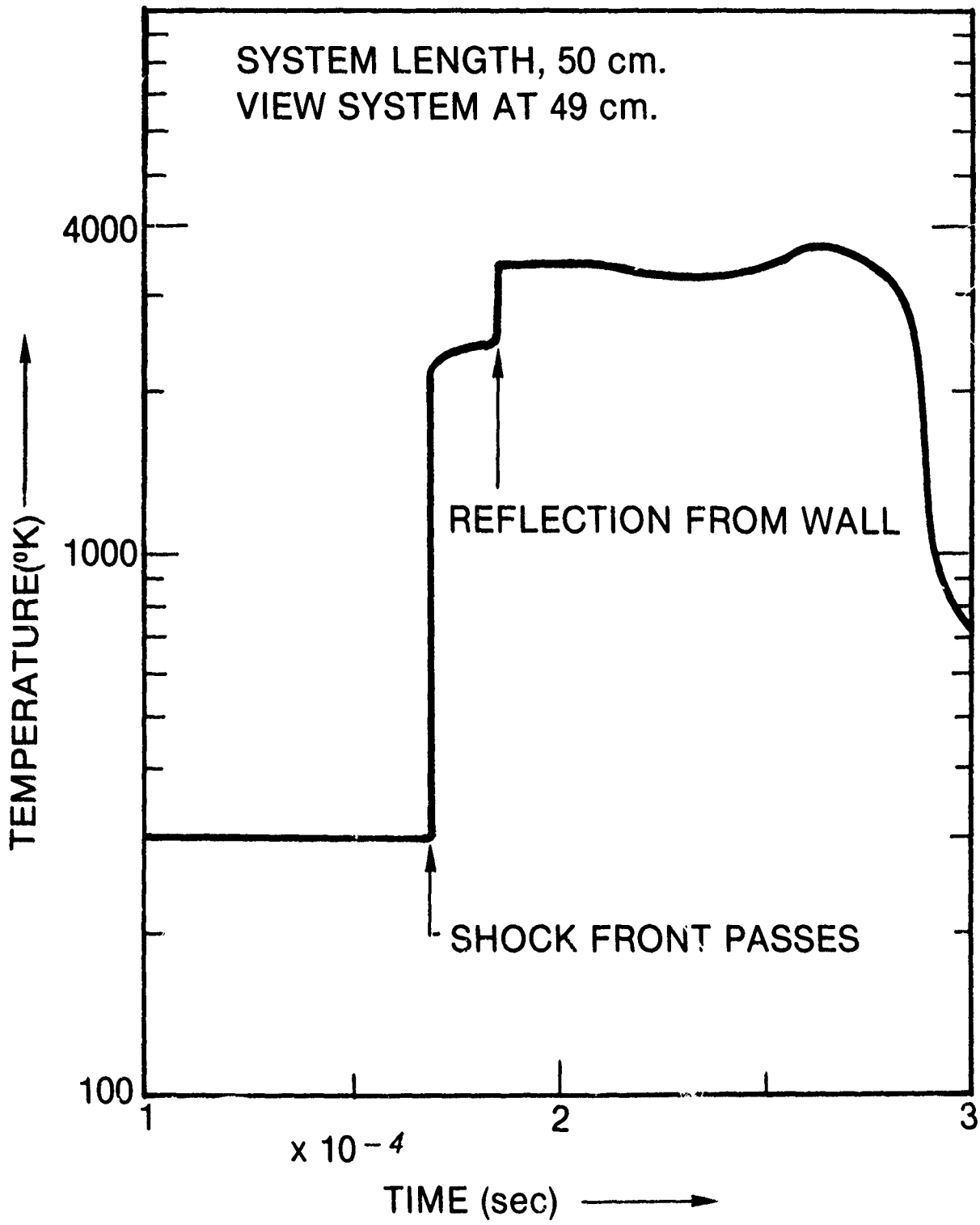

Fig. VIII.11 — Calculations of temperature as a function of time at 39 cm. The shock is reflected at a rigid wall at 50 cm

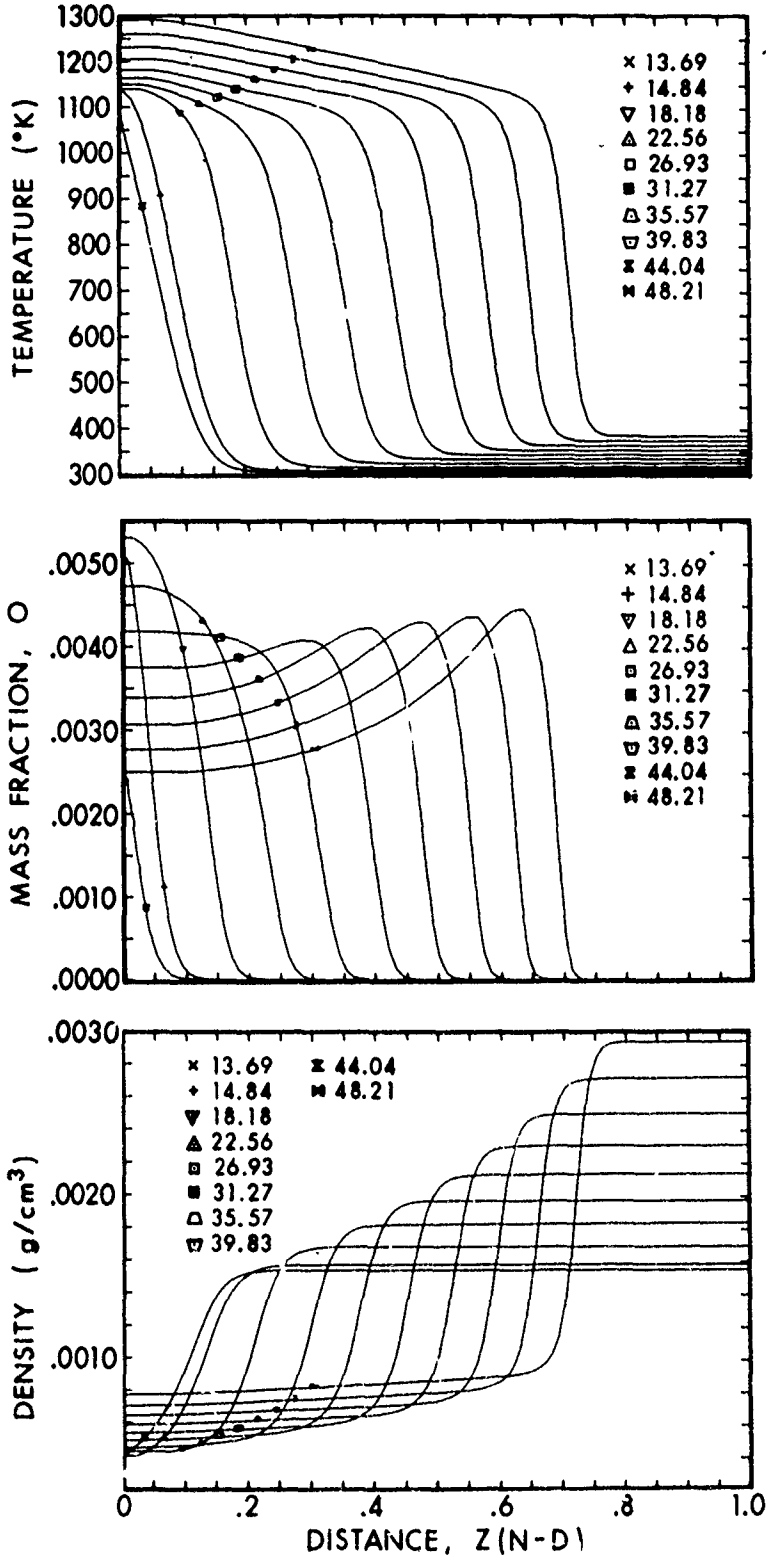

Fig. IX.1 — Profiles of temperature (A), atomic oxygen mass fraction (B), and density (C), as a function of position for a flame in 20% O_3/O_2.

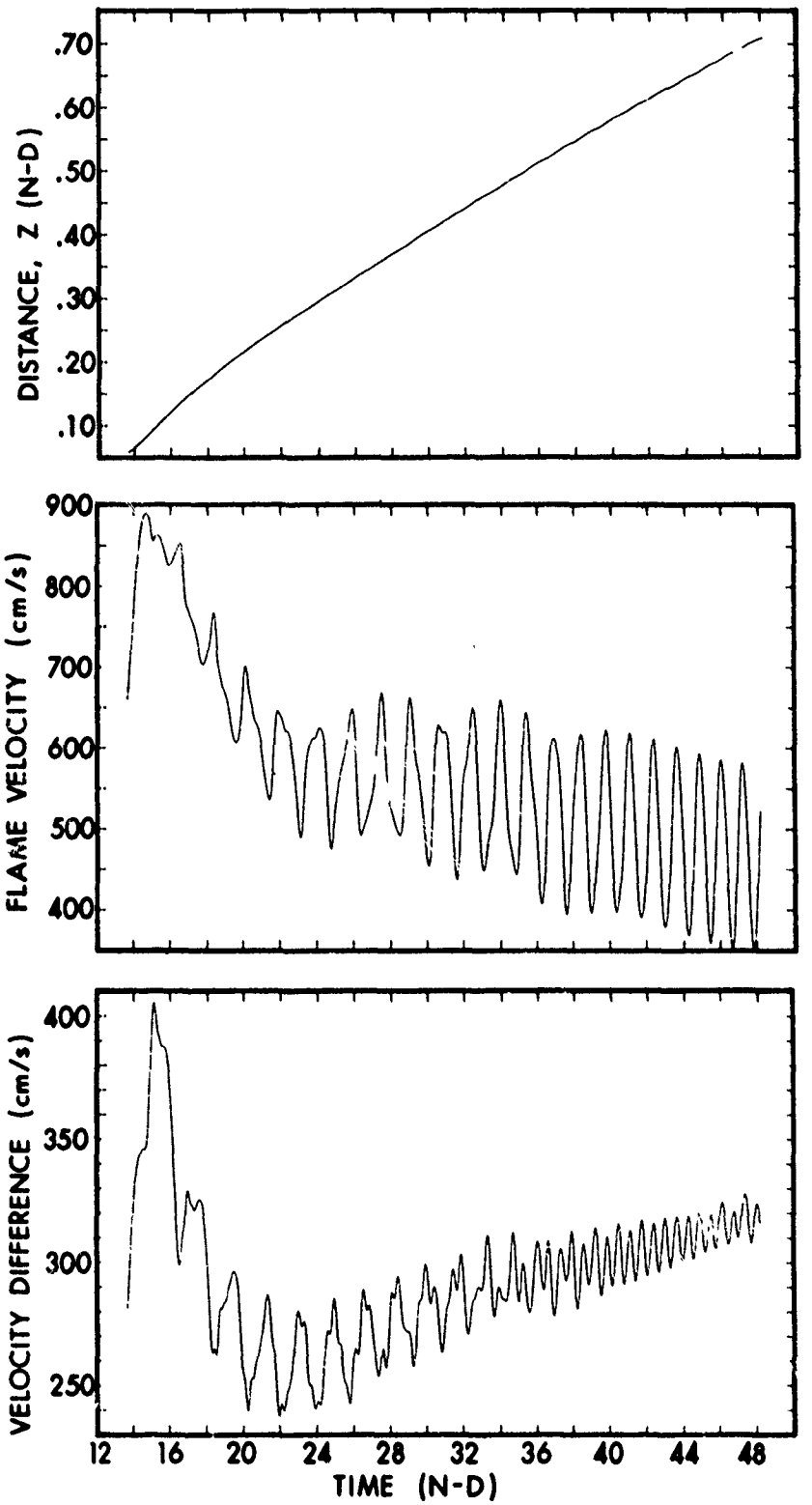

Fig. IX.2 – Position of the flamefront (A), flame velocity in inertial coordinate (B), and fundamental burning velocity (C) as a function of time for the flame shown in Fig. IX.1.

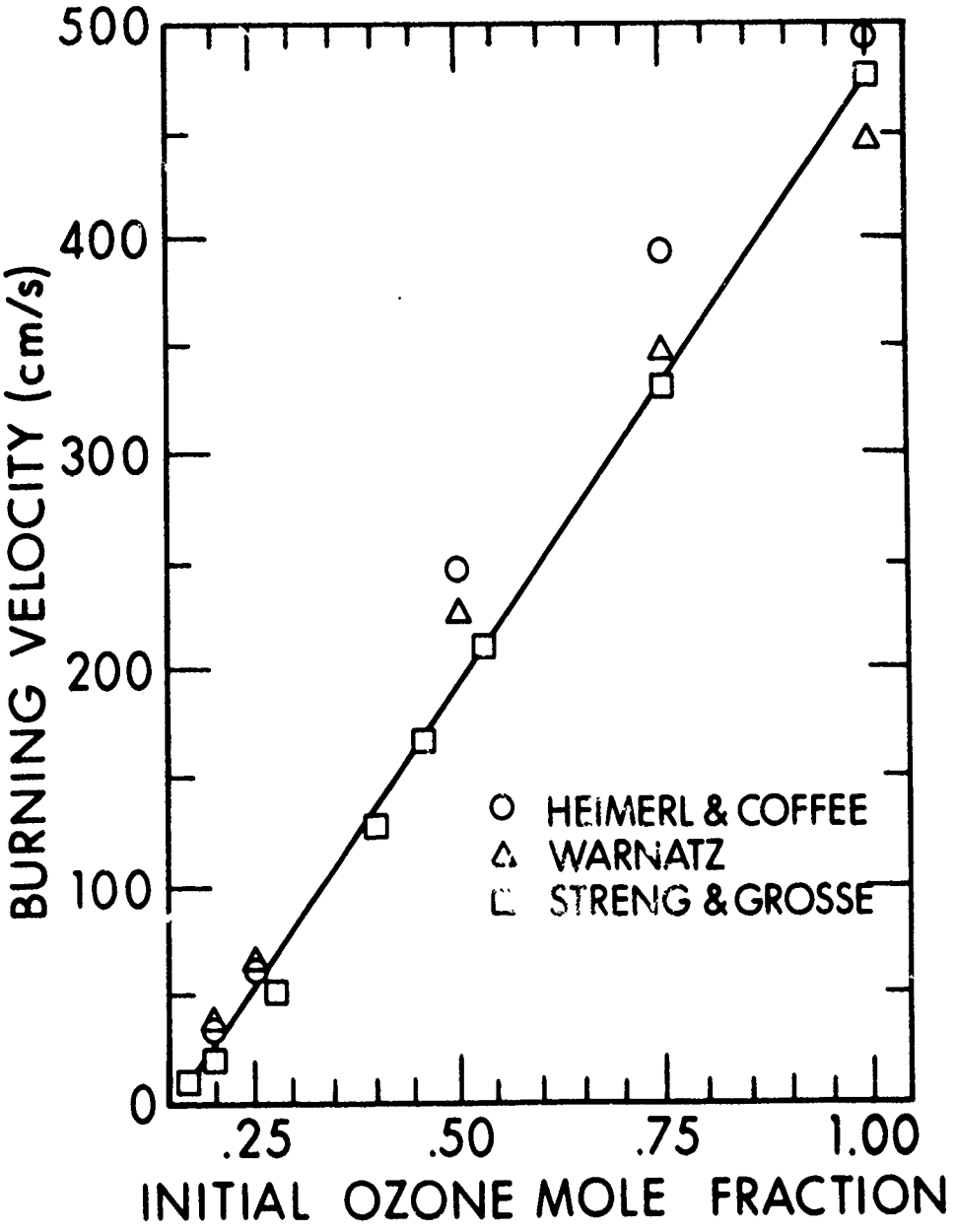

Fig. IX.3 — Comparisons of measured burning velocities [108] as a function of the initial ozone mole fraction to those calculated by Warnatz [98] and Heimerl and Coffee [97].

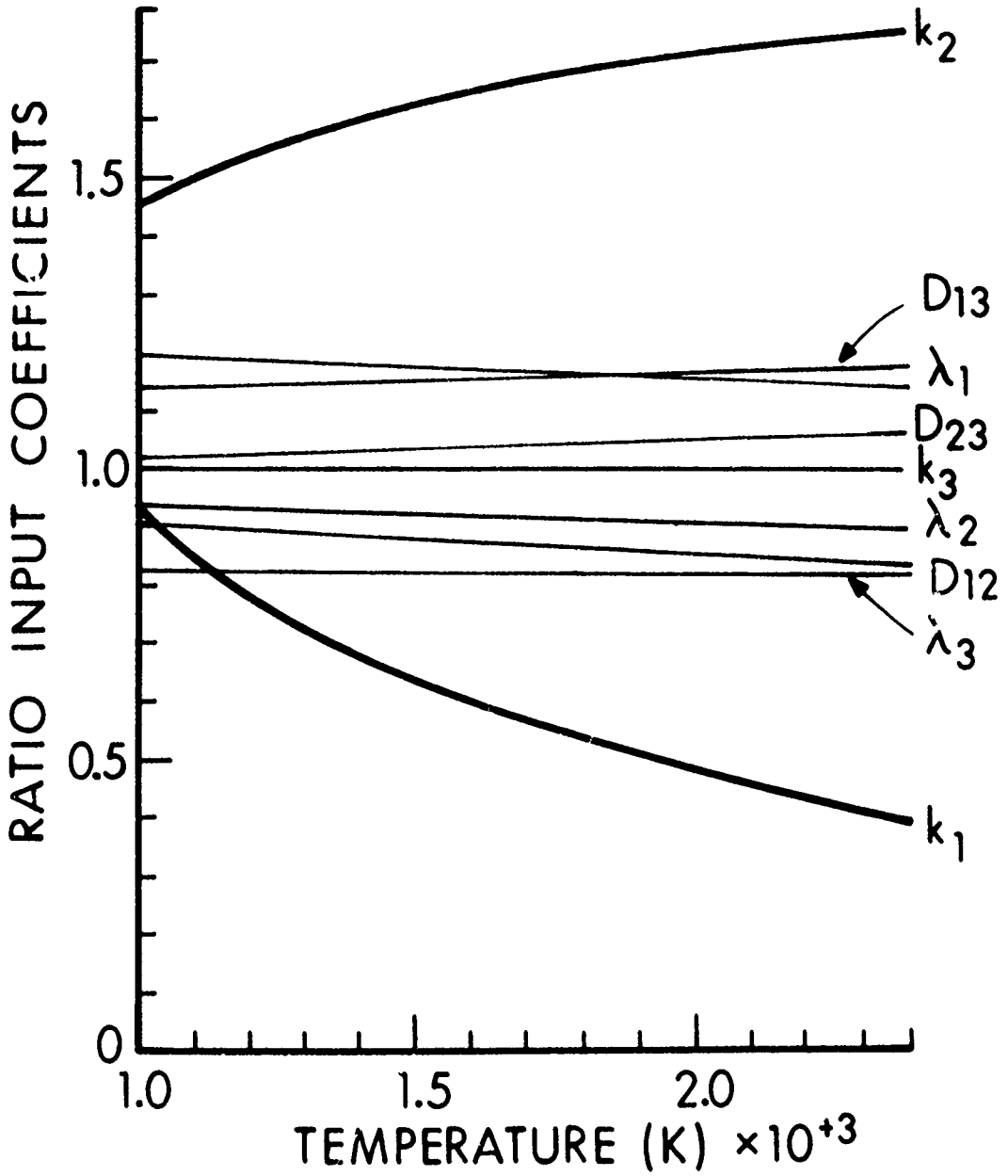

Fig. IX.4 — Ratios of the values of the chemical rates and diffusion coefficients used by Heimerl and Coffee [97] to those used by Warnatz [98]. Each ratio is indicated by the specific coefficient which is defined in the text.

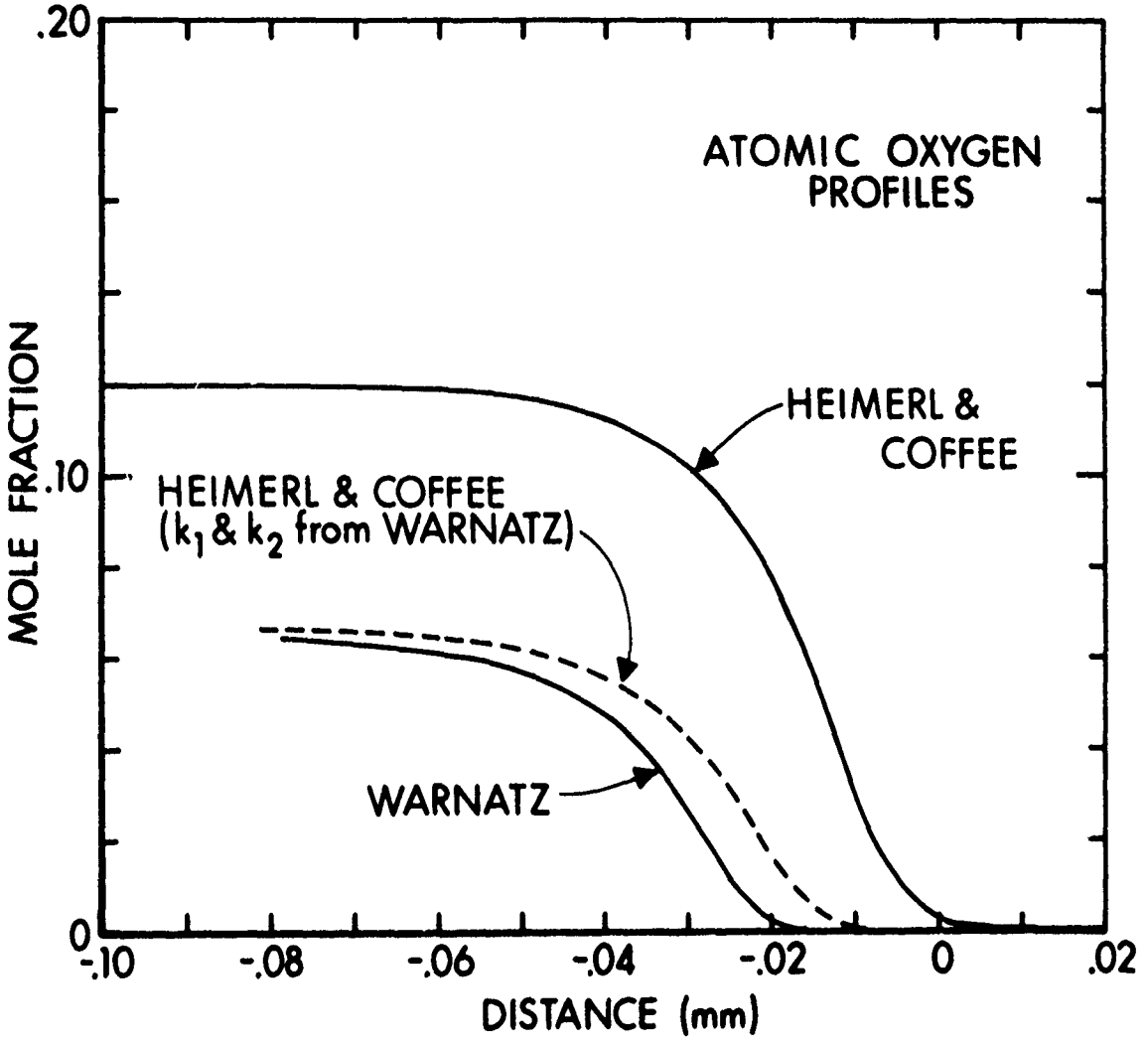

Fig. IX.5a — Mole fraction of atomic oxygen as a function of position as predicted by Heimerl and Coffee [97] and Warnatz [98]. The three curves have been purposely off-set on the distance scale to show their differences in magnitude.

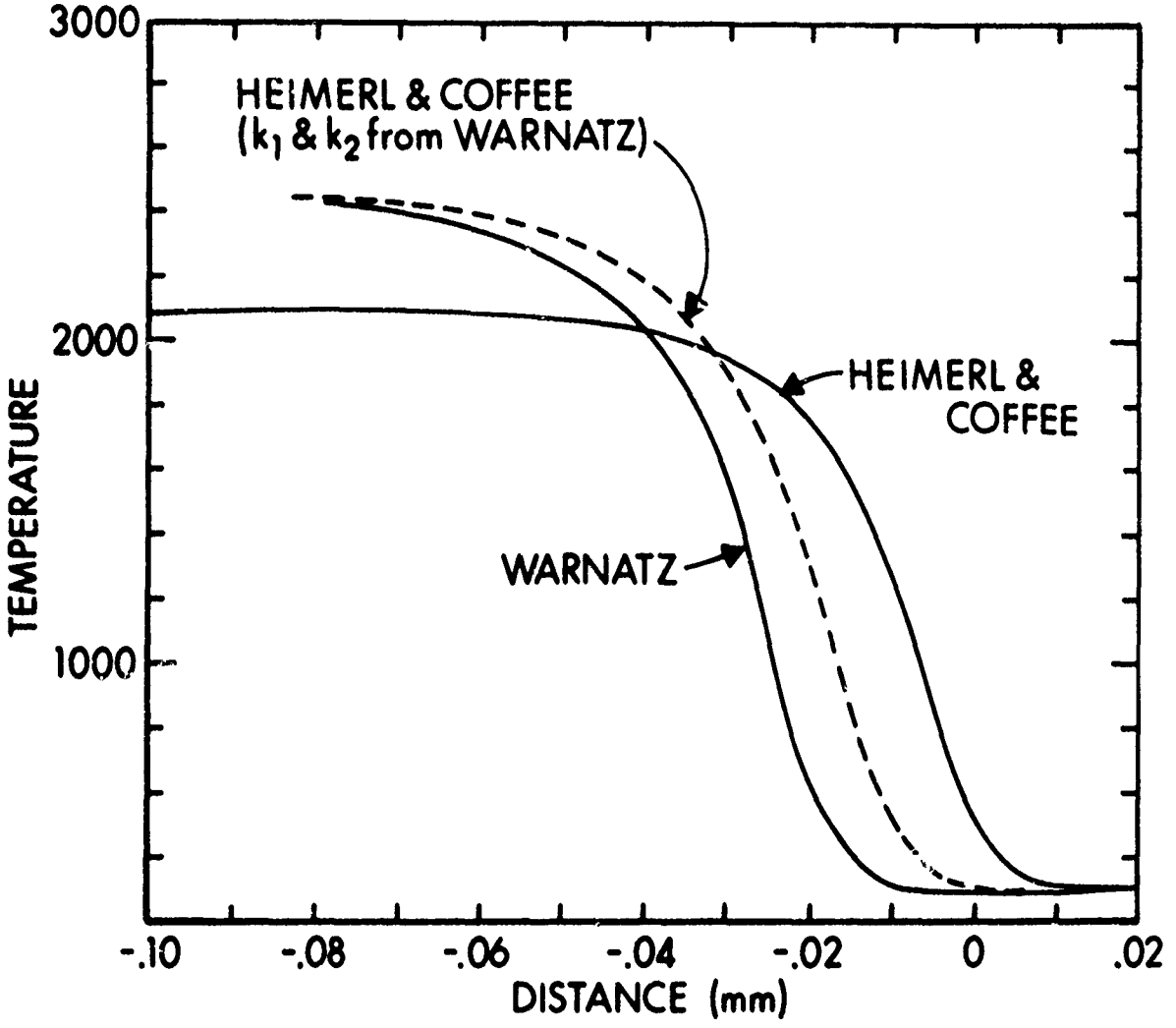

Fig. IX.5b -- Temperature as a function of position for the cases shown in Fig. IX.a.

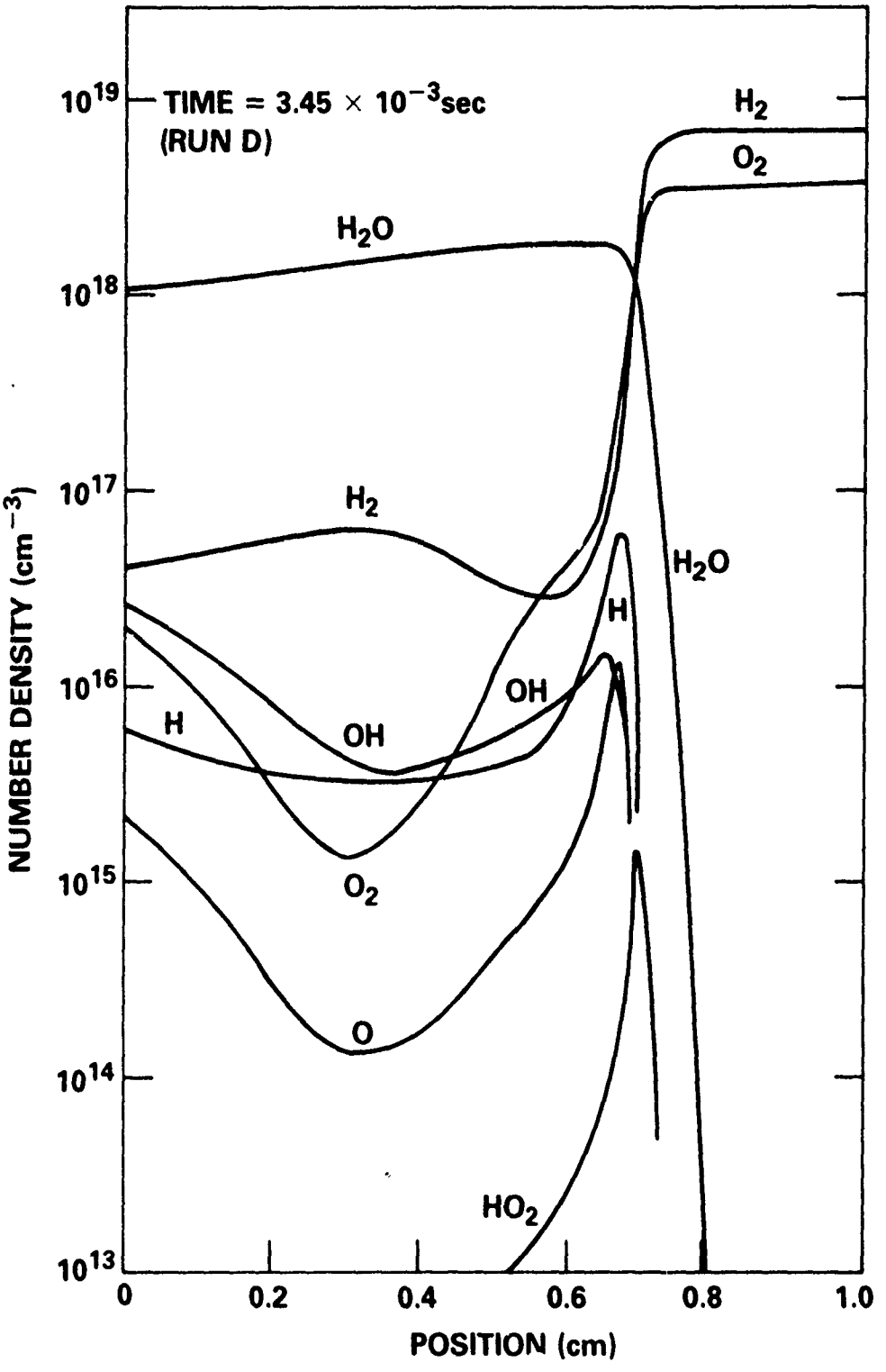

Fig. IX 6 — Species densities as a function of position for an $H_2 - O_2$ flame [78].

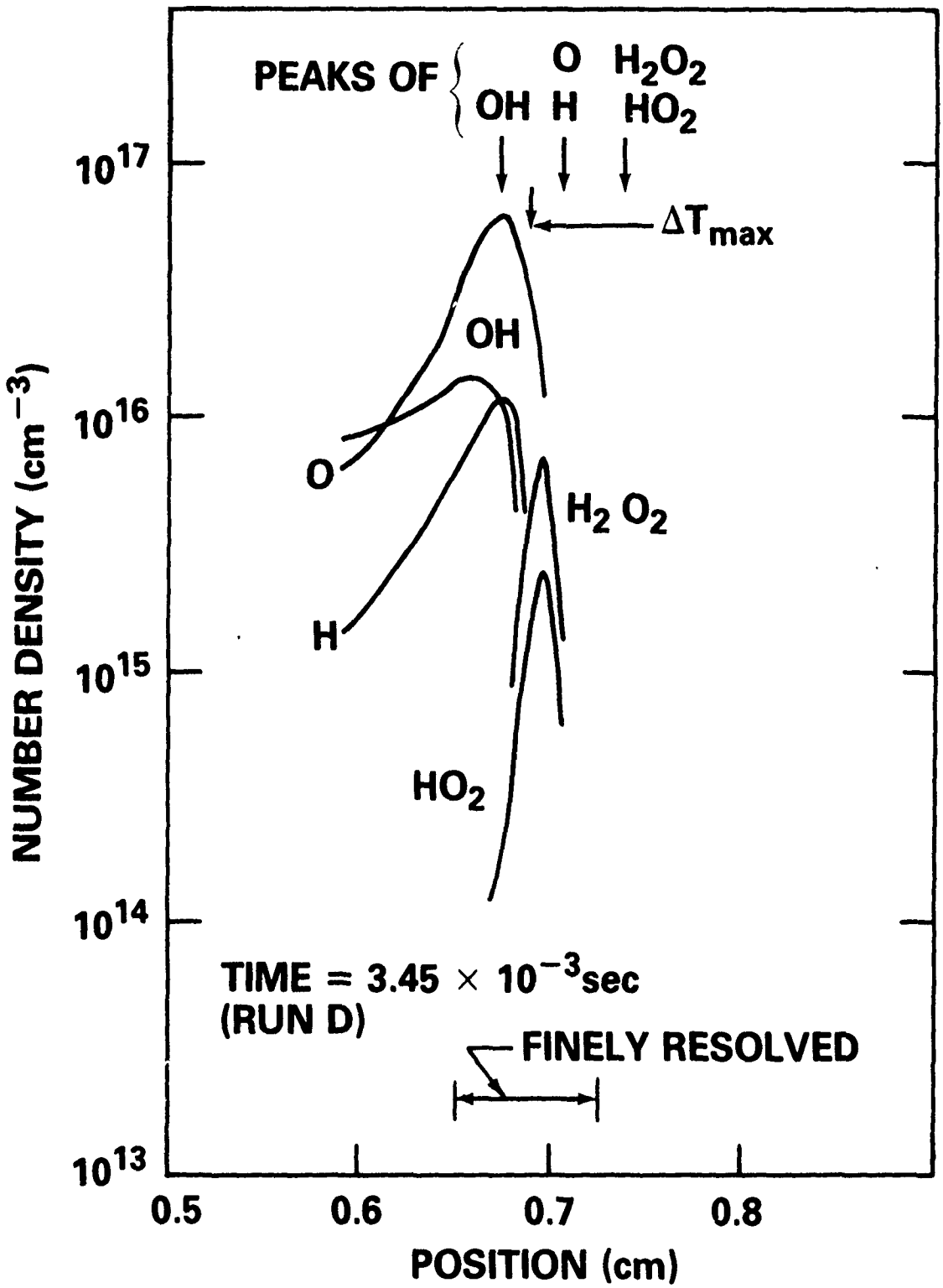

Fig. IX.7 – Expansion of Fig. IX.6 in the region of the flame front. Peaks of OH, O, H, H_2O_2 and HO_2 and the maximum temperature gradient (ΔT max) are noted by arrows. The region around the flamefront which is finely gridded has been marked at the bottom of the figure.

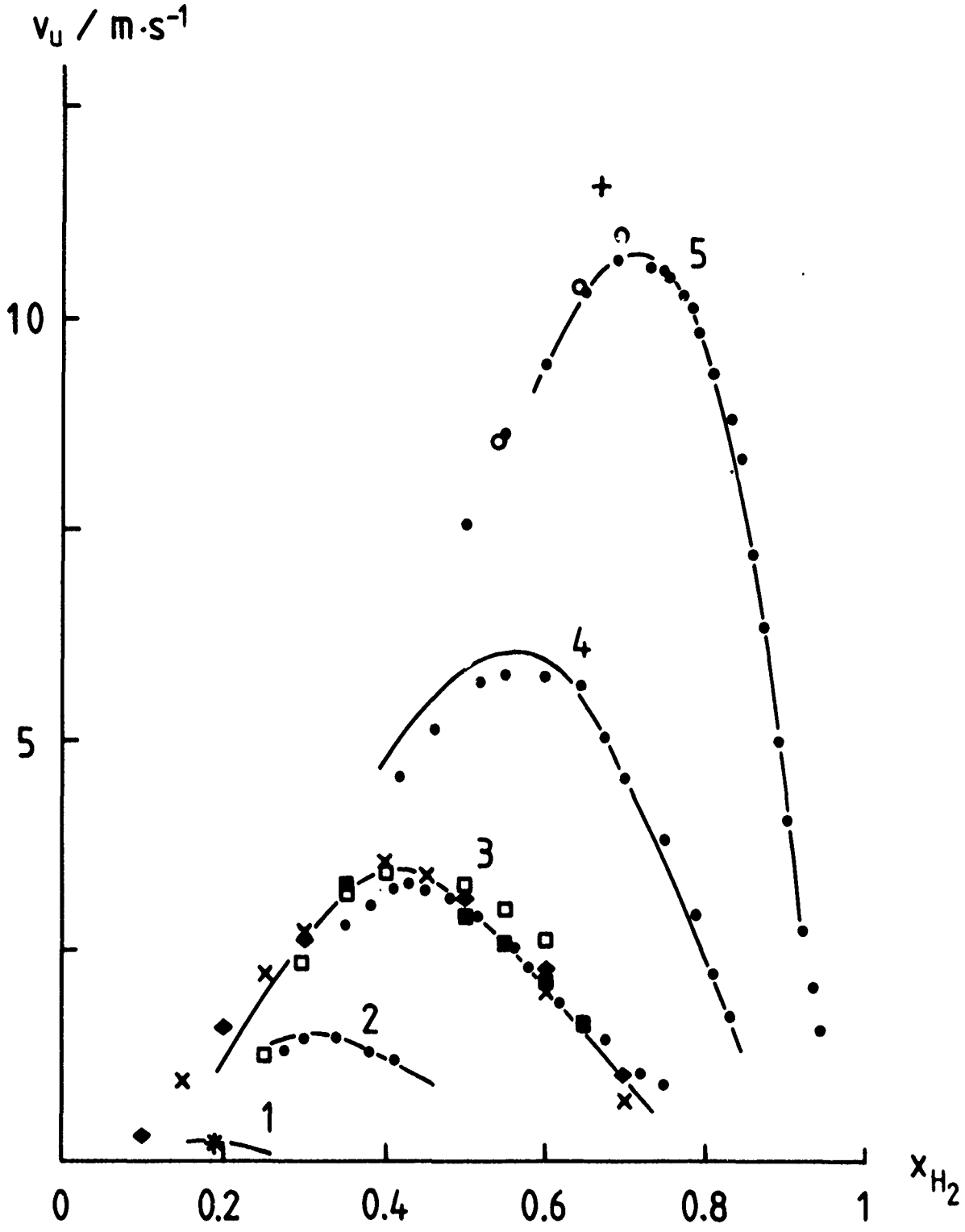

Fig. IX.8 — Comparison between calculated (solid line) and measured flame velocities (other symbols) as a function of mole fraction of H_2 in $H_2 - O_2 - N_2$ flames (298° K and a pressure of 1 bar in unburnt gas). References to the specific measurements are given by Warnatz [98]. The numbers 1 through 5 refer to differ values of the ratio $R = X(O_2)/(X(O_2) + X(N_2))$, where X indicates a mole fraction. Key: 1 → $R = 0.057$, 2 → $R = 0.125$, 3 → $R = 0.21$ (air), 4 → $R = 0.40$, 5 → $R = 1$.

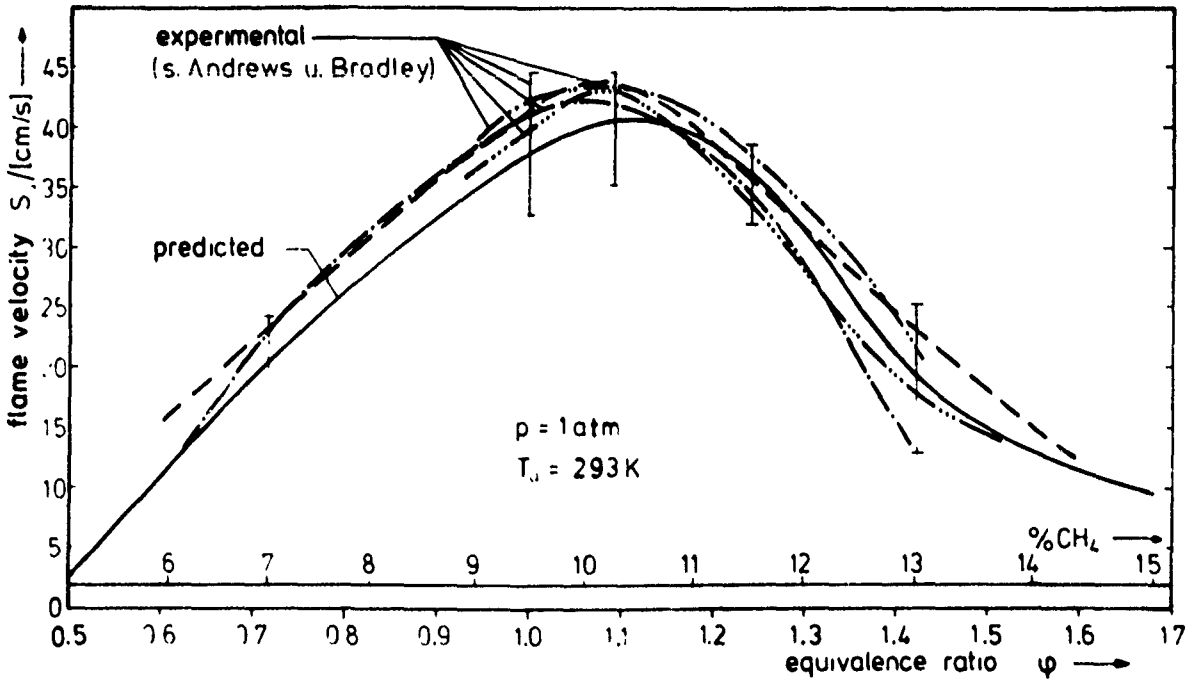

Fig. IX.9 — Comparison of measured and calculated flame velocities for methane-air flames at 1 atm as a function of equivalence ratio [99].

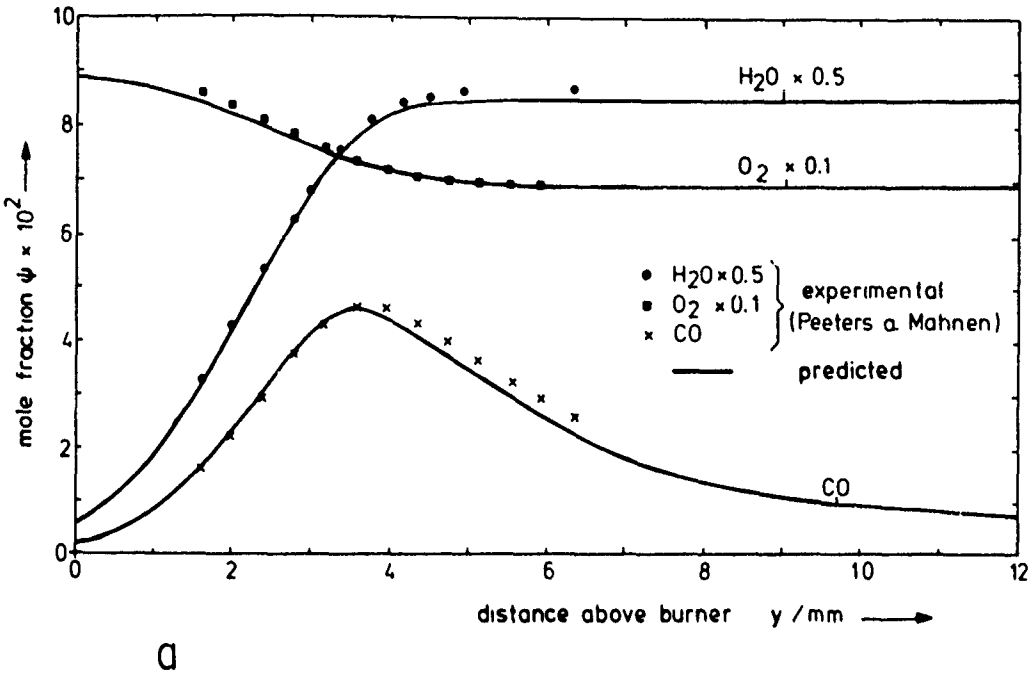

Fig. IX.10a — Comparison of measured and calculated mole fractions of H_2O, O_2, and CO_2 as a function of distance above the burner for a low pressure $CH_4 - O_2$ flame ($P = 0.053$ atm, 9.5% CH_4) [99].

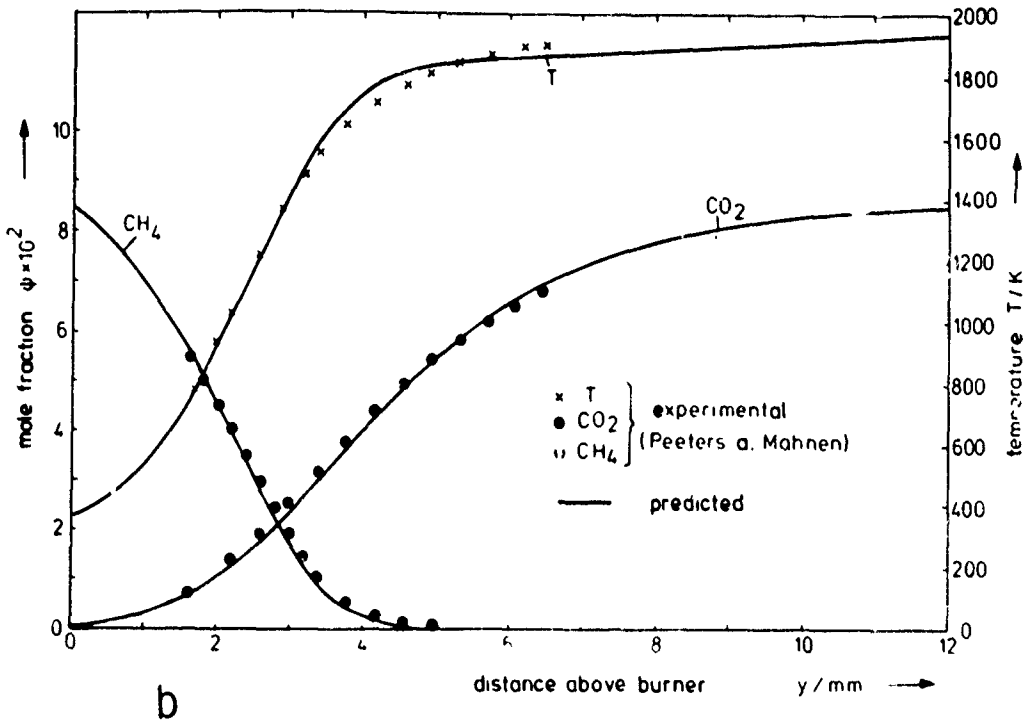

Fig IX.10b — Comparison of measured and calculated temperature and mole fractions of CH_4 and CO_2 for the conditions of Fig 10.a.

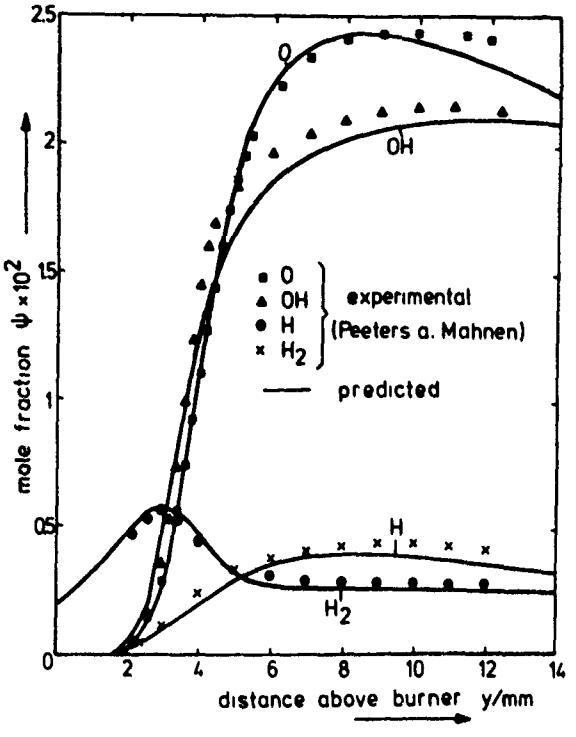

c

Fig. IX.10c — Comparison of measured and calculated mole fractions O, OH, H, and H_2 for the conditions of Fig. IX.10a.

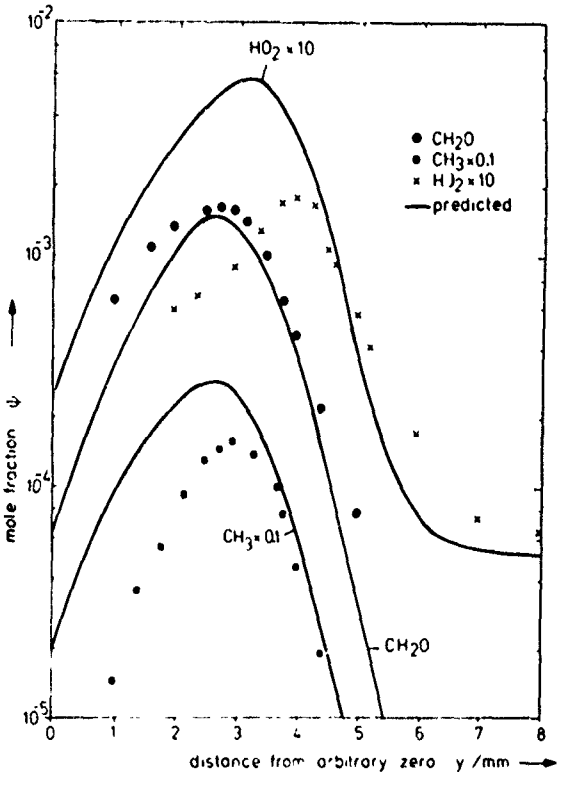

d

Fig. IX.10d — Comparison of measured and calculated mole fractions of HO_2, CH_2O, and CH_3 for the conditions of Fig. IX.10a.

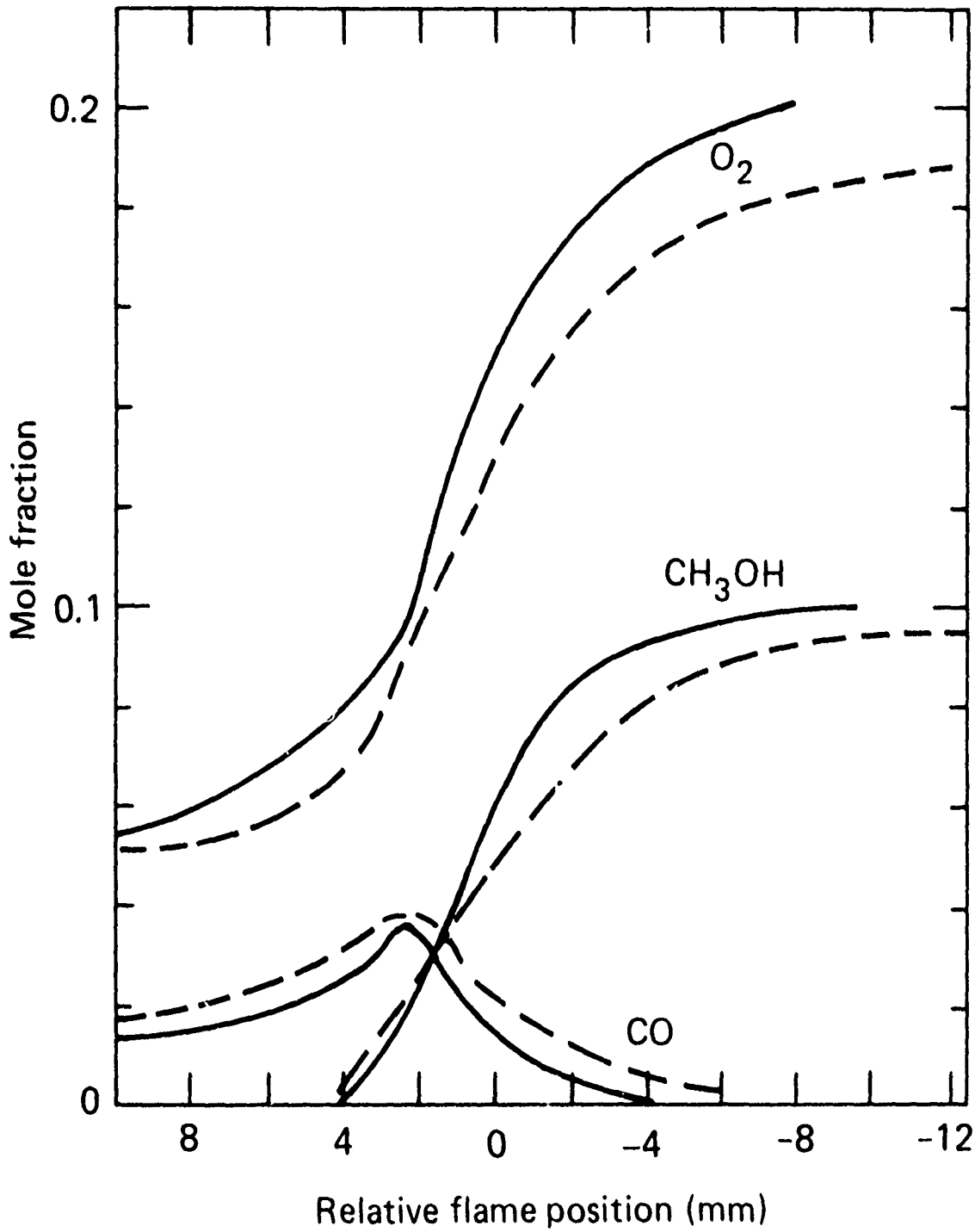

Fig. IX.11 — Comparison of measured (solid line) and calculated (dashed line) species concentrations for a low pressure method-air flame [100] as a function of position (P = 0.1 atm, equivalence ratio = 0.77, and initial unburned temperature = 300°K).

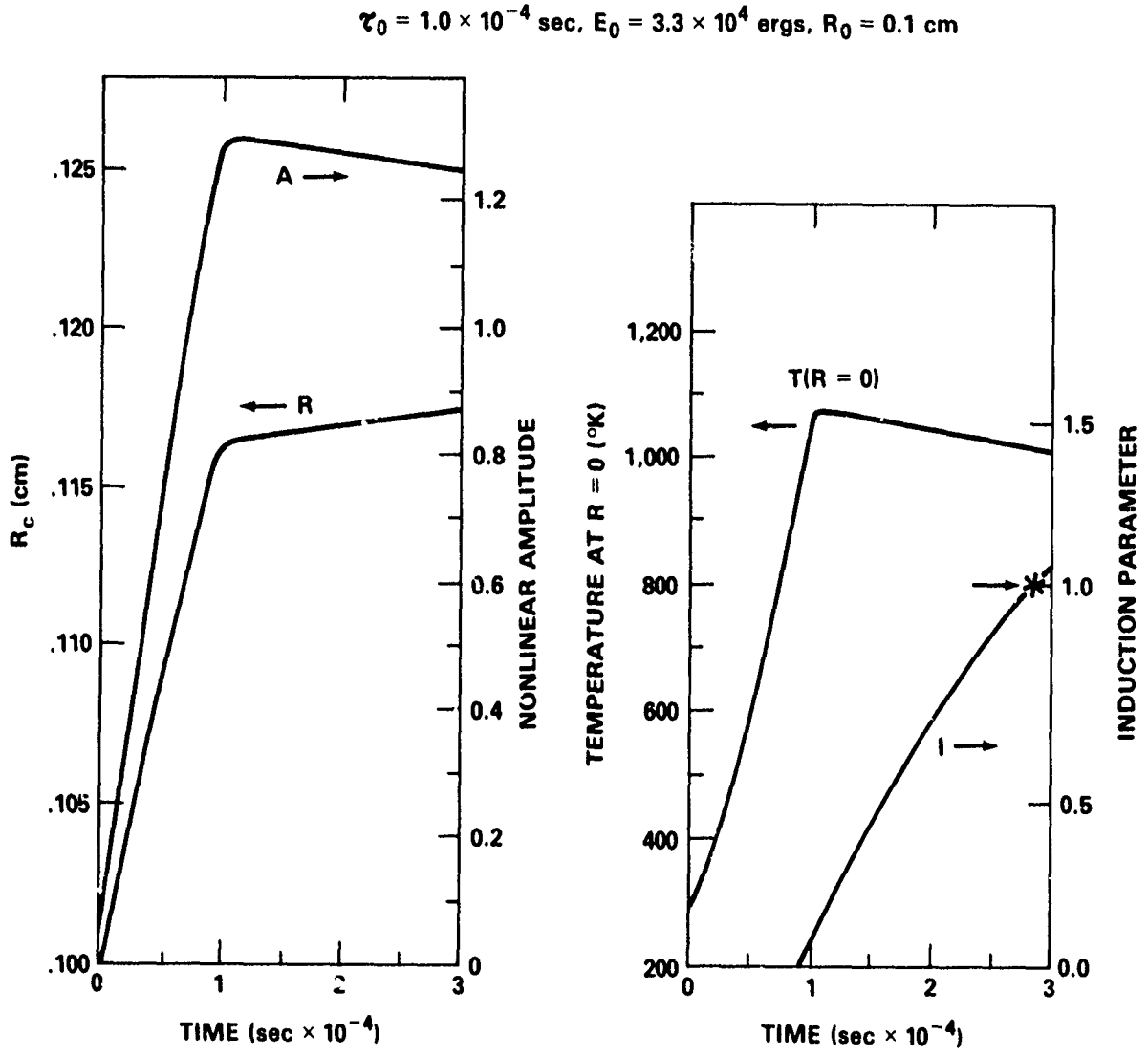

Fig. IX.12 — Similarity solution parameters (characteristic radius, R_c, nonlinear amplitude, A, central temperature, $T(R = 0)$, and induction parameter, I) as a function of time. The '*' indicates the time for which the model predicts ignition for a mixture of H_2: O_2: N_2/2:1:10 at 1 atm and initially at 300°K.

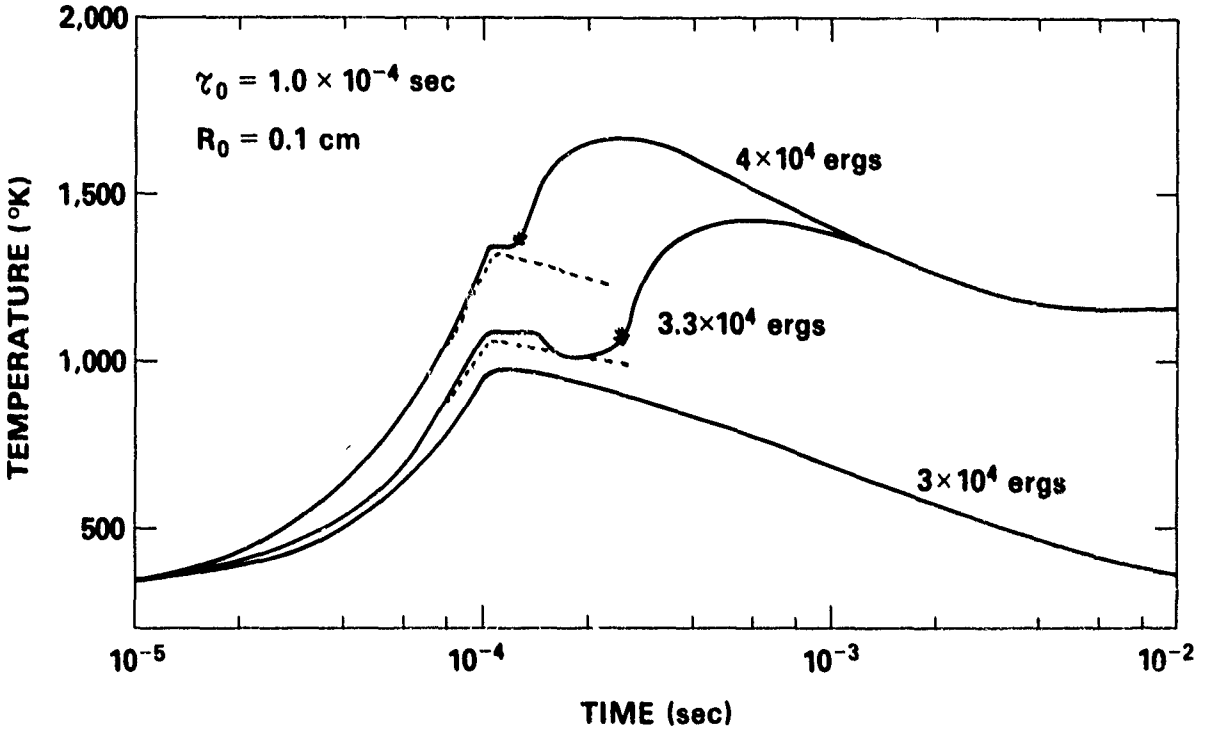

Fig. IX.13 — Comparison of solutions of central temperature as a function of time for the similarity solution (dashed line) and a detailed simulation (solid line) for three values of energy deposited. The '*' indicates the time at which the similarity solution predicts ignition.

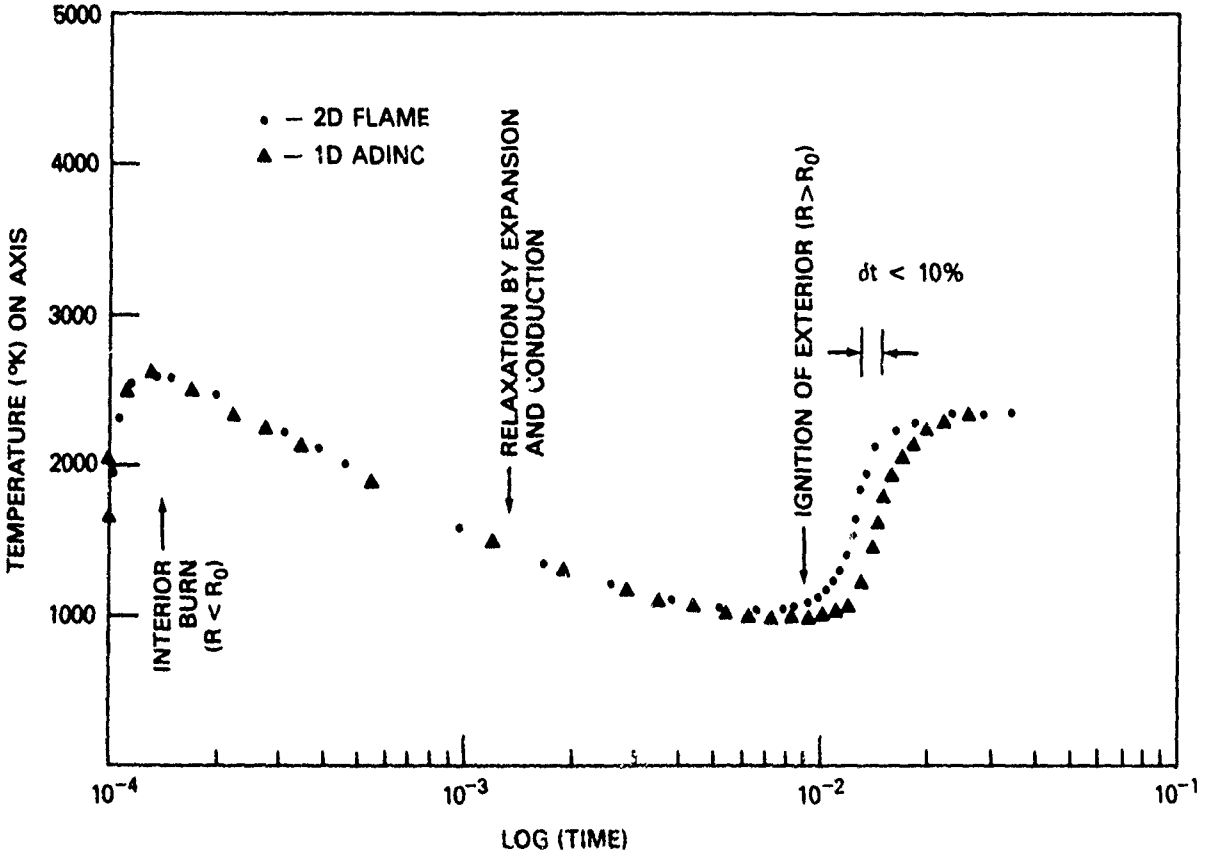

Fig. IX.14 — Velocity vector and reactant density contour plots at times 1.0×10^{-4}, 2×10^{-4}, and 5×10^{-4} seconds, from top to bottom, for the calculation of unsteady combustion in two connected, closed chambers [102].

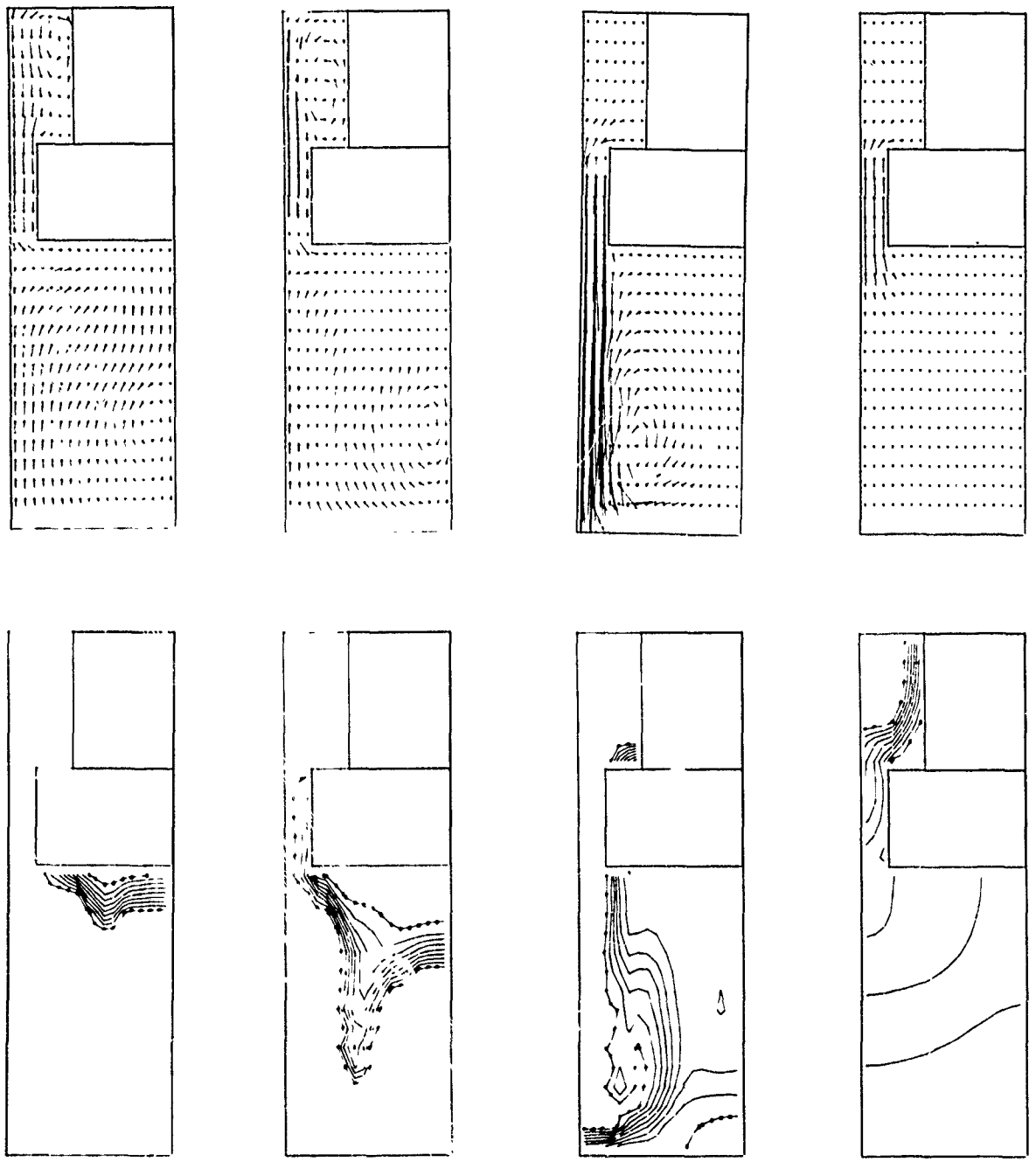

Fig. IX.15 — Calculations of central temperature as a function of time for a propagating flame in an enclosed chamber. Pressure increases in the enclosed chamber cause all of the unburned gas to ignite at once at about 10^{-2} seconds. The results calculated using the one-dimensional and the two-dimensional models differ by about 10% after this time.

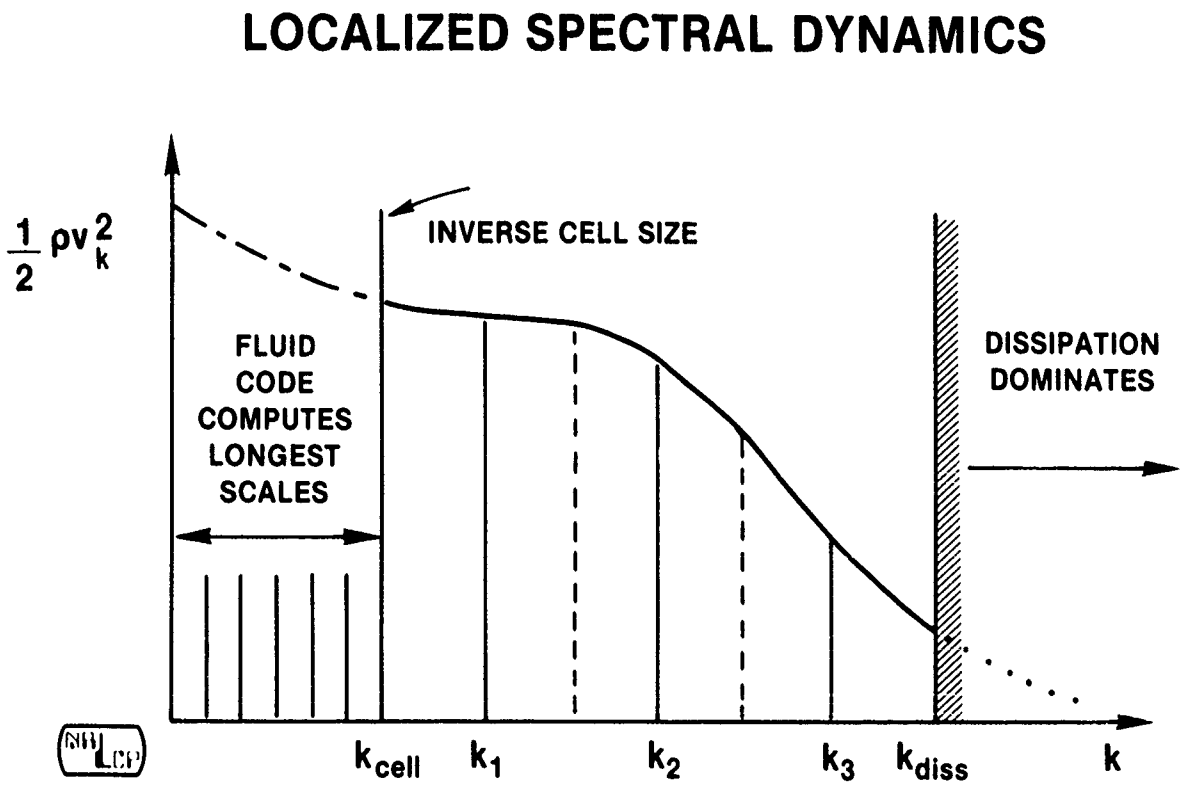

Fig. X.1 — Schematic showing how localized spectral dynamics can describe reactive flow mixing.

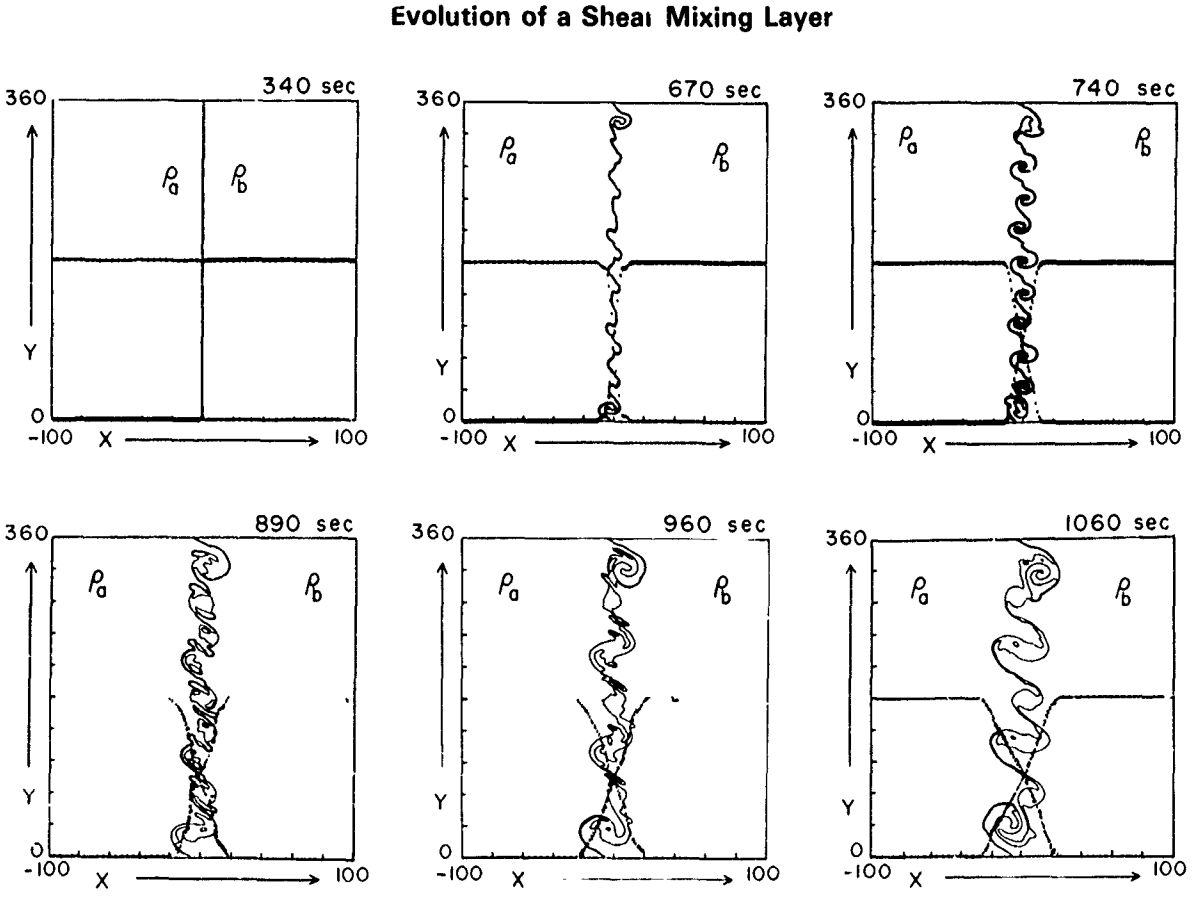

Fig. X.2 — Evolution of a shear mixing layer in a finely resolved two-dimensional ab initio calculation of a two species compressible fluid.

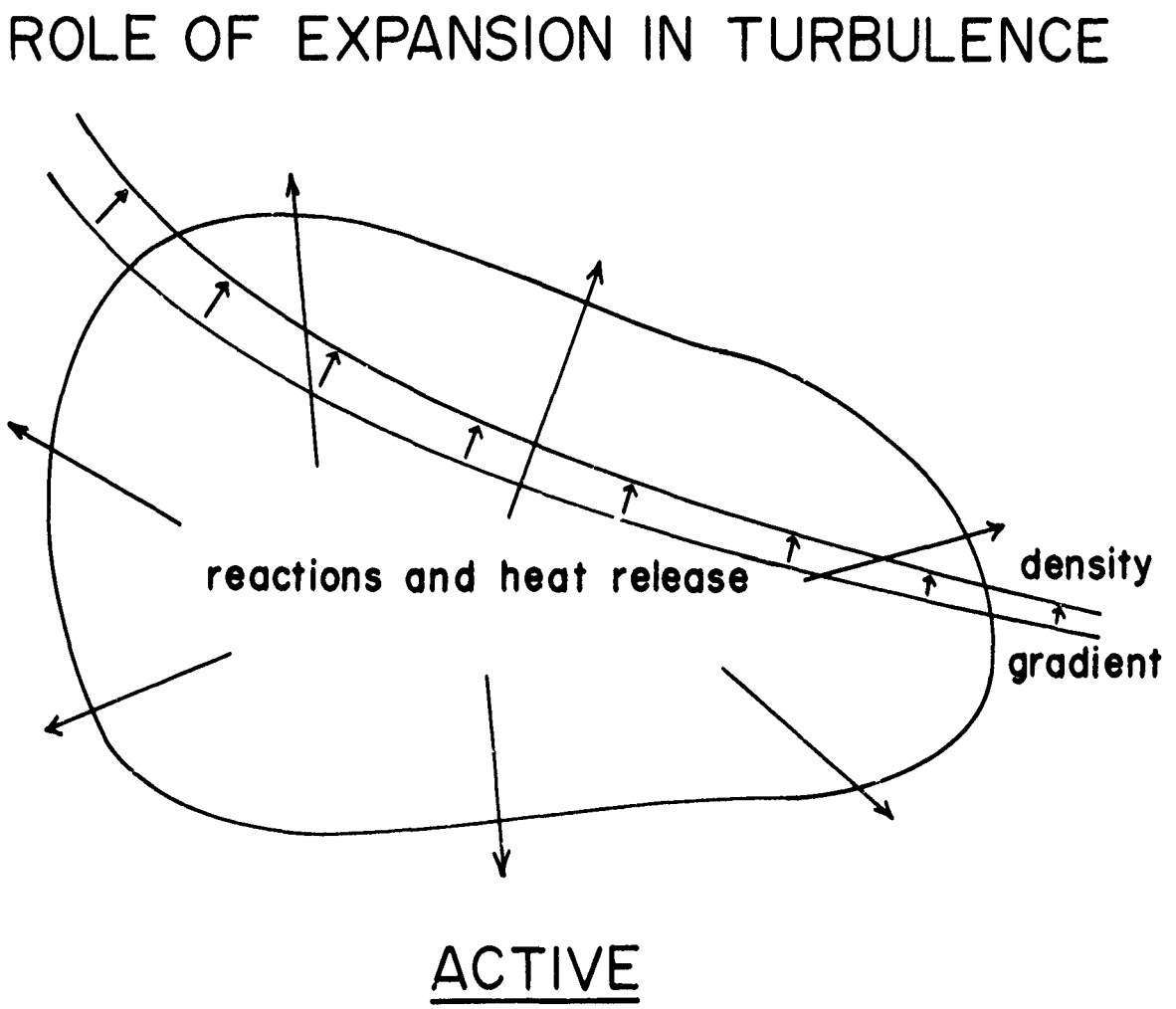

Fig. X.3 — The active role of expansion in the turbulence of reactive flows.

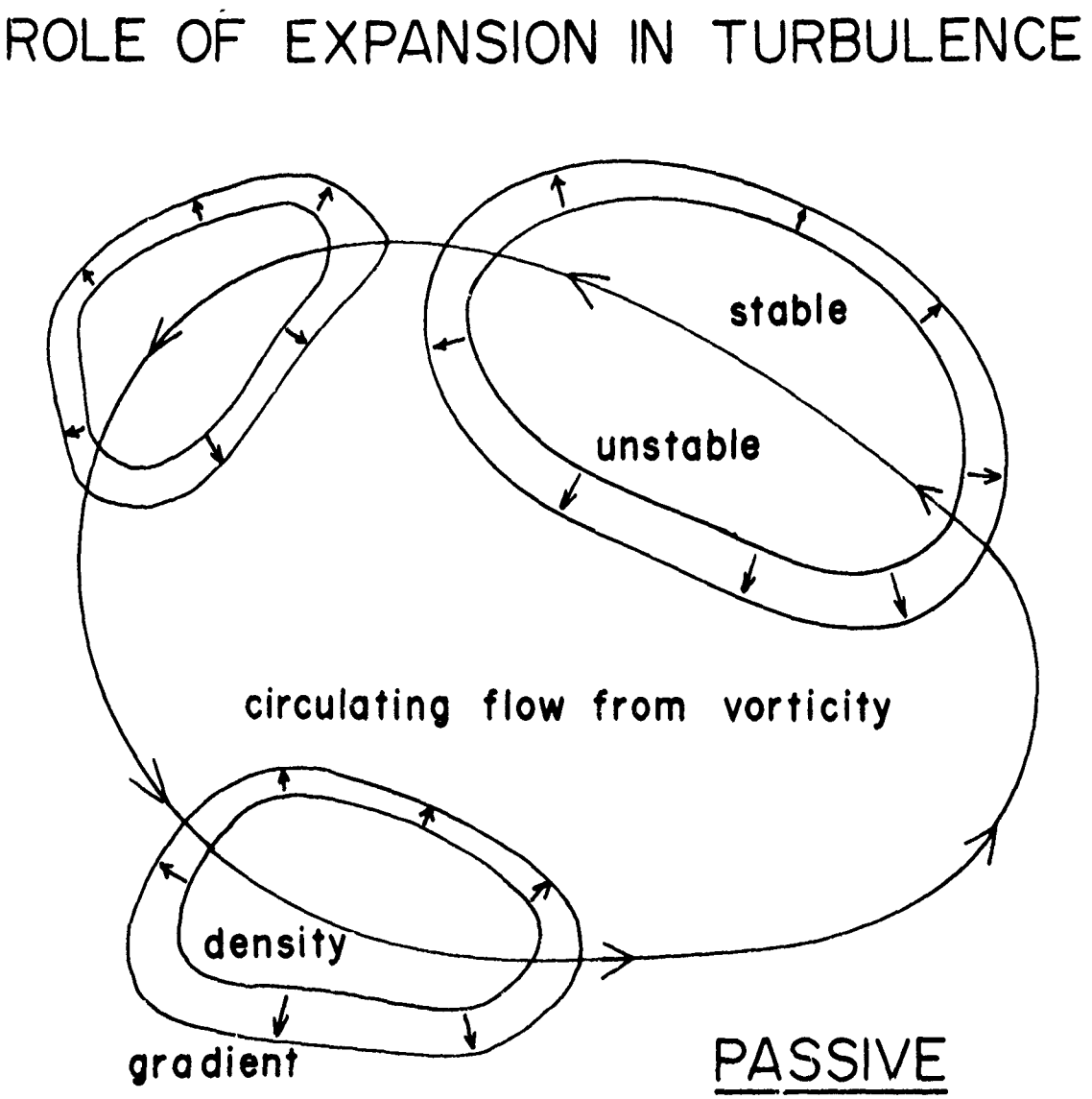

Fig. X.4 – The passive role of expansion in the turbulence of reactive flows.

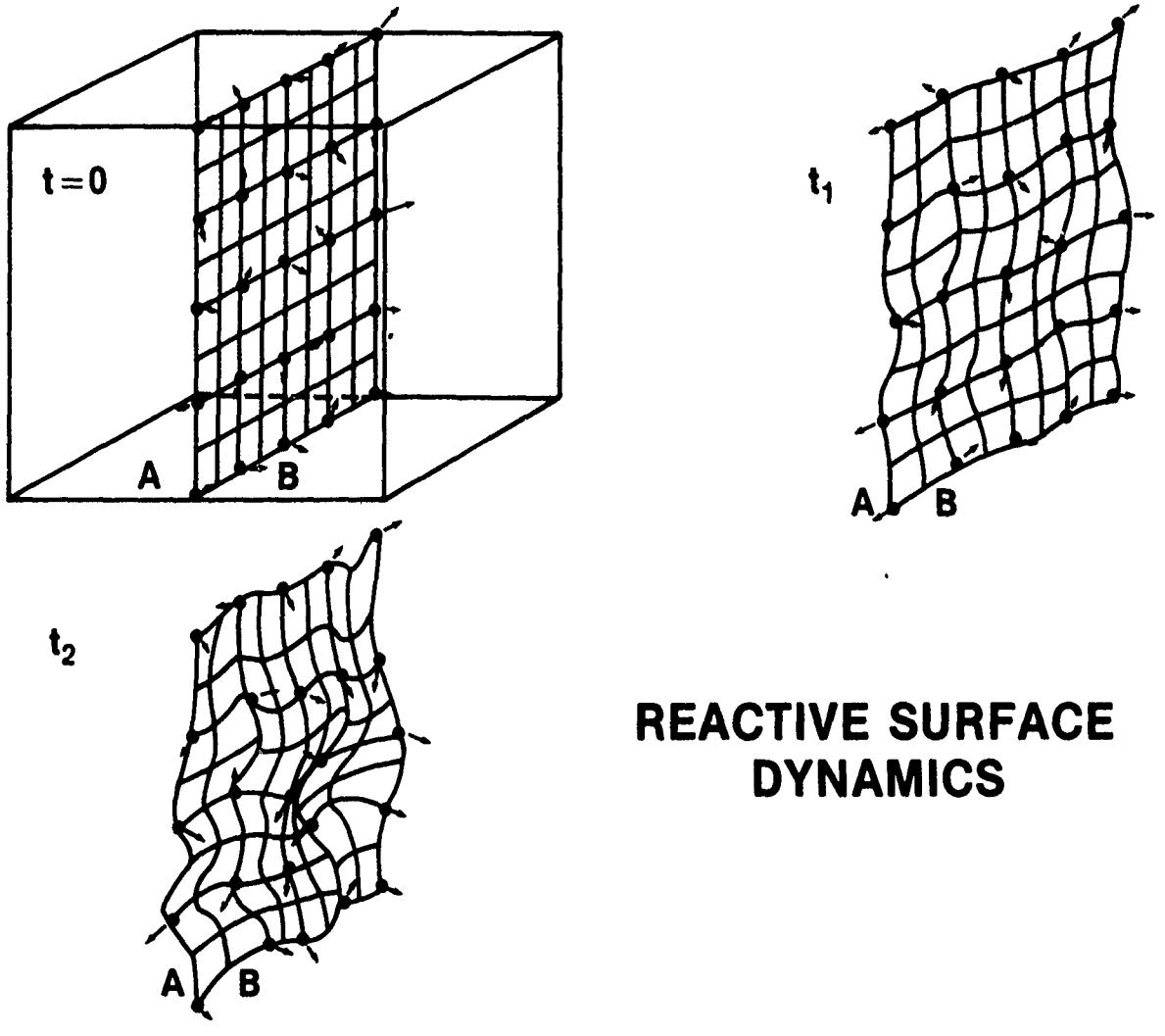

Fig. X.5 — Three stages during the early deformation of a reactive surface between two fluids *A* and *B*. At $t = 0$ (upper left), the surface separating A and B is shown as flat and two-dimensional in a three-dimensional volume of fluid. At later times t_1 (upper right) and t_2 (lower left), the surface progressively deforms as the result of the local Lagrangian motion of surface points shown as small arrows to indicate local direction of flow.

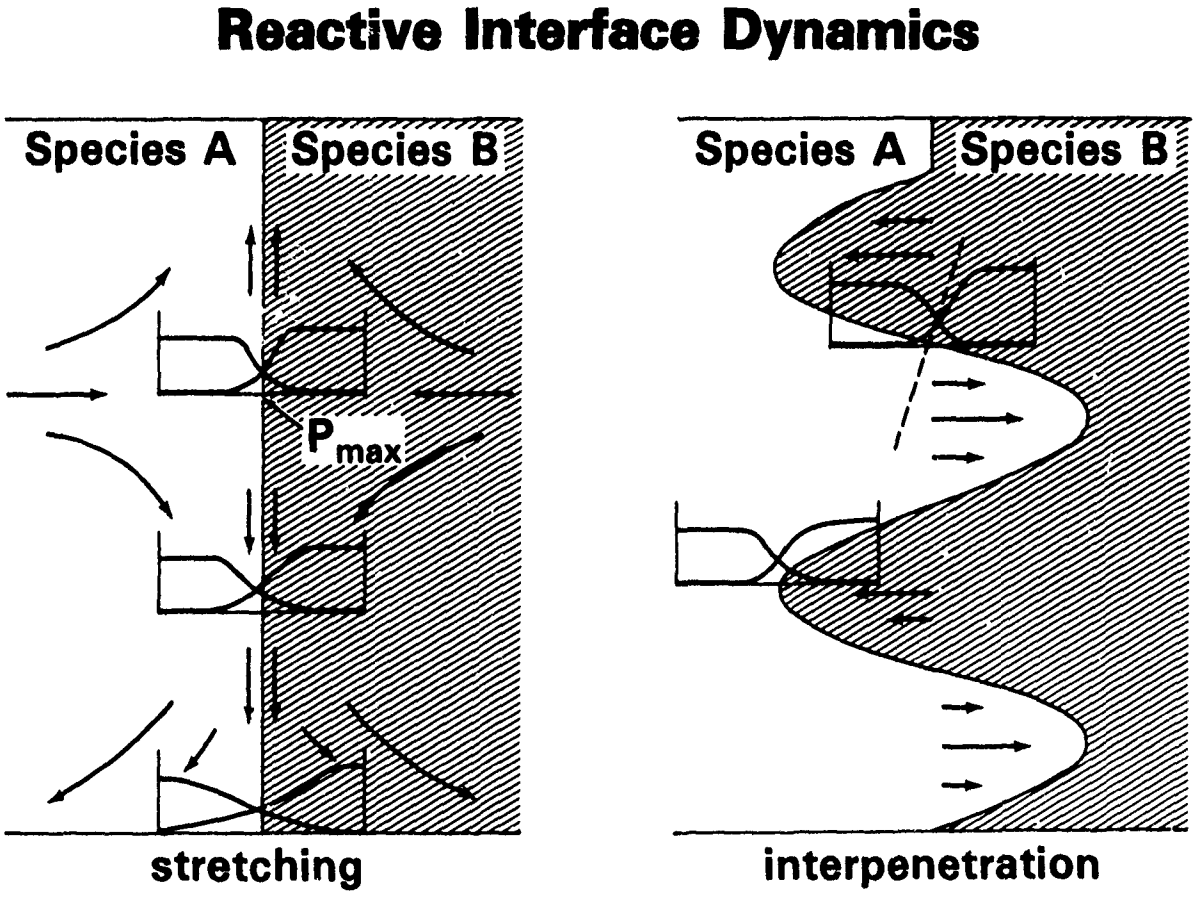

Fig. X.6 — Interpenetration of two species A and B as influenced by local reactive interface dynamics.

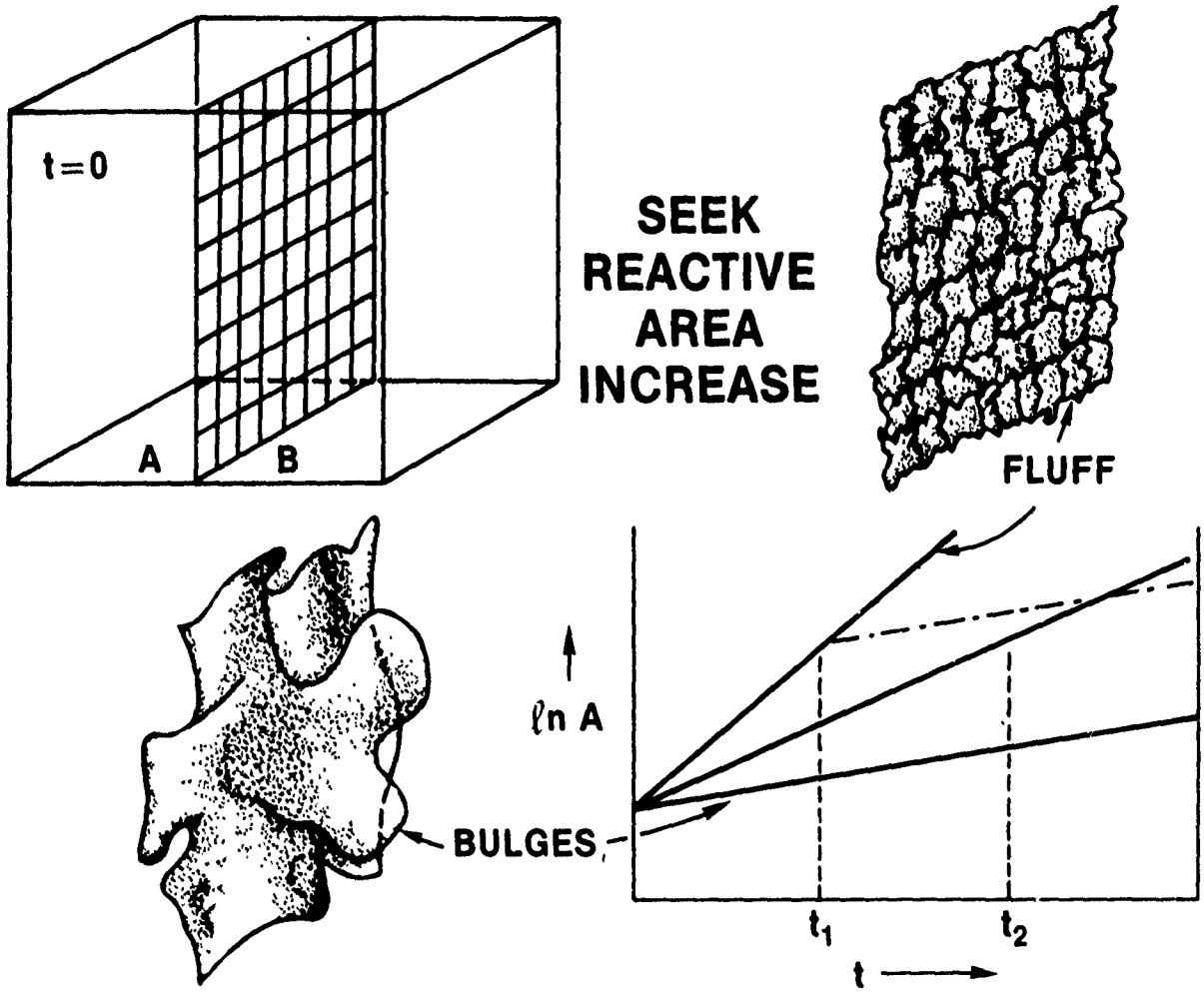

Fig. X.7 — Two different cases for reactive interface area increase are shown. In the upper right a relatively flat fluffy surface results from a turbulent velocity spectrum enhanced at short wavelengths where molecular diffusion is strong. When diffusior. is small and the velocity spectrum large at long wavelengths, smooth bulges result as shown in the lower left.

Ab Initio Simulation of Reactive Flow Mixing

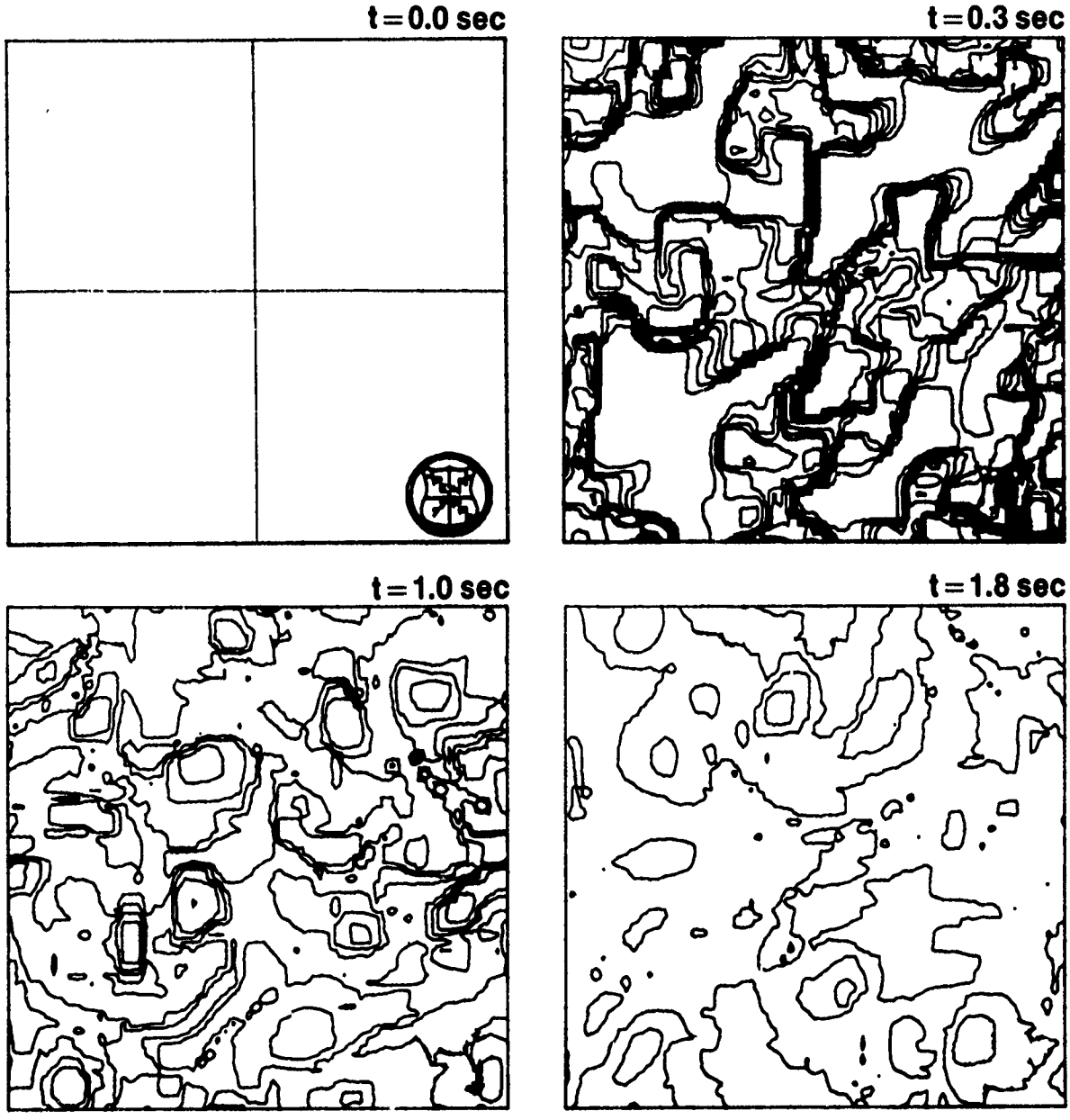

Fig. X.8 — Contour plots of density during a detailed two-dimensional reactive flow simulation designed to show the effects of density differences on the generation of short wavelength turbulence and mixing.

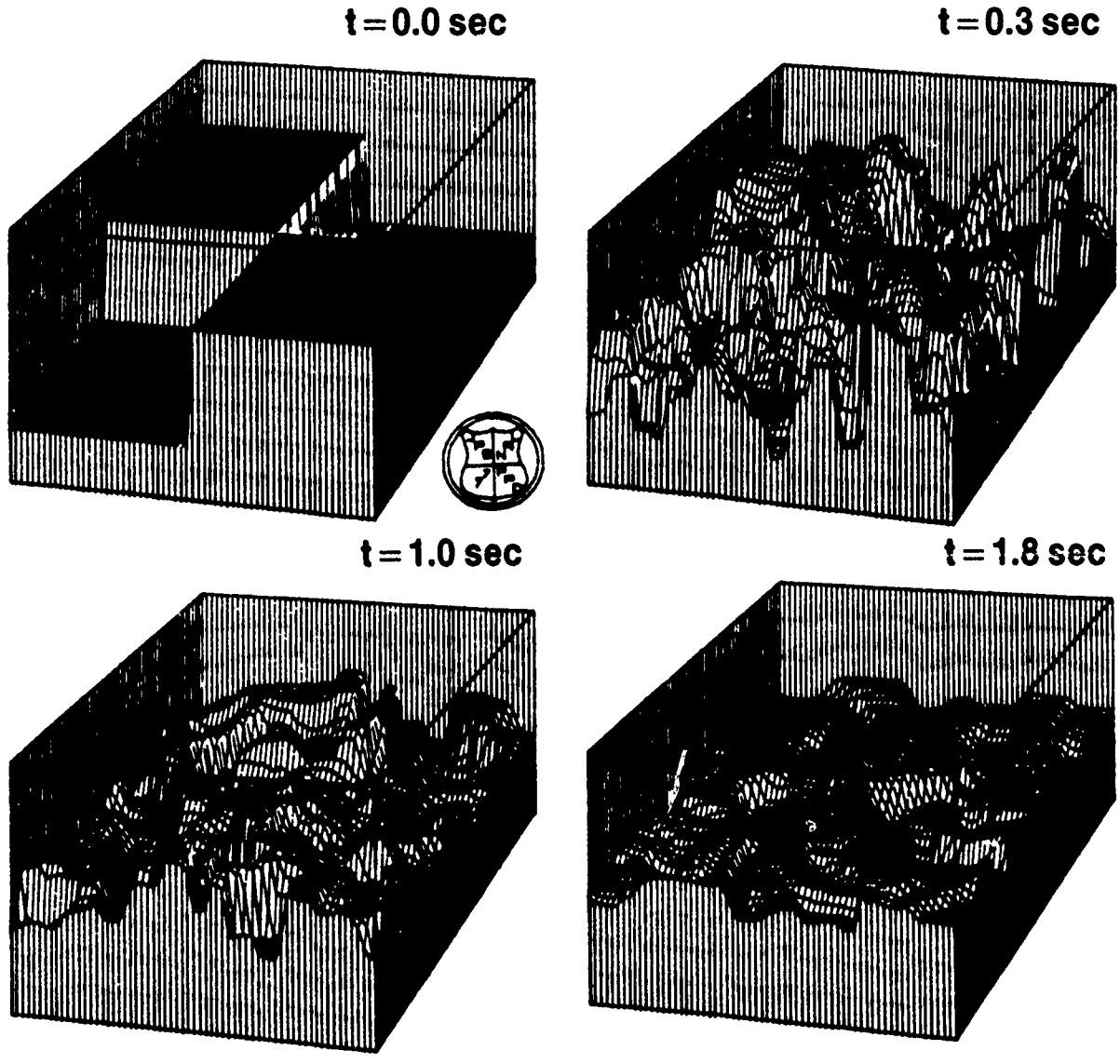

Fig. X.9 — Plots of density as a function of x and y at four times for the ab initio reactive flow mixing calculation of Fig. X.8.

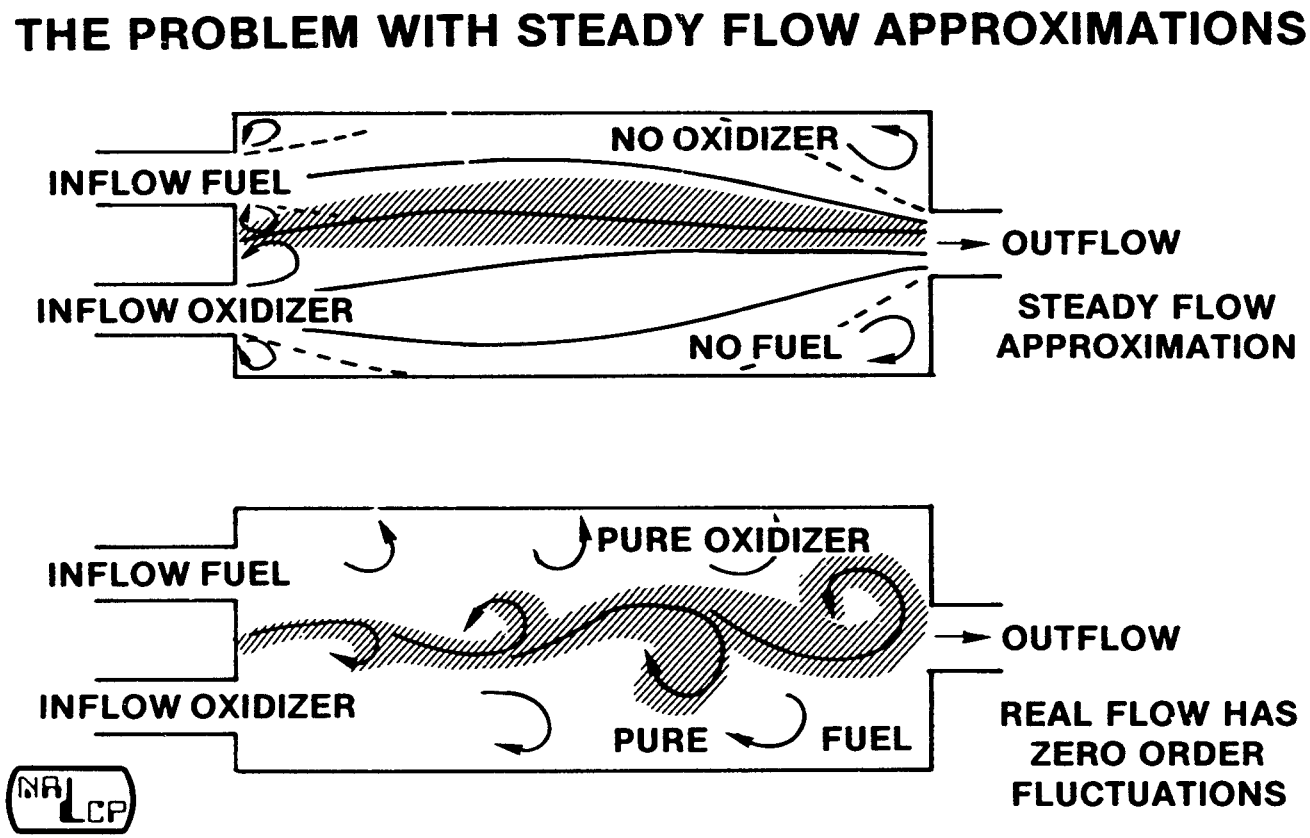

Fig X.10 — A fundamental problem with steady flow approximations.